



**HAL**  
open science

# Discrete Reconfigurations of Cable-Driven Parallel Robots

Lorenzo Gagliardini

► **To cite this version:**

Lorenzo Gagliardini. Discrete Reconfigurations of Cable-Driven Parallel Robots. Automatic. Ecole Centrale de Nantes (ECN), 2016. English. NNT: . tel-01535455v1

**HAL Id: tel-01535455**

**<https://hal.science/tel-01535455v1>**

Submitted on 9 Jun 2017 (v1), last revised 24 Jul 2019 (v2)

**HAL** is a multi-disciplinary open access archive for the deposit and dissemination of scientific research documents, whether they are published or not. The documents may come from teaching and research institutions in France or abroad, or from public or private research centers.

L'archive ouverte pluridisciplinaire **HAL**, est destinée au dépôt et à la diffusion de documents scientifiques de niveau recherche, publiés ou non, émanant des établissements d'enseignement et de recherche français ou étrangers, des laboratoires publics ou privés.

# Thèse de Doctorat

Lorenzo GAGLIARDINI

Mémoire présenté en vue de l'obtention  
**du grade de Docteur de l'École Centrale de Nantes**  
sous le sceau de l'Université Bretagne Loire

École doctorale : Sciences Pour l'Ingénieur, Géosciences, Architecture

*Discipline : Mécanique des solides, des matériaux, des structures et des surfaces*  
*Unité de recherche : Institut de Recherche en Communications et Cybernétique de Nantes*

Soutenue le 19 Septembre 2016

## Reconfigurations discrètes de robots parallèles à câbles

### JURY

Président : **M. Jean-Pierre MERLET**, Directeur de Recherche, INRIA, Sophia Antipolis

Rapporteurs : **M. Marco CARRICATO**, Professeur, University of Bologna, Italie  
**M. Jean-Pierre MERLET**, Directeur de Recherche, INRIA, Sophia Antipolis

Examineurs : **M. Tobias BRUCKMANN**, Professeur associé, University of Duisburg-Essen, Allemagne  
**M. Philippe WENGER**, Directeur de Recherche, CNRS, IRCCyN, École Centrale de Nantes

Invités : **M. Alexis GIRIN**, Docteur, IRT Jules Verne, Bouguenais  
**M. Jean-Louis PIQUEMAL**, Ingénieur de recherche, STX France S.A.

Directeur de thèse : **M. Stéphane CARO**, Chargé de Recherche, HDR, CNRS, IRCCyN, École Centrale de Nantes

Co-encadrant de thèse : **M. Marc GOUTTEFARDE**, Chargé de Recherche, CNRS, LIRMM





## École Doctorale SPIGA

IRCCYN "INSTITUT DE RECHERCHE EN COMMUNICATIONS ET  
CYBERNÉTIQUE"

2015 / 2016

This dissertation is submitted for the degree of  
*Doctor of Philosophy*

**Lorenzo Gagliardini**

**On 19/09/2016**

# DISCRETE RECONFIGURATIONS OF CABLE-DRIVEN PARALLEL ROBOTS

### MEMBERS OF THE JURY

President:	<b>Jean-Pierre MERLET</b>	Directeur de Recherche, INRIA, Sophia Antipolis, France
Reviewer:	<b>Marco CARRICATO</b>	Professor, University of Bologna, Italy
	<b>Jean-Pierre MERLET</b>	Directeur de Recherche, INRIA, Sophia Antipolis, France
Examiners:	<b>Tobias BRUCKMANN</b>	Dr.-Ing, University of Duisburg-Essen, Germany
	<b>Philippe WENGER</b>	Directeur de Recherche, CNRS, IRCCyN, École Centrale de Nantes
	<b>Philippe CARDOU</b>	Associated Professor, Laval University, Québec, QC., Canada
Invited Members:	<b>Alexis GIRIN</b>	Resp. Equipe Recherche Robotique, IRT Jules Verne, France
	<b>Jean-Louis PIQUEMAL</b>	Resp. du Developpement Operationnel, STX-Europe
Thesis Director :	<b>Stéphane CARO</b>	Chargé de Recherche, HDR, CNRS, IRCCyN
Supervisor:	<b>Marc GOUTTEFARDE</b>	Chargé de Recherche, CNRS, LIRMM



## Abstract

*Cable-Driven Parallel Robots* (CDPRs) are parallel robots whose legs consist of cables. CDPRs may be used successfully in several industrial applications such as sandblasting and painting of large and heavy structures. However, the flexible nature of the cables, the possible collisions between the cables and the environment and the cable interferences can limit their use in an industrial context. These drawbacks are usually amplified when the task to be performed is complex and the working environment is cluttered.

Recent developments in CDPRs have shown that the reconfiguration of their geometric parameters can lead to several advantages. CDPR performances can be improved, with respect to a given task, by modifying the position of the exit points, defined as the connection points between the cables and the robot base frame. CDPRs that are able to displace their exit points are defined hereafter as *Reconfigurable Cable-Driven Parallel Robots* (RCDPRs). The research work presented in this manuscript deals mainly with RCDPRs whose cable connection points on the base frame can be positioned at a possibly large but discrete set of possible locations.

The first part of this manuscript is dedicated to the modelling of CDPRs. When the deformations induced by the mass of the cables can be neglected, cables are modelled as linear segments. The linear cable model has been used to describe the static, kinematic and dynamic models of the CDPRs. When the mass of the cables is not negligible, cables are modelled while considering the sagging effect. Heavy cables are generally used when the CDPR has to displace a heavy payload over a large workspace. For this kind of operations, we considered the equilibrium of the robot as quasi-static, describing the CDPR through its geometrico-static model. Finally, two elasto-static models have been introduced in this manuscript, in order to describe the small displacement of the moving platform due to the non-rigid nature of the cables. These models can be used for the modal analysis of the CDPRs, as well. The elasto-static model based on linear cables has been computed including the effect of the pulleys orienting the cables into the CDPR workspace. The elasto-static model based on sagging cables has been computed developing both the passive and active stiffness matrices of the CDPR, while the active stiffness matrix is usually neglected in the literature. The CDPR models based on the linear and the sagging cable models are well known in the literature. In this manuscript, the notation describing these models has been adapted for RCDPRs.

The second part of this manuscript deals with the investigation of the workspace of CDPRs, in terms of their moving platform static and dynamic equilibria, and in terms of their moving platform kinematic constraints. Two novel workspaces have been defined: (i) the *Twist Feasible Workspace* (TFW), defined as the set of twist feasible poses of the CDPR. A pose is said to be twist feasible if the platform of the CDPR can assume a given range of twists while satisfying the cable speed limits imposed by the actuators and the transmission systems; (ii) the *Improved Dynamic Feasible Workspace* (IDFW), defined as the set of dynamic feasible poses of the CDPR. A pose is said to be dynamic feasible if the actuators of the CDPR can provide to the cables the tensions necessary to achieve a given set of moving platform accelerations. With respect to the *Dynamic Feasible Workspace* (DFW), the IDFW does not neglect the contributions of the external wrenches applied on the moving platform on the dynamic equilibrium of the moving platform. Coriolis and centrifugal wrenches are considered as well, by supposing the

twist of the moving platform to be constant. All the workspaces described in this manuscript are valid for both CDPRs and RCDPRs.

The third part of this manuscript describes a generic design strategy for CDPRs. According to the state of the art, the design problem of CDPRs is formulated as an optimization problem. It aims at optimising the design variables with respect to one or several criterion(a), e.g. computing the locations of the cable exit points minimising the size of the CDPR. It may also aim at dimensioning the CDPR components, such as winches, pulleys and actuators while maximising the size of the WFW, TFW or the IDFW. The optimisation is performed while satisfying a set of constraints which validates the feasibility of the required operations with respect to the CDPR capabilities and limitations.

However, when the working environment is cluttered, CDPRs may not be able to accomplish the required task. Under this assumption, RCDPRs may solve this problem. A novel design strategy has been proposed in this thesis. This strategy contemplates the possibility to displace the cable exit points on a predefined grid of locations. The prescribed workspace or path of the moving platform is divided by the designer into  $n_p$  parts. Each part has to be covered by one and only one configuration of the RCDPR. An optimization algorithm defines the optimal configuration to be associated to each part of the prescribed workspace or path. The configurations are selected while optimising one or several global criterion(a), e.g. maximising the number of cable exit point locations shared among two or more configurations. The selection is performed by analysing all the configurations that can be generated by placing the cable exit points in any position of the exit point grid of locations. A case study has been introduced in this manuscript in order to validate the efficiency of this design strategy.

The fourth part of this manuscript introduces an algorithm to compute an optimal reconfiguration strategy for RCDPRs. This strategy can be used when the working environment of the RCDPR is extremely cluttered and it is not possible to predict how many configurations are necessary to complete the task. The moving platform of the RCDPR is supposed to follow a prescribed discretised path. If necessary, a reconfiguration is performed by detaching the cables from given exit point positions and attaching them to new locations. A so-called feasibility map is first generated. For each possible configuration of the RCDPR, this map stores the feasible or unfeasible character of each point of the discretised prescribed path, according to user-defined constraints which ensure a proper functioning of the RCDPR. The feasibility map is next analysed in order to determine minimum sets of configurations, which allow the RCDPR to follow the whole prescribed path. Finally, the corresponding discrete reconfiguration planning problem is represented as a graph whose nodes correspond to feasible RCDPR reconfigurations. The arcs of the graph are weighted by a user-defined cost function, e.g. the number of reconfigurations, the stability of the robot moving platform and the cable tensions, so that the graph can be searched for an optimal reconfiguration strategy using Dijkstra's algorithm. A set of constraints should be satisfied all along the task, including the equilibrium of the moving platform, the cable interference avoidance and the absence of collisions between the cables and the environment. The effectiveness of the algorithm has been studied by analysing a planar and a spatial RCDPRs reproducing some industrial tasks.

**Keywords: Cable-Driven Parallel Robots, Discrete Reconfiguration, Workspace Analysis, Elasto-Static Modelling, Design.**

## Résumé

Les robots parallèles à Câbles (RPCs) sont des robots parallèles dont les jambes se composent de câbles. Les applications industrielles potentielles des RPCs sont nombreuses telles que le grenailage et la peinture de structures massives et de grandes dimensions. Cependant, la flexibilité des câbles, les collisions éventuelles entre les câbles et entre les câbles et l'environnement peuvent limiter leur utilisation dans un contexte industriel. Ces inconvénients sont généralement amplifiés lorsque la tâche à accomplir est complexe et l'environnement de travail est encombré.

Les développements récents dans le domaine de la robotique parallèle à câbles ont montré que la reconfiguration des paramètres géométriques peut conduire à de nombreux avantages. Les performances des RPC peuvent être améliorées, par rapport à une tâche donnée, en modifiant notamment la position des points de sortie des câbles. Les robots parallèles à câbles pour lesquels les points de sortie des câbles peuvent être déplacés sont appelés Robots Parallèles à Câbles Reconfigurables (RPCRs). Les travaux de recherche présentés dans ce manuscrit traitent de RPCRs pouvant avoir un nombre important de reconfigurations mais « discrètes ».

La première partie de ce manuscrit est dédiée à la modélisation des RPCs. Lorsque les déformations induites par la masse des câbles peuvent être négligées, les câbles sont modélisés comme des segments linéaires. Le modèle de câble linéaire a été utilisé pour décrire les modèles statiques, cinématiques et dynamiques des RPCs. Lorsque la masse des câbles n'est pas négligeable, ces derniers sont modélisés en tenant compte de leur affaissement. Les câbles lourds sont généralement utilisés lorsque le RPC doit déplacer une charge utile lourde sur un grand espace de travail. Pour ce genre d'opérations, nous avons considéré l'équilibre du robot quasi-statique, décrivant le RPC grâce à son modèle géométrico-statique. Enfin, deux modèles élasto-statiques ont été introduits dans ce manuscrit, pour décrire le petit déplacement de la plate-forme mobile en raison de la nature non-rigide des câbles. Ces modèles peuvent également être utilisés pour l'analyse modale des RPC. Le modèle élasto-statique basé sur des câbles linéaires a été calculé, y compris l'effet des poulies orientant les câbles dans l'espace de travail du RPC. Le modèle élasto-statique basé sur des câbles pesants a été exprimé en faisant la différence entre la matrice de raideur active et la matrice de raideur passive du RPC, la matrice de raideur active étant généralement négligée dans la littérature. Dans ce manuscrit, la notation a été adaptée afin d'exprimer le modèle élasto-statique de RPCRs.

La deuxième partie de ce manuscrit traite de l'analyse d'espaces de travail de RPCs vis-à-vis de leurs performances statiques et dynamiques. Deux nouveaux espaces de travail ont été définis : (i) l'Espace des Vitesses Générables (EVG), défini comme l'ensemble des situations (positions et orientations) possibles de la plateforme mobile pour lesquelles des intervalles de vitesses linéaires et angulaires de la plateforme peuvent être atteints connaissant les intervalles de vitesses angulaires des moteurs; (ii) l'Espace de Travail Dynamique Amélioré (ETDA) correspondant à l'ensemble des situations de la plateforme mobile pour lesquelles des intervalles d'accélération peuvent être atteints, des intervalles d'efforts extérieurs peuvent être supportés en fonction des tensions admissibles dans les câbles et pour une torseur cinématique constant de la plateforme mobile. Il est à noter que l'ETDA tient compte des efforts de Coriolis et centrifuges appliqués sur la plateforme mobile. Tous les espaces de travail décrits dans ce manuscrit sont valables aussi bien pour les RPCs que pour les RPCRs.

La troisième partie de ce manuscrit décrit une stratégie de conception générique de RPCs. Le problème de conception de RPCs est formulé sous la forme d'un problème d'optimisation. Il vise à optimiser les variables de conception par rapport à un ou plusieurs critère(s) tels que le calcul de l'emplacement des points de sortie des câbles permettant de minimiser la taille du RPC. Il peut également viser le dimensionnement des composants des RPCs, tels que des treuils, des poulies et des actionneurs tout en maximisant la taille de l'Espace des Torseurs Générables (ETG), de l'EVG et de l'ETDA. Le problème d'optimisation est sujet à des contraintes qui doivent être satisfaites afin de valider la faisabilité des opérations nécessaires vis-à-vis des capacités et des limites des RPCs.

Toutefois, lorsque l'environnement de travail est encombré, les RPCs peuvent ne pas être en mesure d'accomplir la tâche requise contrairement aux RPCRs. Une nouvelle stratégie de conception a été proposée dans cette thèse. Cette stratégie envisage la possibilité de déplacer les points de sortie des câbles du RPCR sur une grille prédéfinie d'emplacements. L'espace de travail ou le chemin de la plate-forme mobile prescrit sont divisé par le concepteur en  $n_p$  éléments. Chaque élément doit être couvert par une et une seule configuration du RPCR. Un algorithme d'optimisation définit la configuration optimale qui doit être associée à chaque partie de l'espace de travail ou le chemin prescrit. Les configurations sont choisies tout en optimisant un ou plusieurs critère(s) global(aux), par exemple la maximisation de points de sortie communs à deux ou plusieurs configurations du RPCR. La sélection est effectuée en analysant toutes les configurations qui peuvent être générées en plaçant les points de sortie des câbles dans toutes les positions de la grille de points de sortie des emplacements. Une étude de cas a été introduite dans ce manuscrit afin de valider l'efficacité de cette stratégie de conception.

La quatrième partie de ce manuscrit présente un algorithme pour calculer une stratégie de reconfiguration optimale pour les RPCRs. Cette stratégie peut être utilisée lorsque l'environnement de travail de RPCRs est extrêmement encombré et qu'il n'est pas possible de prévoir le nombre de configurations nécessaires pour compléter la tâche. La plateforme mobile du RPCR est censée suivre un chemin discrétisé prescrit. Si nécessaire, une reconfiguration est effectuée en détachant les câbles de leur point de sortie et les attachant à un nouvel emplacement. Une carte dite de faisabilité est d'abord générée. Pour chaque configuration possible du RPCR, cette carte stocke le caractère réalisable ou irréalisable de chaque point de la trajectoire prescrite discrétisée, en fonction des contraintes définies par l'utilisateur qui assurent un bon fonctionnement du RPCR. La carte de faisabilité est ensuite analysée afin de déterminer des ensembles minimaux de configurations qui permettent au RPCR de suivre tout le parcours prescrit. Enfin, le schéma de reconfigurations discrètes est représenté comme un graphe dont les nœuds correspondent à des reconfigurations du RPCR réalisables. Les arcs du graphe sont pondérés par une fonction de coût définie par l'utilisateur, par exemple le nombre de reconfigurations, un critère de stabilité de la plateforme mobile et les tensions dans les câbles, de sorte que la carte de faisabilité permet de rechercher une stratégie de reconfiguration optimale en utilisant l'algorithme de Dijkstra. Des contraintes doivent être satisfaites tout au long de la tâche telles que l'équilibre de la plateforme mobile, l'évitement des interférences des câbles et l'absence de collisions entre les câbles et l'environnement. L'efficacité de l'algorithme a été analysée en étudiant les reconfigurations d'un robot parallèle à câbles planaire et d'un robot parallèle à câbles spatial en lien avec des applications industrielles.

**Mot-clés: Robots Parallèles à Câbles, Reconfigurations Discrètes, Espaces de travail, Modélisation Elasto-Statique, Conception.**

# Contents

<b>List of Figures</b>	<b>xi</b>
<b>List of Tables</b>	<b>xv</b>
<b>Acronyms and Abbreviations</b>	<b>xvii</b>
<b>1 Introduction</b>	<b>1</b>
1.1 Cable-Driven Parallel Robots (CDPRs)	2
1.1.1 Advantages and Applications	3
1.1.2 Classification of CDPRs	6
1.1.3 Reconfigurable Cable-Driven Parallel Robots (RCDPRs)	8
1.1.4 IRT Jules Verne CAROCA Project	8
1.2 Theoretical Background	9
1.2.1 Direct Geometrico-Static Problem	11
1.2.2 Cable and Stiffness Modelling	11
1.2.3 Workspace Analysis	12
1.2.4 Tension Distribution and Control	13
1.2.5 Design	13
1.2.6 Reconfigurability	14
1.3 Contributions and Thesis Organisation	15
1.3.1 Elasto-Static Modelling	16
1.3.2 Twist and Dynamic Feasible Workspaces	16
1.3.3 Design of CDPRs and RCDPRs	17
1.3.4 Reconfiguration Strategy for Discrete RCDPRs	18
1.3.5 Manuscript Organisation	19

<b>2</b>	<b>Modelling</b>	<b>21</b>
2.1	CDPR Models Based on the Linear Rigid Cable Model . . . . .	22
2.1.1	Robot Representation . . . . .	22
2.1.2	Inverse Geometric Models (IGMs) . . . . .	23
2.1.3	Inverse Static Model (ISM) . . . . .	24
2.1.4	Direct and Inverse First Order Kinematic Models . . . . .	26
2.1.5	Direct and Inverse Second Order Kinematic Models . . . . .	26
2.1.6	Inverse Dynamic Model (IDM) . . . . .	27
2.2	CDPR Models Based on the Sagging Cable Model . . . . .	29
2.2.1	Sagging Cable Model . . . . .	29
2.2.2	Inverse Gometrico-Static Model . . . . .	30
2.3	CDPR Elasto-Static Models . . . . .	33
2.3.1	Linear Non-Rigid Cable Model . . . . .	33
2.3.2	Linear Non-Rigid Cable Model with Pulleys . . . . .	36
2.3.3	Sagging Cable Model . . . . .	39
2.4	Conclusions . . . . .	42
<b>3</b>	<b>Workspace Analysis</b>	<b>43</b>
3.1	Mathematical Definition of Existing Workspaces . . . . .	44
3.1.1	Wrench Feasible Workspace (WFW) . . . . .	44
3.1.2	Wrench Closure Workspace (WCW) . . . . .	46
3.1.3	Static Feasible Workspace (SFW) . . . . .	47
3.1.4	Interference and Collision Free Workspaces . . . . .	48
3.2	Twist Feasible Workspace (TFW) . . . . .	48
3.3	Dynamic Feasible Workspace (DFW) . . . . .	50
3.3.1	Standard Dynamic Feasible Workspace . . . . .	50
3.3.2	Improved Dynamic Feasible Workspace (IDFW) . . . . .	50
3.4	Case Study . . . . .	51
3.5	Conclusions . . . . .	54
<b>4</b>	<b>Design of Reconfigurable Cable-Driven Parallel Robots</b>	<b>57</b>
4.1	Design Strategy for CDPRs . . . . .	58
4.1.1	Design Problem Formulation . . . . .	59
4.1.2	Objective Functions . . . . .	60
4.1.3	Constraint Functions . . . . .	64

4.2	Classes of RCDPRs . . . . .	66
4.2.1	Reconfigurable Elements and Technological Solutions . . . . .	67
4.2.2	Discrete and Continuous Reconfigurations . . . . .	68
4.3	Nomenclature for RCDPRs . . . . .	68
4.4	Design Strategy for RCDPRs . . . . .	69
4.4.1	Design Problem Formulation . . . . .	69
4.4.2	Global Objective Functions . . . . .	71
4.5	Case Study I: Design of a CDPR Based on the Workspace Size . . . . .	73
4.5.1	Problem Description . . . . .	73
4.5.2	Optimisation Results . . . . .	76
4.6	Case Study II : Design of a RCDPR for Sandblasting and Painting of a Large Tubular Structure . . . . .	78
4.6.1	Problem Description . . . . .	78
4.6.2	Optimisation Results . . . . .	84
4.7	Conclusions . . . . .	85
<b>5</b>	<b>Reconfiguration Planning of RCDPRs</b>	<b>89</b>
5.1	Reconfiguration Procedure . . . . .	90
5.2	Reconfiguration Strategy . . . . .	90
5.2.1	<u>Step I: Constant Design Parameters</u> . . . . .	90
5.2.2	<u>Step II: RCDPR Layout Parametrisation</u> . . . . .	91
5.2.3	<u>Step III: RCDPR Configuration Set</u> . . . . .	92
5.2.4	<u>Step IV: Task and Environment</u> . . . . .	93
5.2.5	<u>Step V: Constraint Functions</u> . . . . .	93
5.2.6	<u>Step VI: Feasibility Map</u> . . . . .	94
5.2.7	<u>Step VII: Configuration Selection</u> . . . . .	95
5.2.8	<u>Step VIII: Graph Building</u> . . . . .	98
5.2.9	<u>Step IX: Cost Functions</u> . . . . .	99
5.2.10	<u>Step X: Dijkstra's Algorithm</u> . . . . .	102
5.3	Case Study I: A Planar RCDPR . . . . .	102
5.4	Case Study II: A Spatial RCDPR . . . . .	104
5.4.1	Problem Description . . . . .	105
5.4.2	Results for the Outer Faces of the Tubular Structure . . . . .	111
5.4.3	Results for the Inner Faces of the Tubular Structure . . . . .	117
5.4.4	Computational Time . . . . .	120
5.5	Conclusions . . . . .	120

<b>6</b>	<b>Conclusions and Perspectives</b>	<b>123</b>
6.1	General Conclusions . . . . .	123
6.1.1	Modelling . . . . .	123
6.1.2	Workspace Analysis . . . . .	124
6.1.3	Design of CDPRs and RCDPRs . . . . .	124
6.1.4	Reconfiguration Strategy for discrete RCDPRs . . . . .	125
6.2	Perspectives . . . . .	125
6.2.1	Modelling . . . . .	126
6.2.2	Workspace Analysis . . . . .	126
6.2.3	Reconfiguration of the Cable Connection Points on the Moving Platform . . . . .	126
6.2.4	Routing of the Cables . . . . .	126
6.2.5	Macro-micro RCDPRs and Control Laws . . . . .	127
	<b>Bibliography</b>	<b>129</b>
	<b>Appendix A Modelling Complements</b>	<b>139</b>
A.1	Angular Speeds and Accelerations . . . . .	139
A.2	Wrench Matrix Time Derivative . . . . .	140
A.3	Active Stiffness Matrix Detailed Computation for Sagging Cables . . . . .	141
	<b>Appendix B Routing Inspection Problem</b>	<b>143</b>
	<b>Appendix C Publications</b>	<b>145</b>
	<b>Index</b>	<b>147</b>

# List of Figures

1.1	Original Gough-Stewart platform . . . . .	1
1.2	FlexPicker from ABB . . . . .	2
1.3	SurgiScope at the Surgical Robotics Lab . . . . .	2
1.4	Architecture of a Cable-Driven Parallel Robot (CDPR) . . . . .	2
1.5	NIST RoboCrane painting an aeroplane . . . . .	4
1.6	Patent US6826452 . . . . .	4
1.7	CoGiRo prototye . . . . .	4
1.8	FALCON prototype . . . . .	4
1.9	IPAnema prototye . . . . .	5
1.10	SACSO . . . . .	5
1.11	Skycam . . . . .	5
1.12	CAREX . . . . .	5
1.13	MARIONET-CRANE . . . . .	6
1.14	FAST Project radio telescope . . . . .	6
1.15	Four-Cable Drawing Machine by David Bynoe . . . . .	8
1.16	Flyer of IRT JV CAROCA project . . . . .	10
1.17	Summary of the thesis organisation . . . . .	15
2.1	Schematic of a CDPR . . . . .	22
2.2	Schematic and parametrization of a pulley . . . . .	24
2.3	Scheme of the torque transmission . . . . .	28
2.4	Sagging model of a cable . . . . .	30
2.5	Algorithm for the computation of the geometrico-static model (sagging model) . . . . .	34
3.1	Mapping of $[\tau]_a$ into the wrench space as $[\mathbf{w}_e]_a$ . . . . .	46
3.2	Computation of the RWS $[\mathbf{w}]_r$ . . . . .	52
3.3	Case Study IDFW: Layout of the CDPR . . . . .	53

3.4	Case Study IDFW: IDFW representation . . . . .	53
3.5	Case Study IDFW: DFW representation . . . . .	53
3.6	Case Study IDFW: WFW representation . . . . .	54
3.7	Case Study IDFW: SFW representation . . . . .	54
4.1	Design strategy for CDPRs . . . . .	60
4.2	Minimum Degree of Constraint Satisfaction (MDoCS) . . . . .	62
4.3	CableBot design with cable exit points fixed to a grid . . . . .	67
4.4	CableBot design with cable exit points sliding on rails . . . . .	67
4.5	Schematic of a RCDPR . . . . .	69
4.6	Design strategy for RCDPRs . . . . .	70
4.7	Case Study CDPR Design: Description of the case study and the prescribed workspace . . . . .	74
4.8	Case Study CDPR Design: Moving Platform of the CDPR . . . . .	75
4.9	Case Study CDPR Design: Intersection of the WFW and the TFW for the optimal solution . . . . .	77
4.10	Case Study CDPR Design: TFW of the optimal solution . . . . .	77
4.11	Case Study CDPR Design: Correlation analysis . . . . .	78
4.12	Case Study CDPR Design: Larger WFW . . . . .	78
4.13	Case Study RCDPR Design: Description of the case study . . . . .	79
4.14	Case Study RCDPR Design: Design variables parametrising configuration $\mathcal{C}_1$ . . . . .	81
4.15	Case Study RCDPR Design: Design variables parametrising configuration $\mathcal{C}_2$ . . . . .	83
4.16	Case Study RCDPR Design: Optimal Reconfigurable Cable-Driven Parallel Robot . . . . .	86
4.17	Case Study RCDPR Design: MDoCS . . . . .	87
5.1	Example of reconfiguration procedure . . . . .	91
5.2	Scheme of the optimal reconfiguration planning method . . . . .	92
5.3	Parametrisation of the exit points on a parallelepiped layout . . . . .	92
5.4	Computation an optimal path . . . . .	93
5.5	A feasibility map . . . . .	95
5.6	Example of a feasibility map . . . . .	96
5.7	Flowchart of the graph building algorithm . . . . .	100
5.8	Graph associated to the feasibility map shown in Fig. 5.5 . . . . .	101
5.9	Case Study Planar Reconfiguration: Exit point parametrisation . . . . .	103
5.10	Case Study Planar Reconfiguration: Optimal solution (feasibility map) by minimising $\mu_1$ . . . . .	104
5.11	Case Study Planar Reconfiguration: Optimal solution (RCDPR configurations) by minimising $\mu_1$ . . . . .	104
5.12	Case Study Planar Reconfiguration: Optimal solution (feasibility map) by minimising $\mu_3$ . . . . .	105

5.13	Case Study Planar Reconfiguration: Graph of the two optimisation problems . . . . .	106
5.14	Case Study Spatial Reconfiguration: Graph of the two optimisation problems . . . . .	107
5.15	Case Study Spatial Reconfiguration: Moving platform . . . . .	107
5.16	Case Study Spatial Reconfiguration: Parametrisation of the RCDPR (outer faces) . . . . .	108
5.17	Case Study Spatial Reconfiguration: Parametrisation of the RCDPR (inner faces) . . . . .	109
5.18	Case Study Spatial Reconfiguration: Prescribed path and via points . . . . .	110
5.19	Case Study Spatial Reconfiguration: Eulerian path $\mathcal{P}_{out}$ (outer faces) . . . . .	110
5.20	Case Study Spatial Reconfiguration: Partial representation of the reconfiguration graph . . . . .	112
5.21	Case Study Spatial Reconfiguration: Feasibility map and optimal solutions . . . . .	113
5.22	Case Study Spatial Reconfiguration: Configurations $\mathcal{C}_1^*$ , $\mathcal{C}_5^*$ and $\mathcal{C}_8^*$ for the optimal reconfiguration with respect to $\mu_3$ . . . . .	115
5.23	Case Study Spatial Reconfiguration: Configurations $\mathcal{C}_4^*$ , $\mathcal{C}_5^*$ and $\mathcal{C}_{10}^*$ for the optimal reconfiguration with respect to $\mu_5$ . . . . .	116
5.24	Case Study Spatial Reconfiguration: Parallel graph of the dominant configuration quadruplets . . . . .	117
5.25	Case Study Spatial Reconfiguration: Filtered parallel graph . . . . .	118
5.26	Case Study Spatial Reconfiguration: RCDPR configuration optimising $\mu_2$ and $\mu_3$ for $\mathcal{P}_{in}$ . . . . .	119
5.27	Case Study Spatial Reconfiguration: RCDPR configuration optimising $\mu_4$ and $\mu_5$ for $\mathcal{P}_{in}$ . . . . .	119
6.1	Example of cable routing for a RCDPR . . . . .	127
A.1	RPY angle representation . . . . .	140
B.1	Computation of an optimal path covering the whole set of prescribed segments . . . . .	144



# List of Tables

1.1	ADVANTAGES AND DRAWBACKS OF CABLE-DRIVEN PARALLEL ROBOTS (CDPRs) . . . . .	3
3.1	CASE STUDY IDFW: COMPARISON OF WORKSPACES . . . . .	54
4.1	CDPR RECONFIGURABLE PARAMETER CLASSIFICATION . . . . .	68
4.2	CASE STUDY CDPR DESIGN: DESIGN VARIABLE BOUNDS . . . . .	75
4.3	CASE STUDY RCDPR DESIGN: DESIGN VARIABLES . . . . .	84
4.4	CASE STUDY RCDPR DESIGN: DESIGN VARIABLES OF THE SELECTED OPTIMUM RCDPR . . . . .	85
5.1	CASE STUDY PLANAR RECONFIGURATION: POSSIBLE CONFIGURATIONS . . . . .	103
5.2	CASE STUDY SPATIAL RECONFIGURATION: OPTIMAL CONFIGURATIONS . . . . .	112
5.3	CASE STUDY SPATIAL RECONFIGURATION: OPTIMAL RECONFIGURATION PLANNING FOR THE OUTER FACES . . . . .	114
5.4	CASE STUDY SPATIAL RECONFIGURATION: OPTIMAL RECONFIGURATION PLANNING FOR THE INNER FACES . . . . .	118
5.5	CASE STUDY SPATIAL RECONFIGURATION: ANALYSIS OF THE COMPUTATIONAL TIME . . . . .	120



# Acronyms and Abbreviations

<b>ACTS</b>	Available Cable Tension Set
<b>ACVS</b>	Available Cable Velocity Set
<b>ATS</b>	Available Twist Set
<b>AWS</b>	Available Wrench Set
<b>CDPR</b>	Cable-Driven Parallel Robot
<b>CFW</b>	Collision Free Workspace
<b>CoM</b>	Centre of Mass
<b>DFW</b>	Dynamic Feasible Workspace
<b>DoF</b>	Degrees of Freedom
<b>DKM</b>	Direct Kinematic Model
<b>DSOKM</b>	Direct Second Order Kinematic Model
<b>IDFW</b>	Improved Dynamic Feasible Workspace
<b>IDM</b>	Inverse Dynamic Model
<b>IFW</b>	Interference Free Workspace
<b>IGM</b>	Inverse Geometric Model
<b>IKM</b>	Inverse Kinematic Model
<b>ISOKM</b>	Inverse Second Order Kinematic Model
<b>ISM</b>	Inverse Static Model
<b>MDoCS</b>	Minimum Degree of Constraint Satisfaction
<b>MDoDCS</b>	Minimum Degree of Dynamic Constraint Satisfaction
<b>RAS</b>	Required Acceleration Set
<b>RCDPR</b>	Reconfigurable Cable-Driven Parallel Robot
<b>RDWS</b>	Required Dynamic Wrench Set
<b>REWS</b>	Required External Wrench Set
<b>RPY</b>	Roll Pitch Yaw
<b>RTS</b>	Required Twist Set
<b>RWS</b>	Required Wrench Set
<b>SFW</b>	Static Feasible Workspace
<b>TFW</b>	Twist Feasible Workspace
<b>WCW</b>	Wrench Closure Workspace
<b>WFW</b>	Wrench Feasible Workspace



# Chapter 1

# Introduction

### Chapter Content

- 1.1 Cable-Driven Parallel Robots (CDPRs) . . . . . 2
- 1.2 Theoretical Background . . . . . 9
- 1.3 Contributions and Thesis Organisation . . . . . 15

Parallel robots made their first appearance in 1954, with the original Gough-Stewart platform [Ste65] shown in Fig. 1.1. Parallel robots are closed-loop mechanisms, mainly composed of a platform, connected to a fixed base by several kinematic chains, hereafter defined as legs [Mer06].

These robots proved to be appealing from a scientific and a technical point of view, thanks to their low inertia and their high stiffness, precision, repeatability and payload capabilities.

Parallel robots are used in several industrial contexts for manufacturing [CW03, WS02] and pick and place operations [PRF90]. The Delta robot [CE90], shown in Fig. 1.2, is an example of industrial parallel robot widely used in the food and electronic industries for fast pick-and-place operations. Parallel robots are also efficient in other domains, being used as flight simulators [Cap67, KJ75] and medical devices [Mer01, BBGA07], as illustrated in Fig. 1.3.

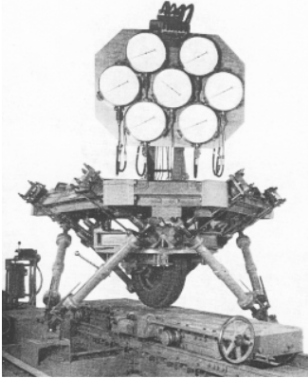


Fig. 1.1 – Original Gough-Stewart platform [Ste65]



**Fig. 1.2** – FlexPicker, a Delta parallel robot from ABB company [[ABB](#)]



**Fig. 1.3** – SurgiScope at the Surgical Robotics Lab, Humboldt-University [[Int](#)]

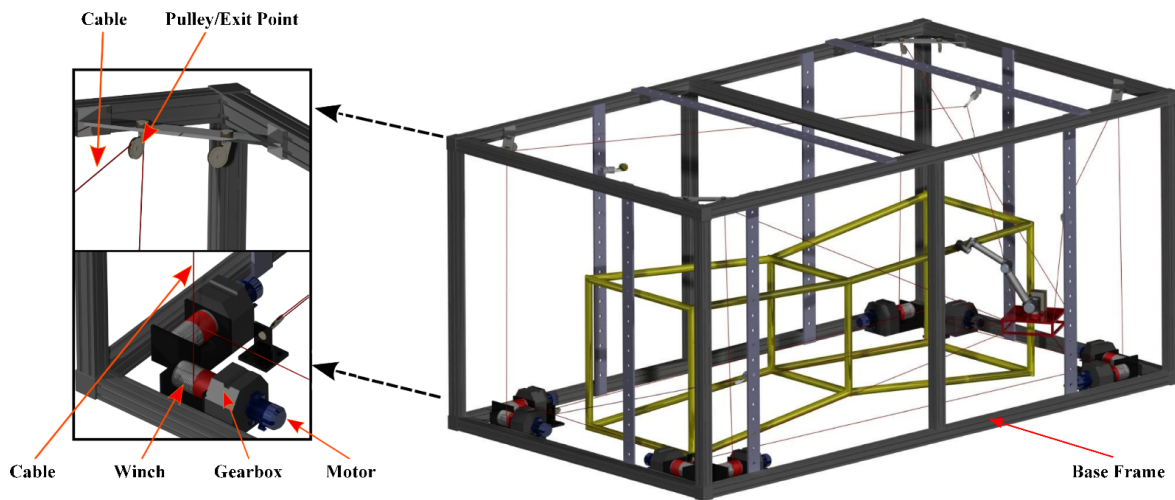


**Fig. 1.4** – Architecture of a Cable-Driven Parallel Robot (CDPR), developed in the framework of the IRT Jules Verne CAROCA project

## 1.1 Cable-Driven Parallel Robots (CDPRs)

Legs of parallel robots are traditionally composed of rigid links. Those rigid links contribute to the high stiffness characterising these robots, which are mainly provided by the parallel architecture of the robots. However, rigid links limit the dimensions of the workspace of parallel robots. This limitation does not concern *Cable-Driven Parallel Robots* (CDPRs), a particular class of parallel robots whose moving platform is connected to a fixed base frame by cables. Hereafter, the connection points between the cables and the base frame will be referred to as *exit points*. The cables are coiled on motorised winches. Passive pulleys may guide the cables from the winches to the exit points. A central control system coordinates the motors actuating the winches. Thereby, the pose and the motion of the moving platform are controlled by modifying the cable lengths. An example of CDPR, developed at IRT Jules Verne in the framework of the CAROCA project, is shown in Fig. 1.4.

**Tab. 1.1 – ADVANTAGES AND DRAWBACKS OF CABLE-DRIVEN PARALLEL ROBOTS (CDPRs)**

<i>Advantages</i>	<i>Drawbacks</i>
<ul style="list-style-type: none"> <li>• Large workspace</li> <li>• High payload-to-weight ratio</li> <li>• Low inertia of the mobile parts</li> <li>• Low cost</li> <li>• Low maintenance effort</li> <li>• Deployability and transportability</li> <li>• Possible reconfigurability</li> </ul>	<ul style="list-style-type: none"> <li>• Mono-directional cable transmission of forces to the platform</li> <li>• Cable interferences</li> <li>• Collisions between the cables and the environment</li> <li>• Cable deformations</li> </ul>

### 1.1.1 Advantages and Applications

CDPRs have several advantages. Thanks to their non-rigid nature, large cable lengths can be coiled on winches. Consequently, CDPRs have potentially very large workspaces with respect to rigid-link parallel robots [Gos13]. From a structural point of view, cable properties provide CDPRs with a high payload capability while the low mass of the cables assures a high payload-to-weight ratio. The low inertia of the mobile parts reduces the energy consumption of CDPRs and improves their dynamic performances with respect to rigid-link robots. Moreover, CDPRs can be manufactured using mostly standard industrial elements, limiting the manufacturing and the maintenance costs. Finally, CDPRs can be eventually designed in such a way to be easily assembled, disassembled and reconfigured. Table 1.1 summarises the advantages and drawbacks of CDPRs.

#### Industrial Applications

Taking advantage of the previous properties, CDPRs have already been used in some industrial applications. Indeed, at the beginning of the 90s, Albus *et al.* developed the NIST RoboCrane [ABD92, ABJ03, BADJ94], taking inspiration from the architecture of a Gough-Stewart platform. The NIST RoboCrane is able to perform several tasks, like displacement of heavy payloads and painting of military aeroplanes (Fig. 1.5).

CDPRs are used as well to handle heavy payloads in large areas. In 2001, Holland and Cannon filed the patent *US6826452 B1* [HC04, GJC01]. They proposed a robotic system composed of four cranes to be used as a CDPR for cargo transportation (Fig. 1.6). Later on, Hassan and Khajepour investigated the performances of large CDPRs for warehouse applications [HK09] while other research studies focused on large-scale assembly operations [WXB08, PMV10]. Recent studies have been performed in the framework of the CoGiRo (Control of Giant Robot) ANR Project [Pro]. The goal of this project is the definition of novel design and control strategies for CDPRs of large size and carrying heavy payloads. Some contributions of this project are: The integration in the control system of feedbacks from external sensors, such as camera [LGCH13]; The development of a simplified cable model [GCRB12]; The investigation of an efficient cable layout [GCRB15]. The CoGiRo CDPR prototype, represented in Fig. 1.7, is 15 m long, 11 m wide and 6 m high. It is able to carry payloads up to 500 kg. The ratio between the CDPR workspace and the CDPR volume is higher than 0.75.

Besides, CDPRs are good candidates for pick-and-place operations, thanks to their dynamic motion capabilities (low mass and inertia of moving parts). The FALCON (*Fast Load Conveyance*) CDPR has been developed in Japan at the end of the 90s [KCTP95, KKW00] (Fig. 1.8). This CDPR is able to reach linear speeds of 13 m/s and



**Fig. 1.5** – NIST RoboCrane painting an aeroplane [[ABD92](#), [ABJ03](#)]

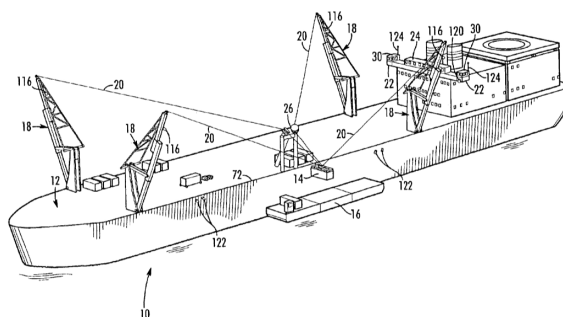


**Fig. 1.6** – Concept of a four-crane CDPR (Patent US6826452 [[HC04](#), [GJC01](#)])



**Fig. 1.7** – CoGiRo prototype, designed by the LIRMM and Tecnia [[Pro](#)]



**Fig. 1.8** – FALCON prototype [[KCTP95](#), [KKW00](#)]

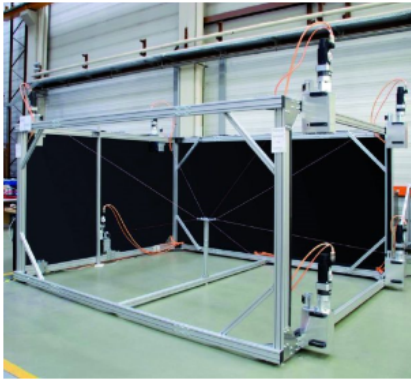


**Fig. 1.9** – IPAnema prototype, designed by the Fraunhofer IPA [PMK+13]

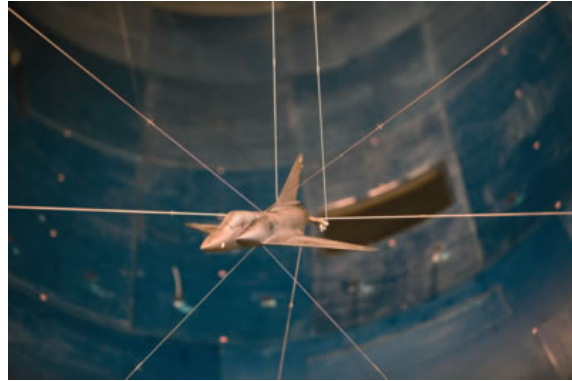


**Fig. 1.10** – SACSO, a CDPR for wind tunnel tests, designed by ONERA [LLR02, Laf04]



**Fig. 1.11** – Skycam, a CDPR for broadcasting of sport events [Sky]



**Fig. 1.12** – CAREX, a cable-driven arm exoskeleton [MA12]

linear accelerations of 43 G. Similar applications have been investigated by Maeda *et al.* for the assembly of light components [MTT+99]. In 2013, Pott *et al.* designed another family of CDPRs, the IPAnema series [PMK+13], for fast pick-and-place and other industrial operations (Fig. 1.9).

Finally, CDPRs have been used as well for aerodynamic tests in wind tunnel [ZLL10, SWB11]. Figure 1.10 shows SACSO, an application developed by ONERA for vertical wind tunnels [LLR02, Laf04].

### Other Applications

The first commercialised application of CDPRs is the broadcasting of sport events [TB05, NAD06, Cabb, Sky, Spy]. These CDPRs can be installed indoor and outdoor, for example in stadium, as shown in Fig. 1.11. They can cover large spaces, reach speeds up to 40 km/h and their cables do not obstruct the field of view of the audience.

Thanks to their low inertia, high stiffness and large workspace, CDPRs are widely spread in the domain of haptic interfaces [Wi198, GRR01, ZRS+09, FCCG14]. Haptic interfaces can be used in several fields, including virtual reality [HS92, IS94, DPL07, HkMP15], teleoperation [MI93] and as locomotion interfaces [PG07, OMDT+08]. One of the first application, WireMan, has been designed by Bonivento *et al.* in order to simulate the touch-rendering of bas-relief virtual surfaces [BEM+97].



**Fig. 1.13** – MARIONET-CRANE during a search and rescue simulation [Mer08, MD10]



**Fig. 1.14** – Design of FAST project radio telescope [KZW06, Dua99, DQZZ09]

In the medical field, CDPRs have been widely proposed for rehabilitation of injured people and post-stroke patients. Most of the research works focused on upper limb rehabilitation [HA95, GR02, LCH04, RABG07, RGM07, ZRMR14], like Sophia-3 and the wearable exoskeleton CAREX shown in Fig. 1.12 [MA12]. An exception is represented by STRING-MAN, a CDPR for gait rehabilitation [SZB07].

In France, Merlet *et al.* created MARIONET, a family of CDPRs which includes MARIONET-ASSIST, MARIONET-CRANE and MARIONET-REHAB. This family of robots proposes several architectures and actuation systems, being designed to use both linear and rotational motors. MARIONET-REHAB, for example, is actuated by linear motors and can be used for rehabilitation purposes or for fast displacements of small payloads. MARIONET-ASSIST can be used to assist elderlies or people with motion disabilities. MARIONET-CRANE [Mer08, MD10] can be used in search and rescue operations, as illustrated in Fig. 1.13, being portable and deployable. Alternative solutions to the search and rescue problem have been proposed by several research teams [TVHT99, BWT05, TET<sup>+</sup>05]. Takemura *et al.* provided a particular design. In their innovative concept, the moving platform of the CDPR consists of an aero-static balloon. A camera or a thermal sensor are mounted on the balloon in order to locate the injured people from the sky.

The high payload capabilities of CDPRs suggested another innovative use case. The Chinese project FAST is currently developing a *Five hundred meter Aperture Spherical Telescope* [KZW06, Dua99, DQZZ09]. The telescope receiver will be controlled using a CDPR [YTWH10, YLZ13]. A rendering illustrating the model of the final structure appears in Fig. 1.14.

The investigation of CDPR capabilities leads to several other applications, including: Artistic painting [Hek], 3D scanning of artefacts [DLP<sup>+</sup>07], sport training [MKK97, MKK98], inspection of building façades [IGCS13], actuation of underwater vehicle-manipulator systems [EGGC15], aerostat positioning systems [LNC07] and entertainment [TSPE15].

### 1.1.2 Classification of CDPRs

According to the geometry of the CDPR, the moving platform is characterised by its number  $n$  of *Degrees of Freedom* (DoF). CDPRs can be classified in two families: *Fully constrained* and *under-constrained* CDPRs. This classification is based on the number of moving platform DoF that can be controlled by the CDPR actuators.

*Fully constrained* CDPRs assure the control of all the  $n$  DoF of the moving platform. The pose of the moving

platform is completely determined and can be described according to the geometric constraints of the CPDR, such as the lengths of its cables. In order to assure the control of the moving platform, at least  $n$  cables should be tensed. Fully constrained CDPRs usually consist of at least  $n + 1$  cables [RGL98]. Since cables cannot push the moving platform, redundant cables are used to guarantee the moving platform to be in a static equilibrium, assuming that external wrenches can be exerted on the moving platform along any direction.

If the external wrench applied on the moving platform is constant or the moving platform is connected to a passive constraining mechanism [BK05a],  $n$  cables may be sufficient to fully control the CDPR. Fully constrained CDPRs with  $n$  cables usually consist of a suspended architecture. In suspended CDPRs, all the cable exit points are located above the prescribed workspace of the moving platform [ABD92, SD00, GCRB15]. The static equilibrium of the moving platform is assured by the gravity force generated by the payload of the moving platform: The gravity force is equivalent to a virtual cable pulling the moving platform with a constant force along the gravity direction.

Suspended and non-suspended fully constrained CDPRs are characterised by different advantages and drawbacks. Since all the cables are located above the moving platform, fully constrained suspended CDPRs free the space below the moving platform. The payload of the moving platform is shared among all the cables. Consequently, suspended CDPRs usually offer higher payload capabilities and lower energy consumption. However, performances of suspended CDPRs are directly related to the payload of the moving platform. When the payload is low, the stiffness of the CDPR is reduced. Hence, the CDPR can be prone to low platform positioning accuracy, vibrations and instability.

According to the previous considerations, the minimum number of cables for a 2T1R planar CDPR to be fully constrained is 4, where T stands for translational DoF and R for rotational DoF. By definition, a *planar CDPR* is a CDPR whose moving platform motion is constrained on a plane, being the payload of the moving platform compensated along the orthogonal direction. An example of planar CDPR is described in Fig. 1.15. This CDPR consists of a drawing platform. It has been designed by David Bynoe for the Telus Spark Science Centre in Calgary [Fou] and it is composed of four cables supporting a metallic sphere used to trace lines on the sand.

The minimum number of cables for a 3R3T spatial CDPR to be fully constrained is equal to  $m = 6$ . Examples of spatial fully constrained CDPRs are: IPAnema [PMK<sup>+</sup>13], a fully constrained 3T3R CDPR with  $m = 8$  cables and  $n = 6$  DoF; CoGiRo [Pro], a suspended 3T3R CDPR with  $m = 8$  cables and  $n = 6$  DoF for logistic and warehouse applications; Skycam [Sky], a suspended 3T CDPR with  $m = 4$  cables and  $n = 3$  DoF; FALCON [KCTP95], a fully constrained 3T3R CDPR with  $m = 7$  cables and  $n = 6$  DoF for fast pick and place operations of lightweight products; RoboCrane [BADJ94] and FAST [YTW10], two suspended CDPRs composed of  $m = 6$  cables and  $n = 6$  DoF.

In *under-constrained* CDPRs, at least one DoF of the moving platform is not controlled by the actuators [CM13, AC15, BMC16]. In general, the number of cables,  $m$ , is usually smaller than the number of moving platform DoF,  $n$ , allowing the CDPR to control at most  $m$  of the  $n$  DoF of the CDPR. The computation of the moving platform pose of under-constrained CDPRs requires the simultaneous analysis of both the kinematic constraints and the static equilibrium of the CDPR. It has to be noticed that the same CDPR may behave as a fully constrained or a under-constrained CDPR according to the pose of the moving platform and the external wrench acting on it. In particular, CDPRs with at least  $n$  cables may behave as under-constrained CDPRs, if one or more cables become slack, and the number of tensed cables is lower than  $n$ .

Comparing fully constrained CDPRs with  $m \geq n$  cables and under-constrained CDPRs with  $m < n$  cables, several advantages and drawbacks can be mentioned. Fully constrained CDPRs with  $m \geq n$  cables provide often



**Fig. 1.15** – Four-Cable Drawing Machine by David Bynoe [Fou]

the possibility to lower cable tensions by redistributing the moving platform payload on a larger number of cables. Furthermore, a high number of cables increases the dexterity of the CDPR and improves the controllability of its internal wrenches: thus, the CDPR is able to balance a wider range of external wrenches acting on the moving platform and to adjust its stiffness. On the one hand, the presence of additional cables improves the reliability of the system. If a cable breaks down, the remaining cables can ensure the stability, and eventually the controllability, of the moving platform. On the other hand, under-constrained CDPRs with  $m < n$  cables are cheaper and are intrinsically less prone to cable interferences and collisions. They can be used in applications where a limited number of DoF should be controlled, like in rehabilitation applications [SZB07, RGM07], measuring [GMP11], and search and rescue operations [TVHT99, MD10].

### 1.1.3 Reconfigurable Cable-Driven Parallel Robots (RCDPRs)

In most applications described in Sec. 1.1.1, the CDPR has a fixed configuration which is determined during its design. In the sequel, a CDPR *configuration* refers to the positions of the cable exit points, the positions of the connection points between the cables and the moving platform, and the cable layout between these two sets of points. Hereafter, the connection points between the cables and the base frame will be referred to as exit points. While fixed-configuration CDPRs are relevant in many cases, some more demanding applications require reconfiguration capabilities. One notable case is a cluttered environment where cable collisions with objects in the CDPR workspace cannot be completely avoided so that reconfigurations are necessary. Reconfigurable Cable-Driven Parallel Robots (RCDPRs) are a class of CDPRs whose geometric parameters, such as the locations of the exit points and the cable connection points on the moving platform, can be modified.

By changing the robot configuration, its workspace may be enlarged and collisions between the cables and the environment can be avoided. At the same time, some robot performances may be improved such higher RCDPR stiffness and payload capability and lower cable tensions and energy consumption.

### 1.1.4 IRT Jules Verne CAROCA Project

Nowadays, several industrial sectors are facing with the necessity to manufacture novel products having large dimensions and complex shapes. In order to improve such manufacturing processes, the *IRT Jules Verne* (IRT JV)

promoted the investigation of new technologies for metallic, composite and hybrid structures in the domain of the advanced manufacturing. The investigation is dedicated to several engineering fields including naval, automotive, aeronautics and renewable energy engineering and it is organised into three main axes: (i) product/process integrated design, (ii) innovative process, (iii) flexible and intelligent systems.

CAROCA project<sup>1</sup> deals with the third research axis. It aims at investigating the performance of CDPRs and RCDPRs for manufacturing large products in cluttered industrial environments. The CDPR should be able to improve the productivity and the flexibility of the industrial processes, while releasing operators from repetitive and sometimes dangerous tasks. Some of the investigated applications are the following:

- The assembly and displacement of heavy and/or large parts.
- The inspection and measurement of large parts.
- The sandblasting and painting of large tubular structures.

In order to investigate these applications, the CAROCA project requires: (i) the consolidation of the existing CDPR design tools, in order to improve the efficiency of the design processes; (ii) the definition of a new design and reconfiguration procedure for RCDPRs. Accordingly, the following research axes have been considered in the framework of CAROCA project.

- The improvement of a stiffness model for large CDPRs. This model is required in order to model the displacements of the moving platform of CDPRs subjected to variations in the external wrenches.
- The development of a tool to analyse the workspaces of CDPRs with respect to their static equilibrium, dynamic equilibrium and kinematic constraints.
- The formulation of a design problem and a design strategy for CDPRs. The design problem should be used to determine the positions of the cable exit points and the characteristics of the motors, the winches and the gearboxes of the CDPRs.
- The formulation of a design problem and a design strategy for RCDPRs.
- The definition of a reconfiguration strategy for RCDPRs.

Three industrial partners are involved in the CAROCA project, namely, STX, DCNS and AIRBUS companies. Moreover, the two following joint research units take part in the CAROCA project: (i) The Institut de Recherche en Communications et Cybernetique de Nantes (IRCCyN, UMR CNRS 6597) and the Laboratoire d'Informatique, de Robotique et de Microelectronique de Montpellier (LIRMM, UMR CNRS 5506). A flyer of the CAROCA project is shown in Fig. 1.16.

## 1.2 Theoretical Background

Much of the research studies conducted on CDPRs have been developed in the last two decades. Several advances in modelling, design and control of CDPRs have been obtained. However, some fundamental open problems have not been solved yet. The following sections describe briefly some recent advances in CDPRs and some unsolved open problems.

---

<sup>1</sup>Evaluation des Capacités de la RObotique à Câbles dans un contexte industriel

# CAROCA

▶ ADAPTIVE AND SMART MANUFACTURING SYSTEMS  
▶ ROBOTIC TECHNOLOGIES FOR INDUSTRIAL PROCESSES

*A project to assess the capabilities of cable robotics in an industrial context*

**IRT  
JULES  
VERNE**

Using methods like modelling, identification, simulation and prototyping, the Caroca project (CAROCA for Evaluation des CAPacités de la RObotique à Câbles dans un contexte industriel) aims at identifying the industrial operations that can be handled by cable-driven parallel robots. This involves assessing the capabilities of cable-driven parallel robots to carry out different industrial operations, such as painting, shot blasting, part assembly, measurements and inspection of oversized parts.

### Technical and economic impacts

- ▶ Easy access to large structures
- ▶ Improved safety
- ▶ Optimized robot multi-tasking through reconfigurations

### Keywords

Robotics // Cables  
Reconfigurability  
Large Volumes

January 2014: Project launch  
 December 2014: Modelling and simulation  
 January 2015: Installation of a 1:50 scale demonstrator  
 June 2015: Robot reconfigurations tool  
 January 2016: Installation of a 1:5 scale demonstrator  
 June 2016: Experimental validations  
 January 2017: End of project

### INDUSTRIAL CONTEXT

The processes considered thus far require moving operators or effectors over large distances in cluttered environments. The constraints for these heterogeneous processes are quite different in terms of robot accuracy, external wrenches and mass in motion. Therefore, there is a need, to develop robotic solutions to make these operations safer, less arduous and more efficient.

TRL 1
TRL 2
TRL 3
TRL 4
TRL 5
TRL 6
TRL 7
TRL 8
TRL 9

### INNOVATIVE FEATURES

- ▶ Development of cable robots for shot-blasting and painting operations on offshore wind turbine jackets
- ▶ Development of a robotic system for moving and assembling heavy oversized parts
- ▶ Ideas: cable robots carrying another active system; reconfigurable cable robots
- ▶ Fast and accurate robotic systems covering a large workspace
- ▶ Robot reconfigurability for work/operations in congested areas

### Partners

- ▶ IRT JULES VERNE
- ▶ AIRBUS
- ▶ DCNS
- ▶ STX FRANCE
- ▶ IRCCYN (UMR CNRS, ECN, EMN, UNIVERSITE NANTES)
- ▶ LIRMM (UMR CNRS, UNIV MONTPELLIER)

### INDUSTRIAL APPLICATIONS

Optimizing the reconfiguration should make it possible to move the tools around oversized parts in order to perform a wide range of operations. This could be of interest to a number of industries.

### Equipment

- ▶ Two cable-driven parallel robots: the first 1 is one meter high, the second one is 5 meters high

### Budget

- ▶ 605 k€

Sales contact  
Philippe Piard  
philippe.piard@irt-jules-verne.fr

Press contact  
Sophie Péan  
communication@irt-jules-verne.fr

Fig. 1.16 – Flyer of IRT JV CAROCA project

### 1.2.1 Direct Geometrico-Static Problem

The direct geometrico-static problem aims at determining the poses of a CDPR moving platform and the cable tensions required to assure its static equilibrium, supposing that the lengths of the cables are known. A CDPR being a particular type of parallel robot, the solving of the direct geometrico-static problem is a challenging issue. However, in the case of CDPRs, the complexity of this problem is higher, due to the unilateral nature of the kinematic constraints: Cables can only pull on the moving platform and not push on it. The complexity of the problem has been highlighted by Carricato *et al.* for suspended CDPRs with less than six cables [CM13]. In particular, it has been proved that the direct geometrico-static problem is equivalent to finding the roots of a univariate polynomial of degree 156, for a 3-cable CDPR [Car13], and of degree 216, for a 4-cable CDPR [CA13]. In 2015, the analysis was extended to a generic under-constrained CDPR with  $n$  cables [AC15].

One of the most efficient methods for the computation of the moving platform pose has been presented by Berti *et al.* in [BMC13, BMC15, BMC16]. Their method is based on an interval-analysis algorithm, which can be applied to both fully constrained and under-constrained CDPRs. The algorithm provides the complete solution of the direct geometrico-static problem, describing all the possible poses of the moving platform that can be generated by a given set of cable lengths. Interval analysis has been used as well to investigate the kinematics of CDPRs with sagging cables [Mer15a]. At the cost of a high computational effort, the algorithm can find all the solutions to the direct geometrico-static problem.

Another relevant contribution to the resolution of the direct geometrico-static problem has been provided by Collard and Cardou [CC13]. They propose a novel method to compute the lowest equilibrium pose of a suspended CDPR. By definition, the lowest equilibrium pose is the moving platform pose where the Centre of Mass (CoM) of the moving platform is the closest to the ground. The design problem is formulated as an optimisation problem aiming at minimising the potential energy of the CDPR moving platform. The algorithm efficiency is proportional to the number of cables of the suspended CDPR.

### 1.2.2 Cable and Stiffness Modelling

In CDPRs, motion is transmitted to the moving platform by means of cables. The use of non-rigid links affects the positioning accuracy of the moving platform, as well as its static and dynamic equilibrium. The accuracy of the moving platform positioning may be related as well to other technical aspects, like measurement uncertainties or manufacturing assembly imprecisions. Nevertheless, cable deformations are one of the principal sources of inaccuracy. Cable deformations are due to gravity and to the force applied by the moving platform on the cables. Indeed, under the action of gravity, the self-weight of a cable leads to sagging, especially for large diameter cables which have a non-negligible mass linear density (mass per unit of length). The force applied to the cable end produces as well a longitudinal elongation of the cable according to its axial stiffness.

According to the previous considerations, the moving platform stiffness and the moving platform positioning accuracy of a CDPR are strictly related to the cable properties. Cables can be modelled as linear segments when their mass is negligible and the axial stiffness is sufficient to describe their deformation [VHT98, KKW00, BK05b, SRK13].

When the cables are heavy and the CDPR covers a wide workspace, the cables may sag under their own weights [KZW06, RGBP10b, Ars13]. Cable sagging has been described by Irvine in [Irv92] by means of the elastic catenary model which takes into account both the axial stiffness of the cable and the deformations due to its weight. Comparisons between the two models show that the sagging model is usually more accurate than the

linear one. A simplified model of a sagging cable has been proposed by Gouttefarde *et al.* [GCRB12, NG13]. As proved experimentally, for a given range of cable properties, the proposed cable and stiffness models provide a good moving platform positioning accuracy and the possibility to solve these models in real-time applications.

Stiffness influences as well the dynamic behaviour of CDPRs. The presence of wind, or fast movements of the moving platform, can generate vibrations. Once again, cables have a higher influence over the compliance of the robot than the other components. In order to analyse the dynamic behaviour of the cables, they have been modelled as linear massless springs, as taut massless strings [DM09, MD05] and as sagging cables [YCD15]. The CDPR dynamic stiffness has been investigated by means of the dynamic stiffness matrix [KZW06, YCD15] or by means of the finite element method [DDB13].

### 1.2.3 Workspace Analysis

The non-rigid nature of the cables affects the equilibrium of the moving platform. Cables are not able to push the moving platform, behaving as unilateral actuators. Hence, the static equilibrium, the dynamic equilibrium and the kinematic constraints of the moving platform should be investigated carefully, being influenced by several factors, including: The configuration of the cables, the pose of the moving platform and the characteristics of the CDPR components, i.e. the nominal and the pick power of the actuators and the winch diameters.

The equilibrium of the moving platform is investigated analysing the workspace of the CDPR. In serial and parallel robots, the workspace is usually defined as the set of end-effector poses at which a number of kinematic constraints are satisfied. In CDPRs, the workspace is usually defined as the set of poses where the CDPR satisfies one or more conditions including the static or the dynamic equilibrium of the moving platform, with the additional constraint of non-negative cable tensions. Several workspaces and equilibrium conditions have been studied in the literature.

The first investigations focused on the static equilibrium of the moving platform [GG04, GG06, SK04, SK06]. Most of the proposed approaches are based on the *Wrench Closure Workspace* (WCW). WCW has been widely used in grasping problems, in order to verify if the fingers of the gripper can assure a stable static equilibrium of the grasped object. It has to be noticed that the grasper can apply only pushing forces to the object [EUV04]. In the case of CDPRs, cables are only able to transmit non-negative pulling forces to the moving platform. A pose of the moving platform belongs to the WCW if and only if the static equilibrium of the moving platform is assured by non-negative cables tensions, whichever is the external wrench on the platform. Therefore, cable tensions do not present any upper bound, which is the main limitation of the WCW analysis.

The feasible static equilibria of the moving platform can be analysed using the *Wrench Feasible Workspace* too (WFW) [BREU06, BGM08, GK10, GDM11]. By definition, the WFW is the set of wrench feasible moving platform poses. A pose is *wrench feasible* when the cables can balance a set of external moving platform wrenches while the cable tensions stay in between given cable tension upper and lower bounds. The *Static Feasible Workspace* (SFW) represents a special case of the WFW, where no external wrench is applied on the moving platform. The static equilibrium is achieved compensating only the weight of the moving platform [PFAM04]. The lower cable tension bound,  $\tau_{min}$ , is defined in order to prevent the cables to become slack. The upper cable tension bound,  $\tau_{max}$ , is defined in order to prevent the CDPR to be damaged.

The dynamic equilibrium of the moving platform can be investigated using the *Dynamic Feasible Workspace* (DFW). By definition, the DFW is the set of dynamic feasible moving platform poses. A pose is *dynamic feasible* if a prescribed set of moving platform accelerations is feasible, with cable tensions lying in between given lower

and upper bounds. The concept of dynamic workspace has already been investigated in [BG05] for planar CDPRs. Barrette *et al.* solved the dynamic equations of a planar CDPR analytically, providing the possibility to compute the boundary of the DFW. This strategy cannot be directly applied to spatial CDPRs due to the complexity of their dynamic model. In 2014, Kozlov studied in [Koz14] the possibility to investigate the DFW by using a tool developed by Guay *et al.* for the analysis of the WFW [GCCC14]. However, the dynamic model proposed by Kozlov is incomplete: It does not take into account the dynamics of the cables, the dynamics of the winches and the external wrenches acting on the moving platform. Furthermore, it considers the moving platform as a point mass, neglecting centrifugal and Coriolis forces.

#### 1.2.4 Tension Distribution and Control

The set of cable tensions which assures the static or the dynamic equilibrium of a CDPR is strictly dependent on the pose of the moving platform and the external wrenches acting on the moving platform. When cable tensions are not distributed homogeneously, some cable tensions may approach the upper and the lower cable tension limits: In the first case, cables can be damaged. In the second case, cables may become slack. Slack cables decrease the stiffness of the moving platform and may lead to the loss of the CDPR control. In order to avoid this problem, it may be necessary to control the tension of each cable using a tension distribution algorithm. Tension distribution algorithms optimise the cable tensions according to a given criterion while taking into account the tension limits of the cables. A minimum cable tension prevent the cables to become slack while a maximum cable tension prevent the CDPR to be damaged. Under the assumption of rigid cables, tension distribution can be applied to fully constrained CDPRs, whose static equilibrium consists of an under-determined system of equations, by modifying their internal wrenches. The internal wrenches are defined as the set of cable wrenches whose linear combination does not modify the pose of the CDPR.

Cable tension distribution can be computed using several algorithms. Each algorithm has its own advantages and drawbacks. Some of the developed methods are based on linear programming [BJS<sup>+</sup>09] and quadratic programming [TB11]. Linear programming requires a low computational time but may lead to discontinuities. Discontinuities can be avoided using quadratic programming, which assures the cable tension minimisation. Alternative methods are based on the analysis of the vertices of the intersection between the space of the available cable tension set and the affine space of the cable tensions which satisfy the static equilibrium of the moving platform [BMHS07, BMB<sup>+</sup>09b, LG13]. These methods provide continuous solutions and they are quite easy to implement. Recent developments lead to the formulation of the closed-form method [PBM09], the corner projection method [BMB<sup>+</sup>09b] and the puncture method [MRB15]. The last method is quite intuitive, easy to be implemented, and its solutions are closer to the ones produced by the quadratic programming.

The previous tension distribution algorithms have been tested on some fully constrained CDPRs [MBHS08, PBM09, GG11]. They are also integrated in some CDPR control schemes. Several control schemes have been provided in the literature. Their structure is inspired by the control schemes of serial and rigid-link parallel robots, including: PID control schemes [FFT<sup>+</sup>04, OA05], impedance control schemes [RMB15] and adaptive control schemes [SDJB08, LGCH13]. Some control schemes integrate exteroceptive sensors, such as cameras [DGAD12].

#### 1.2.5 Design

Few research works on CDPRs focus on the development of a CDPR design strategy, aiming at determining the optimal number of cables and cable arrangements as well as the optimal dimensions of the robot at hand.

Several CDPR designs rely on the intuition of their designers, such as in [KCTP95, Laf04, BG07]. One of the preliminary trajectory-based design approaches was proposed by Pusey *et al.* in 2004 [PFAM04]. The design problem is formulated as an optimisation problem aiming at improving the size of the CDPR workspace and other global conditioning indices. A generic numerical task-based approach has been proposed by Bruckmann *et al.* in [BMB<sup>+</sup>09a]. The design problem is formulated as a constrained optimisation problem, as well. The problem aims at maximising the workspace of the CDPR, while assuring the wrench feasibility of the moving platform through the corresponding workspace and along the prescribed trajectory. Several optimisation methods have been tested, including interval-based global optimisation techniques, simulated annealing, genetic algorithms and gradient based algorithms. Gouttefarde *et al.* focused on the use of an interval-based global optimisation techniques [GKC<sup>+</sup>08]. With respect to the method described in [BMB<sup>+</sup>09a], the approach proposed in [GKC<sup>+</sup>08] is based on the investigation of the WCW. In 2015, Blanchet developed a design strategy based on the interval analysis [Bla15], which takes into account the WFW. Recently, an analytical method has been proposed by Azizian and Cardou in order to synthesise planar CDPRs [AC12]. This method has been extended numerically to spatial CDPRs [AC13].

Specific design problems have been dedicated to the design of the actuators [ABAASV11] and the cables [RGBP10a]. In 2014, Khakpour *et al.* introduced the use of cables differentials in the architecture of planar CDPRs, analysing the advantages and the drawbacks of these components [KBT14]. The selection of the cable layout has been investigated briefly by Tadokoro *et al.* in [TMH<sup>+</sup>02]. A more efficient strategy, aiming at selecting the geometry of fully constrained suspended CDPRs, has been recently described in [GCRB15].

### 1.2.6 Reconfigurability

Manufacturing processes over large products may not be executed by a fixed-configuration CDPR, because of cable collisions. The most efficient way of avoiding cable collisions is to permit CDPR cable exit point reconfigurations. Exit point reconfigurations can be performed in a continuous or in a discrete manner. The first one consists in cable exit points mounted on mobile bases, e.g. a trolley on a rail [NGCP14] or a flying platform [FMKK11, JK13, MDRC13]. Such a RCDPR has a *continuous* set of possible configurations. On the contrary, the set of possible reconfigurations is *discrete* when the cable exit points can be positioned at a possibly large but finite number of locations, such as those of a grid of possible exit point positions. From a technical point of view, modifying a cable exit point amounts to move or change the last pulley which directs the cable toward the moving platform. Hereafter, the RCDPRs whose cable exit points can be installed on a grid are defined as *discrete reconfigurable cable-driven parallel robots*.

Preliminary studies on RCDPRs have already been performed by the NIST as a part of the *NIST RoboCrane* project [BJP<sup>+</sup>00]. Izard *et al.* [IGM<sup>+</sup>13] also studied a family of RCDPRs, named *ReelAx*, in order to investigate the potentialities of CDPRs in industrial contexts. However, no reconfiguration strategy has been proposed by the authors. More detailed studies have been performed by Rosati *et al.* [RZA11, ZRMR14], which focused on planar RCDPRs. They suggested to use movable exit points in order to maximise a local performance index across the RCDPR workspace. The corresponding continuous reconfiguration problem is solved by means of an analytical description of the desired optimal cable configuration, which can however hardly be extended to spatial RCDPRs.

In 2012, Zhou *et al.* [ZTK12] suggested to increase the number of DoFs of a CDPR by mounting the winches on mobile bases, which results in a type of RCDPRs. In [ZJK13, ZJK14], Zhou used an alternative concept for RCDPRs. A set of cables with constant lengths are connected to linear motors. The cables are either attached to the moving platform [ZJK14] or pull the moving platform by means of idler pulleys [ZJK13]. In both cases, a

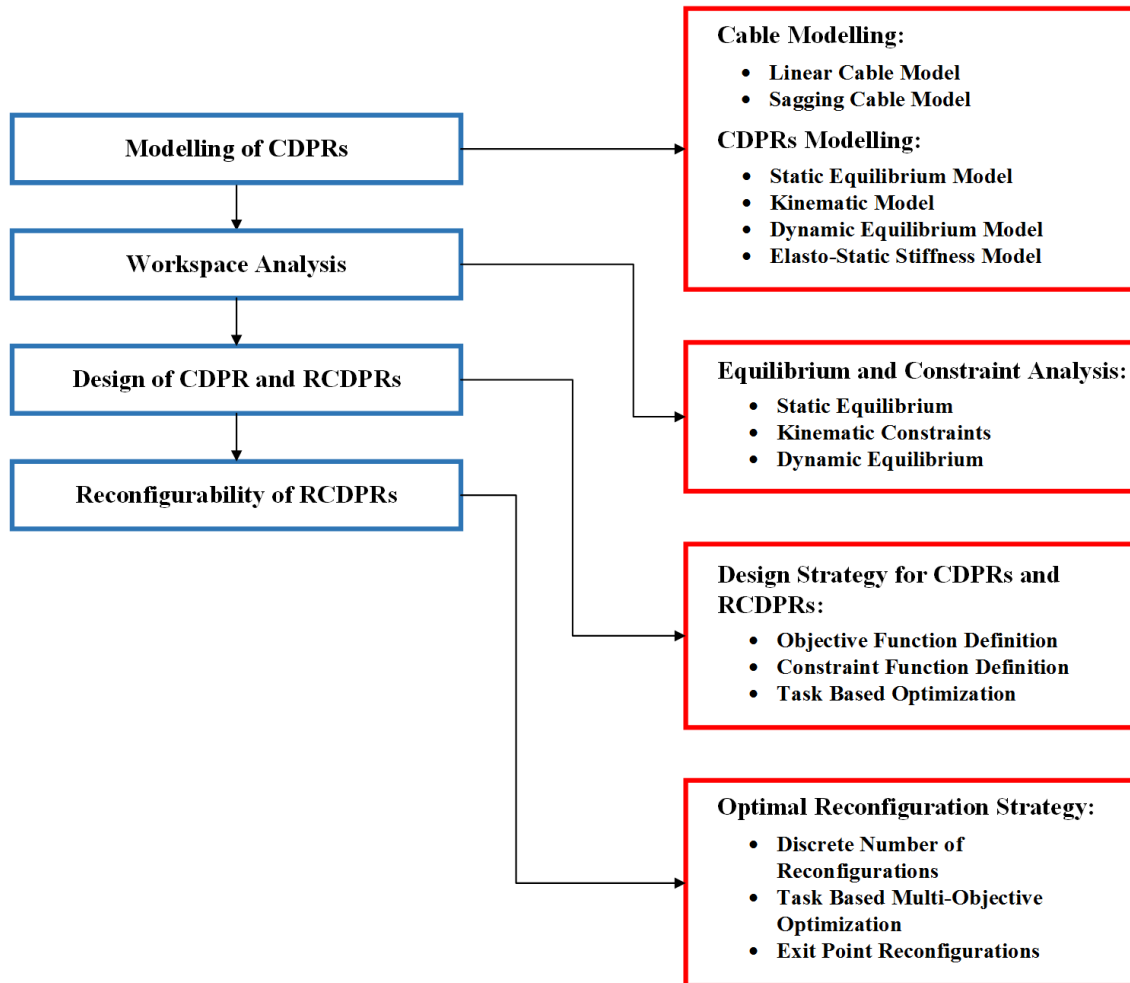


Fig. 1.17 – Summary of the thesis organisation

planar case study has been investigated to show the concept advantages, namely: An even distribution of the load among the cables, a decoupling between the cable lengths and the cable tensions and the elimination of the cable length errors. However, Zhou's solution has not been extended to a spatial case study.

Recently, Nguyen *et al.* [NGCP14,NG14b] proposed a reconfiguration strategy which consists in solving two sub-optimisation problems. The first problem aims at defining bounds on the reconfiguration parameter such that the CDPR reconfiguration is formulated as a box-constrained optimisation problem. The latter forms the second sub-optimisation problem which, for example, can be solved by means of gradient based optimisation algorithms.

### 1.3 Contributions and Thesis Organisation

The research work presented in this manuscript aims mainly at defining a reconfiguration strategy for RCDPRs whose exit points can be positioned on a discrete grid of possible locations. Several steps have to be accomplished before the definition of a reconfiguration strategy. These steps are listed hereafter and summarised in Fig. 1.17.

### 1.3.1 Elasto-Static Modelling

A set of models are required in order to analyse and design CDPRs and RCPDRs. Two cable models are used in our research work: (i) the massless model, where the cables are represented as elastic straight line segments; (ii) the sagging model, where the deformations induced by the mass of the cables are taken into account [Irv92]. The cable model is chosen according to the cable properties and the task to be executed. When the linear density of the cable is low, the straight line segment cable model is used to describe the geometric, elasto-static, kinematic and dynamic behaviour of the RCDPR. When heavy payloads have to be displaced, the sagging model is more appropriate to describe the geometric and the elasto-static behaviour of the RCDPR. Under these assumptions, the dynamic model of the RCDPR is neglected, the motion of the moving platform being considered quasi-static. The CDPR models based on the linear and the sagging cable models are well known in the literature. In this manuscript, the notation describing these models has been adapted for RCDPRs.

The analysis of the elasto-static behaviour of CDPRs and RCDPR is still an open problem. This thesis proposes a formal definition of the elasto-static model of a RCDPR with linear nono-rigid cables. The model has been derived for a generic spatial RCDPR. It has been computed developing the vectorial form of the equations describing the kinematics and the statics of the RCDPR. The calculated stiffness matrix corresponds to the model proposed in [BK05b]. However, the formalism and the assumption which lead to the computation of the elasto-static model are more rigorous than the one performed in [BK05b].

The inverse geometrico-static model of a RCDPR with sagging cables has been implemented as well, according to the strategy proposed in [KZW06, RGK<sup>+</sup>09, YCD15]. Being coupled, the inverse geometric problem and the static problem are solved at the same time. The inverse geometrico-static problem aims at defining the cable lengths of the RCDPR and the cable tensions with respect to the pose of the moving platform. The solution to the problem is computed numerically. Then, the elasto-static problem has been formulated. This model can be used in order to analyse the small pose variations of the moving platform, due to the non-rigid nature of the cables, and the dynamic response of the CDPR by means of modal analysis.

The stiffness matrix of the RCDPR is decomposed in two components: The passive stiffness matrix and the active stiffness matrix. The passive stiffness matrix takes into account the stiffness of the cable sagging model. The active stiffness matrix is strictly related to the cable tensions. It has been obtained developing the Jacobian of the cable wrenches with respect to the moving platform pose. Note that, in most of the models appearing in the literature, the active stiffness matrix is neglected, e.g. in [KZW06].

### 1.3.2 Twist and Dynamic Feasible Workspaces

The analysis of RCDPRs requires the development of several tools. Part of these tools is dedicated to the analysis of the moving platform static equilibrium, the dynamic equilibrium and the kinematic constraints. When mechanical brakes are not active, the maximum tension in the cables depends mostly on the characteristics of the actuators, such as their nominal or peak torque. The actuators influence also the twist (linear and angular velocities) that the CDPR moving platform can attain, assuming the nominal speed of the actuators proportional to the coiling/uncoiling speed of the cables.

In this manuscript, the concept of wrench feasibility has been extended to the moving platform kinematic analysis, introducing the so called *Twist Feasible Workspace* (TFW). The TFW is the set of twist feasible moving platform poses [GCG15a]. A pose is *twist feasible* when the actuators, according to their nominal speed, are able to move the platform within a given range of linear and rotational velocities. The TFW is computed using the

algorithm presented by Gouttefarde *et al.* in order to analyse the WFW [GK10]. The same algorithm is also used to compute an *Improved Dynamic Feasible Workspace* (IDFW) [GGC16a]. With respect to the definition proposed in [BG05], the IDFW considered in this manuscript takes into account: (i) the inertia of the moving platform; (ii) the external wrenches applied on the moving platform; (iii) the centrifugal and the Coriolis forces induced by a constant moving platform twist. The *Required Wrench Set* (RWS), defined here as the set of internal wrenches the cables should be able to transmit to the moving platform in order to guarantee its dynamic equilibrium, is calculated summing the three components of the dynamic equilibrium.

### 1.3.3 Design of CDPRs and RCDPRs

The models and the tools presented in Sec. 1.3.1 and Sec. 1.3.2 can be used in order to design a CDPR. In this manuscript, according to the methods proposed in the literature (e.g. in [BMB<sup>+</sup>09a]), the CDPR design has been formulated as an optimisation problem. The selected design strategy is task-based. The design problem is formulated taking into account the tasks the CDPR has to perform, i.e. following a prescribed path or covering a prescribed workspace defined for the CoM of the moving platform. Several design variables can be optimised, including the exit point locations, the positions of the connection points between the cables and the moving platform, the cables properties, the actuators and the winch properties. The optimisation is performed referring to one or more objective functions. For example, the actuators and the winches can be optimised maximising the size of WFW, the TWF and the DFW. The position of the exit points can be optimised as well, e.g., aiming at minimising the size of the CDPR [GCG<sup>+</sup>14]. A set of constraints has to be satisfied during the task execution. As typical examples, this manuscript considers cable collision, wrench-feasibility and the moving platform displacement due to the non-rigid nature of the cables. A case study will be investigated in order to analyse the design procedure for CDPRs.

However, the use of CDPRs is justified only when the task to be accomplished is simple and the working environment is not cluttered. In a cluttered environment, one configuration can hardly allow the CDPR moving platform to cover the entire prescribed path or the entire prescribed workspace without cable collisions, so that several reconfigurations are generally required. In this manuscript, the reconfigurations are limited to the displacement of the exit points which is generally sufficient to avoid cable interferences and collisions between the cables and the environment. The proposed design strategy is oriented by the task the RCDPR should accomplish [GCG<sup>+</sup>15b]. The user discretises the prescribed workspace or the prescribed path and divides them in  $n_t$  portions. Each portion should be covered by one and only one configuration of the CDPR. Then, each configuration is parametrised and the corresponding possible locations of the cables exit are thereby. The parameters defining the locations of the exit points can take a discrete set of values. By combining these values, it is possible to generate a large number of configurations. Each configuration is first analysed in order to verify if it is *feasible*, i.e., if it can cover the assigned portion of the prescribed path or the prescribed workspace while satisfying a set of constraints. Then, the feasible configurations are analysed to compose all the possible  $n_t$  dimensional combinations of configurations that allow the RCDPR to accomplish the prescribed task. The retained RCDPRs are the ones which satisfy one or more objective functions.

A case study has been considered in order to validate the proposed design strategy. The RCDPR should sandblast and paint a three-dimensional tubular structure. These operations are performed by appropriate tools embarked on the robot moving platform. The robot moving platform approaches each external side of the structure following a prescribed path while the tools perform their work. Three of the external sides of the structure is sandblasted and painted by means of a different configuration of the cable exit points. To reconfigure the RCDPR

from one side of the structure to another one, one or several cables are disconnected from their current exit points and moved to new ones. This procedure is repeated until all the sides of the structure are sandblasted and painted. The variables of the corresponding design problems are the Cartesian coordinates of the exit points of the three required configurations associated to the paths of the external sides of the structure. In this case study, the total number of exit points on the base is minimised, selecting the exit point locations that can be shared between two or more configurations. Thereby, during a configuration change, not all the cable exit points need to be modified. Furthermore, according to a hierarchical optimisation, the design problem aims at minimising the robot overall size and the average of the cable tensions along the prescribed path.

The feasibility of each configuration has to be guaranteed: Cable interferences as well as cable collisions with the structure are not permitted.

### 1.3.4 Reconfiguration Strategy for Discrete RCDPRs

When the task to be solved is complicated, it is not always possible to predict the number of configurations necessary to complete it. Therefore, the design algorithm introduced in Sec. 1.3.3 cannot always find a feasible solution. In this context, it is preferable to design an arbitrary RCDPR with a large number of possible cable exit point locations. Given such a complex RCDPR, where the number of cable exit point locations can be extremely large, a reconfiguration algorithm is required in order to complete a given task. In the previous research works, summarised in Sec. 1.2.6, two general problems are tackled. The *first problem* is related to RCDPR design optimisation. It consists in determining reconfiguration parameter values allowing the RCDPR to work adequately across a prescribed workspace. The RCDPR is then only occasionally reconfigured. The *second problem* is to continuously resolve the reconfiguration parameter values so as to optimise some performance criterion along a prescribed path. All these research works deal with continuous RCDPR reconfigurations. In our study, discrete reconfigurations are considered because the use of continuous reconfigurations for industrial applications over large structures can be prohibitive since several additional motorised DOFs must be used in order to continuously reconfigure the cable exit points. Hence, the aforementioned second problem is irrelevant since, in this manuscript, the set of possible values of the cable exit point positions (reconfiguration parameters) is not continuous but discrete. The first problem is relevant to a discrete reconfiguration problem, but, to the best of our knowledge, in the case of a discrete set of possible configurations, the issue of optimising the sequence of reconfigurations which allow the RCDPR moving platform to follow a prescribed path has never been dealt with before.

This manuscript introduces a reconfiguration algorithm for discrete RCDPRs [GCG<sup>+</sup>15c, GCGG16, GGC<sup>+</sup>16b]. The algorithm is able to compute the optimal sequence of cable exit point reconfigurations permitting the moving platform of a RCDPR to follow a prescribed path. The prescribed path is discretised into a finite set of points. The cable exit points of the RCDPR can be positioned at the points of a user-defined grid of possible locations. The user also defines a set of constraint functions which ensure a proper functioning of the RCDPR. The prescribed path is deemed to be successfully followed if all these constraints are satisfied at all points of the discretised path.

The computation of the reconfiguration strategy is based on the following contributions. A so-called feasibility map is firstly generated. *For each possible RCDPR configuration*, this map stores the feasibility of the points of the prescribed path. A point is feasible if the corresponding moving platform pose satisfies all constraint functions, it is unfeasible otherwise. From this map, *feasibility transitions* are then defined. These transitions represent the reconfigurations that can be possibly performed along the prescribed path. The feasibility map is next analysed in order to find so-called dominant configurations and then to determine minimum sets of configurations which allow the RCDPR moving platform to follow the whole prescribed path while satisfying all constraint functions,

resulting in a reduced feasibility map. This analysis aims at reducing the number of configurations to be considered in the next step. This next step uses the feasibility transitions to build a graph whose nodes represent the feasible RCDPR reconfigurations along the prescribed path and whose arcs are weighted by means of a user-defined cost function. Some possible cost functions are presented, a relevant example being the number of cable exit point changes required for a given reconfiguration. Finally, the graph is searched using Dijkstra's algorithm which eventually determines the optimal reconfiguration strategy, i.e., the sequence of feasible reconfigurations that permit to follow the whole prescribed path while optimising a cost function.

Two case studies are dealt within this manuscript. The first case study involves the reconfiguration of a planar CDPR. In the second case study, the considered applications involve low force operations over the surface of a large (metallic) structure, e.g. painting and sandblasting. The CDPR environment is cluttered because the structure is located into the workspace and occupies a significant part of it. The task to be performed is simplified to that of following a prescribed path which is defined by the user in such a way that the entire surface of the structure is eventually treated. The moving platform orientation is constant. Tools and/or active devices may have to be embarked on the CDPR moving platform but the corresponding issues are not dealt with in this thesis.

### **1.3.5 Manuscript Organisation**

This manuscript is organised as follows. Chapter II introduces the geometric, kinematic, elasto-static and dynamic models of CDPRs used in the thesis. Chapter III describes the tools used to analyse the workspace of CDPRs. The workspace analysis is useful in Chap. IV, which introduces a strategy to design CDPRs and discrete RCDPRs. Chapter V presents the main steps of a discrete reconfiguration planning method, detailing the feasibility map computation, its analysis to reduce the number of considered configurations, the graph building, and the graph search for an optimal discrete reconfiguration strategy. Chapter VI concludes this manuscript by summarising the main contributions of this doctorate thesis and by discussing some research perspectives.



# Chapter 2

## Modelling

### Chapter Content

2.1	CDPR Models Based on the Linear Rigid Cable Model . . . . .	22
2.2	CDPR Models Based on the Sagging Cable Model . . . . .	29
2.3	CDPR Elasto-Static Models . . . . .	33
2.4	Conclusions . . . . .	42

The performances of CDPRs can be affected by their models. The choice of a relevant model allows to control and predict the behaviour of a CDPR in terms of moving platform positioning accuracy and cable tension distribution. Several geometric, elasto-static, kinematic and elasto-dynamic models have been proposed in the literature. These models mainly differ in the cable descriptions and characteristics. Most of the models are based on massless cables.

Massless cables are described as linear segments and provide a good accuracy when their linear density is low. The effect of the pulleys on the CDPR geometric model, and consequently on the moving platform pose, is usually neglected. However, in order to improve the robot performances, Bruckmann included the effects of the pulleys in the geometric models of its prototype [Bru10]. Similarly, Surdilovic *et al* investigated the influence of pulleys on the elasto-static behaviour of CDPRs [SRK13].

In Sec. 2.1.2 and Sec. 2.1.3 the geometric and the static models of CDPRs with massless cables are presented. In Sec. 2.1.4, Sec. 2.1.5 and Sec. 2.1.6 the kinematic and dynamic models of CDPRs with massless cables are described. For sake of simplicity, the effect of the pulleys on the kinematic and dynamic models of CDPRs is not considered.

When a CDPR is designed to displace heavy loads, the cables used to perform the task have a large diameter and consequently a high linear density. As a consequence, the deformations of the cables due to gravity effect may not be negligible anymore and should be considered [KZW06, RGK<sup>+</sup>09, RGBP10b]. The cables are then described using the sagging model defined in [Irv92]. The sagging cable model and the related geometric model of the CDPR are detailed in Sec. 2.2.1 and Sec. 2.2.2, respectively. These models neglect the effect of pulleys that have already been considered in Gouttefarde *et al*. [GNB14]. Since heavy cables are mostly used for quasi-static operations [Ars13, NG14a], the dynamic models of the sagging cable are not taken into account in the scope of this thesis.

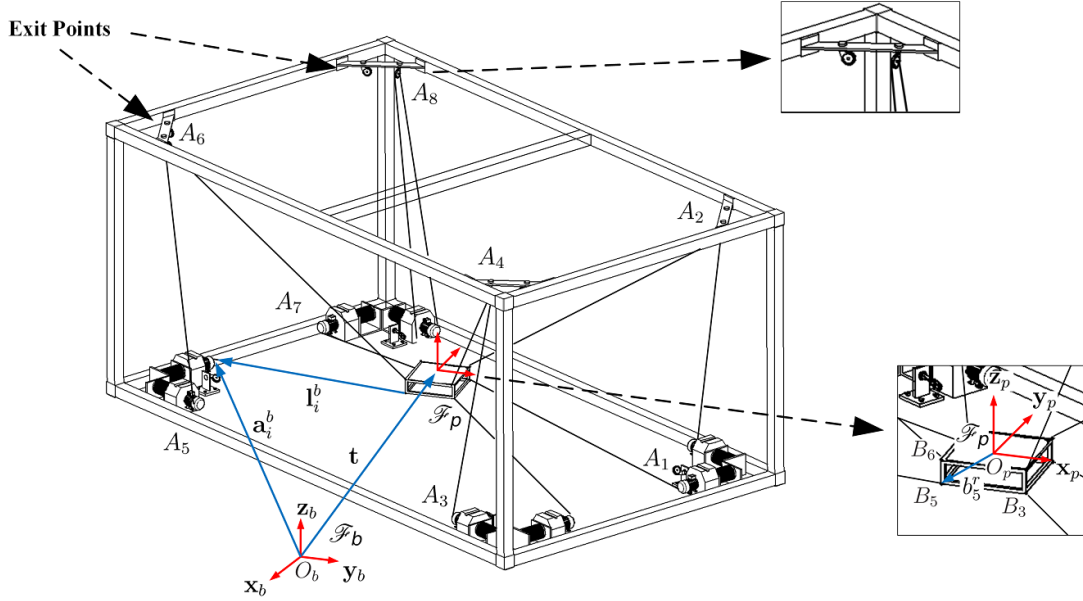


Fig. 2.1 – Schematic of a CDPR

Some of the geometric and static models of CDPRs described in the literature take into account the longitudinal elasticity of the cables in order to lower the moving platform positioning error due to the cable deformations. The elasto-static model based on linear cables will be presented in Sec. 2.3.1. In Sec. 2.3.2 pulleys are integrated into the elasto-static modelling of CDPRs. These models have been derived using a more formal approach with respect to the one proposed in [BK05b, Ars10, SRK13]. Section 2.3.3 describes the elasto-static model of CDPRs while considering sagging cables.

The elasto-static model of a CDPR is expressed by means of its *stiffness matrix*. This stiffness matrix is composed of two parts, namely, a *passive stiffness matrix* that strictly depends on the cables properties and an *active stiffness matrix* that strictly depends on the cable tensions. It is noteworthy that most of the existing elasto-static CDPR models with sagging cables neglect the active part of the stiffness matrix, except for the ones proposed in [Ars13, NG14a, Li15]. In this manuscript, the elasto-static model of CDPRs with sagging cables has been expressed while computing the active stiffness matrix by developing the Jacobian of the cable wrenches with respect to the moving platform pose.

## 2.1 CDPR Models Based on the Linear Rigid Cable Model

### 2.1.1 Robot Representation

Figure 2.1 depicts a CDPR. The moving platform is actuated by  $m$  cables. The  $i$ -th cable connection point on the moving platform is denoted by  $B_i$ . The cables are actuated by winches, fixed on the base of the robot. The cables are routed to exit points by means of pulleys. The  $i$ -th exit point is defined as  $A_i$ .

$\mathcal{F}_b$ , of origin  $O_b$  and axes  $\mathbf{x}_b, \mathbf{y}_b, \mathbf{z}_b$ , denotes a fixed reference frame. Vector  $\mathbf{b}_i^b$  is the position vector of point  $B_i$  expressed in frame  $\mathcal{F}_b$ . Vector  $\mathbf{b}_i^p$  denotes the position vector of point  $B_i$  expressed in the moving platform frame  $\mathcal{F}_p$  of origin  $O_p$  and axes  $\mathbf{x}_p, \mathbf{y}_p, \mathbf{z}_p$ . Vector  $\mathbf{a}_i^b$  denotes the position vector of point  $A_i$  expressed in the

base frame  $\mathcal{F}_b$ .

## 2.1.2 Inverse Geometric Models (IGMs)

### IGM without Pulleys

The *Inverse Geometric Model* (IGM) of the CDPDR provides the lengths  $l_i, i = 1, \dots, m$ , of the cables, for a given pose  $\mathbf{p} = [\mathbf{t}^\top, \mathbf{r}^\top]^\top$  of its moving platform. The pose  $\mathbf{p}$  is defined in the reference frame  $\mathcal{F}_b$ .  $\mathbf{t} = [t_x, t_y, t_z]^\top$  is the position vector of the origin  $O_p$  of frame  $\mathcal{F}_p$ , which usually coincides with the moving platform CoM. Vector  $\mathbf{r}$  contains the Roll, Pitch, and Yaw (RPY) angles,  $\phi$ ,  $\theta$  and  $\psi$ , around the axes  $\mathbf{z}_b$ ,  $\mathbf{y}_b$  and  $\mathbf{x}_b$ , respectively. These angles define the moving platform orientation with respect to  $\mathcal{F}_b$ . Here, the weight of the cables is neglected and the cables are thus considered to be straight line segments.

The IGM is based on the loop closure equations of the cable vectors,  $\mathbf{l}_i^b, i = 1, \dots, m$ , defined in  $\mathcal{F}_b$ , as follows:

$$\mathbf{l}_i^b = \mathbf{a}_i^b - \mathbf{b}_i^b = \mathbf{a}_i^b - \mathbf{t} - \mathbf{R}\mathbf{b}_i^p = \mathbf{a}_i^b - \mathbf{t} - \mathbf{b}_i^r, \quad i = 1, \dots, m \quad (2.1)$$

where vector  $\mathbf{l}_i^b$  is directed along the  $i$ -th cable from point  $B_i$  to point  $A_i$ .  $\mathbf{b}_i^r = \mathbf{R}\mathbf{b}_i^p$  is the vector pointing from the origin  $O_p$  of frame  $\mathcal{F}_p$  to the attachment point  $B_i$  of the  $i$ -th cable. Vector  $\mathbf{b}_i^r$  is expressed in frame  $\mathcal{F}_b$ .  $\mathbf{R} = \mathbf{R}_z(\phi)\mathbf{R}_y(\theta)\mathbf{R}_x(\psi)$  is the rotation matrix defining the moving platform orientation:

$$\mathbf{R} = \mathbf{R}_z(\phi)\mathbf{R}_y(\theta)\mathbf{R}_x(\psi) = \begin{bmatrix} c\phi c\theta & c\phi s\theta s\psi - s\phi c\psi & c\phi s\theta c\psi + s\phi s\psi \\ s\phi c\theta & s\phi s\theta s\psi + c\phi c\psi & s\phi s\theta c\psi - c\phi s\psi \\ -s\theta & c\theta s\psi & c\theta c\psi \end{bmatrix} \quad (2.2)$$

where c and s stand for cosinus and sinus, respectively.

The length  $l_i$  of the  $i$ -th cable is then defined by the 2-norm of the cable vector  $\mathbf{l}_i^b$ , namely,  $l_i = \|\mathbf{l}_i^b\|_2, i = 1, \dots, m$ . The unit vectors associated to  $\mathbf{l}_i, i = 1, \dots, m$  are defined, with respect to  $\mathcal{F}_b$ , as:

$$\mathbf{d}_i^b = \frac{\mathbf{l}_i^b}{l_i}, \quad i = 1, \dots, m \quad (2.3)$$

### IGM with Pulleys

Considering the static equilibrium of the moving platform, each cable and the associated pulley lie in a plane. The plane of the  $i$ -th cable is described through a local reference frame,  $\mathcal{F}_i$ , of origin  $A_i$  and axes  $\mathbf{x}_i^b, \mathbf{y}_i^b$  and  $\mathbf{z}_i^b$ . Axis  $\mathbf{z}_i^b$  is vertical and lies along the gravity direction. Axis  $\mathbf{x}_i^b$  is orthogonal to axis  $\mathbf{z}_i^b$  and lies in the cable plane, i.e.  $\mathbf{y}_i^b = \mathbf{z}_i^b \times \mathbf{x}_i^b$  is orthogonal to the two foregoing vectors axes.

The geometric model of a pulley is represented in Fig. 2.2. The geometry of the pulley affects the cable exit point location, and consequently the IGM. Pulleys are composed of rollers mounted on vertical axis revolute joints.  $r_p$  is the radius of the pulleys. The orientation of the  $i$ -th roller around the vertical axis, and consequently of the  $i$ -th cable local reference frame, is given by angle  $\theta_i = \text{atan2}(-l_{y,i}, -l_{x,i})$ , where  $l_{x,i}$  and  $l_{y,i}$  are the components of  $\mathbf{l}_i$  along  $\mathbf{x}_b$  and  $\mathbf{y}_b$ , respectively. Knowing the orientation of the pulley, the position of the centre point of the  $i$ -th roller,  $O_i$ , is computed as follows:

$$\mathbf{o}_i^b = \mathbf{a}_i^b + r_p \mathbf{R}_i \mathbf{x}_b = \mathbf{a}_i^b + r_p \mathbf{x}_i^b \quad (2.4)$$



The external wrench  $\mathbf{w}_e$  is a 6-dimensional vector expressed in frame  $\mathcal{F}_b$  and takes the form:

$$\mathbf{w}_e = [\mathbf{f}_e^T, \mathbf{m}_e^T]^T = [f_x, f_y, f_z, m_x, m_y, m_z]^T \quad (2.9)$$

$f_x$ ,  $f_y$  and  $f_z$  are the  $x$ ,  $y$  and  $z$  components of the external force vector  $\mathbf{f}_e$ .  $m_x$ ,  $m_y$  and  $m_z$  are the  $x$ ,  $y$  and  $z$  components of the external moment vector  $\mathbf{m}_e$ , respectively. The components of the external wrench  $\mathbf{w}_e$  are assumed to be bounded as follows:

$$\underline{f} \leq f_x, f_y, f_z \leq \bar{f} \quad (2.10)$$

$$\underline{m} \leq m_x, m_y, m_z \leq \bar{m} \quad (2.11)$$

where  $\underline{f}$  and  $\bar{f}$  are the lower and the upper bounds of the external force components, while  $\underline{m}$  and  $\bar{m}$  are the lower and the upper bounds of the external moment components.

In order to balance the external wrench, each cable generates on the moving platform a wrench, proportional to its tension  $\tau_i = 1, \dots, m$ . The cables balance the external wrench  $\mathbf{w}_e$ , according to the following equation [RGL98]:

$$\mathbf{W}\boldsymbol{\tau} + \mathbf{w}_e = \mathbf{0} \quad (2.12)$$

The cable tensions are collected into the vector  $\boldsymbol{\tau} = [\tau_1, \dots, \tau_m]^T$  and multiplied by the wrench matrix  $\mathbf{W}$  whose columns are composed of the unit wrenches  $\mathbf{w}_i$  exerted by the cables on the moving platform [RGL98]:

$$\mathbf{W} = \begin{bmatrix} \mathbf{d}_1^b & \mathbf{d}_2^b & \dots & \mathbf{d}_m^b \\ \mathbf{Rb}_1^p \times \mathbf{d}_1^b & \mathbf{Rb}_2^p \times \mathbf{d}_2^b & \dots & \mathbf{Rb}_m^p \times \mathbf{d}_m^b \end{bmatrix} \quad (2.13)$$

When the effect of pulleys is not neglected, Eq. (2.13) can be rewritten as follows:

$$\mathbf{W} = \begin{bmatrix} \mathbf{D}_1^b & \mathbf{D}_2^b & \dots & \mathbf{D}_m^b \\ \mathbf{Rb}_1^p \times \mathbf{D}_1^b & \mathbf{Rb}_2^p \times \mathbf{D}_2^b & \dots & \mathbf{Rb}_m^p \times \mathbf{D}_m^b \end{bmatrix} \quad (2.14)$$

Most of the CDPRs and RCDPRs considered in this thesis are redundantly actuated, i.e., the number of cables is greater than the number of DOFs of the moving platform. Then, the *Inverse Static Model* (ISM) (determination of  $\boldsymbol{\tau}$  in Eq. (2.12)) of CDPRs modelled with linear rigid cables generally leads to an infinite number of solutions. Considering that the cable tensions must be non-negative and satisfy Eq. (2.12), a possible solution is described by the following equation:

$$\boldsymbol{\tau} = \boldsymbol{\tau}_n + \boldsymbol{\tau}_0 = -\mathbf{W}^\dagger \mathbf{w}_e + \mathbf{N}\boldsymbol{\lambda}, \quad \boldsymbol{\tau} \geq \mathbf{0} \quad (2.15)$$

where  $\mathbf{W}^\dagger$  is the Moore-Penrose generalised inverse of  $\mathbf{W}$ ,  $\boldsymbol{\lambda} \in \mathbb{R}^{(m-n)}$  and  $\mathbf{N}$  is a matrix whose columns span the null space of  $\mathbf{W}$  [RGL98].  $n$  is the dimension of the task space. In the framework of this thesis, the solution that minimises the 2-norm of the cable tension vector  $\boldsymbol{\tau}$  is used.

### 2.1.4 Direct and Inverse First Order Kinematic Models

The kinematic model of the CDPR describes the twist of the moving platform in terms of the cable coiling/uncoiling velocities:

$$\mathbf{J}\dot{\mathbf{l}} - \dot{\mathbf{p}} = \mathbf{J}\dot{\mathbf{l}} - \begin{bmatrix} \dot{\mathbf{t}} \\ \boldsymbol{\omega} \end{bmatrix} = 0 \quad (2.16)$$

where  $\dot{\mathbf{t}} = [\dot{l}_x, \dot{l}_y, \dot{l}_z]^T$  is the vector of the moving platform linear velocity,  $\boldsymbol{\omega} = [\omega_x, \omega_y, \omega_z]^T$  is the vector of the moving platform angular velocity and  $\dot{\mathbf{l}}$  is the vector of the cable velocities,  $\dot{\mathbf{l}} = [\dot{l}_1, \dots, \dot{l}_m]^T$ .  $\mathbf{J}$  is the kinematic Jacobian matrix of the CDPR. The columns of the Jacobian matrix represent the twist  $\dot{\mathbf{p}}_i$  associated to each cable. The moving platform angular velocity can be expressed as a function of the RPY angular velocities, according to the description provided in App. A.1.

Considering the duality between the kinematic model and static model of the CDPR, the static equilibrium of the moving platform is rewritten as:

$$\boldsymbol{\tau} = \mathbf{J}^T \mathbf{w}_e \quad (2.17)$$

Comparing Eq. (2.12) and Eq. (2.17) we observe that:

$$\mathbf{J}^T \mathbf{w}_e = -\mathbf{W}^\dagger \mathbf{w}_e \quad (2.18)$$

Therefore, the kinematic Jacobian matrix of the CDPR is computed as:

$$\mathbf{J} = -\mathbf{W}^{\dagger T} \quad (2.19)$$

The *Direct Kinematic Model* (DKM) of a CDPR defines the twist  $\dot{\mathbf{p}}$  of the moving platform as a function of vector  $\dot{\mathbf{l}}$ :

$$\dot{\mathbf{p}} = \mathbf{J}\dot{\mathbf{l}} = -\mathbf{W}^{\dagger T} \dot{\mathbf{l}} \quad (2.20)$$

The *Inverse Kinematic Model* (IKM) is computed by inverting Eq. (2.20), i.e.:

$$\dot{\mathbf{l}} = \mathbf{J}^\dagger \dot{\mathbf{p}} = -\mathbf{W}^T \dot{\mathbf{p}} \quad (2.21)$$

where  $\mathbf{J}^\dagger$  is the Moore-Penrose pseudo-inverse of  $\mathbf{J}$ .

### 2.1.5 Direct and Inverse Second Order Kinematic Models

The *Second Order Direct Kinematic Model* (SODKM) is computed differentiating Eq. (2.20):

$$\ddot{\mathbf{p}} = \begin{bmatrix} \ddot{\mathbf{t}} \\ \boldsymbol{\alpha} \end{bmatrix} = \dot{\mathbf{J}}\dot{\mathbf{l}} + \mathbf{J}\ddot{\mathbf{l}} \quad (2.22)$$

where  $\ddot{\mathbf{t}} = [\ddot{l}_x, \ddot{l}_y, \ddot{l}_z]^T$  is the vector of the moving platform linear acceleration,  $\boldsymbol{\alpha} = [\alpha_x, \alpha_y, \alpha_z]^T$  is the vector of the moving platform angular acceleration,  $\ddot{\mathbf{l}} = [\ddot{l}_1, \dots, \ddot{l}_m]^T$  is the vector collecting the second derivative of the cable lengths and  $\dot{\mathbf{J}}$  is the time derivative of the kinematic Jacobian  $\mathbf{J}$ . The moving platform angular acceleration can be expressed as a function of the RPY angular velocities and accelerations, according to the description provided in App. A.1.

The *Second Order Inverse Kinematic Model* (SOIKM) is defined inverting Eq. (2.22) or differentiating Eq. (2.21):

$$\ddot{\mathbf{l}} = \mathbf{J}^\dagger (\ddot{\mathbf{p}} - \dot{\mathbf{J}}\dot{\mathbf{l}}) = -\dot{\mathbf{W}}^T \dot{\mathbf{p}} - \mathbf{W}^T \ddot{\mathbf{p}} \quad (2.23)$$

The time derivative of the wrench matrix,  $\dot{\mathbf{W}}$ , is detailed in App. A.2.

### 2.1.6 Inverse Dynamic Model (IDM)

The dynamic equilibrium used in this thesis takes into account the dynamics of the moving platform, as well as the dynamics of the motors and the winches. However, assuming that the diameters of the cables and the pulleys are small, the dynamics of the pulleys and the cables is neglected. A scheme of the actuation system is described in Fig. 2.3. The dynamic equilibrium of the moving platform is described by the following equation:

$$\mathbf{W}\boldsymbol{\tau} - \mathbb{I}_p \ddot{\mathbf{p}} - \mathbf{C}\dot{\mathbf{p}} + \mathbf{w}_e + \mathbf{w}_g = 0 \quad (2.24)$$

In order to generalise the dynamic model of CDPBs, this thesis considers the possibility that the CoM of the moving platform,  $G$ , may not coincide with the origin  $O_p$  of frame  $\mathcal{F}_p$ . Being  $M$  the mass of the moving platform, the wrench  $\mathbf{w}_g$  due to the gravity acceleration  $\mathbf{g}$  is defined as follows:

$$\mathbf{w}_g = \begin{bmatrix} M\mathbf{I}_3 \\ \mathbf{M}\hat{\mathbf{S}}_p \end{bmatrix} \mathbf{g} \quad (2.25)$$

$\mathbf{I}_3$  is the  $3 \times 3$  identity matrix;  $\mathbf{M}\mathbf{S}_p = \mathbf{R} [Mx_p, My_p, Mz_p]^T$  is the first momentum of the moving platform defined with respect to frame  $\mathcal{F}_b$ . Vector  $\mathbf{S}_p = [x_p, y_p, z_p]^T$  describes the position of the moving platform CoM,  $G$ , with respect to the origin  $O_p$  of frame  $\mathcal{F}_p$ .  $\mathbf{M}\hat{\mathbf{S}}_p$  is the skew-symmetric matrix associated to  $\mathbf{M}\mathbf{S}_p$ .

Matrix  $\mathbb{I}_p$  represents the spatial inertia of the moving platform:

$$\mathbb{I}_p = \begin{bmatrix} M\mathbf{I}_3 & -\mathbf{M}\hat{\mathbf{S}}_p \\ \mathbf{M}\hat{\mathbf{S}}_p & \mathbf{I}_p \end{bmatrix} \quad (2.26)$$

$\mathbf{I}_p$  is the inertia tensor of the moving platform, computed applying the Huygens-Steiner theorem to the moving platform inertia tensor,  $\mathbf{I}_g$ , defined with respect to the CoM of the moving platform itself.  $\mathbf{I}_p$  takes the form:

$$\mathbf{I}_p = \mathbf{R}\mathbf{I}_g\mathbf{R}^T - \frac{\mathbf{M}\hat{\mathbf{S}}_p\mathbf{M}\hat{\mathbf{S}}_p}{M} \quad (2.27)$$

$\mathbf{C}$  is the matrix of the centrifugal and Coriolis wrenches, defined such that:

$$\mathbf{C}\dot{\mathbf{p}} = \begin{bmatrix} \hat{\boldsymbol{\omega}}\hat{\boldsymbol{\omega}}\mathbf{M}\mathbf{S}_p \\ \hat{\boldsymbol{\omega}}\mathbf{I}_p\boldsymbol{\omega} \end{bmatrix} \quad (2.28)$$

where  $\hat{\boldsymbol{\omega}}$  is the skew-symmetric matrix of  $\boldsymbol{\omega}$ .

The input motor torques  $\boldsymbol{\tau}_M$  are computed by using the dynamic equilibrium of the motors:

$$\boldsymbol{\tau}_M = \boldsymbol{\tau}_R + \mathbf{I}_M\ddot{\mathbf{q}} + \mathbf{F}_v\dot{\mathbf{q}} + \mathbf{F}_c\text{sign}(\dot{\mathbf{q}}) \quad (2.29)$$

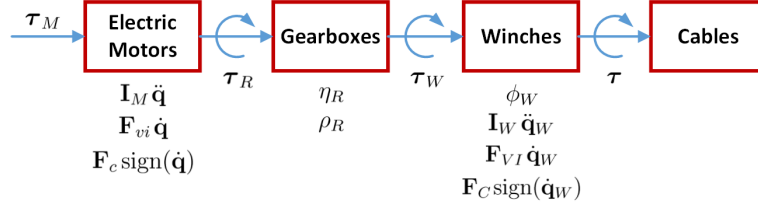


Fig. 2.3 – Scheme of the torque transmission from the electric motors to the cables

$\mathbf{F}_{vi}$  and  $\mathbf{F}_c$  are the diagonal matrices of the viscous and the Coulomb friction coefficients of the motors, respectively;  $\mathbf{I}_M$  is the inertia matrix of the motors;  $\tau_R$  is the vector of the torques transmitted by the motors to the gearboxes.

Gearboxes are usually integrated directly in the motor block. They transmit to the winches higher torques,  $\tau_W$ , and lower rotational speeds,  $\dot{\mathbf{q}}_W$ . The inertia of the gearbox is usually negligible.

$$\tau_W = \eta_R \rho_R \tau_R \quad (2.30)$$

$$\dot{\mathbf{q}}_W = \mu_R \dot{\mathbf{q}} = \frac{1}{\rho_R} \dot{\mathbf{q}} \quad (2.31)$$

$\rho_R$  is the gearbox ratio and  $\eta_R$  is the efficiency coefficient.

The cables are coiled around the winches, which are connected to the motors through the gearboxes. The dynamic equilibrium of the winches is defined as follows:

$$\tau_W = \frac{\phi_W}{2} \tau + \mathbf{I}_W \ddot{\mathbf{q}}_W + \mathbf{F}_{VI} \dot{\mathbf{q}}_W + \mathbf{F}_C \text{sign}(\dot{\mathbf{q}}_W) \quad (2.32)$$

$\mathbf{I}_W$  is the diagonal matrix of the winch inertia,  $\phi_W$  is the nominal diameter of the winches,  $\mathbf{F}_{VI}$  and  $\mathbf{F}_C$  are the viscous and Coulomb friction matrices of the winches, respectively.  $\ddot{\mathbf{q}}_W$  is the vector of the rotational acceleration of the winches. Considering a constant gearbox ratio,  $\rho_R = \frac{\dot{\mathbf{q}}}{\dot{\mathbf{q}}_W}$ , it turns out that:

$$\ddot{\mathbf{q}}_W = \frac{\ddot{\mathbf{q}}}{\rho_R} \quad (2.33)$$

Considering  $\dot{\mathbf{q}}_W = 2 \frac{\dot{\mathbf{q}}}{\phi_W}$  and its time derivative  $\ddot{\mathbf{q}}_W = 2 \frac{\ddot{\mathbf{q}}}{\phi_W}$ , the dynamic equilibrium of the whole robot is obtained substituting Eq.s (2.21), (2.23), and (2.29-2.33) in Eq. (2.24):

$$\frac{2}{\phi_W} \eta_R \rho_R \mathbf{W} \tau_M + \mathbf{A} \ddot{\mathbf{p}} + \mathbf{B} + \mathbf{D} + \mathbf{w}_e = 0 \quad (2.34)$$

where:

$$\mathbf{A} = -\mathbb{I}_p + \frac{4}{\phi_W^2} \mathbf{W} (\eta_R \rho_R^2 \mathbf{I}_m + \mathbf{I}_W) \mathbf{W}^T \quad (2.35)$$

$$\begin{aligned} \mathbf{B} = & -\mathbf{C}\dot{\mathbf{p}} + \frac{4}{\phi_W^2} \mathbf{W} (\eta_R \rho_R^2 \mathbf{I}_m + \mathbf{I}_W) \mathbf{W}^T \dot{\mathbf{p}} + \\ & + \frac{4}{\phi_W^2} \mathbf{W} (\eta_R \rho_R^2 \mathbf{F}_{vi} + \mathbf{F}_{VI}) \mathbf{W}^T \dot{\mathbf{p}} \end{aligned} \quad (2.36)$$

$$\mathbf{D} = \mathbf{w}_g - \frac{2}{\phi_W} \mathbf{W} (\eta_R \rho_R \mathbf{F}_c + \mathbf{F}_C) \text{sign}(-\mathbf{W}^T \dot{\mathbf{p}}) \quad (2.37)$$

Thus, the motor torques  $\tau_M$  are computed according to the *Inverse Dynamic Model* (IDM):

$$\tau_M = -\frac{\phi_W}{2\eta_R \rho_R} \mathbf{W}^\dagger (\mathbf{A}\ddot{\mathbf{p}} + \mathbf{B} + \mathbf{D} + \mathbf{w}_e) \quad (2.38)$$

## 2.2 CDPR Models Based on the Sagging Cable Model

When the payload of the CDPR is heavy and the acceleration of the moving platform are low, the motion of the CDPR moving platform can be considered quasi-static. The geometric and the elasto-static models of the CDPR provided in this section take into account the weight of the cables, according to the sagging model provided by Irvine in [Irv92].

### 2.2.1 Sagging Cable Model

The sagging cable model is usually described with respect to the reference frame of the cable,  $\mathcal{F}_i$ , as shown in Fig. 2.4. Assuming that  $P$  is an arbitrary point of the strained cable profile parametrised by its linear abscissa  $p$ , the geometric constraint for a differential cable element around the point  $P$  is expressed as:

$$\left(\frac{dx}{dp}\right)^2 + \left(\frac{dz}{dp}\right)^2 = 1 \quad (2.39)$$

The static equilibrium of the unstrained cable element can be parametrised according to a curvilinear abscissa  $s$ :

$$f_p \frac{dx}{dp} = f_{p,x} \quad (2.40)$$

$$f_p \frac{dz}{dp} = f_{p,z} + \lambda_0 \mathbf{g}(s - L_{0,i}) \quad (2.41)$$

where  $f_p = \|\mathbf{f}_p\|_2$  is the tension of the cable at point  $P$ , defined as the 2-norm of the cable tension vector at point  $P$ ,  $\mathbf{f}_p = [f_{p,x}, f_{p,y}, f_{p,z}]^T$ .  $L_{0,i}$  is the initial length of the  $i$ -th unstrained cable. The tension satisfies the Hooke's law:

$$f_p = EA_0 \left( \frac{dp}{ds} - 1 \right) \quad (2.42)$$

where  $E$  is the Young Modulus of the cable and  $A_0$  is the section area of the unstrained cable.

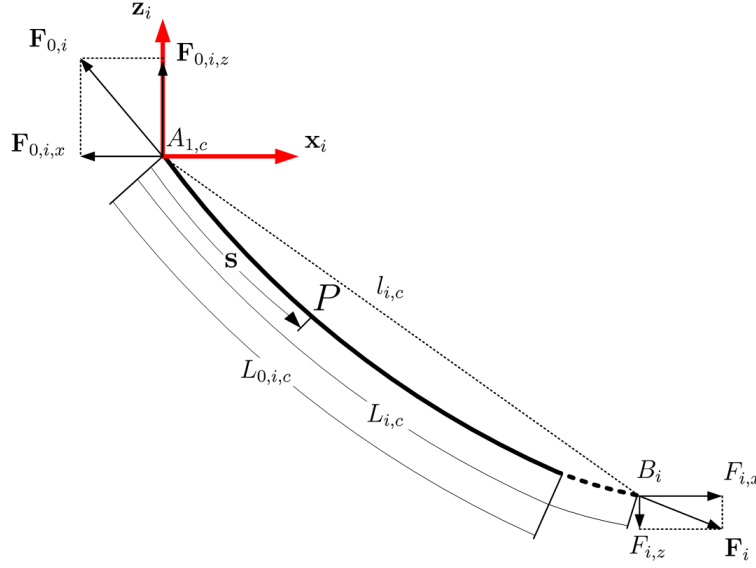


Fig. 2.4 – Sagging model of a cable

By combining Eq.s (2.39-2.42), the profile of the cable is parametrised as a function of  $s$  [Irv92]:

$$x_i(s) = \frac{F_{x,i}s}{EA_0} + \frac{\|F_{x,i}\|_2}{\lambda_0 g} \left[ \sinh^{-1} \left( \frac{F_{z,i} + \lambda_0 g(s - L_{0,i})}{F_{x,i}} \right) \right] - \sinh^{-1} \left( \frac{F_{z,i} - \lambda_0 g L_{0,i}}{F_{x,i}} \right) \quad (2.43)$$

$$y_i(s) = 0 \quad (2.44)$$

$$z_i(s) = \frac{F_{z,i}s}{EA_0} + \frac{\lambda_0 g}{EA_0} \left( \frac{s^2}{2} - L_{0,i}s \right) \quad (2.45)$$

$$+ \frac{1}{\lambda_0 g} \left[ \sqrt{F_{x,i}^2 + (F_{z,i} + \lambda_0 g(s - L_{0,i}))^2} - \sqrt{F_{x,i}^2 + (F_{z,i} - \lambda_0 g L_{0,i})^2} \right] \quad (2.46)$$

where  $\lambda_0$  is the linear density of the unstrained cable and  $F_{x,i}, F_{y,i}, F_{z,i}$  are the components of the forces transmitted by the moving platform on the cables at point  $B_i$ . These components are collected in vector  $\mathbf{F}_i = [F_{x,i}, F_{y,i}, F_{z,i}]^T$ .

## 2.2.2 Inverse Gometrico-Static Model

### Problem Description

The objective of the IGM is to compute the lengths of the cables for a given pose of the moving platform. Observing the equations describing the profile of the sagging cables, we notice that the profile of the cables and the force  $\mathbf{F}_i, i = 1, \dots, m$  exerted on the cables at point  $B_i, i = 1, \dots, m$  are strictly correlated through a set of non-linear equations. Hence, the geometric and the static problems can not be decoupled. The pose of the moving platform,  $\mathbf{p}$ , is specified, as well as the external wrench applied on the moving platform. The unknown variables of the geometrico-static problem are the cable lengths  $L_{0,i}, i = 1, \dots, m$  and the forces transmitted by the moving platform to the cables,  $\mathbf{F}_i, i = 1, \dots, m$ . Each force is parametrised according to its non-null components,  $F_{i,x}$  and  $F_{i,z}$ . Therefore, for a given CDP, the number of unknown variables for the geometrico-static problem is equal to  $3m$ .

The locations of the cable connection points on the moving platform,  $B_i, i = 1, \dots, m$ , are computed, with

respect to the local frames  $\mathcal{F}_i$  according to the cable profile described in Eq. (2.43) and Eq. (2.46) [KZW06].

$$b_{x,i}^l = \frac{F_{x,i}L_{0,i}}{EA_0} + \frac{\|F_{x,i}\|_2}{\lambda_0 g} \left[ \sinh^{-1} \left( \frac{F_{z,i}}{F_{x,i}} \right) - \sinh^{-1} \left( \frac{F_{z,i} - \lambda_0 g L_{0,i}}{F_{x,i}} \right) \right] \quad (2.47)$$

$$b_{y,i}^l = 0 \quad (2.48)$$

$$b_{z,i}^l = \frac{F_{z,i}L_{0,i}}{EA_0} - \frac{\lambda_0 g L_{0,i}}{2EA_0} + \frac{1}{\lambda_0 g} \left[ \sqrt{F_{x,i}^2 + F_{z,i}^2} - \sqrt{F_{x,i}^2 + (F_{z,i} - \lambda_0 g L_{0,i})^2} \right] \quad (2.49)$$

The previous components are collected into the vector  $\mathbf{b}_i^l = [b_{x,i}^l, b_{y,i}^l, b_{z,i}^l]^T$ . The geometric constraints have to be solved simultaneously with the static equilibrium equations of the moving platform:

$$\sum_{i=1}^m \mathbf{R}_i \mathbf{F}_i - \mathbf{f}_e = 0 \quad (2.50)$$

$$\sum_{i=1}^m \mathbf{R} \mathbf{b}_i^l \times \mathbf{R}_i \mathbf{F}_i - \mathbf{m}_e = 0 \quad (2.51)$$

Hence, the geometrico-static problem consists of  $2m$  geometric constraints and  $n$  static equilibrium equations. For a spatial CDPR, when the number of cables is equal to the DoF of its moving platform,  $m = n = 6$ , the geometrico-static problem contains as many unknowns as equations. For fully constrained CDPRs, with  $m > n$ , the number of unknowns is greater than the number of equations,  $3m > 2m + n$ . In both cases, as proved by Merlet in [Mer15b], the inverse geometrico-static problem may admit several solutions. The solutions have to be computed numerically since there is no known analytical solution for the problem at hand.

## Numerical Solution

The inverse geometrico-static problem can be solved numerically as an optimisation problem. The unknowns, collected in the vector  $\mathbf{x}$ , are the cable force components,  $F_{x,i}, F_{z,i}$ ,  $i = 1, \dots, m$ , and the cable unstrained lengths,  $L_{0,i}$ ,  $i = 1, \dots, m$ . A unique solution for the inverse geometrico-static problem can be found by minimising the cable lengths (and consequently the cable sagging) or the cable tensions [RGK<sup>+</sup>09]. The objective function aiming at minimising the cable length is:

$$\mathcal{V}_1 = \|\mathbf{L}\|_2 \quad (2.52)$$

where  $\mathbf{L}$  is the vector collecting all the cable lengths  $\mathbf{L} = [L_1, \dots, L_m]^T$  and  $\|\mathbf{L}\|_2$  is its 2-norm. The objective function aiming at minimising the cable tension expressed as:

$$\mathcal{V}_2 = \|\boldsymbol{\tau}_s\|_2 \quad (2.53)$$

where  $\boldsymbol{\tau}_s$  is the vector collecting all the maximum tensions measured along the cables,  $\boldsymbol{\tau}_s = [\tau_{s,1}, \dots, \tau_{s,m}]^T$ , and  $\|\boldsymbol{\tau}_s\|_2$  is its 2-norm. In order to assure the static equilibrium of the moving platform, Eq.s (2.47-2.51) are translated into a set of constraints. The geometric constraints verify that the computed locations of points  $B_i$ ,  $i = 1, \dots, m$  expressed in frame  $\mathcal{F}_i$  are sufficiently close to the desired locations,  $\tilde{\mathbf{b}}_i^l = [\tilde{b}_{x,i}^l, \tilde{b}_{y,i}^l, \tilde{b}_{z,i}^l]^T$ , calculated with respect to the prescribed moving platform pose:

$$c_{1,i} := \|b_{x,i}^l - \tilde{b}_{x,i}^l\| < \varepsilon_1 \quad i = 1, \dots, m \quad (2.54)$$

$$c_{2,i} := \|b_{z,i}^l - \tilde{b}_{z,i}^l\| < \varepsilon_2 \quad i = 1, \dots, m \quad (2.55)$$

where  $\varepsilon_1$  and  $\varepsilon_2$  represent the user-defined precision required to satisfy the previous constraints. Similarly, the static equilibrium should be satisfied by the following constraint equations:

$$\mathbf{c}_3 := \left\| \sum_{i=1}^m \mathbf{R}_i \mathbf{F}_i - \mathbf{f}_e \right\| < \varepsilon_3 \quad (2.56)$$

$$\mathbf{c}_4 := \left\| \sum_{i=1}^m \mathbf{R} \mathbf{b}_i^p \times \mathbf{R}_i \mathbf{F}_i - \mathbf{m}_e \right\| < \varepsilon_4 \quad (2.57)$$

In this thesis, the optimisation problem is solved using the *fmincon* function of *Matlab*<sup>®</sup> and the related active-set solver. The optimisation problem can be rewritten in the following form:

$$\min_{\mathbf{x}} \mathcal{J}_2(\mathbf{x}) \quad \text{such that} \quad \begin{cases} \mathbf{c}(\mathbf{x}) \leq \boldsymbol{\varepsilon} \\ \mathbf{x}_{lb} \leq \mathbf{x} \leq \mathbf{x}_{ub} \end{cases} \quad (2.58)$$

where  $\mathbf{c}(\mathbf{x})$  represents the set of constraint functions described in Eq.s (2.54-2.57).  $\boldsymbol{\varepsilon}$  is the vector collecting the precision required by each constraint, while  $\mathbf{x}_{lb}$  and  $\mathbf{x}_{ub}$  are the lower and upper bounds of vector  $\mathbf{x}$ , respectively. Since the function searches for a local minimum, vector  $\mathbf{x}$  has to be initialised inside the domain defined by the bounds  $\mathbf{x}_{lb}$  and  $\mathbf{x}_{ub}$ . The convergence and the efficiency of the solution are related to the initial guess,  $\mathbf{x}_0$ . The initial guess of the optimisation problem are computed solving the IGM and the ISM based on the linear rigid cable model. These models have been presented in Sec. 2.1.2 and Sec. 2.1.3, respectively. As a reminder, for fully constrained CDPs with  $m > n$ , the ISM is computed while minimising the 2-norm of the cable tensions,  $\|\boldsymbol{\tau}\|_2$ . Alternatively, the initial guess can be computed according to the simplified hefty cable CDP model presented by Gouttefarde *et al.* in [GCRB12]. In general, the simplified hefty cable model assures a better initial estimate than the linear rigid cable model.

Once the geometrico-static problem has been solved, the cable lengths is computed as follows [KZW06]:

$$\begin{aligned} L_i = L_{0,i} + \frac{1}{2\rho_0 g EA_0} & \left[ F_{z,i} \sqrt{F_{x,i}^2 + F_{z,i}^2} + F_{x,i}^2 \sinh^{-1} \left( \frac{F_{z,i}}{\|F_{x,i}\|_2} \right) + \right. \\ & - (F_{z,i} - \lambda_0 g L_{0,i}) \sqrt{F_{x,i}^2 + (F_{z,i} - \lambda_0 g L_{0,i})^2} + \\ & \left. - F_{x,i}^2 \sinh^{-1} \left( \frac{F_{z,i} - \lambda_0 g L_{0,i}}{\|F_{x,i}\|_2} \right) \right]^2 \quad i = 1, \dots, m \end{aligned} \quad (2.59)$$

It is noteworthy that the cable tensions vary along the cables:

$$f_i(s) = \sqrt{F_{x,i}^2 + (F_{z,i} + \lambda_0 g (s - L_{0,i}))^2}, \quad i = 1, \dots, m \quad (2.60)$$

The minimum and the maximum tensions are located at the extremities of the cables:

$$f_i^0 = \|\mathbf{F}_0\|_2 = \sqrt{F_{x,i}^2 + (F_{z,i} - \lambda_0 g L_{0,i})^2} \quad i = 1, \dots, m \quad (2.61)$$

$$f_i(L_{0,i}) = \|\mathbf{F}_i\|_2 = \sqrt{F_{x,i}^2 + F_{z,i}^2} \quad i = 1, \dots, m \quad (2.62)$$

### Cable Tension Distribution over a Prescribed Path

Section 2.2.2 describes the procedure to solve the inverse geometrico-static problem for a given pose of the moving platform. When the CoM of the moving platform has to follow a prescribed path, the algorithm described in Fig. 2.5 can be applied to ensure the cable tension continuity. The prescribed path,  $\mathcal{P}$ , is discretised into a set of  $n_P$  points  $P_j, j = 1, \dots, n_P$ . The steps of the algorithms are described as follows:

- Step I. The initial point of the path,  $P_1$ , is analysed using the IGM and the ISM based on the linear rigid cable model or the hefty cable model. By using the linear rigid cable model, Eq. (2.1.2) provides the cable lengths while assuming massless cables. The cable tensions are computed according to Eq. (2.15) by minimising  $\|\boldsymbol{\tau}\|_2$ . The solutions correspond to the initial guess,  $\mathbf{x}_{0,1}$ , of the geometrico-static problem for a CDPR with sagging cables. The bounds of the geometrico-static optimisation problem,  $\mathbf{x}_{lb}$  and  $\mathbf{x}_{ub}$ , are initialised: The cable lengths are bounded between 0 and  $l_{max}$ , while the cable tensions are bounded between  $\tau_{min}$  and  $\tau_{max}$ .  $l_{max}$  is the maximum cable length that can be coiled onto the winches.
- Step II. For the given point  $P_j$ , the statico-geometric problem is solved numerically according to Eq. (2.58) with respect to the given initial guess,  $\mathbf{x}_{0,j}$ , and the given bounds,  $\mathbf{x}_{lb}$  and  $\mathbf{x}_{ub}$ . The solution,  $\mathbf{x}_j$ , provides the lengths of the cables and their tension at point  $P_j$ .
- Step III. If point  $P_j$  is the last point of the path,  $P_e$ , the algorithm will stop. Otherwise, the initial guess and the bounds of the optimisation problem in Eq. (2.58) are updated. The initial guess associated to point  $P_{j+1}$  is equal to the solution of the geometrico-static problem obtained for point  $P_j$ ,  $\mathbf{x}_{0,j+1} = \mathbf{x}_j$ . The bounds  $\mathbf{x}_{lb}$  and  $\mathbf{x}_{ub}$  are updated while considering the surrounding of  $\mathbf{x}_j$ :

$$\mathbf{x}_{lb} = \mathbf{x}_j - \Delta_P \quad (2.63)$$

$$\mathbf{x}_{ub} = \mathbf{x}_j + \Delta_P \quad (2.64)$$

where  $\Delta_P$  is a user-defined vector used to define the bounds of the optimisation at the next iteration. The inverse geometrico-static problem associated to point  $P_{j+1}$  is solved according to the updated parameters by going back to Step II.

## 2.3 CDPR Elasto-Static Models

### 2.3.1 Linear Non-Rigid Cable Model

In order to quantify the stiffness of the CDPR, an elasto-static model is used. The elastic behaviour of the moving platform is described by the following equation:

$$\delta \mathbf{w}_e = \begin{bmatrix} \delta \mathbf{f}_e \\ \delta \mathbf{m}_e \end{bmatrix} = \mathbf{K} \delta \mathbf{p} = \mathbf{K} \begin{bmatrix} \delta \mathbf{t} \\ \delta \mathbf{r} \end{bmatrix} \quad (2.65)$$

where  $\delta \mathbf{w}_e$  represents the infinitesimal (sufficiently small) change in the external wrench applied to the moving platform,  $\delta \mathbf{p}$  is the infinitesimal (sufficiently small) displacement screw of the moving platform, and  $\mathbf{K}$  is the stiffness matrix. In this case,  $\delta \mathbf{r} = [\delta r_x, \delta r_y, \delta r_z]^T$  represents the vector of the infinitesimal (sufficiently small) rotations of the moving platform around the axes  $\mathbf{x}_b$ ,  $\mathbf{y}_b$  and  $\mathbf{z}_b$ , respectively.

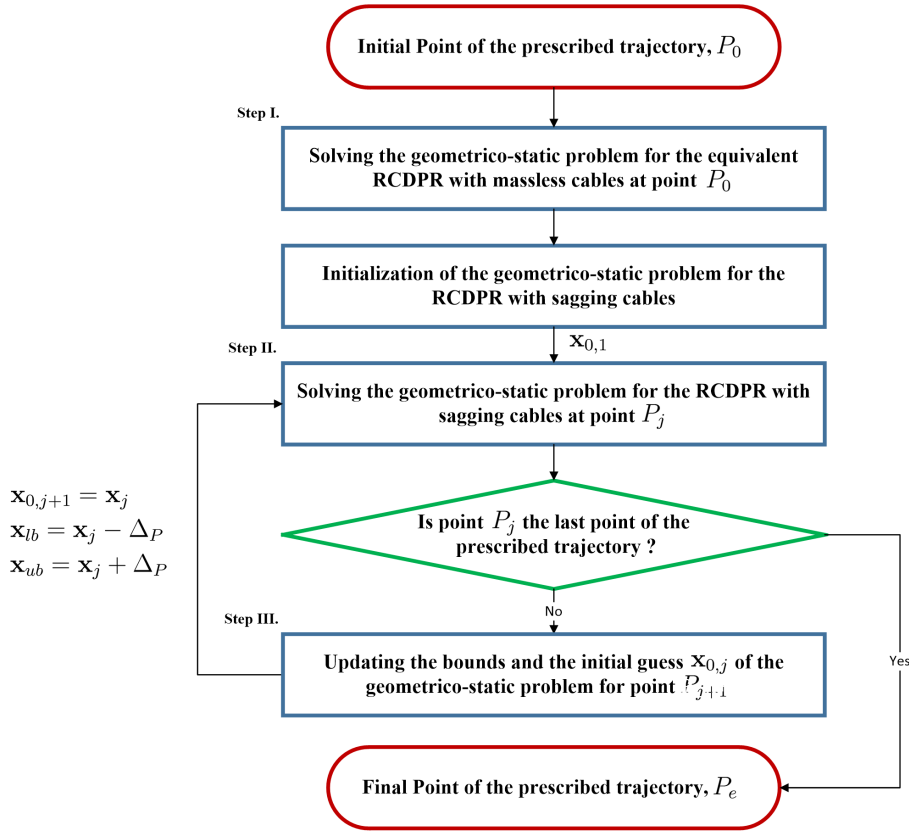


Fig. 2.5 – Algorithm for the computation of the geometrico-static model of a CDPR subjected to sagging effect.

According to Behzadipour and Khajepour [BK05b], it is possible to define the stiffness matrix  $\mathbf{K}$  as:

$$\mathbf{K} = \frac{d\mathbf{w}_e}{d\mathbf{p}} \quad (2.66)$$

Substituting Eq. (2.12) in Eq. (2.66), the stiffness matrix is decomposed into two terms: The active stiffness matrix,  $\mathbf{K}_a = -\frac{d\mathbf{W}}{d\mathbf{p}}\tau$ , depending on the cable tensions; The passive stiffness matrix,  $\mathbf{K}_p = -\mathbf{W}\frac{d\tau}{d\mathbf{p}}$ , depending on the cable properties.

$$\mathbf{K} = -\frac{d\mathbf{W}\tau}{d\mathbf{p}} = \mathbf{K}_a + \mathbf{K}_p = -\frac{d\mathbf{W}}{d\mathbf{p}}\tau - \mathbf{W}\frac{d\tau}{d\mathbf{p}} \quad (2.67)$$

### Passive Stiffness Matrix Computation

The cable elasticity is modelled according to the linear spring model, where  $k_i$  represents the elastic coefficient of the  $i$ -th cable and  $\delta l_i$  the length variation of the cable induced by the cable tension  $\tau_i$ .

$$\tau_i = k_i \delta l_i \quad (2.68)$$

The elastic behaviour of all the cables is thus defined as follows:

$$\boldsymbol{\tau} = \mathbf{K}_l \boldsymbol{\delta l} \quad (2.69)$$

where the general cables-stiffness matrix,  $\mathbf{K}_l = \text{diag}\{k_1, k_2, \dots, k_m\}$ , is a diagonal matrix containing the elastic coefficients  $k_i, i = 1, \dots, m$  of all the cables,  $\boldsymbol{\delta l} = [\delta l_1, \dots, \delta l_m]^T$  is the vector containing the length variations of all the cables of the CDPR.

Taking into account Eq. (2.21) and Eq. (2.69), where  $\mathbf{l} = [l_1, \dots, l_m]^T$  is the vector of the cable lengths, the passive stiffness matrix  $\mathbf{K}_p$  takes the following form:

$$\mathbf{K}_p = -\mathbf{W}\mathbf{K}_l \frac{d\mathbf{l}}{d\mathbf{p}} = \mathbf{W}\mathbf{K}_l \mathbf{W}^T = \sum_{i=1}^m k_i \begin{bmatrix} \mathbf{d}_i^b \mathbf{d}_i^{b^T} & \mathbf{d}_i^b \mathbf{d}_i^{b^T} \hat{\mathbf{b}}_i^{r^T} \\ \hat{\mathbf{b}}_i^r \mathbf{d}_i^b \mathbf{d}_i^{b^T} & \hat{\mathbf{b}}_i^r \mathbf{d}_i^b \mathbf{d}_i^{b^T} \hat{\mathbf{b}}_i^{r^T} \end{bmatrix} \quad (2.70)$$

$\hat{\mathbf{b}}_i^r$  represents the cross product matrix of vector  $\mathbf{b}_i^r = [b_{i,x}^r, b_{i,y}^r, b_{i,z}^r]^T$ :

$$\hat{\mathbf{b}}_i^r = \begin{bmatrix} 0 & -b_{i,z}^r & b_{i,y}^r \\ b_{i,z}^r & 0 & -b_{i,x}^r \\ -b_{i,y}^r & b_{i,x}^r & 0 \end{bmatrix} \quad (2.71)$$

### Active Stiffness Matrix Computation

Hereafter, the active stiffness matrix,  $\mathbf{K}_a$ , will be developed:

$$\frac{d\mathbf{W}}{d\mathbf{p}} \boldsymbol{\tau} = \sum_{i=1}^m \frac{d\mathbf{w}_i}{d\mathbf{p}} \tau_i \quad (2.72)$$

The Jacobian matrix  $\frac{d\mathbf{w}_i}{d\mathbf{p}}$  is decomposed as follows:

$$\frac{d\mathbf{w}_i}{d\mathbf{p}} = \begin{bmatrix} \frac{d\mathbf{d}_i^b}{d\mathbf{t}} & \frac{d\mathbf{d}_i^b}{d\mathbf{r}} \\ \frac{d(\mathbf{b}_i^r \times \mathbf{d}_i^b)}{d\mathbf{t}} & \frac{d(\mathbf{b}_i^r \times \mathbf{d}_i^b)}{d\mathbf{r}} \end{bmatrix} \quad (2.73)$$

The differential form of Eq. (2.1) is:

$$d\mathbf{l}_i^b = -d\mathbf{t} - d\mathbf{b}_i^r = -d\mathbf{t} + \mathbf{b}_i^r \times d\mathbf{r} = -d\mathbf{b}_i^b \quad (2.74)$$

Alternatively, the IGM can be differentiated as follows:

$$d\mathbf{l}_i^b = d(l_i \mathbf{d}_i^b) = dl_i \mathbf{d}_i^b + l_i d\mathbf{d}_i^b \quad (2.75)$$

Taking into account that  $l_i^2 = \mathbf{l}_i^{b^T} \mathbf{l}_i^b$ , we can conclude that  $2l_i dl_i = 2\mathbf{l}_i^{b^T} d\mathbf{l}_i^b$ . Hence:

$$dl_i = \frac{\mathbf{l}_i^{b^T}}{l_i} d\mathbf{l}_i^b = \mathbf{d}_i^{b^T} d\mathbf{l}_i^b = \mathbf{d}_i^{b^T} (-d\mathbf{t} + \mathbf{b}_i^r \times d\mathbf{r}) = -\mathbf{d}_i^{b^T} d\mathbf{b}_i^b \quad (2.76)$$

Comparing Eq. (2.74) and Eq. (2.75) we obtain the following expression:

$$-d\mathbf{b}_i^b = -\mathbf{d}_i^{bT} d\mathbf{b}_i^b + l_i^b d\mathbf{d}_i^b \quad (2.77)$$

Observing Eq. (2.77) we can obtain the first components of matrix  $\mathbf{K}_a$  of Eq. (2.73):

$$d\mathbf{d}_i^b = -\frac{1}{l_i} \left( \mathbf{I}_{3,3} - \mathbf{d}_i^b \mathbf{d}_i^{bT} \right) d\mathbf{b}_i^b = -\frac{1}{l_i} \left( \mathbf{I}_{3,3} - \mathbf{d}_i^b \mathbf{d}_i^{bT} \right) (d\mathbf{t} - \mathbf{b}_i^r \times d\mathbf{r}) \quad (2.78)$$

These components are:

$$\frac{d\mathbf{d}_i^b}{d\mathbf{t}} = -\frac{1}{l_i} \left( \mathbf{I}_{3,3} - \mathbf{d}_i^b \mathbf{d}_i^{bT} \right) \quad (2.79)$$

$$\frac{d\mathbf{d}_i^b}{d\mathbf{r}} = \frac{1}{l_i} \left( \mathbf{I}_{3,3} - \mathbf{d}_i^b \mathbf{d}_i^{bT} \right) \hat{\mathbf{b}}_i^r \quad (2.80)$$

The missing components of the active stiffness matrix  $\mathbf{K}_a$  in Eq. (2.73) are obtained by differentiating  $\mathbf{b}_i^r \times \mathbf{d}_i^b$ , namely,

$$\begin{aligned} d(\mathbf{b}_i^r \times \mathbf{d}_i^b) &= d\mathbf{b}_i^r \times \mathbf{d}_i^b + \mathbf{b}_i^r \times d\mathbf{d}_i^b = (d\mathbf{r} \times \mathbf{b}_i^r) \times \mathbf{d}_i^b + \mathbf{b}_i^r \times d\mathbf{d}_i^b = \\ &= \mathbf{d}_i^b \times \mathbf{b}_i^r \times d\mathbf{r} - \frac{1}{l_i} \mathbf{b}_i^r \times \left( \mathbf{I}_{3,3} - \mathbf{d}_i^b \mathbf{d}_i^{bT} \right) (d\mathbf{t} - \mathbf{b}_i^r \times d\mathbf{r}) \end{aligned} \quad (2.81)$$

These components are:

$$\frac{d(\mathbf{b}_i^r \times \mathbf{d}_i^b)}{d\mathbf{t}} = -\frac{1}{l_i} \hat{\mathbf{b}}_i^r \left( \mathbf{I}_{3,3} - \mathbf{d}_i^b \mathbf{d}_i^{bT} \right) \quad (2.82)$$

$$\frac{d(\mathbf{b}_i^r \times \mathbf{d}_i^b)}{d\mathbf{r}} = \left[ \hat{\mathbf{d}}_i^b + \frac{\hat{\mathbf{b}}_i^r}{l_i} \left( \mathbf{I}_{3,3} - \mathbf{d}_i^b \mathbf{d}_i^{bT} \right) \right] \hat{\mathbf{b}}_i^r \quad (2.83)$$

where  $\hat{\mathbf{d}}_i^b$  denotes the cross product matrix of vector  $\mathbf{d}_i^b$ .

Hence, the active stiffness matrix  $\mathbf{K}_a$  takes the form:

$$\mathbf{K}_a = -\sum_{i=1}^m \tau_i \begin{bmatrix} -\frac{1}{l_i} \left( \mathbf{I}_{3,3} - \mathbf{d}_i^b \mathbf{d}_i^{bT} \right) & \frac{1}{l_i} \left( \mathbf{I}_{3,3} - \mathbf{d}_i^b \mathbf{d}_i^{bT} \right) \hat{\mathbf{b}}_i^r \\ -\frac{1}{l_i} \hat{\mathbf{b}}_i^r \left( \mathbf{I}_{3,3} - \mathbf{d}_i^b \mathbf{d}_i^{bT} \right) & \left[ \hat{\mathbf{d}}_i^b + \frac{\hat{\mathbf{b}}_i^r}{l_i} \left( \mathbf{I}_{3,3} - \mathbf{d}_i^b \mathbf{d}_i^{bT} \right) \right] \hat{\mathbf{b}}_i^r \end{bmatrix} \quad (2.84)$$

### 2.3.2 Linear Non-Rigid Cable Model with Pulleys

The elasto-static model provided in Sec. 2.3.1 has been improved by taking into account the effect of pulleys. Once again, the stiffness is described through the stiffness matrix of Eq. (2.66) and its components.

#### Passive Stiffness Matrix Computation

The structure of the passive stiffness matrix does not present major modifications with respect to Eq. (2.70):

$$\mathbf{K}_p = \sum_{i=1}^m k_i \begin{bmatrix} \mathbf{D}_i^b \mathbf{D}_i^{bT} & \mathbf{D}_i^b \mathbf{D}_i^{bT} \hat{\mathbf{b}}_i^{bT} \\ \hat{\mathbf{b}}_i^b \mathbf{D}_i^b \mathbf{D}_i^{bT} & \hat{\mathbf{b}}_i^b \mathbf{D}_i^b \mathbf{D}_i^{bT} \hat{\mathbf{b}}_i^{bT} \end{bmatrix} \quad (2.85)$$

### Active Stiffness Matrix Computation

However, the active stiffness matrix is quite different. The components of the Jacobian presented in Eq. (2.73) should be computed. This computation requires the derivation of a set of unit vectors, including  $d\mathbf{D}_i^b$ :

$$d\mathbf{D}_i^b = \frac{d\mathbf{L}_i^b - \left(d\mathbf{L}_i^{bT} \mathbf{D}_i^b\right) \mathbf{D}_i^b}{l_i} \quad (2.86)$$

The IGM described in Eq. (2.8) is differentiated as follows:

$$d\mathbf{L}_i^b = -r_p \left(\mathbf{z}_i^b + \mathbf{D}_i^b\right) \times d\mathbf{y}_i^b - r_p d\mathbf{D}_i^b \times \mathbf{y}_i^b - d\mathbf{b}_i^b \quad (2.87)$$

with:

$$\mathbf{y}_i^b = \frac{\mathbf{l}_i^b \times \mathbf{z}_i^b}{N_i} \quad (2.88)$$

Equation (2.88) is differentiated according to the formula presented in Eq. (2.86) and Eq. (2.87):

$$d\mathbf{y}_i^b = \frac{d\mathbf{N}_i^b - \left(d\mathbf{N}_i^{bT} \mathbf{y}_i^b\right) \mathbf{y}_i^b}{N_i} \quad (2.89)$$

Reminding that  $\mathbf{N}_i^b = \mathbf{l}_i^b \times \mathbf{z}_i^b$  and that the unit vector  $\mathbf{z}_i^b$  is constant, the differentiation of  $\mathbf{N}_i^b$  is:

$$d\mathbf{N}_i^b = d\mathbf{l}_i^b \times \mathbf{z}_i^b = \mathbf{z}_i^b \times d\mathbf{b}_i^b \quad (2.90)$$

Hence, Eq. (2.89) is rewritten as follows:

$$N_i d\mathbf{y}_i^b = \mathbf{z}_i^b \times d\mathbf{b}_i^b - \left(\left(\mathbf{z}_i^b \times d\mathbf{b}_i^b\right)^T \mathbf{y}_i^b\right) \mathbf{y}_i^b \quad (2.91)$$

We can notice that  $N_i d\mathbf{y}_i^b$  is the component of  $\mathbf{z}_i^b \times d\mathbf{b}_i^b$  normal to  $\mathbf{y}_i^b$ , and consequently parallel to  $\mathbf{x}_i^b$ :

$$N_i d\mathbf{y}_i^b = \left(\left(\mathbf{z}_i^b \times d\mathbf{b}_i^b\right)^T \mathbf{x}_i^b\right) \mathbf{x}_i^b = \left(\left(\mathbf{x}_i^b \times \mathbf{z}_i^b\right)^T d\mathbf{b}_i^b\right) \mathbf{x}_i^b = -\left(\mathbf{y}_i^{bT} d\mathbf{b}_i^b\right) \mathbf{x}_i^b \quad (2.92)$$

Consequently, according to Eq. (2.92), the differentiation of unit vector  $\mathbf{y}_i^b$  is:

$$d\mathbf{y}_i^b = -\frac{\mathbf{y}_i^{bT} d\mathbf{b}_i^b}{N_i} \mathbf{x}_i^b \quad (2.93)$$

The differential of  $\mathbf{y}_i^b$  is substituted in Eq. (2.87):

$$d\mathbf{L}_i^b = r_p \left(\mathbf{z}_i^b + \mathbf{D}_i^b\right) \times \left(\frac{\mathbf{y}_i^{bT} d\mathbf{b}_i^b}{N_i} \mathbf{x}_i^b\right) - r_p d\mathbf{D}_i^b \times \mathbf{y}_i^b - d\mathbf{b}_i^b \quad (2.94)$$

Hence, the projection of  $d\mathbf{L}_i^b$  on  $\mathbf{D}_i^b$  is expressed as:

$$d\mathbf{L}_i^{bT} \mathbf{D}_i^b = r_p \left( (\mathbf{z}_i^b + \mathbf{D}_i^b) \times \left( \frac{\mathbf{y}_i^{bT} d\mathbf{b}_i^b}{N_i} \mathbf{x}_i^b \right) \right)^T \mathbf{D}_i^b - r_p \left( d\mathbf{D}_i^b \times \mathbf{y}_i^b \right)^T \mathbf{D}_i^b - d\mathbf{b}_i^{bT} \mathbf{D}_i^b \quad (2.95)$$

Considering that vector  $(\mathbf{z}_i^b + \mathbf{D}_i^b) \times \mathbf{x}_i^b$  is parallel to  $\mathbf{y}_i^b$ , the first term of the previous equation is null. Thus, post-multiplying Eq. (2.95) by  $\mathbf{D}_i^b$  we obtain:

$$\left( d\mathbf{L}_i^{bT} \mathbf{D}_i^b \right) \mathbf{D}_i^b = -r_p \left( \left( d\mathbf{D}_i^b \times \mathbf{y}_i^b \right)^T \mathbf{D}_i^b \right) \mathbf{D}_i^b - \left( d\mathbf{b}_i^{bT} \mathbf{D}_i^b \right) \mathbf{D}_i^b = -r_p d\mathbf{D}_i^b \times \mathbf{y}_i^b - \left( d\mathbf{b}_i^{bT} \mathbf{D}_i^b \right) \mathbf{D}_i^b \quad (2.96)$$

As a matter of fact, since  $\mathbf{D}_i^b$  is a unit vector, i.e.  $d\mathbf{D}_i^{bT} \mathbf{D}_i^b = 0$  and  $\mathbf{D}_i^{bT} \mathbf{D}_i^b = 1$ , the projection of  $(d\mathbf{D}_i^b \times \mathbf{y}_i^b)^T \mathbf{D}_i^b$  on  $\mathbf{D}_i^b$  is equal to:

$$\left( \left( d\mathbf{D}_i^b \times \mathbf{y}_i^b \right)^T \mathbf{D}_i^b \right) \mathbf{D}_i^b = \left( \|d\mathbf{D}_i^b \times \mathbf{y}_i^b\|_2 \mathbf{D}_i^{bT} \mathbf{D}_i^b \right) \mathbf{D}_i^b = \|d\mathbf{D}_i^b \times \mathbf{y}_i^b\|_2 \mathbf{D}_i^b = d\mathbf{D}_i^b \times \mathbf{y}_i^b \quad (2.97)$$

The differential unit vector  $d\mathbf{D}_i^b$  is obtained substituting Eq. (2.94) and Eq. (2.96) into Eq. (2.86)

$$d\mathbf{D}_i^b = \frac{1}{l_i} \left[ \frac{r_p}{N_i} \left( \mathbf{y}_i^{bT} d\mathbf{b}_i^b \right) (\mathbf{z}_i^b + \mathbf{D}_i^b) \times \mathbf{x}_i^b - d\mathbf{b}_i^b + \left( d\mathbf{b}_i^{bT} \mathbf{D}_i^b \right) \mathbf{D}_i^b \right] \quad (2.98)$$

By definition,  $\mathbf{z}_i^b \times \mathbf{x}_i^b = \mathbf{y}_i^b$ . The triple cross product  $\mathbf{D}_i^b \times \mathbf{x}_i^b = \mathbf{D}_i^b \times (\mathbf{y}_i^b \times \mathbf{z}_i^b)$  can be developed with the triple cross product formula, concluding that  $\mathbf{D}_i^b \times \mathbf{x}_i^b = \left( \mathbf{D}_i^{bT} \mathbf{z}_i^b \right) \mathbf{y}_i^b$ . Finally, the differential vector  $d\mathbf{D}_i^b$  takes the form

$$\begin{aligned} d\mathbf{D}_i^b &= \frac{1}{l_i} \left[ \frac{r_p}{N_i} \left( \mathbf{y}_i^{bT} d\mathbf{b}_i^b \right) \left( \mathbf{y}_i^b + \left( \mathbf{D}_i^{bT} \mathbf{z}_i^b \right) \mathbf{y}_i^b \right) + \mathbf{D}_i^b \left( \mathbf{D}_i^{bT} d\mathbf{b}_i^b \right) - d\mathbf{b}_i^b \right] = \\ &= \frac{1}{l_i} \left[ \frac{r_p}{N_i} \mathbf{y}_i^b \left( 1 + \mathbf{D}_i^{bT} \mathbf{z}_i^b \right) \mathbf{y}_i^{bT} + \mathbf{D}_i^b \mathbf{D}_i^{bT} - \mathbf{I}_3 \right] d\mathbf{b}_i^b = \\ &= \frac{1}{l_i} \left[ \frac{r_p}{N_i} \mathbf{y}_i^b \left( 1 + \mathbf{D}_i^{bT} \mathbf{z}_i^b \right) \mathbf{y}_i^{bT} + \mathbf{D}_i^b \mathbf{D}_i^{bT} - \mathbf{I}_3 \right] \left( dt - \hat{\mathbf{b}}_i^r dr \right) \end{aligned} \quad (2.99)$$

Equation (2.99) leads to the first components of the active stiffness matrix  $\mathbf{K}_a$ :

$$\frac{d\mathbf{D}_i^b}{dt} = -\frac{1}{l_i} \left( \mathbf{I}_3 - \mathbf{D}_i^b \mathbf{D}_i^{bT} - \mathbf{H} \right) \quad (2.100)$$

$$\frac{d\mathbf{D}_i^b}{dr} = \frac{1}{l_i} \left( \mathbf{I}_3 - \mathbf{D}_i^b \mathbf{D}_i^{bT} - \mathbf{H} \right) \hat{\mathbf{b}}_i^r \quad (2.101)$$

where  $\mathbf{H} = \left[ \frac{r_p}{N_i} \mathbf{y}_i^b \left( 1 + \mathbf{D}_i^{bT} \mathbf{z}_i^b \right) \mathbf{y}_i^{bT} \right]$ . The missing components of the active stiffness matrix,  $\mathbf{K}_a$ , are obtained upon differentiation of  $\mathbf{b}_i^r \times \mathbf{D}_i^b$ :

$$\begin{aligned} d \left( \mathbf{b}_i^r \times \mathbf{D}_i^b \right) &= d\mathbf{b}_i^r \times \mathbf{D}_i^b + \mathbf{b}_i^r \times d\mathbf{D}_i^b = \left( dr \times \mathbf{b}_i^r \right) \times \mathbf{D}_i^b + \mathbf{b}_i^r \times d\mathbf{D}_i^b = \\ &= \hat{\mathbf{D}}_i^b \hat{\mathbf{b}}_i^r dr + \frac{\hat{\mathbf{b}}_i^r}{l_i} \left( \mathbf{H} + \mathbf{D}_i^b \mathbf{D}_i^{bT} - \mathbf{I}_3 \right) \left( dt - \hat{\mathbf{b}}_i^r dr \right) \end{aligned} \quad (2.102)$$

where  $\hat{\mathbf{D}}_i^b$  denotes the cross product matrix of vector  $\mathbf{D}_i^b$ . The last components of the active stiffness matrix are:

$$\frac{d(\mathbf{b}_i^r \times \mathbf{d}_i^b)}{dt} = -\frac{\hat{\mathbf{b}}_i^r}{l_i} (\mathbf{I}_3 - \mathbf{D}_i^b \mathbf{D}_i^{bT} - \mathbf{H}) \quad (2.103)$$

$$\frac{d(\mathbf{b}_i^r \times \mathbf{d}_i^b)}{dr} = \left[ \hat{\mathbf{D}}_i^b + \frac{\hat{\mathbf{b}}_i^r}{l_i} (\mathbf{I}_3 - \mathbf{D}_i^b \mathbf{D}_i^{bT} - \mathbf{H}) \right] \hat{\mathbf{b}}_i^r \quad (2.104)$$

As a result, the active stiffness matrix  $\mathbf{K}_a$  is expressed as:

$$\mathbf{K}_a = -\sum_{i=1}^m \tau_i \begin{bmatrix} -\frac{1}{l_i} (\mathbf{I}_3 - \mathbf{D}_i^b \mathbf{D}_i^{bT} - \mathbf{H}) & \frac{1}{l_i} (\mathbf{I}_3 - \mathbf{D}_i^b \mathbf{D}_i^{bT} - \mathbf{H}) \hat{\mathbf{b}}_i^r \\ -\frac{\hat{\mathbf{b}}_i^r}{l_i} (\mathbf{I}_3 - \mathbf{D}_i^b \mathbf{D}_i^{bT} - \mathbf{H}) & \left[ \hat{\mathbf{D}}_i^b + \frac{\hat{\mathbf{b}}_i^r}{l_i} (\mathbf{I}_3 - \mathbf{D}_i^b \mathbf{D}_i^{bT} - \mathbf{H}) \right] \hat{\mathbf{b}}_i^r \end{bmatrix} \quad (2.105)$$

### 2.3.3 Sagging Cable Model

The sagging cable description requires to define a novel stiffness model adapted to this cable profile. The stiffness is still described by the stiffness matrix defined in Eq. (2.66). For CDPRs with sagging cables, the static equilibrium is described by Eq. (2.50) and Eq. (2.51). The static equilibrium is rewritten as follows:

$$\sum_{i=1}^m \begin{bmatrix} \mathbf{R}_i \\ \hat{\mathbf{b}}_i^r \mathbf{R}_i \end{bmatrix} \mathbf{F}_i - \mathbf{w}_e = 0 \quad (2.106)$$

Substituting Eq. (2.106) into Eq. (2.66), the stiffness matrix is decomposed into the active and passive stiffness matrices:

$$\mathbf{K} = \sum_{i=1}^m \frac{d}{d\mathbf{p}} (\mathbf{W}_i \mathbf{F}_i) = \sum_{i=1}^m \frac{d\mathbf{W}_i}{d\mathbf{p}} \mathbf{F}_i + \sum_{i=1}^m \mathbf{W}_i \frac{d\mathbf{F}_i}{d\mathbf{p}} \quad (2.107)$$

where:

$$\mathbf{W}_i = \begin{bmatrix} \mathbf{R}_i \\ \hat{\mathbf{b}}_i^r \mathbf{R}_i \end{bmatrix} \quad (2.108)$$

#### Passive Stiffness Matrix

According to Eq. (2.107), it has to be noted that vectors  $\mathbf{F}_i$  are differentiated with respect to the moving platform pose vector  $\mathbf{p}$ . Since vectors  $\mathbf{F}_i$  are expressed in the local frames  $\mathcal{F}_i$ , a projection is required:

$$\frac{d\mathbf{F}_i}{d\mathbf{p}} = \frac{d\mathbf{F}_i}{db_i^l} \frac{db_i^l}{d\mathbf{p}} \quad (2.109)$$

The Jacobian  $\frac{db_i^l}{d\mathbf{p}}$  is computed considering the following equation:

$$\dot{\mathbf{b}}_i^l = \mathbf{R}_i^T (\dot{\mathbf{t}} - \hat{\mathbf{b}}_i^l \omega) = \begin{bmatrix} \mathbf{R}_i^T & -\mathbf{R}_i^T \hat{\mathbf{b}}_i^l \end{bmatrix} \begin{bmatrix} \dot{\mathbf{t}} \\ \omega \end{bmatrix} \quad (2.110)$$

where the twist of point  $B_i$  is defined, with respect to frame  $\mathcal{F}_i$ , by vector  $\mathbf{b}_i^l$ . Considering sufficiently small displacements and rotations, Eq. (2.110) is rewritten in the differential form:

$$\delta \mathbf{b}_i^l = \mathbf{W}_i^T \delta \mathbf{p} \quad (2.111)$$

from which it is possible to deduce  $\frac{d\mathbf{b}_i^l}{d\mathbf{p}} = \mathbf{W}_i^T$ .

Thus, the passive stiffness  $\mathbf{K}_p$  is detailed as follows:

$$\mathbf{K}_p = \sum_{i=1}^m \mathbf{W}_i \frac{d\mathbf{F}_i}{d\mathbf{b}_i^l} \mathbf{W}_i^T \quad (2.112)$$

### Cable Stiffness Matrix

The passive stiffness matrix contains the Jacobian  $\frac{d\mathbf{F}_i}{d\mathbf{b}_i^l}$ . This Jacobian represents the stiffness matrix  $\mathbf{K}_i$  of the  $i$ -th cable expressed in the local reference frame  $\mathcal{F}_i$ :

$$d\mathbf{F}_i = \mathbf{K}_i d\mathbf{b}_i^l \quad (2.113)$$

The matrix  $\mathbf{K}_i$  is derived from the corresponding compliant matrix:

$$\mathbf{C}_i = \mathbf{K}_i^{-1} = \left( \frac{d\mathbf{F}_i}{d\mathbf{b}_i^l} \right)^{-1} = \begin{bmatrix} \frac{\partial b_{x,i}^l}{\partial F_{x,i}} & \frac{\partial b_{x,i}^l}{\partial F_{y,i}} & \frac{\partial b_{x,i}^l}{\partial F_{z,i}} \\ \frac{\partial b_{y,i}^l}{\partial F_{x,i}} & \frac{\partial b_{y,i}^l}{\partial F_{y,i}} & \frac{\partial b_{y,i}^l}{\partial F_{z,i}} \\ \frac{\partial b_{z,i}^l}{\partial F_{x,i}} & \frac{\partial b_{z,i}^l}{\partial F_{y,i}} & \frac{\partial b_{z,i}^l}{\partial F_{z,i}} \end{bmatrix} = \begin{bmatrix} C_i^{11} & 0 & C_i^{13} \\ 0 & 0 & 0 \\ C_i^{31} & 0 & C_i^{33} \end{bmatrix} \quad i = 1, \dots, m \quad (2.114)$$

The components of matrix  $\mathbf{C}_i$  is computed from Eq. (2.47) and Eq. (2.49) as follows [KZW06]:

$$C_i^{11} = \frac{L_{0,i}}{EA_0} + \frac{1}{\rho_0 g} \left[ \frac{F_{x,i}}{\|\mathbf{F}_{x,i}\|} \left( \sinh^{-1} \left( \frac{F_{z,i}}{F_{x,i}} \right) - \sinh^{-1} \left( \frac{-F_{z,i}^0}{F_{x,i}} \right) \right) - \frac{F_{z,i}}{\|\mathbf{F}_i\|} - \frac{F_{z,i}^0}{\|\mathbf{F}_i^0\|} \right] \quad (2.115)$$

$$C_i^{13} = \frac{1}{\rho_0 g} \left( \frac{F_{x,i}}{\|\mathbf{F}_i\|} - \frac{F_{x,i}}{\|\mathbf{F}_i^0\|} \right) \quad (2.116)$$

$$C_i^{32} = \frac{1}{\rho_0 g} \left( \frac{F_{x,i}}{\|\mathbf{F}_i\|} - \frac{F_{x,i}}{\|\mathbf{F}_i^0\|} \right) \quad (2.117)$$

$$C_i^{33} = \frac{L_{0,i}}{EA_0} + \frac{1}{\rho_0 g} \left( \frac{F_{z,i}}{\|\mathbf{F}_i\|} + \frac{F_{z,i}^0}{\|\mathbf{F}_i^0\|} \right) \quad (2.118)$$

where  $F_{z,i}^0 = \rho_0 g L_{0,i} - F_{z,i}$  represents the vertical component of the  $i$ -th cable tension at point  $A_i$ . The cable tension at point  $A_i$  is defined as  $\mathbf{F}_i^0 = [F_{x,i}^0, F_{y,i}^0, F_{z,i}^0]$ .

In order to compute the stiffness matrix  $\mathbf{K}_i$  it is possible to use the following formula:

$$\mathbf{K}_i = \frac{1}{C_i^{11}C_i^{33} - C_i^{13}C_i^{31}} \begin{bmatrix} C_i^{33} & 0 & -C_i^{31} \\ 0 & 0 & 0 \\ -C_i^{13} & 0 & C_i^{11} \end{bmatrix} \quad (2.119)$$

### Active Stiffness Matrix

The active stiffness matrix is decomposed as follows:

$$\mathbf{K}_a = \sum_{i=1}^m \frac{dW_i}{d\mathbf{p}} \mathbf{F}_i = \sum_{i=1}^m \begin{bmatrix} \frac{d\mathbf{R}_i}{d\mathbf{p}} \\ d(\hat{\mathbf{b}}_i^r \mathbf{R}_i) \\ \frac{d\mathbf{p}}{d\mathbf{p}} \end{bmatrix} \mathbf{F}_i \quad (2.120)$$

The first term of Eq. (2.120) is decomposed as:

$$\frac{d\mathbf{R}_i}{d\mathbf{p}} \mathbf{F}_i = \frac{d\mathbf{R}_i}{d\theta_i} \frac{d\theta_i}{d\mathbf{p}} \mathbf{F}_i = \sum_{j=1}^3 \frac{d\mathbf{R}_{i,j}}{d\theta_i} \frac{d\theta_i}{d\mathbf{p}}^T F_{i,j} \quad (2.121)$$

where  $\mathbf{R}_{i,j}$  represents the  $j$ -th column of  $\mathbf{R}_i$ . The derivative of  $\mathbf{R}_i$  with respect to  $\theta_i$  is:

$$\frac{d\mathbf{R}_i}{d\theta_i} = \begin{bmatrix} -\sin \theta_i & -\cos \theta_i & 0 \\ \cos \theta_i & -\sin \theta_i & 0 \\ 0 & 0 & 0 \end{bmatrix} \quad (2.122)$$

and the differential  $\frac{d\theta_i}{d\mathbf{p}}$  is:

$$\frac{d\theta_i}{d\mathbf{p}} = \begin{bmatrix} \frac{l_{y,i}}{l_{x,i}^2 + l_{y,i}^2} & -\frac{l_{x,i}}{l_{x,i}^2 + l_{y,i}^2} & 0 & \frac{b_{z,i}^b l_{x,i}}{l_{x,i}^2 + l_{y,i}^2} & \frac{b_{z,i}^b l_{y,i}}{l_{x,i}^2 + l_{y,i}^2} & -\frac{b_{x,i}^b l_{x,i} + b_{y,i}^b l_{y,i}}{l_{x,i}^2 + l_{y,i}^2} \end{bmatrix}^T \quad (2.123)$$

The Jacobian matrix  $\frac{d(\hat{\mathbf{b}}_i^r \mathbf{R}_i)}{d\mathbf{p}}$  is decomposed into two terms:

$$\sum_{i=1}^m \left( \frac{d(\hat{\mathbf{b}}_i^r \mathbf{R}_i)}{d\mathbf{p}} \right) \mathbf{F}_i = \sum_{i=1}^m \frac{d\hat{\mathbf{b}}_i^r}{d\mathbf{p}} \mathbf{R}_i \mathbf{F}_i + \sum_{i=1}^m \hat{\mathbf{b}}_i^r \frac{d\mathbf{R}_i}{d\mathbf{p}} \mathbf{F}_i \quad (2.124)$$

These terms are developed as follows:

$$\frac{d\hat{\mathbf{b}}_i^r}{d\mathbf{p}} \mathbf{R}_i \mathbf{F}_i = \sum_{j=1}^3 \left[ \frac{d\hat{\mathbf{b}}_i^r}{dt_x} \mathbf{R}_{i,j}, \frac{d\hat{\mathbf{b}}_i^r}{dt_y} \mathbf{R}_{i,j}, \frac{d\hat{\mathbf{b}}_i^r}{dt_z} \mathbf{R}_{i,j}, \frac{d\hat{\mathbf{b}}_i^r}{dr_x} \mathbf{R}_{i,j}, \frac{d\hat{\mathbf{b}}_i^r}{dr_y} \mathbf{R}_{i,j}, \frac{d\hat{\mathbf{b}}_i^r}{dr_z} \mathbf{R}_{i,j} \right] F_{i,j} \quad (2.125)$$

$$\hat{\mathbf{b}}_i^r \frac{d\mathbf{R}_i}{d\mathbf{p}} \mathbf{F}_i = \sum_{j=1}^3 \hat{\mathbf{b}}_i^r \frac{d\mathbf{R}_{i,j}}{d\theta_i} \frac{d\theta_i}{d\mathbf{p}}^T F_{i,j} \quad (2.126)$$

A detailed development of the active stiffness matrix is described in App. A.3.

## 2.4 Conclusions

This chapter dealt with the modelling of CDPRs, which is the basis for the workspace analysis, the design and the reconfiguration procedures described in the following chapters. Cables have been modelled using the massless and the sagging models. Massless cables have been used to model the static, kinematic and dynamic behaviour of CDPRs, when the effect of the cable mass is negligible [RGL98, LGCH13]. The dynamic model has been developed taking into account the actuation and the transmission systems, including the dynamics of the motors, the gearboxes and the winches. The inertia and the efficiency coefficients of these components have been considered too.

When the cable mass can not be neglected, sagging cables have been used to model the geometrico-static behaviour of CDPRs. This model is more accurate, despite its increasing complexity due to non-linearities. The coupling of the geometric and static problems has been treated. A strategy to solve the foregoing problem for a given pose or a given path of the moving platform has been described, developing the solutions proposed in [RGK<sup>+</sup>09, YCD15].

The elasto-static behaviour of the cables has been considered too. The massless elastic cable model, for sufficiently small pose displacements, has been derived with a more formal approach than the ones proposed in the literature [BK05b, SRK13]. The model has been developed for a spatial CDPR while considering the influence of the pulleys. Then, the elasto-static model of a CDPR with sagging cables has been derived. The model considers the effects of both the passive and the active stiffness matrices, while the active stiffness matrix is usually neglected in the literature. The proposed model is similar to the ones described in [Ars13, NG14a], despite it has been developed according to a different strategy.

All the models described in this chapter are valid for both CDPRs and RCDPRs.

# Chapter 3

## Workspace Analysis

### Chapter Content

3.1	Mathematical Definition of Existing Workspaces . . . . .	44
3.2	Twist Feasible Workspace (TFW) . . . . .	48
3.3	Dynamic Feasible Workspace (DFW) . . . . .	50
3.4	Case Study . . . . .	51
3.5	Conclusions . . . . .	54

One of the main differences between CDPRs and classical parallel robots is the unilateral nature of the cables. The latter are only able to push the moving platform while rigid links can apply bidirectional forces on the moving platform. Consequently, the static and dynamic equilibria of the CDPR moving platform can be assured only by non-negative cable tensions. Moreover, CDPRs can be prone to collisions with the surrounding environment and to cable interferences. Both cable collisions and interferences should usually be avoided to prevent damages to the CDPR and to objects in the working environment. These requirements form a set of constraints, to which supplementary constraints may be added, that define the CDPR workspace.

The analysis of the moving platform equilibrium can be performed by means of the static, kinematic and dynamic models of the CDPR. Section 3.1 provides a formal description of the *Wrench Closure Workspace* (WCW), the *Wrench Feasible Workspace* (WFW) and other CDPR workspaces, including the static, the dynamic, the interference-free and the collision-free workspaces, which have already been defined in the literature. A pose of the moving platform belongs to the WCW if and only if the static equilibrium of the moving platform is assured by non-negative cables tensions, whichever is the external wrench on the platform. The WFW is defined as the set of poses of the moving platform where the static equilibrium is satisfied with respect to a set of external wrenches applied on the moving platform and the cable tension bounds [BREU06, BGM08, GDM11].

The *Static Feasible Workspace* (SFW) represents a particular case of the WFW, where only the gravity wrench due to the weight of the moving platform is considered. The *Interference Free Workspace* (IFW) consists of the set of accessible poses of the moving platform where the cables are not colliding with each other. Similarly, the *Collision Free Workspace* (CFW) consists of the set of accessible poses of the moving platform where the cables are not colliding with the surrounding environment.

The static equilibrium of the moving platform is mostly influenced by the geometry of the CDPR, the properties of the cables, the motor nominal torques and speeds, and the winch diameters. These factors influence

the kinematic constraints of the CDPR too. In Sec. 3.2, the kinematic constraints of the moving platform are investigated by means of the *Twist Feasible Workspace* (TWF). This novel workspace corresponds to the moving platform poses where a prescribed set of moving platform twists is feasible, under cable coiling and uncoiling speed limitations.

The *Dynamic Feasible Workspace* (DFW) was defined by Barrette *et al.* in [BG05]. It consists of the moving platform poses which are able to guarantee a given moving platform acceleration vector. The proposed DFW does not take into account the influence of the external wrenches acting on the moving platform while considering the mass and inertia of the moving platform. In this chapter, a new formulation of the DFW, the so called *Improved Dynamic Feasible Workspace* (IDFW), has been introduced. According to the IDFW, both the moving platform inertia and the external wrenches applied to the moving platform are considered. Coriolis and centrifugal forces have been included in the dynamic model of the CDPR, assuming that the twist of the moving platform is constant. The IDFW will be presented in Sec. 3.3.

Section 3.4 investigates the different workspaces of a spatial CDPR. The layout of the CDPR is inspired by the CoGiRo prototype [Pro] while the dimensions are equal to the ones of the prototype developed in the framework of the IRT JV CAROCA project. The SFW, WFW, DFW and IDFW have been traced. The analysis highlights the differences between the dimensions of the four workspaces.

All the workspaces introduced in this chapter are valid for both CDPRs and RCDPRs.

## 3.1 Mathematical Definition of Existing Workspaces

The workspace of a classical serial or parallel manipulator depends on the robot geometry and its joint limits. However, several workspaces have been defined for CDPRs. Those workspaces depend on the robot geometry (i.e., the location of the exit points and the cable connection points on the moving platform), the cable tension limits, the external wrench applied on the moving platform, and the acceleration required to the moving platform. For CDPRs, several workspaces have been defined, as described in [EUV04]. A review of the most significant workspace previously defined in the literature is provided in this section.

### 3.1.1 Wrench Feasible Workspace (WFW)

#### Definition

The moving platform of the CDPR is assumed to be a rigid body with  $m$  cables attached to it. Each cable generates a wrench on the moving platform. The cable wrenches,  $\mathbf{w}_i = \hat{\mathbf{w}}_i \boldsymbol{\tau}_i, i = 1, \dots, m$ , where  $\hat{\mathbf{w}}_i, i = 1, \dots, m$  are the columns of the wrench matrix  $\mathbf{W}$ , have to balance the external wrench acting on the moving platform. The external wrench acting on the moving platform is assumed to be bounded:

$$f_{min} \leq f_x, f_y, f_z \leq f_{max} \quad (3.1)$$

$$m_{min} \leq m_x, m_y, m_z \leq m_{max} \quad (3.2)$$

The set of external wrenches applied to the moving platform, and that the cables have to balance, is defined as the *Required External Wrench Set* (REWS),  $[\mathbf{w}_e]_r$ . According to Eq. (3.1) and Eq. (3.2), the REWS is a hyperrectangle.

Cable tensions,  $\tau_i, i = 1, \dots, m$ , are also bounded. Due to the unilateral nature of the cables, cable tensions are always non-negative. A lower tension,  $\tau_{min} > 0$ , can be defined by the user in order to prestress the cables and to account for the fact that cables should not be slack. Cable tensions should be lower than an upper bound,  $\tau_{max}$ , associated to the physical characteristics of the cables, the nominal torque of the motors, and the breaking loads of various mechanical elements of the robot. The set of admissible cable tensions is defined hereafter as the *Available Cable Tension Set* (ACTS):

$$[\tau]_a = \{\tau \mid \tau_{min} \leq \tau_i \leq \tau_{max}, i = 1, \dots, m\} \quad (3.3)$$

Due to the previous constraints, cables can apply on the moving platform only a bounded set of wrenches, defined as the *Available Wrench Set* (AWS),  $[\mathbf{w}_e]_a$ . The AWS can be computed from the ACTS using Eq. (2.12). Considering that  $[\mathbf{w}_e]_a$  is the image of  $[\tau]_a$  under the linear mapping described by the wrench matrix  $\mathbf{W}$ ,  $[\mathbf{w}_e]_a$  belongs to a particular class of polytopes called zonotopes [BGM08].

Accordingly, the static equilibrium of the moving platform is feasible if and only if the moving platform pose is wrench feasible.

**Definition 3.1.** A moving platform pose is said to be *wrench feasible* if and only if the CDPR can balance any external wrench  $\mathbf{w}_e$  included in  $[\mathbf{w}_e]_r$  while satisfying the cable tension limits expressed by  $[\tau]_a$ . The *Wrench Feasible Workspace* (WFW) is the set of wrench feasible poses,  $[\mathbf{p}]_{WFW}$ .

$$[\mathbf{p}]_{WFW} = \left\{ (\mathbf{t}, \mathbf{R}) \in \mathbb{R}^3 \times SO(3) : \forall \mathbf{w}_e \in [\mathbf{w}_e]_r, \exists \tau \in [\tau]_a \quad \text{s.t.} \quad \begin{cases} \mathbf{w}_e \in [\mathbf{w}_e]_a \\ \mathbf{W}\tau + \mathbf{w}_e = 0 \end{cases} \right\} \quad (3.4)$$

where  $SO(3)$  is the group of proper rotation matrices.

### Computation

Boscher *et al.* proposed in [BREU06] a basic method to analyse the wrench feasibility of a moving platform pose. The method aims at finding the analytical closed-form expression of the WFW bounds for spatial CDPRs. The bounds are defined as the set of equations describing the contact between one vertex of  $[\mathbf{w}_e]_r$  and the facets of  $[\mathbf{w}_e]_a$ . In fact, from a geometrical point of view, a pose is wrench feasible if  $[\mathbf{w}_e]_r$  is fully included in  $[\mathbf{w}_e]_a$  (as shown in Fig. 3.1):

$$[\mathbf{w}_e]_r \subseteq [\mathbf{w}_e]_a \quad (3.5)$$

Bouchard *et al.* were the first to notice, in 2009, that the AWS is a zonotope. As a zonotope, the AWS can be defined as: (i) the linear combinations of the cable wrench vectors, according to cable tension limits,  $\tau_{min}$  and  $\tau_{max}$  (the Minkowski sum of the cable wrenches); (ii) the affine transformation of a hypercube, from the cable tension space to the moving platform wrench space. The AWS can be described by means of its vertices or by means of its facet supporting hyperplanes. According to Bouchard *et al.*, a basic method to determine the AWS consists in computing the convex hull of the linear combinations (Minkowski sum) of the cable wrench vector. This method usually requires an iterative procedure. An alternative method has been proposed and called the hyperplane shifting algorithm. A subset of  $n - 1$  columns of the wrench matrix,  $\hat{\mathbf{w}}_i$ , is selected in order to create a set of hyperplanes. This operation is repeated until all the linearly independent combinations of  $n - 1$

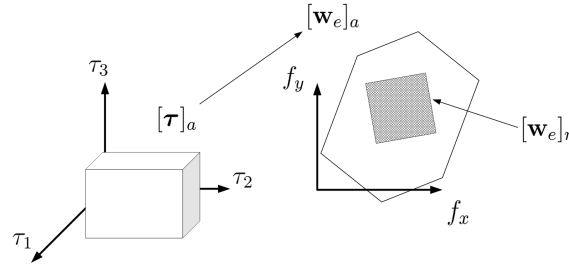


**Fig. 3.1** – Mapping of  $[\tau]_a$  into the wrench space as  $[w_e]_a$ . Example of a planar CDPR with 3 actuators

wrench matrix columns are analysed and all the supporting hyperplanes are defined. An improved version of the hyperplane shifting method has been provided by Gouttefarde and Krut in [GK10].

The wrench feasibility can be verified by determining the distances between all the vertices of  $[w_e]_r$  and the facets of  $[w_e]_a$  through the following inequality:

$$\mathbf{C}w_e \leq \mathbf{d}, \quad \forall w_e \in [w_e]_r \quad (3.6)$$

Equation (3.6) is the mathematical representation of the AWS obtained by means of the hyperplane shifting method. The rows of matrix  $\mathbf{C}$  represent the norms of the hyperplanes describing the facets of  $[w_e]_a$  and vector  $\mathbf{d}$  collects the distances between these facets and the origin of the wrench space.

In order to analyse the WFW with the previous methods, the Cartesian space is usually discretised into a grid of points. Each point of the grid is analysed in order to verify whether it belongs to the WFW of the CDPR or not. The main limitation associated to such a discretisation is related to the fact that the results can not be extended directly to a continuous domain. A finer grid can improve the quality of the results in such a way that the results should be consistent with respect to a continuous analysis. Anyway, the WFW being in general a non-convex set represented by non-linear inequalities, holes and separated feasible regions may exist and may not be detected by a discretisation.

An alternative solution, based on interval analysis, has been proposed by Gouttefarde *et al.* in [GDM11]. The Cartesian space is recursively divided into a set of boxes and a wrench feasibility analysis over the continuous domain of each box is performed. Thereby, interval analysis can guarantee that all the poses contained inside a box belong to the WFW, or that all poses inside the box are outside the WFW, or else cannot conclude. In the latter case, the box is bisected. This method is thus a useful alternative to discretisation. However, the computation time is not deterministic and, provided that the discretisation grid is relatively coarse, is usually higher than the one required to compute the WFW by means of a discretisation.

### 3.1.2 Wrench Closure Workspace (WCW)

#### Definition

The WCW is a particular instance of the WFW, where the sole constraint on the cable tensions is non-negativity. The ACTS is then defined as follows:

$$[\tau]_a = \{\tau \mid \tau_i \geq 0, i = 1, \dots, m\} \quad (3.7)$$

According to the absence of a cable tension upper bound, cables can be tightened without taking into account their structural limits or the actuation system limits. Therefore, the WCW depends only on the CDPR geometry. The CDPR should be able to bare any possible external wrench applied to the moving platform, where  $[\mathbf{w}_e]_r = \mathbb{R}^3 \times \mathbb{R}^3$ . Therefore, the WCW can be formally defined as follows.

**Definition 3.2.** The *Wrench-Closure Workspace* (WCW) is the set of poses of the moving platform for which any wrench can be exerted on the moving platform by tightening the cables [GG06].

$$[\mathbf{p}]_{WCW} = \{(\mathbf{t}, \mathbf{R}) \in \mathbb{R}^3 \times SO(3) : \forall \mathbf{w}_e \in \mathbb{R}^3 \times \mathbb{R}^3, \exists \boldsymbol{\tau} \in [\boldsymbol{\tau}]_a \text{ s.t. } \mathbf{W}\boldsymbol{\tau} + \mathbf{w}_e = \mathbf{0}\} \quad (3.8)$$

It has to be noticed that, according to its definition, the WCW can be only used on non-suspended fully constrained CDPRs.

### Computation

The first analysis of the WCW has been performed by Veroheven in [VH00]. Veroheven proved that the WCW of fully constrained CDPRs is bounded by polynomial surfaces expressed through an explicit formula. Later on, a technique was proposed to compute cross sections of the WCW of spatial CDPRs and it was showed that the constant orientation workspace is bounded by cubic surfaces [GG06]. Stump and Kumar developed an analytical technique to delineate the WCW bounds of CDPRs. The method is inspired by the work performed by Ebert-Uphoff and Voglewede in [EUV04]. By means of semi-definite programming, they obtained a closed-form expression of the bounds of the WCW. Recently, Sheng *et al.* provided a similar method to compute the bounds of the WCW analytically [SPSA15].

An alternative evaluation of the WCW has been provided by Arsenault in [Ars10]. In this context, the analysis is performed while observing the active stiffness matrix of the CDPR. According to Eq. (2.15), the static equilibrium of the moving platform can be assured multiplying the null space of the wrench matrix,  $\mathbf{W}$ , by an appropriate vector of scaling factors,  $\boldsymbol{\lambda}$ . Vector  $\boldsymbol{\lambda}$  represents the so called pre-stress. The active stiffness matrix of the CDPR,  $\mathbf{K}_a$ , is partially dependent on the pre-stress. For a given pose of the moving platform, Arsenault proved that, if a vector  $\boldsymbol{\lambda}$  exists such that the active stiffness matrix related to the cable pre-stress is positive definite, then this pose will belong to the WCW.

### 3.1.3 Static Feasible Workspace (SFW)

According to some tasks, like quasi-static displacements of heavy-objects, the weight of the moving platform is the only external wrench taken into account,  $[\mathbf{w}_e]_r = \mathbf{w}_g$ . In this case, the workspace of the CDPR can be described through the SFW. Similarly to the WFW, it is possible to take into account the cable tension limits defined in Eq. (3.3).

**Definition 3.3.** The *Static Feasible Workspace* (SFW) is the set of moving platform poses where the CDPR can balance the weight of the possibly loaded moving platform,  $\mathbf{w}_g$  according to the cable tension limits expressed by  $[\boldsymbol{\tau}]_a$ .

$$[\mathbf{p}]_{SFW} = \{(\mathbf{t}, \mathbf{R}) \in \mathbb{R}^3 \times SO(3) : \exists \boldsymbol{\tau} \in [\boldsymbol{\tau}]_a \text{ s.t. } \mathbf{W}\boldsymbol{\tau} + \mathbf{w}_g = \mathbf{0}\} \quad (3.9)$$

### 3.1.4 Interference and Collision Free Workspaces

One of the main drawbacks associated to CDPRs is the possible interferences between cables and the possible collisions between the cables, the moving platform and the working environment. Some symbolical and numerical hybrid methods let verify cable interferences and collisions [MTT<sup>+</sup>99, PG07, MD06]. These methods can be applied successfully when the trajectory of the moving platform is defined a priori. However, they do not assure the possibility to observe which portion of the prescribed workspace is free of interferences and collisions. In 2004 Merlet computed by means of numerical algorithms the interference free regions of a CDPR [Mer04]. Taking inspiration from Merlet work, Perreault *et al.* improved the method to compute, for a given constant orientation of the moving platform, the so called *Interference Free Workspace* (IFW) [PCGO10].

**Definition 3.4.** The *Interference Free Workspace* (IFW) is the set of accessible moving platform poses,  $[\mathbf{p}]_{IFW}$ , without collisions between cables.

When interferences occur, the cables lie in the same plane. The algorithm proposed by Perreault *et al.* analyses the possible cable interference loci in this plane, parametrising the interference equations and solving them as a function of the moving platform pose. This algorithm can be used as well to compute, for a given constant orientation of the moving platform, the so-called *Collision Free Workspace* (CFW).

**Definition 3.5.** The *Collision Free Workspace* (CFW) is the set of accessible moving platform poses,  $[\mathbf{p}]_{CFW}$ , without collisions between the cables, the moving platform, and the environment.

## 3.2 Twist Feasible Workspace (TFW)

The definition of the WFW is based on the linearity of the static equilibrium equation,  $\mathbf{W}$  being a linear map between the cable tension space and the space of the external wrench acting on the moving platform:

$$\mathbf{w}_e = \sum_{i=1}^m \hat{\mathbf{w}}_i \tau_i \quad (3.10)$$

The kinematic problem described in Eq. (2.16) presents a similar structure. The kinematic Jacobian matrix,  $\mathbf{J}$ , is a linear map between the space of the cable velocities and the space of the moving platform twists. In this manuscript, the kinematic Jacobian  $\mathbf{J}$  is computed according to Eq. (2.19). As a matter of fact, Eq. (2.16) can be rewritten as a linear combination of the cable twists,  $\dot{\mathbf{p}}_i$ ,  $i = 1, \dots, m$  ( $\hat{\mathbf{p}}_i$ ,  $i = 1, \dots, m$  being the column vectors of  $\mathbf{J}$ ):

$$\dot{\mathbf{p}} = \sum_{i=1}^m \hat{\mathbf{p}}_i \dot{t}_i \quad (3.11)$$

Due to the similarities of the static and kinematic problems, the considerations made in Sec. 3.1.1 can be extended to the kinematics of the CDPR moving platform. In this specific context, the workspace will focus on the analysis of the twist that the moving platform will be able to achieve.

During the task execution, the moving platform velocities are supposed to lie within given ranges:

$$\dot{t}_{min} \leq \dot{t}_x, \dot{t}_y, \dot{t}_z \leq \dot{t}_{max} \quad (3.12)$$

$$\omega_{min} \leq \omega_x, \omega_y, \omega_z \leq \omega_{max} \quad (3.13)$$

where  $\dot{i}_x$ ,  $\dot{i}_y$  and  $\dot{i}_z$  represent the components of the moving platform linear velocity,  $\dot{\mathbf{t}}$ , along  $\mathbf{x}_b$ ,  $\mathbf{y}_b$  and  $\mathbf{z}_b$ , respectively.  $\omega_x$ ,  $\omega_y$  and  $\omega_z$  represent the components of the moving platform rotational velocity,  $\omega$ , about  $\mathbf{x}_b$ ,  $\mathbf{y}_b$  and  $\mathbf{z}_b$ , respectively.  $\dot{i}_{min}$  and  $\dot{i}_{max}$  are the lower and the upper bounds on the linear velocity components. Analogously,  $\omega_{min}$  and  $\omega_{max}$  are the lower and the upper bounds on the rotational velocity components. The set of twists,  $[\dot{\mathbf{p}}]_r$ , which is limited by the previous lower and upper bounds, is defined as the *Required Twist Set* (RTS).

Similarly to the WFW, matrix  $\mathbf{J}$  depends on the moving platform pose. Thus, the TFW is a function of the moving platform pose. The TFW depends as well on the power of the actuators. The nominal speed of the motors limits the cable coiling/uncoiling velocities. The maximum coiling speed is defined as  $\dot{i}_{max}$ ; for most of the actuators, considering  $\dot{i}_{min} = -\dot{i}_{max}$ , the cable coiling/uncoiling velocities are bounded as follows:

$$\dot{i}_{min} \leq \dot{i}_i \leq \dot{i}_{max}, \forall i = 1, \dots, m \quad (3.14)$$

The set of possible cable coiling/uncoiling velocities is defined hereafter as the *Available Cable Velocity Set* (ACVS),  $[\dot{\mathbf{i}}]_a$ :

$$[\dot{\mathbf{i}}]_a = \{\dot{\mathbf{i}} \mid \dot{i}_{min} \leq \dot{i}_i \leq \dot{i}_{max}, \forall i = 1, \dots, m\} \quad (3.15)$$

According to Eq. (3.15) and Eq. (2.16), the moving platform can assume only a bounded set of twists, defined hereafter as the *Available Twist Set* (ATS),  $[\dot{\mathbf{p}}]_a$ . The ATS, which is a convex polytope, can be computed from the ACVS using the Jacobian matrix as a linear map from the cable velocity space to the moving platform twist space.

In order to satisfy the velocity constraints in Eq. (3.15), the CDPR can assume only the poses contained inside the TFW.

**Definition 3.6.** A moving platform pose is said to be *twist feasible* when the CDPR moving platform can assume any twist  $\dot{\mathbf{p}}$  included in  $[\dot{\mathbf{p}}]_r$  according to the bounds on the cable velocities,  $[\dot{\mathbf{i}}]_a$ . The *Twist Feasible Workspace* (TFW) is the set of twist feasible poses,  $[\mathbf{p}]_{TFW}$ .

$$[\mathbf{p}]_{TFW} : \forall \dot{\mathbf{p}} \in [\dot{\mathbf{p}}]_r, \exists \dot{\mathbf{i}} \in [\dot{\mathbf{i}}]_a \text{ s.t. } \begin{cases} \dot{\mathbf{p}} \in [\dot{\mathbf{p}}]_a \\ \mathbf{J}\dot{\mathbf{i}} - \dot{\mathbf{p}} = 0 \end{cases} \quad (3.16)$$

Alternatively, the twist feasibility condition can be described as:

$$[\dot{\mathbf{p}}]_r \subseteq [\dot{\mathbf{p}}]_a \quad (3.17)$$

Therefore, the TFW can be investigated, similarly to the WFW, using the improved hyperplane shifting method presented in [GK10]:

$$\mathbf{C}^* \dot{\mathbf{p}} \leq \mathbf{d}^*, \quad \forall \dot{\mathbf{p}} \in [\dot{\mathbf{p}}]_r \quad (3.18)$$

where the rows of matrix  $\mathbf{C}^*$  represent the norms of the hyperplane describing the facets of  $[\dot{\mathbf{p}}]_a$  and vector  $\mathbf{d}^*$  the distances between the origin of the twist space and those facets.

### 3.3 Dynamic Feasible Workspace (DFW)

#### 3.3.1 Standard Dynamic Feasible Workspace

The concept of SFW has been extended to take into account the CDPR moving platform dynamics. When the acceleration of the moving platform can not be neglected, the DFW takes into account its inertia. The first studies on the DFW have been realised by Barrette *et al.* in [BG05]. The bounds of the DFW have been computed for a generic planar CDPR developing the equations of its dynamic model. Since this method can not be easily extended to spatial CDPRs, Kozlov proposed to use the method described in [GCCC14] in order to compute the DFW of a fully-constrained CDPR [Koz14]. Similarly to the WFW, the proposed method takes into account the cable tension limits in order to compute the AWS. The AWS has to assure the dynamic equilibrium of the moving platform in presence of its inertial forces associated to the following accelerations:

$$\ddot{i}_{min} \leq \ddot{x}_C, \ddot{y}_C, \ddot{z}_C \leq \ddot{i}_{max} \quad (3.19)$$

$$\alpha_{min} \leq \alpha_x, \alpha_y, \alpha_z \leq \alpha_{max} \quad (3.20)$$

where  $\ddot{i}_{min}, \ddot{i}_{max}, \alpha_{min}, \alpha_{max}$  represent the bounds on the moving platform linear and rotational accelerations. The demanded moving platform accelerations belong to the so called *Required Acceleration Set* (RAS),  $[\ddot{\mathbf{p}}]_r$ . The RAS can be projected into the wrench space by means of matrix  $\mathbf{A}$ , defined in Eq. (2.35), which basically collects the inertia matrix of the moving platform and the inertia matrices of motors and winches. The set of wrenches,  $[\mathbf{w}_d]_r$ , generated by this linear mapping is defined as the *Required Dynamic Wrench Set* (RDWS). No external wrench is applied to the moving platform. According to the previous requirements, the DFW can be defined as follows:

**Definition 3.7.** A moving platform pose is said to be *dynamic feasible* when the moving platform of the CDPR can reach any acceleration included in  $[\ddot{\mathbf{p}}]_r$  according to cable tension limits expressed by  $[\boldsymbol{\tau}]_a$ . The *Dynamic Feasible Workspace* (DFW) is the set of dynamic feasible poses,  $[\mathbf{p}]_{DFW}$ .

$$[\mathbf{p}]_{DFW} = \{(\mathbf{t}, \mathbf{R}) \in \mathbb{R}^3 \times SO(3) : \forall \ddot{\mathbf{p}} \in [\ddot{\mathbf{p}}]_r, \exists \boldsymbol{\tau} \in [\boldsymbol{\tau}]_a \text{ s.t. } \mathbf{W}\boldsymbol{\tau} + \mathbf{A}\ddot{\mathbf{p}} = \mathbf{0}\} \quad (3.21)$$

#### 3.3.2 Improved Dynamic Feasible Workspace (IDFW)

The DFW described in Sec. 3.3.1 has several limitations. The main drawback is associated to the fact that the proposed DFW takes into account neither the external wrenches applied to the moving platform nor its weight. Furthermore, the model used to verify the dynamic equilibrium of the moving platform neglects the Coriolis and the centrifugal wrenches associated to the CDPR dynamic model.

In the IDFW, at a given moving platform pose, the CDPR dynamic equilibrium should be assured as well when a set of external wrenches is applied to the moving platform. Hence, the AWS should compensate both the contribution associated to the REWS,  $[\mathbf{w}_e]_r$ , and the RDWS,  $[\mathbf{w}_d]_r$ . The components of the REWS are bounded according to Eq. (3.1) and Eq. (3.2) while the components of the RDWS are bounded according to Eq. (3.19) and Eq. (3.20).

The dynamic equilibrium of the moving platform is described by Eq. (2.38), where  $\mathbf{B}$  is related to the Coriolis and centrifugal forces of the moving platform and  $\mathbf{D}$  to its weight. These terms depend only on the pose and the twist of the moving platform. For a given pose and twist of the moving platform, these terms are constant. The influence of the friction and the efficiency coefficients of motors, gearboxes and winches are considered as well.

Therefore, with respect to the listed modifications, the IDFW can be defined as follows.

**Definition 3.8.** A moving platform pose is said to be *dynamic feasible* when the CDPR can balance any external wrench  $\mathbf{w}_e$  included in  $[\mathbf{w}_e]_r$ , while the moving platform can assume any acceleration  $\ddot{\mathbf{p}}$  included in  $[\ddot{\mathbf{p}}]_r$  and a given twist  $\dot{\mathbf{p}}$ . The *Improved Dynamic Feasible Workspace* (IDFW) is the set of dynamic feasible poses,  $[\mathbf{p}]_{IDFW}$ .

$$[\mathbf{p}]_{IDFW} : \forall \mathbf{w}_e \in [\mathbf{w}_e]_r, \forall \ddot{\mathbf{p}} \in [\ddot{\mathbf{p}}]_r \exists \tau \in [\tau]_a \quad \text{s.t.} \quad \frac{2}{\phi_W} \eta_{RP} \rho_R \mathbf{W} \tau_M + \mathbf{A} \ddot{\mathbf{p}} + \mathbf{B} \dot{\mathbf{p}} + \mathbf{D} + \mathbf{w}_e = 0 \quad (3.22)$$

Analysing the previous definition, we may notice that the feasibility conditions are expressed according to three components defined in the wrench space. The first component,  $[\mathbf{w}_d]_r$ , is computed projecting the vertices of  $[\ddot{\mathbf{p}}]_r$  into the wrench space. For a 3-dimensional case study,  $[\ddot{\mathbf{p}}]_r$  is composed of 64 vertices. The second component,  $[\mathbf{w}_e]_r$ , is composed as well of 64 vertices, when defined for a 3-dimensional case study. By supposing the twist of the moving platform is constant, the last component of the dynamic equilibrium,  $\mathbf{w}_c = \{\mathbf{B} \dot{\mathbf{p}} + \mathbf{D}\}$ , represents a constant wrench. According to the polytope algebra [BR15], the composition of these components still generates a polytope,  $[\mathbf{w}]_r$ , namely defined as the *Required Wrench Set* (RWS).  $[\mathbf{w}]_r$  can be computed using the Minkowski sum over  $[\mathbf{w}_e]_r$ ,  $[\mathbf{w}_d]_r$  and  $\mathbf{w}_c$ , as illustrated in the example of Fig. 3.2:

$$[\mathbf{w}]_r = [\mathbf{w}_e]_r \oplus [\mathbf{w}_d]_r \oplus \mathbf{w}_c \quad (3.23)$$

Thus, Def. 3.8 can be rewritten as a function of  $[\mathbf{w}]_r$ :

**Definition 3.9.** A moving platform pose is said to be *dynamic feasible* when the CDPR can balance any wrench  $\mathbf{w}$  included in  $[\mathbf{w}]_r$ . The *Improved Dynamic Feasible Workspace* is the set of dynamic feasible poses,  $[\mathbf{p}]_{IDFW}$ .

$$[\mathbf{p}]_{IDFW} : \forall \mathbf{w} \in [\mathbf{w}]_r, \exists \tau \in [\tau]_a \quad \text{s.t.} \quad \frac{2}{\phi_W} \eta_{RP} \rho_R \mathbf{W} \tau_M + \mathbf{A} \ddot{\mathbf{p}} + \mathbf{B} \dot{\mathbf{p}} + \mathbf{D} + \mathbf{w}_e = 0 \quad (3.24)$$

The mathematical representation provided by Eq. (3.24) is similar to the one describing the WFW. In fact, from a geometrical point of view, a moving platform pose is dynamic feasible if  $[\mathbf{w}]_r$  is fully included in  $[\mathbf{w}]_a$ :

$$[\mathbf{w}]_r \subseteq [\mathbf{w}]_a \quad (3.25)$$

Once again, the dynamic feasibility of a pose can be verified according to the hyperplane shifting method presented by Gouttefarde *et al.* in [GK10] and Guay *et al.* in [GCCC14]. The distances between the facets of the available wrench set,  $[\mathbf{w}]_a$ , and the vertices of the RWS,  $[\mathbf{w}]_r$ , is verified according to the following inequality:

$$\mathbf{C} \mathbf{w}_r \leq \mathbf{d}_d, \quad \forall \mathbf{w} \in [\mathbf{w}]_r \quad (3.26)$$

## 3.4 Case Study

This section aims at comparing the SFW, WFW, DFW and Improved DFW (IDFW) of the spatial suspended CDPR illustrated in Fig. 3.3. It has the layout the CoGiRo robot [GCRB15] and the size of the IRT JV CAROCA

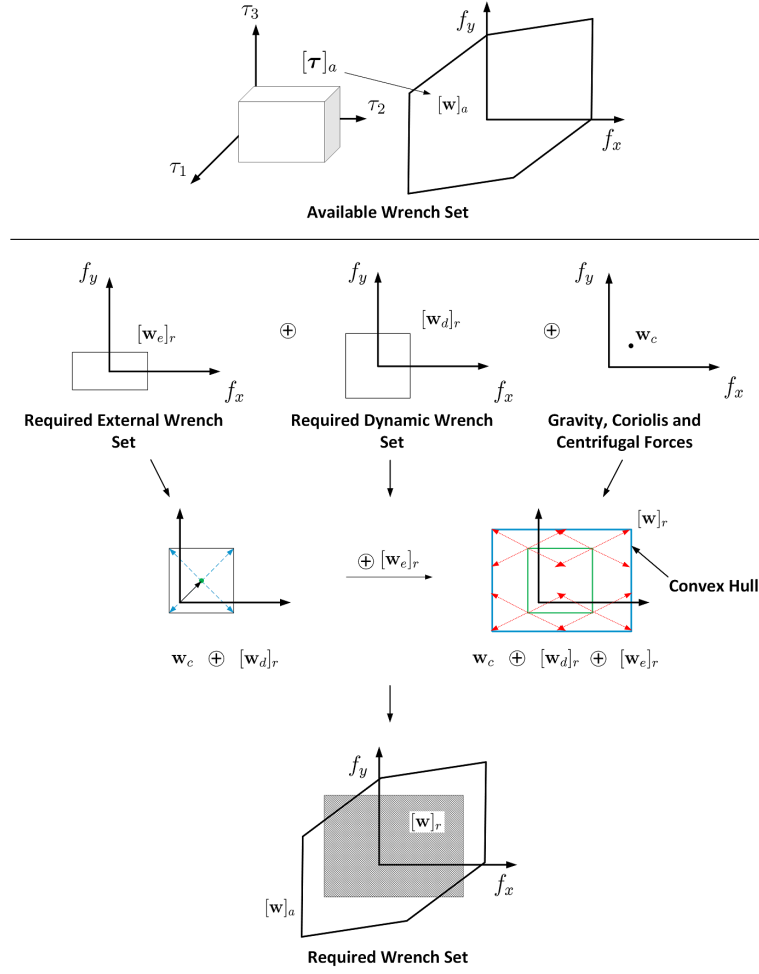


**Fig. 3.2** – Computation of the RWS  $[w]_r$ . Example of a planar CDPR with 3 actuators and 2 translational DoF

prototype. The robot consists of a moving platform connected to the fixed base frame by  $m = 8$  cables. It is 7 m long, 4 m width and 3.5 m high. The maximum cable tension is equal to 6990 N. The moving platform consists of a parallelepiped. Its width,  $w_p$ , its length,  $l_p$ , and its height,  $h_p$ , are equal to 20 cm, 20 cm and 25 cm, respectively. The mass of the moving platform,  $M$ , is equal to 100 kg. In the proposed case study, the CoM of the moving platform,  $G$ , does not coincide with the origin  $O_p$  of frame  $\mathcal{F}_p$ , being  $\mathbf{S} = [1 \text{ cm}, 1 \text{ cm}, 1 \text{ cm}]^T$ .

The volume inside the base frame has been discretized homogeneously into  $n_p = 882$  points. Each point has been analysed in order to verify if the corresponding poses of the CDPR belong to the improved DFW. The analysis has been performed assuming that the moving platform is aligned with respect to the axes of frame  $\mathcal{F}_p$ . The linear velocity of the moving platform is equal to  $\dot{\mathbf{t}} = [1 \text{ m/s}, 1 \text{ m/s}, 1 \text{ m/s}]^T$  and its angular velocity is equal to  $\omega = [0.05 \text{ rad/s}, 0.05 \text{ rad/s}, 0.05 \text{ rad/s}]^T$ . The external wrenches acting on the moving platform are bounded as follows:

$$-100 \text{ N} \leq f_x, f_y, f_z \leq 100 \text{ N} \quad (3.27)$$

$$-1 \text{ Nm} \leq m_x, m_y, m_z \leq 1 \text{ Nm} \quad (3.28)$$

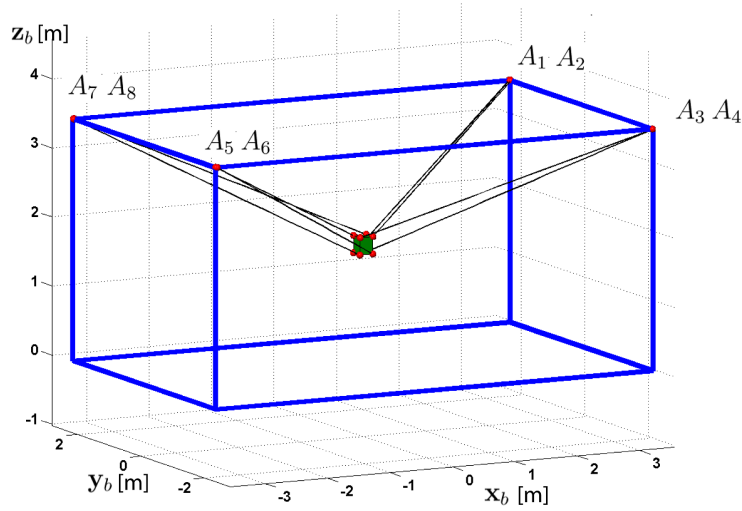


**Fig. 3.3** – Layout of the CoGiRo cable-suspended parallel robot [GCRB15] with the size of the IRT JV CAROCA prototype

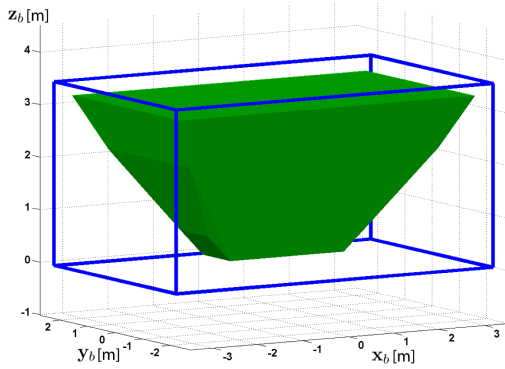


**Fig. 3.4** – Improved DFW of the CDPR under study covering 47.96% of its volume

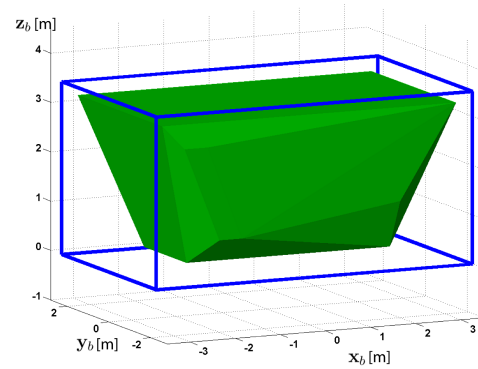


**Fig. 3.5** – DFW of the CDPR under study covering 63.27% of its volume

Similarly, the range of accelerations of the moving platform is limited according to the following inequalities:

$$-2 \text{ m/s}^2 \leq \ddot{t}_x, \ddot{t}_y, \ddot{t}_z \leq 2 \text{ m/s}^2 \quad (3.29)$$

$$-0.1 \text{ rad/s}^2 \leq \alpha_x, \alpha_y, \alpha_z \leq 0.1 \text{ rad/s}^2 \quad (3.30)$$

For the foregoing conditions, the improved DFW of the CDPR covers the 47.96% of its volume. Figure 3.4 illustrates the improved DFW of the CDPR under study.

The results have been compared with respect to the dynamic feasibility conditions described by Def. 3.9. By considering only the weight and the inertia of the moving platform, the DFW covers the 63.27% of the volume occupied by the DFW, as shown in Fig. 3.5. Neglecting the effects of the external wrenches and the Coriolis forces, the volume of the DFW is 32% larger than the the volume of the improved DFW.

Similarly, by neglecting the inertia of the CDPR and taking into account only the external wrenches  $\mathbf{w}_e$ , the WFW occupies the 79.25% of the CDPR volume, as shown in Fig. 3.6. By taking into account only the weight of

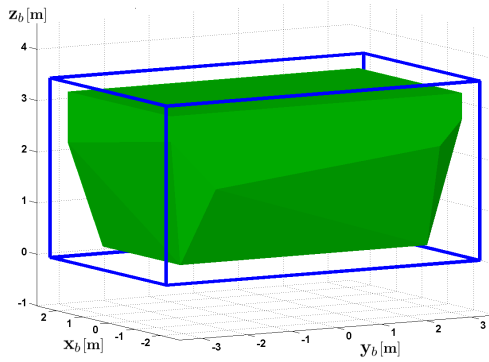


**Fig. 3.6** – WFW of the CDPR under study covering 79.25% of its volume

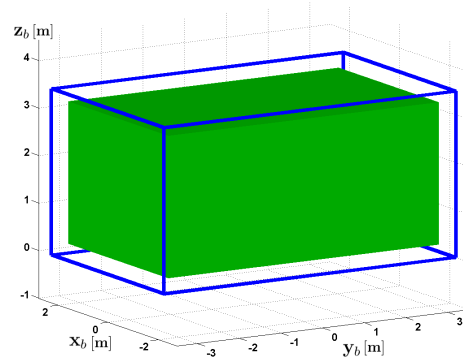


**Fig. 3.7** – SFW of the CDPR under study covering 99.32% of its volume

**Tab. 3.1** – COMPARISON OF THE *SFW*, *WFW*, *DFW* AND *IDFW* OF THE CDPR UNDER STUDY

Workspace type	<i>SFW</i>	<i>WFW</i>	<i>DFW</i>	<i>IDFW</i>
Covered Volume of the CDPR	99.32%	79.25%	63.27%	47.95%

the moving platform, the SFW covers 99.32% of the CDPR volume, as illustrated in Fig. 3.7. These results are summarized in Table 3.1.

### 3.5 Conclusions

This chapter dealt with the workspace analysis of CDPRs. Workspace analysis is one of the fundamental tools in order to design CDPRs and investigated their potentialities. The workspaces and the tools presented in this chapter are dedicated to CDPRs models neglecting the cable mass. They can be applied to RCDPRs as well.

A formal mathematical definition of several workspaces has been provided. Those workspaces are focused on the analysis of the static and dynamic equilibria of CDPRs. The advantages and drawbacks of these workspaces have been highlighted. According to our study, none of the existing workspace takes into account CDPR moving platform velocities. Therefore, part of this chapter has been dedicated to the definition of a novel workspace, the TFW [GCG15a]. This workspace can be used in order to evaluate the twist feasibility, namely, determining twists the moving platform can reach.

Major improvements have been performed on the DFW. The basic DFW is mainly focused on the analysis of the moving platform inertia. In the IDFW, the dynamic equilibria of the CDPR considers the effect of the possible external wrenches applied on the moving platform and the CDPR payload too [GGC16a]. The conditions verifying the so-called dynamic feasibility of the CDPR consider as well the dynamic contribution of the moving platform centrifugal and Coriolis forces. In order to preserve the linear form of the dynamic equations, the twist of the moving platform is supposed constant.

Both the TFW and the IDFW are defined through systems of linear equations, which formally describe a set of polytopes. Hence, the twist feasibility and the dynamic feasibility can be verified according to the hyperplane shifting method. Therefore, similarly to other workspaces, the TFW and the IDFW can be easily integrated into

the dimensioning problem of the actuators, the gearboxes and the winches of CDPRs, as described in the following chapter.

As an illustrative example, the static, wrench-feasible, dynamic and improved dynamic workspaces of a spatial suspended cable-driven parallel robot, with the dimensions of a prototype developed in the framework of the IRT JV CAROCA project, are traced. It turns out that the IDFW of the CDPR under study is respectively 1.32 times, 1.65 times and 2.07 times smaller than its DFW, WFW and SFW.



## Chapter 4

# Design of Reconfigurable Cable-Driven Parallel Robots

### Chapter Content

4.1 Design Strategy for CDPRs . . . . .	58
4.2 Classes of RCDPRs . . . . .	66
4.3 Nomenclature for RCDPRs . . . . .	68
4.4 Design Strategy for RCDPRs . . . . .	69
4.5 Case Study I: Design of a CDPR Based on the Workspace Size . . . . .	73
4.6 Case Study II : Design of a RCDPR for Sandblasting and Painting of a Large Tubular Structure . . . . .	78
4.7 Conclusions . . . . .	85

The models and the tools described in Chap. 2 and Chap. 3 are used in this chapter to define a design strategy for CDPRs and RCDPRs. The design of CDPRs is usually formulated as an optimisation problem. One of the first task-based design was proposed by Pusey *et al.* in 2004 [PFAM04]. The authors aimed at maximising the size of the CDPR workspace. Bruckmann *et al.* generalised this design approach, formulating it as a constrained optimisation problem aiming at optimising one or several criterion(a) [BMB<sup>+</sup>09a]. The optimisation problem was solved by using local and global search algorithms, showing the efficiency of genetic and simulated annealing algorithms. Similar results have been obtained by Azizian and Cardou in [AC13]. An alternative has been proposed by Gouttefarde *et al.*, which used an interval based analysis to implement the design process [GKC<sup>+</sup>08]. In 2015, Blanchet proposed a new design strategy, based on the interval analysis, guaranteeing the static equilibrium of the CDPR when a set of external wrenches are acting on the moving platform [Bla15].

In this manuscript, CDPRs are designed according to [PFAM04, BMB<sup>+</sup>09a]. The design strategy is described in Sec. 4.1.1. The CDPR design optimisation problem is formulated based on the industrial tasks to be performed and the prescribed workspace or path of the *Centre of Mass* (CoM) of the moving platform. The optimisation problem is solved by means of global search algorithms. While other design variables can be considered, this manuscript focuses on the locations of cable exit points and the properties of winches and actuators. The design variables are continuous and bounded. A list of objective functions is described in Sec. 4.1.2. The proposed objective functions are related to the workspace size, the cable tensions, the CDPR stiffness, and the CDPR size.

Section 4.1.3 gives a set of constraints proposed for the design optimisation problems. The constraints take into account: The cable interference, the cable collisions with the working environment, and the *Minimum Degree of Constraint Satisfaction* (MDoCS) [GCCC14].

CDPRs can be used successfully if the tasks to be fulfilled are simple and the working environment is not cluttered. When these hypotheses are not satisfied, RCDPRs may be required to achieve the prescribed goal. In general, several parameters can be reconfigured, as described in Sec. 4.2. These parameters can be reconfigured selecting them between a discrete or a continuous set of values. Contrary to most of the previous research works [RZA11, JK13, NGCP14, NG14b], we will take into account only discrete reconfigurations, namely the locations of the cable exit points are selected from a finite set of values. Hereafter, the class of RCDPRs whose exit points can be placed on a discrete set of exit points is defined as *discrete RCDPRs*. In this manuscript, reconfigurations are limited to the cable exit point locations.

To the best of our knowledge, no design strategy has been formulated in the literature for discrete RCDPRs. Section 4.4 describes a novel task-based design strategy for discrete RCDPRs. By taking into account the working environment, the designer divides the prescribed workspace or path into  $n_t$  parts. Each part will be covered by one and only one configuration of the RCDPR. Then, for each configuration, the designer selects a cable layout, parametrising the position of the cable exit points. The grid of locations where the cable exit points can be located is defined by the designer as well. Placing the exit points on the provided set of possible locations, it is possible to generate many CDPR configurations. All the possible configurations are analysed with respect to a set of constraints, in order to verify the parts of the prescribed workspace or path that can be covered by each configuration. The configurations satisfying the constraints are compared in order to find the combinations of  $n_t$  configurations that accomplish the required task and optimise at the same time one or several objective function(s). A set objective functions, dedicated to RCDPRs, is provided in Sec. 4.4.2. These objective functions aim at maximising the productivity (production cycle time) and reducing the reconfiguration time of the cable exit points.

In order to analyse the advantages and the limitations of the proposed design strategies, two case studies are proposed. The first case study, presented in Sec. 4.5, requires the dimensioning of the actuators, the winches and the gearboxes of a CDPR. The optimisation is performed with respect to the size of the WFW and the TWF of the CDPR. The second case study, described in Sec. 4.6, involves the design of a RCDPR for sandblasting and painting of a three-dimensional tubular structure. The tools performing these operations are embarked on the moving platform, which follows the profile of the tubular structure. Each side of the tubular structure is associated to a single configuration. Cable exit points are reconfigured switching from one side of the tubular structure to another, until all the three external sides of the structure are sandblasted and painted. The cable exit point locations of the three configurations subjected to design are optimised so that the number of cable attachment/detachment operations required to switch from a configuration to another is minimised. The size of the RCDPR is also minimised while its stiffness is maximised along the paths to be followed.

## 4.1 Design Strategy for CDPRs

The design of a CDPR requires the dimensioning of several components. Some components are chosen based on the experience of the designer, with respect to the tasks to be performed by the CDPR. The properties of these components represent the so called *constant design parameters*. The remaining components, which cannot be chosen intuitively, can be dimensioned by means of a proper optimal design strategy, of which the *design variables* characterise those components.

Cables are usually selected based on their material, and in particular their Young modulus and diameter. These parameters influence the structural resistance, the elasticity and the linear density of the cables. In this manuscript, cable properties are considered as design constants.

The architecture of the CDPR consists of the number of cables, the locations of the exit points and the locations of the cable connection points on the moving platform. The number of cables is usually defined a priori, as well as the dimensions of the moving platform. Optimisation is usually required to define the locations of the cable exit points and of the cable connection points on the moving platform.

The actuators, the winches and possibly the gearboxes have an important role with respect to the static and dynamic performance of the CDPR. Their properties can be considered as constant parameters or design variables depending on the design problem at hand.

### 4.1.1 Design Problem Formulation

In order to find the optimal design variables of a CDPR, this manuscript introduces a design strategy composed of six steps. The design is formulated as an optimisation problem, which aims at optimising one or several objective functions subject to a set of constraints. The steps of the proposed design strategy are described hereafter and illustrated in Fig. 4.1.

- Step I. *Task and Environment*. The designer describes the task to be performed. It specifies the nature of the problem, defining if the motion of the moving platform is static, quasi-static or dynamic. According to nature of the problem, the designer defines the external wrenches applied to the moving platform and, possibly, the required moving platform twist and accelerations. The prescribed workspace or path of the CoM of the moving platform is given. A description of the environment is provided as well, including the possible obstacles encountered during the task execution.
- Step II. *Constant Design Parameters*. The designer defines a set of constant design parameters and their values. The parameters are collected in the constant design parameter vector  $\mathbf{q}$ .
- Step III. *Design Variables and their Bounds*. The designer defines a set of design variables. Lower and upper bounds are assigned to each design variable. The design variables are collected in the design variable vector  $\mathbf{x}$ . The lower and the upper bounds on the design variables are collected in vectors  $\mathbf{x}_{low}$  and  $\mathbf{x}_{up}$ , respectively.
- Step IV. *Objective Functions*. The designer defines one or several objective function(s),  $\mathcal{V}_t, t = 1, \dots, n_{\mathcal{V}}$ , where  $n_{\mathcal{V}}$  is equal to the number of objective function(s). If  $n_{\mathcal{V}}$  is greater than 1, the objective functions can be solved simultaneously or hierarchically. When several objective functions have to be solved simultaneously, the multi-objective optimisation problem is transformed into a mono-objective problem. The objective function is composed of the weighted sum of the objective functions:

$$\mathcal{V} = \sum_{t=1}^{n_{\mathcal{V}}} \mu_t \mathcal{V}_t, \quad \mu_t \in [0, 1], \quad \sum_{t=1}^{n_{\mathcal{V}}} \mu_t = 1 \quad (4.1)$$

The weighting factors  $\mu_t, t = 1, \dots, n_{\mathcal{V}}$ , are defined according to the priority assigned to each criterion. The criteria  $\mathcal{V}_t$  are bounded between 0 and 1.

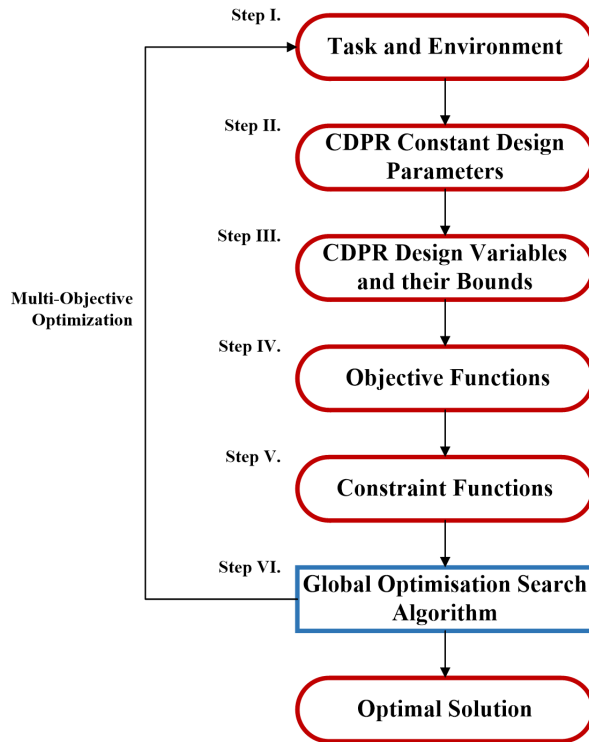


Fig. 4.1 – Design strategy for CDPRs

Step V. *Constraint Functions*. The designer defines a set of  $n_\phi$  constraint functions,  $\phi_k, k = 1, \dots, n_\phi$  that the CDPR should satisfy over the prescribed workspace or along the prescribed path.

Step VI. *Global Optimisation Algorithm*. The optimisation problem associated to the design problem is solved by means of an algorithm aiming at finding a candidate for the global optimum. Several global minimum search algorithms can be used, including genetic algorithms, gradient-based algorithms [ULP<sup>+</sup>07], simulated annealing and swarm particle optimisations. The choice of the algorithm depends on the complexity of the problem, the nature of the constraint functions, and the nature of the objective functions. Mono-objective optimisation problems are solved with respect to the constant design parameters provided in Step II, the design variables described in Step III and the given objective function. Hierarchical multi-objective problems require to solve several optimisation problems in series, by repeating the previous steps with respect to each of the  $n_\psi$  objective functions and the corresponding design parameters and design variables.

### 4.1.2 Objective Functions

#### Workspace Size

One of the main advantages of the CDPR is the possibility to displace payloads over large workspaces. Logistics and pick and place operations may require the moving platform of the CDPR to span a large space. In that case, the design problem can be defined as an optimisation problem aiming at maximising the workspace of the CDPR. The

design problem can be formulated in such a way to optimise the cable exit point locations, the cable connection point locations on the moving platform, the cable layout, and the characteristics of the actuators and the winches.

The workspace can be the WFW. The designer defines the maximum volume the CDPR can span, providing the bounds on the possible cable exit point locations. This volume represents the prescribed workspace, which is later on discretised into a set of  $n_p$  points  $\mathcal{P} = P_k, k = 1, \dots, n_p$ .

The objective function is defined as the percentage  $p_f$  of the wrench feasible points belonging to  $\mathcal{P}$ :

$$\mathcal{V}_1 = p_f = \frac{\sum_{k=1}^{n_p} F_k}{n_p} 100 \quad (4.2)$$

where  $F_k, k = 1, \dots, n_p$  is a set of binary values associated to points  $P_k, k = 1, \dots, n_p$ .  $F_k = 1$  when the  $k$ -th point  $P_k$  is wrench feasible, otherwise  $F_k = 0$ .

Alternatively, the objective function can be described as the regular volume included into the WFW of the CDPR. The regular volume represents the largest polygon included in the WFW of the CDPR. For example, a regular volume can assume the shape of a parallelepiped.

As described in Chap. 3, several workspaces can be used to analyse the behaviour of the CDPRs. Therefore, the optimisation of the CDPR workspace can be performed as well using the TFW and the IDFW when the kinematic constraints and the dynamic equilibrium of the CDPR are taken into account, respectively.

### Minimum Degree of Constraint Satisfaction

When the dimensions of the prescribed workspace of the CDPR are fixed a priori by the designer, the *Minimum Degree of Constraint Satisfaction* (MDoCS) of the CDPR may be optimised [GCC14]. The MDoCS quantifies how "close" the RCDPR is to a non static equilibrium condition with respect to a prescribed set of external wrenches,  $[\mathbf{w}_e]_r$ .

Provided a set of  $n_p$  points  $\mathcal{P} = P_k, k = 1, \dots, n_p$  composing the discretised prescribed workspace or path, the objective function  $\mathcal{V}_2$  can be defined, with respect to the wrench feasibility, as the average of the MDoCS computed for the  $n_t$  points belonging to  $\mathcal{P}$ :

$$\mathcal{V}_2 = \frac{\sum_{k=1}^{n_p} S_k}{n_p} \quad (4.3)$$

where the MDoCS,  $S_k$ , measured at point  $P_k$ , is defined as follows:

$$S_k = \min_{j=1, \dots, n_j} \left( \min_{l=1, \dots, n_l} (s_{k,j,l}) \right) \quad (4.4)$$

$s_{k,j,l}$  being the signed "distance" from the  $j$ -th vertex of  $[\mathbf{w}_e]_r$  to the  $l$ -th facet of the *Available Wrench Set* (AWS),  $[\mathbf{w}_e]_a$ , as illustrated in Fig. 4.2.  $n_j$  and  $n_l$  are equal to the number of vertices of the *Required External Wrench Set* (REWS),  $[\mathbf{w}_e]_r$ , and the number of facets of  $[\mathbf{w}_e]_a$ , respectively.

It has to be noticed that the units of the components of vector  $\mathbf{w}_e$  and matrix  $\mathbf{W}$  (2.12) are not homogeneous.

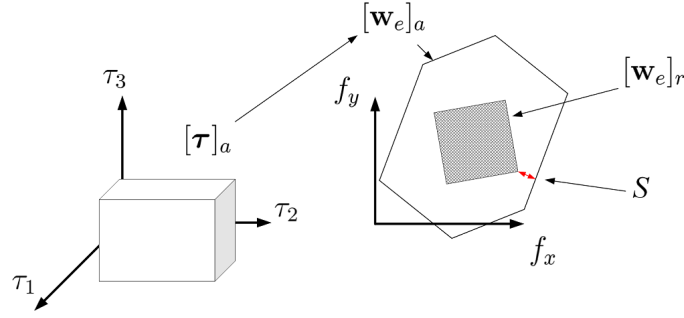


Fig. 4.2 – Minimum Degree of Constraint Satisfaction (MDoCS) for a planar CDPR

In order to compute the MDoCS, they are normalised as follows:

$$\mathbf{W}_n = \begin{bmatrix} \mathbb{I}_3 & \mathbf{0}_3 \\ \mathbf{0}_3 & \frac{1}{r_g} \mathbb{I}_3 \end{bmatrix} \mathbf{W} \quad (4.5)$$

$$\mathbf{w}_{e, n} = \begin{bmatrix} \mathbb{I}_3 & \mathbf{0}_3 \\ \mathbf{0}_3 & \frac{1}{r_g} \mathbb{I}_3 \end{bmatrix} \mathbf{w}_e \quad (4.6)$$

$r_g$  being the radius of gyration taking the form  $r_g^2 = \frac{1}{m} \sum_{i=1}^m \|\mathbf{b}_i^b\|_2^2$ .  $\mathbb{I}_3$  and  $\mathbf{0}_3$  are the  $(3 \times 3)$  identity and null matrices, respectively.

The MDoCS can be defined as well in terms of the dynamic equilibrium. In this case, the *Minimum Degree of Dynamic Constraint Satisfaction* (MDoDCS) should take into account the task requirements influencing the dynamic equilibrium of the moving platform, such as the acceleration of the moving platform,  $[\ddot{\mathbf{p}}]_r$ .

The MDoDCS,  $S_k^d$ , measured at point  $P_k$ , is defined as follows:

$$S_k^d = \min_{j=1, \dots, n_j} \left( \min_{l=1, \dots, n_l} (s_{k,j,l}^d) \right) \quad (4.7)$$

where  $s_{k,j,l}^d$  is the signed "distance" from the  $j$ -th vertex of the *Required Wrench Set* (RWS)  $[\mathbf{w}]_r$  to the  $l$ -th facet of  $[\mathbf{w}]_a$ . In this case,  $n_j$  and  $n_l$  are equal to the number of vertices of  $[\mathbf{w}]_r$  and the number of facets of  $[\mathbf{w}]_a$ , respectively. The terms composing the RWS should be normalised by means of the radius of gyration, according to the procedure illustrated for the WFW.

### Cable Tensions

During the execution of the task, cable tensions may increase considerably in the neighbourhood of singularities or workspace bounds. The higher the cables tensions, the higher the energy consumption and the higher the risk to damage mechanical parts of the CDPR. The CDPR can be designed in such a way that the average of the cable tensions is minimised. Given a prescribed workspace or a prescribed path discretised in  $n_p$  points,  $\mathcal{P} = P_k, k = 1, \dots, n_p$ , the geometry of the CDPR can be optimised by minimising the mean of the cable tensions,  $\|\overline{\boldsymbol{\tau}}\|_2$ , over a given workspace or along a given path. Thus, the objective function can be formulated as follows:

$$\gamma_3 = \frac{\|\overline{\boldsymbol{\tau}}\|_2}{n_p} = \frac{\sum_{k=1}^{n_p} \|\boldsymbol{\tau}_k\|_2}{n_p} \quad (4.8)$$

where  $\|\tau_k\|_2$  is the 2-norm of the cable tension vector,  $\tau$ , computed at point  $P_k$ .

### Cable Tension Variations

The task execution may induce important variations in cable tensions, according to the pose assumed by the moving platform, the moving platform accelerations and the external wrench. The reduction of variations in the cable tensions can be performed by means of an appropriate CDPR design, whose objective function aims at minimising the variations in the cable tensions over the prescribed workspace or path. The objective function is defined as the standard deviation  $\sigma_\tau$  of the 2-norm of the cable tension vector for all point  $P_k, k = 1, \dots, n_p$  belonging to the prescribed workspace or path to be followed by the CDPR:

$$\mathcal{V}_4 = \sigma_\tau = \sqrt{\frac{\sum_{k=1}^{n_p} \left( \|\tau_k\|_2 - \overline{\|\tau\|_2} \right)^2}{n_p}} \quad (4.9)$$

### CDPR Size

CDPRs may be used in small or cluttered environments. According to this assumption, the designer may want to reduce the size of the CDPR as much as possible. A compact design may be also required for deployable CDPRs, which require to be deployed, disassembled and moved easily. The size of the CDPR can be measured through the volume  $V$  of the convex hull of its cable exit points,  $A_i, i = 1, \dots, m$ ,  $\mathcal{V}_5 = V(A_i)$  being the objective function.

### Moving Platform Infinitesimal Displacement Due To Cable Deformations

The pose assumed by the moving platform is usually influenced by cable deformations. The variations in moving platform pose due to the non-rigid nature of the cables can be minimised. By minimising this infinitesimal displacement it is also possible to increase the stiffness of the CDPR.

The following objective function,  $\mathcal{V}_6$ , aims at minimising the 2-norm of the positioning infinitesimal displacement of the RCDPR moving platform. This objective function is expressed as the mean of the 2-norm of the positioning infinitesimal displacement,  $\overline{\|\delta\mathbf{t}\|_2}$ , for the  $n_p$  points  $P_k, k = 1, \dots, n_p$  of the discretised prescribed workspace  $\mathcal{P}$ :

$$\mathcal{V}_6 = \frac{\overline{\|\delta\mathbf{t}\|_2}}{n_p} = \frac{\sum_{k=1}^{n_p} \|\delta\mathbf{t}_k\|_2}{n_p} \quad (4.10)$$

where  $\|\delta\mathbf{t}_k\|_2$  is the 2-norm of the point-displacement vector at point  $P_k$ . The previous consideration can be extended as well to the moving platform orientation, by defining the following objective function:

$$\mathcal{V}_7 = \frac{\overline{\|\delta\mathbf{r}\|_2}}{n_p} = \frac{\sum_{k=1}^{n_p} \|\delta\mathbf{r}_k\|_2}{n_p} \quad (4.11)$$

where  $\overline{\|\delta\mathbf{r}\|_2}$  is the mean of the 2-norm of the orientation variation vector for the  $n_p$  points  $P_k, k = 1, \dots, n_p$  of the discretised prescribed workspace  $\mathcal{P}$  and  $\|\delta\mathbf{r}_k\|_2$  is the 2-norm of the orientation variation vector at point  $P_k$ , according to the definition provided in Sec. 2.3.1.

### 4.1.3 Constraint Functions

#### Wrench Feasibility

Since cables can only pull on the moving platform, the tensions in the cables must always be non-negative. Moreover, cable tensions must be lower than an upper bound,  $\tau_{max}$ , which corresponds either to the maximum tension  $\tau_{max1}$  the cables (or other mechanical parts) can bare, or to the maximum tension  $\tau_{max2}$  the motors can provide.

The cable tension bounds can thus be written as:

$$0 \leq \tau_i \leq \tau_{max}, \quad \forall i = 1, \dots, m \quad (4.12)$$

where  $\tau_{max} = \min\{\tau_{max1}, \tau_{max2}\}$ .

The maximum tension  $\tau_{max1}$ , due to the structural limit of the cables is expressed as follows:

$$\tau_{max1} = \pi \frac{\phi_c^2}{4} E \quad (4.13)$$

where  $E$  is the Young modulus of the cables and  $\phi_c$  the diameter of the cables. The motor power limits both the tension transmitted to the cables and the rotational speed of the winches. In this manuscript,  $\tau_M$  and  $\omega_M$  refer to the nominal torque and speed of the motors, respectively. A gearbox is connected to the motor. The winches are connected to the gearboxes. They transmit a tension  $\tau_{max2}$  to the cable, proportional to the inverse of the winches radius,  $\rho_W = \frac{2}{\phi_w}$ :

$$\tau_{max2} = \rho_W \tau_G = \rho_W \rho_R \tau_M = \frac{2}{\phi_w} \rho_R \tau_M \quad (4.14)$$

Due to the cable tension bounds, CDPRs can balance only a bounded set of external wrenches. Then, when the motion of the moving platform is quasi-static, the analysis of the WFW is required. According to Def. 3.1, the following constraint requires the poses of a RCDPR moving platform to be wrench feasible:

$$\forall \mathbf{w}_e \in [\mathbf{w}_e]_r, \exists \boldsymbol{\tau} \in [\boldsymbol{\tau}] \text{ s.t. } \begin{cases} \mathbf{w}_e \in [\mathbf{w}_e]_a \\ \mathbf{W}\boldsymbol{\tau} + \mathbf{w}_e = 0 \end{cases} \quad (4.15)$$

With respect to Eq. (3.6), this constraint can be simplified as follows:

$$\mathbf{C}\mathbf{w}_e \leq \mathbf{d}, \quad \forall \mathbf{w}_e \in [\mathbf{w}_e]_r \quad (4.16)$$

It has to be noticed that the wrench feasibility analysis verifies implicitly the absence of singularities. Singularities of a CDPR can be detected by analysing the singularities of the wrench matrix. This analysis is included in the WFW computation, namely, the singularity of the wrench matrix  $\mathbf{W}$  implies that the corresponding pose is not wrench feasible.

#### Dynamic Feasibility

When the accelerations of the moving platform are not negligible, the dynamic of the CDPR has to be taken in consideration. Therefore, the analysis of dynamic feasibility becomes necessary. The constraint associated to the

DFW can be deduced from Def. 3.9:

$$\forall \mathbf{w}_e \in [\mathbf{w}_e]_r, \forall \dot{\mathbf{p}} \in [\dot{\mathbf{p}}]_r \exists \boldsymbol{\tau} \in [\boldsymbol{\tau}]_a \quad \text{s.t.} \quad \frac{2}{\phi_W} \eta_R \rho_R \mathbf{W} \boldsymbol{\tau}_M + \mathbf{A} \dot{\mathbf{p}} + \mathbf{B} \dot{\mathbf{p}} + \mathbf{D} + \mathbf{w}_e = 0 \quad (4.17)$$

Using the IDFW computation strategy proposed in Sec. 3.3.2, the constraint can be rewritten as follows:

$$\mathbf{C}_d \mathbf{w}_r \leq \mathbf{d}_d, \quad \forall \mathbf{w} \in [\mathbf{w}]_r \quad (4.18)$$

### Twist Feasibility

According to the specifications of the tasks to be performed, the analysis of the TFW can be demanded. For the given points  $P_k, k = 1, \dots, n_p \in \mathcal{P}$  of the prescribed workspace or path, the constraint associated to the twist feasibility is issued from Def. 3.6:

$$\forall \dot{\mathbf{p}} \in [\dot{\mathbf{p}}]_r, \exists \dot{\mathbf{i}} \in [\dot{\mathbf{i}}]_a \quad \text{s.t.} \quad \begin{cases} \dot{\mathbf{p}} \in [\dot{\mathbf{p}}]_a \\ \mathbf{J} \dot{\mathbf{i}} - \dot{\mathbf{p}} = 0 \end{cases} \quad (4.19)$$

and can be rewritten according to the following equation:

$$\mathbf{C}^* \dot{\mathbf{p}} \leq \mathbf{d}^*, \quad \forall \dot{\mathbf{p}} \in [\dot{\mathbf{p}}]_r \quad (4.20)$$

### Cable Lengths

Due to technological reasons, cable lengths are bounded between a maximum cable length,  $l_{max}$ , and a minimum cable length,  $l_{min}$ . The maximum cable length depends on the properties of the winches, in particular their lengths and their diameters. The minimum cable length is defined according to the routing of the cable and the geometry of the CDPR:

$$l_{min} \leq l_i \leq l_{max}, \quad \forall i = 1, \dots, m \quad (4.21)$$

### Cable Interferences

If two or more cables collide, the geometric and static models of the CDPR are not valid any more and the cables can be damaged or their life time severely reduced. In order to verify that cables do not interfere, it is sufficient to determine the distances between them. Modelling the cables as linear segments, the distance  $d_{i,j}^{cc}$  between the  $i$ -th cable and the  $j$ -th cable can be computed, e.g. by means of the method presented in [Lum85]. There is no interference if the distance is larger than the diameter of the cables,  $\phi_c$ :

$$d_{i,j}^{cc} \geq \phi_c \quad \forall i, j = 1, \dots, m, \quad i \neq j \quad (4.22)$$

The number of possible cable interferences to be verified is equal to  $C_{m,2} = \frac{m!}{2!(m-2)!}$ . Note that, depending on the way the cables are routed from the winches to the moving platform, possible interferences of the cable segments between the winches and the pulleys may have to be considered.

### Collisions Between the Cables and the Environment

Industrial environments may be cluttered. Collisions between the environment and the cables of the CDPR should be avoided. For fast collision detection, the environment objects (obstacles) are enclosed in bounding volumes such as spheres and cylinders. When more complex shapes have to be considered, their surfaces are approximated with polygonal meshes. Thus, the collision analysis is performed by computing the distances between the edges of those polygons and the cables, e.g. by using [Lum85].

### Pose Infinitesimal Displacement Due to the Non-Rigid Nature of Cables

Cables are not perfectly rigid body. Consequently, the cables are subjected to some deformations that may induce some moving platform pose infinitesimal displacements. The pose infinitesimal displacement can be computed by inverting Eq. (2.65).

$$\delta \mathbf{p} = \mathbf{K}^{-1} \delta \mathbf{w}_c \quad (4.23)$$

$\delta \mathbf{t} = [\delta t_x, \delta t_y, \delta t_z]^T$  and  $\delta \phi = [\delta \gamma, \delta \beta, \delta \alpha]^T$  characterise the positioning and orientation moving platform variations due to the cable elasticity, respectively.

The pose variation should be bounded by: The positioning error threshold vector,  $\delta \mathbf{t}_c = [\delta t_{x,c}, \delta t_{y,c}, \delta t_{z,c}]^T$ , where  $\delta t_{x,c}$ ,  $\delta t_{y,c}$  and  $\delta t_{z,c}$  represent the bounds on the positioning errors along the axes  $\mathbf{x}_b$ ,  $\mathbf{y}_b$  and  $\mathbf{z}_b$  and the orientation error threshold vector,  $\delta \phi = [\delta \gamma_c, \delta \beta_c, \delta \alpha_c]^T$ , where  $\delta \gamma_c$ ,  $\delta \beta_c$  and  $\delta \alpha_c$  represent the bounds on the moving platform orientation errors about the axes  $\mathbf{x}_b$ ,  $\mathbf{y}_b$  and  $\mathbf{z}_b$ , i.e.:

$$-[\delta t_{x,c}, \delta t_{y,c}, \delta t_{z,c}]^T \leq [\delta t_x, \delta t_y, \delta t_z]^T \leq [\delta t_{x,c}, \delta t_{y,c}, \delta t_{z,c}]^T \quad (4.24)$$

$$-[\delta \gamma_c, \delta \beta_c, \delta \alpha_c]^T \leq [\delta \gamma, \delta \beta, \delta \alpha]^T \leq [\delta \gamma_c, \delta \beta_c, \delta \alpha_c]^T \quad (4.25)$$

### Vibrations

By displacing the CDPR moving platform with high accelerations, vibrations can affect the CDPR during the task execution. Vibration analysis can be performed computing the vibration modes of the CDPR by analysing the CDPR stiffness matrix  $\mathbf{K}$  and its eigenvalues. The analysis based on the stiffness matrix issued by the elasto-static modelling of the CDPR (i.e. the ones described in Sec. 2.4) can provide a partial description of the vibration modes. An accurate analysis should be performed over the dynamic stiffness matrix of the CDPR, as highlighted by Yuan *et al.* in [YCD15].

## 4.2 Classes of RCDPRs

CDPRs consist usually of several standard components, notably: A fixed base, a moving platform, a set of  $m$  cables connecting the moving platform to the fixed base through a set of pulleys, a set of  $m$  winches, gearboxes, actuators and a set of internal and external sensors. These components are usually dimensioned in such a way the geometry of the CDPR does not vary during the task. However, by modifying the CDPR geometry, the capacities of CDPRs can be improved. As a matter of fact, RCDPRs are defined as follows:

**Definition 4.1.** A RCDPR is a CDPR whose geometry can be adapted reconfiguring part of its components.

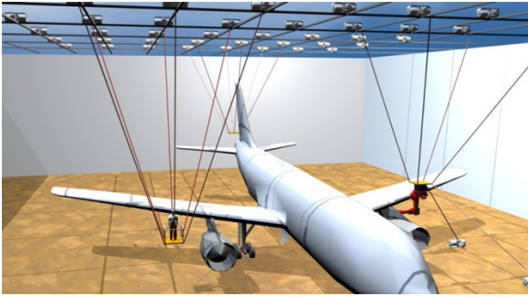


**Fig. 4.3** – CableBot design with cable exit point fixed to a grid. Courtesy of the European FP7 Project CableBot [Caba]

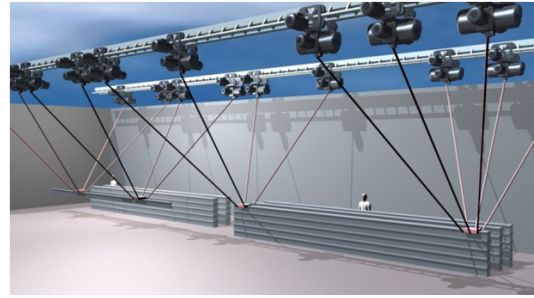


**Fig. 4.4** – CableBot design with cable exit point sliding on rails. Courtesy of the European FP7 Project CableBot [Caba]

### 4.2.1 Reconfigurable Elements and Technological Solutions

According to Def. 4.1, part of the components of a RCDPR may be reconfigured in order to improve its performances. The geometry of the RCDPRs is mostly dependent on the locations of the cable exit points, the locations of the cable attachment points on the moving platform and the number of cables.

The locations of the cable exit points,  $\mathbf{a}_i^b, i = 1, \dots, m$ , have to be reconfigured when the environment is strongly cluttered. Indeed, changing of the cable exit point locations can increase the IFW of the RCDPR. Furthermore, the reconfiguration of cable exit points provides the possibility to modify the layout of the cables and improve the performances of the RCDPR (such as its stiffness). From a technological point of view, points  $A_i, i = 1, \dots, m$  are displaced by moving the pulleys orienting the cables and guiding them to the moving platform. Pulleys are connected on the base of the RCDPR. They can be displaced by sliding them on linear guides or fixing them on a grid of locations, as proposed in the concepts of Fig. 4.3 and Fig. 4.4, respectively. These concepts have been developed in the framework of the European FP7 Project CableBot [Caba]. Alternatively, pulleys can be connected to several terrestrial or aerial unmanned vehicles, as proposed in [JK13, MDRC13, ZTK12].

The geometry of the RCDPR and the cable layout can be modified as well by displacing the cable connection points on the moving platform,  $B_i, i = 1, \dots, m$ . A change in the locations  $\mathbf{b}_i^p, i = 1, \dots, m$  let improve the stiffness of the RCDPR and the MDoCS margin, permitting to compensate higher external wrenches along a prescribed direction. A modification of the cable attachment points may result as well in an improvement of the dimensions of the IFW. The reconfiguration of points  $B_i, i = 1, \dots, m$  can be performed by attaching and detaching the cables at different locations of the moving platform.

The number of cables,  $m$ , has a major influence over the geometry and the performances of the RCDPR. A higher number of cables may lead to an increase of the workspace dimensions and a reduction of the cable tensions and vibrations. However, increasing the number of cables lead to a higher risk of collisions. Accessibility problems can be limited by modifying  $m$ . In this case, the reconfiguration can be performed attaching or detaching one or more additional cable(s) to the moving platform and to a new set of exit points. Furthermore, by attaching and detaching one or more cable(s), the architecture of the RCDPRs can be modified, having access to both suspended and non-suspended configurations and their advantages.

**Tab. 4.1** – CDPDR RECONFIGURABLE PARAMETER CLASSIFICATION

Reconfigurable Parameter	Discrete Domain	Continuous Domain
Exit Point Locations	Yes	Yes
Moving Platform Connection Point Locations	Yes	Yes
Cable Number	Yes	No

### 4.2.2 Discrete and Continuous Reconfigurations

According to the reconfigured components and the associated technology, reconfiguration parameters can be selected over a continuous or a discrete domain of values, as resumed in Table 4.1. Reconfigurations performed over a *discrete domain* let select the reconfigurable parameters within a finite set of values. The variation of the number of cables is a typical example of discrete reconfiguration. Discrete reconfigurations apply as well to the connection points between the cables and the platform, when the dimensions of the moving platform are fixed and the cables can be installed on the moving platform only at some specific locations, e.g. its corners. Another example of discrete RCDPR is represented in Fig. 4.3. In this concept, developed in the framework of the European FP7 Project CableBot, cable exit points are installed on a predefined grid of locations on the ceiling. Discrete reconfigurations are performed off-line, interrupting the task the RCDPR is executing. For this reason, the set-up time of these RCDPRs can be relative large. On the contrary, the costs associated to a discrete RCDPR are moderate, since discrete RCDPRs do not require to motorise the cable exit points.

Reconfigurations performed over a *continuous domain* provides the possibility to select the geometric parameters over a continuous set of values delimited by upper and lower bounds. A typical example of continuous RCDPR is represented in Fig. 4.4, which illustrates another concept developed in the framework of the European FP7 Project CableBot. In this example, the cable exit points slide on some rails fixed on the ceiling. Reconfigurations can be performed on-line, by modifying smoothly the reconfigurable parameters during the task execution. The main advantages of continuous reconfigurations are the reduced set-up time and the local optimisation of the RCDPR properties. However, modifying the locations of the exit points in real time may require the design of a complex control scheme. Furthermore, the cost of RCDPRs with continuous reconfigurations is generally higher than the cost of discrete RCDPRs, since the displacement of the pulleys should be fully actuated.

## 4.3 Nomenclature for RCDPRs

Similarly to CDPDRs, a RCDPR is mainly composed of a moving platform connected to the base through a set of cables, as illustrated in Fig. 4.5. The main difference between CDPDRs and RCDPRs consists of the possibility to displace the cable exit points on a grid of locations. Therefore, the nomenclature associated to the RCDPR models requires some modifications in order to distinguish the possible configurations the RCDPR can assume.

The connection points of the  $i$ -th cable on the moving platform are denoted as  $B_{i,c}$ , where  $c$  represents the configuration number. For the  $c$ -th configuration, the exit point of the  $i$ -th cable is denoted by  $A_{i,c}$ ,  $i = 1, \dots, 8$ . The Cartesian coordinates of each point  $A_{i,c}$ , with respect to  $\mathcal{F}_b$ , are given by the vector  $\mathbf{a}_{i,c}^b$ . Therefore, the IGM of the RCDPR can be rewritten according to the following equation:

$$\mathbf{l}_{i,c}^b = \mathbf{a}_{i,c}^b - \mathbf{t} - \mathbf{R}\mathbf{b}_i^p \quad i = 1, \dots, m \quad (4.26)$$

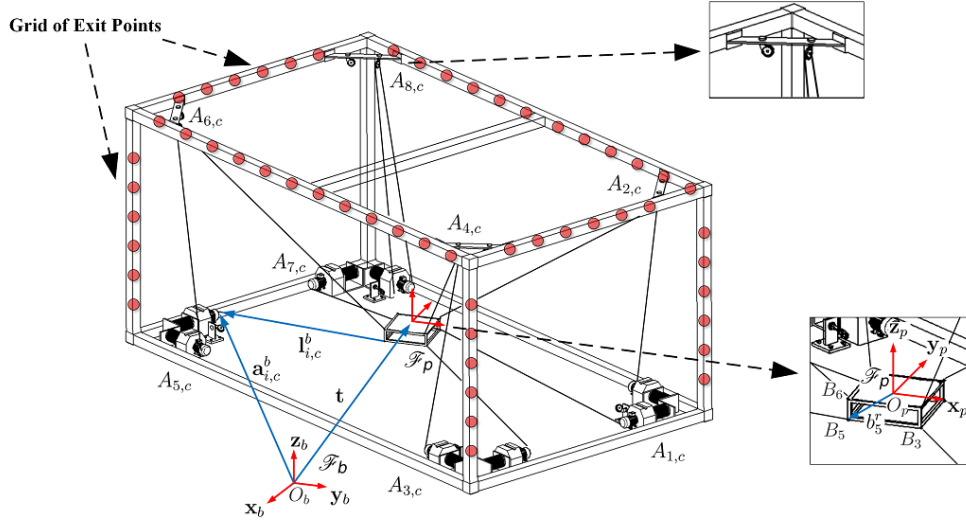


**Fig. 4.5** – Schematic of a RCDPR. The red points represent the possible locations of the cable exit points, where the pulleys can be fixed

where vector  $\mathbf{l}_{i,c}^b$  is directed along the  $i$ -th cable from point  $B_i$  to point  $A_{i,c}$ . The length of the  $i$ -th cable is then defined by the 2-norm of the cable vector  $\mathbf{l}_{i,c}^b$ , namely,  $l_{i,c} = \|\mathbf{l}_{i,c}^b\|_2$ ,  $i = 1, \dots, m$ .

The wrench matrix  $\mathbf{W}$  characterising the static equilibrium of the moving platform can be described as follows:

$$\mathbf{W}_c = \begin{bmatrix} \mathbf{d}_{1,c}^b & \mathbf{d}_{2,c}^b & \dots & \mathbf{d}_{m,c}^b \\ \mathbf{Rb}_1^p \times \mathbf{d}_{1,c}^b & \mathbf{Rb}_2^p \times \mathbf{d}_{2,c}^b & \dots & \mathbf{Rb}_m^p \times \mathbf{d}_{m,c}^b \end{bmatrix} \quad (4.27)$$

where  $\mathbf{d}_{i,c}^b$ ,  $i = 1, \dots, m$  are the unit cables vectors associated to the  $c$ -th configuration. According to the provided examples, the notations of all the RCDPR models introduced in Chap. 2 can be updated in order to distinguish between the different configurations.

## 4.4 Design Strategy for RCDPRs

Similarly to CDPRs, the design of RCDPRs requires the dimensioning of all its components. In this manuscript, the design of RCDPRs focuses on the selection of the cable exit point locations. The other components of the RCDPR are supposed to be already chosen.

### 4.4.1 Design Problem Formulation

The RCDPR design strategy proposed in this section consists of ten steps, as shown in Fig. 4.6. The design can be formulated as a mono-objective or a hierarchical multi-objective optimisation problem. The design defines a prescribed workspace or a prescribed path and divides it into  $n_t$  parts. Each part has to be covered by one and only one configuration. The design variables are the locations of the cable exit points for the  $n_t$  configurations covering the  $n_t$  parts of the prescribed workspace of path. The *global objective functions* investigated in Sec. 4.4.2 aim at improving the performance of the RCDPR, e.g. reducing the reconfiguration time. The optimisation is performed while verifying a set of user-defined constraints, typically the ones described in Sec. 4.1.3.

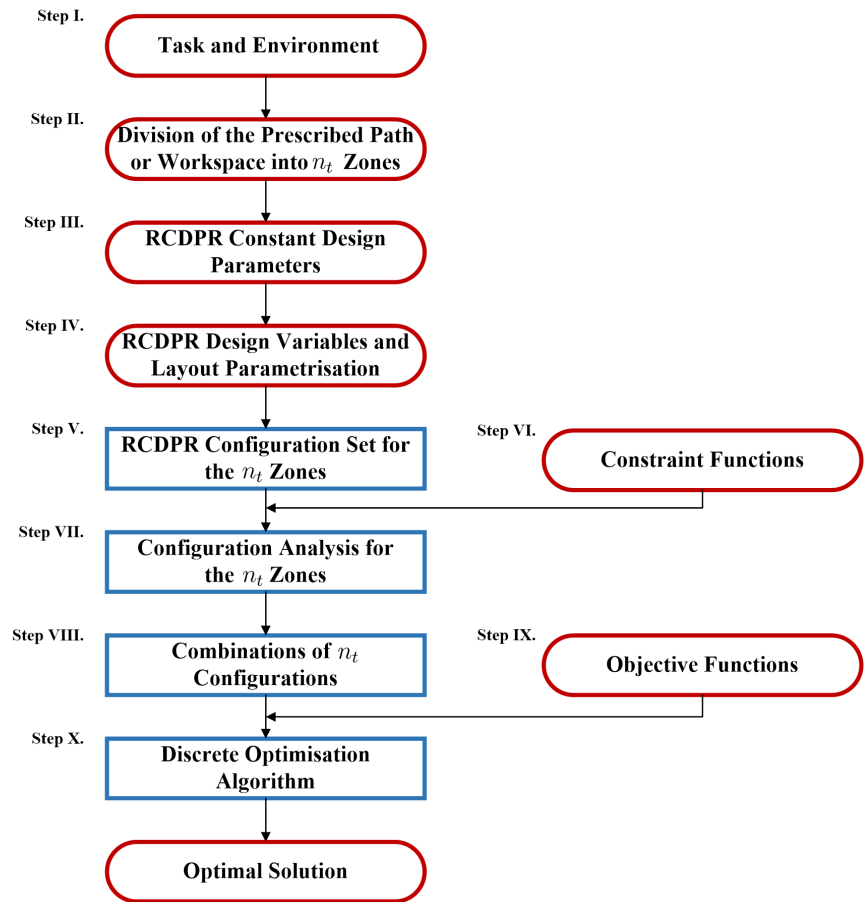


Fig. 4.6 – Design strategy for RCDPRs

Step I. *Task and Environment*. The designer describes the task to be performed, according to the same procedure presented for CDPRs.

Step II. *Division of the Prescribed Workspace or Path*. Given the prescribed workspace or moving platform path, the designer divided it into  $n_t$  parts, assuming that each of them is accessible by one and only one configuration of the RCDPR. The division may be performed trying to predict the possible collisions of the cables and the working environment.

Step III. *Constant Design Parameter*. The designer defines a set of constant design parameters and their values. The parameters are collected in the constant design parameter vector  $\mathbf{q}$ .

Step IV. *Design Variables and Layout Parametrisation*. For each part of the prescribed workspace or moving platform path, the designer defines the cable layout of the associated configuration. The cable layout associated to the  $t$ -th part of the prescribed workspace or path defines the locations of the cable exit points, parametrised with respect to a set of  $n_{t,v}$  design variables,  $u_{t,v}, v = 1, \dots, n_{t,v}$ . The design variables are defined as a discrete set of  $\varepsilon_{t,v}$  values,  $[u]_{t,v}, v = 1, \dots, n_{t,v}$ .

Step V. *RCDPR Configuration Set*. For each part of the prescribed workspace or path, all the possible configurations that can be generated combining the values  $[u]_{t,v}, v = 1, \dots, n_{t,v}$  of the  $n_{t,v}$  design variables

are computed. Therefore,  $n_{t,\mathcal{C}} = \prod_{v=1}^{n_{t,v}} \varepsilon_{t,v}$  possible configurations are generated for the  $t$ -th part of the prescribed workspace or path.

- Step VI. *Constraint Functions.* The user defines a set of  $n_\phi$  constraint functions,  $\phi_k, k = 1, \dots, n_\phi$ . These functions are applied to all the possible configurations associated to all the  $n_t$  part of the prescribed workspace or path.
- Step VII. *Configuration Analysis.* For each portion of the prescribed workspace or path, all the possible configurations generated at Step V with respect to the  $n_\phi$  user-defined constraint functions are tested. The  $n_{f,t}$  configurations satisfying the constraints all over the  $t$ -th part of the prescribed workspace or path are defined hereafter as feasible configurations.
- Step VIII. *Feasible Configuration Combination.* The  $n_t$ -dimensional sets of configurations that lead to the achievement of the prescribed task are computed. Each set is composed combining the  $n_{f,t}$  feasible configurations associated to each part of the prescribed workspace or path. The number of  $n_t$ -dimensional sets of feasible configurations generated during this step is equal to  $n_\mathcal{C}$ .
- Step IX. *Objective Functions.* The designer defines one or more global objective function(s),  $\mathcal{V}_l, l = 1, \dots, n_\mathcal{V}$ , where  $n_\mathcal{V}$  is equal to the number of global objective functions taken into account. With respect to the objective functions described in Sec. 4.2.1, the global objective functions do not focus only on a single configuration. They analyse the properties of the entire RCDPR, considering at once all the  $n_t$  configurations composing the RCDPR. If more global objective functions have to be solved simultaneously, the optimisation problem can be reduced to a mono-objective optimisation, according to Eq. (4.1). If several global optimisation functions have to be solved hierarchically, the designer will number the objective functions according to their priority,  $l = 1, \dots, n_\mathcal{V}$ , having  $\mathcal{V}_1$  the highest priority and  $\mathcal{V}_{n_\mathcal{V}}$  the lowest one.
- Step X. *Discrete Optimisation Algorithm.* The design problem is formulated as an optimisation problem and solved by analysing all the  $n_\mathcal{C}$  sets of feasible configurations. The analysis is performed with respect to the global objective functions defined at Step IX. The  $n_t$ -dimensional set of feasible configurations with the best global objective function is detected. If a hierarchical multi-objective optimisation is required, the following procedure is applied:
- The algorithm analyses the  $n_\mathcal{C}$  sets of feasible configurations with respect to a global objective function,  $\mathcal{V}_l$ , which is initialised as the highest priority global objective function,  $\mathcal{V}_l = \mathcal{V}_1$ .
  - If only a  $n_t$ -dimensional set of feasible configurations optimises  $\mathcal{V}_l$ , this set is considered as the optimal one. On the contrary, if  $n_{\mathcal{C},l}$  set of feasible configurations optimise  $\mathcal{V}_l$ , the algorithm proceeds to the following step.
  - The algorithm analyses the  $n_{\mathcal{C},l}$  sets of optimal solutions with respect to the global objective function with lower priority,  $\mathcal{V}_{l+1}$ . Then, the algorithm moves to Step b.

#### 4.4.2 Global Objective Functions

The design strategy proposed in the previous section aims at optimising the characteristics of the RCDPR. The optimisation may be performed with respect to one or more *global objective functions*. The objective functions used in this manuscript are described hereafter.

### RCDPR Size

The design optimisation problem may aim at minimising the size of the robot, defined as the convex hull of the cable exit points. The Cartesian coordinates of exit point  $A_{i,c}$  are defined as  $\mathbf{a}_{i,c} = [a_{i,c}^x, a_{i,c}^y, a_{i,c}^z]^T$ . The variables  $\underline{s}_x$ ,  $\underline{s}_y$  and  $\underline{s}_z$  denote the smallest Cartesian coordinates of the cable exit points along the axes  $\mathbf{x}_b$ ,  $\mathbf{y}_b$  and  $\mathbf{z}_b$ , respectively:

$$\underline{s}_x = \min a_{i,c}^x, \forall i = 1, \dots, m, c = 1, \dots, n_t \quad (4.28)$$

$$\underline{s}_y = \min a_{i,c}^y, \forall i = 1, \dots, m, c = 1, \dots, n_t \quad (4.29)$$

$$\underline{s}_z = \min a_{i,c}^z, \forall i = 1, \dots, m, c = 1, \dots, n_t \quad (4.30)$$

where  $m$  is the number of cables and  $n_t$  the number of configurations of the RCDPR.

The upper bounds on the Cartesian coordinates of the RCDPR cable exit points, along the axes  $\mathbf{x}_b$ ,  $\mathbf{y}_b$ ,  $\mathbf{z}_b$ , are denoted by  $\bar{s}_x$ ,  $\bar{s}_y$  and  $\bar{s}_z$ , respectively.

$$\bar{s}_x = \max a_{i,c}^x, \forall i = 1, \dots, m, c = 1, \dots, n_t \quad (4.31)$$

$$\bar{s}_y = \max a_{i,c}^y, \forall i = 1, \dots, m, c = 1, \dots, n_t \quad (4.32)$$

$$\bar{s}_z = \max a_{i,c}^z, \forall i = 1, \dots, m, c = 1, \dots, n_t \quad (4.33)$$

Hence, the objective function related to the size of the robot is expressed as follows:

$$\mathcal{V}_1 = (\bar{s}_x - \underline{s}_x)(\bar{s}_y - \underline{s}_y)(\bar{s}_z - \underline{s}_z) \quad (4.34)$$

### Number of Cable Reconfigurations

According to the reconfiguration strategy proposed in this manuscript, reconfiguration operations require the displacement of the cable exit points, and consequently attaching/detaching operations of the cables. These operations are time consuming. The following objective function aims at minimising the number of reconfigurations,  $n_r$ , defined as the number of exit point changes to be performed in order to switch from configuration  $\mathcal{C}_i$  to configuration  $\mathcal{C}_j$ :

$$\mathcal{V}_2 = n_r \quad (4.35)$$

By reducing the number of cable attaching/detaching operations, the RCDPR set-up time could be significantly decreased.

### Number of Configuration Changes

During the reconfiguration of the exit points, the task executed by the RCDPR has to be interrupted. These interruptions impact the task execution time. Therefore, it may be necessary to minimise the number of interruptions,  $n_i$ , in order to improve the effectiveness of the RCDPR. The objective function  $\mathcal{V}_3$  associated to this goal measures the number of configuration changes,  $n_i$ , to be performed during a prescribed task,  $\mathcal{V}_3 = n_i$ .

### RCDPR Complexity

The complexity of the RCDPR increases according to the number of configurations  $n_{\mathcal{C}}$  required to cover the prescribed workspace of moving platform path. When the RCDPR demands a high number of configurations, the base frame of the CDPR may become complex. In order to minimise the complexity of the RCDPR, it is possible to reduce the overall number of exit point locations,  $\mathcal{C}_4 = n_e$ , required by the  $n_{\mathcal{C}}$  configurations. Therefore, the optimisation aims at maximising the number of exit point locations shared among two or more configurations.

## 4.5 Case Study I: Design of a CDPR Based on the Workspace Size

### 4.5.1 Problem Description

Designing a CDPR is a complex task which requires the dimensioning of several components and parameters. Most of the research works involving the design of CDPRs are focused on the dimensioning of the moving platform and the selection of the exit point locations. The present case study focuses on the dimensioning of:

- The actuators, which in this case study are electric motors, whose nominal torque and speed are defined as  $\tau_M$  and  $\omega_M$ , respectively.
- The winches, having a drum whose diameter is equal to  $\phi_w$ .
- The gearboxes, connecting the winches to the motors, whose transmission ratio is equal to  $\rho_R$ .

### Task and Environment

The dimensioning of the motors, the winches and the gearboxes has a great influence on the WFW and the TFW. In order to increase the size of both the workspaces, the design procedure has been formulated as an optimisation problem according to the strategy presented in Sec. 4.1.1. A prescribed workspace,  $\mathcal{P}$ , is defined. It consists of a box, as shown in Fig. 4.7. The box has been discretised into a set of  $n_P = 1881$  points,  $P_k$ ,  $k = 1, \dots, n_P \in \mathcal{P}$ , whose coordinates along  $\mathbf{x}_b$ ,  $\mathbf{y}_b$  and  $\mathbf{z}_b$  are defined according to the sets of values  $[\mathbf{x}]$ ,  $[\mathbf{y}]$  and  $[\mathbf{z}]$ , respectively:

$$[\mathbf{x}] = \{-0.45 \text{ m} : 0.05 \text{ m} : 0.45 \text{ m}\} \quad (4.36)$$

$$[\mathbf{y}] = \{-0.25 \text{ m} : 0.05 \text{ m} : 0.25 \text{ m}\} \quad (4.37)$$

$$[\mathbf{z}] = \{-0.2 \text{ m} : 0.05 \text{ m} : 0.2 \text{ m}\} \quad (4.38)$$

The component of the external forces acting on the moving platform,  $f_x$ ,  $f_y$  and  $f_z$ , have been constrained between  $\pm 20$  N. The components of the external moments,  $m_x$ ,  $m_y$  and  $m_z$ , are bounded between  $\pm 0.1$  Nm:

$$-20 \text{ N} \leq f_x, f_y, f_z \leq 20 \text{ N} \quad (4.39)$$

$$-0.1 \text{ Nm} \leq m_x, m_y, m_z \leq 0.1 \text{ Nm} \quad (4.40)$$

Analogously, the twist components of the moving platform,  $\dot{i}_x$ ,  $\dot{i}_y$  and  $\dot{i}_z$ , have been constrained between  $\pm 0.1$  m/s. The moving platform orientation is assumed to be constant, the frame  $\mathcal{F}_p$  being aligned with the base

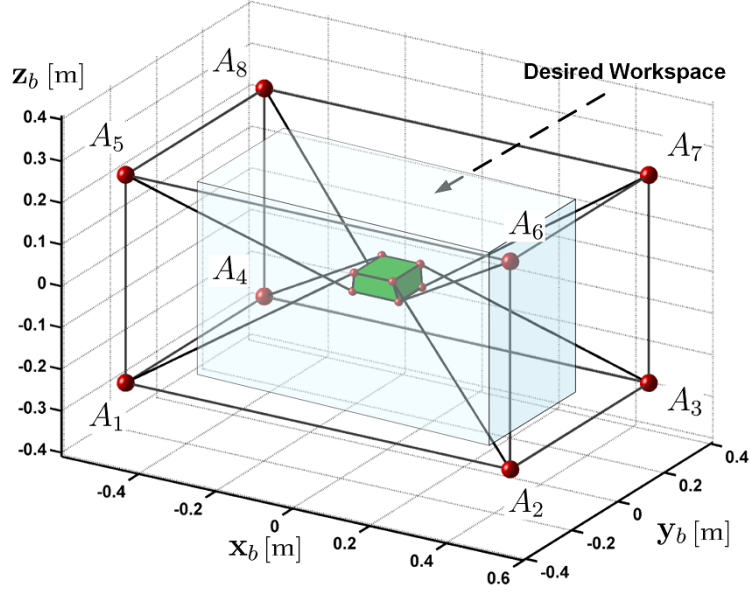


Fig. 4.7 – Case Study I: Description of the case study and the prescribed workspace

frame  $\mathcal{F}_b$ .

$$-0.1 \frac{\text{m}}{\text{s}} \leq \dot{t}_x, \dot{t}_y, \dot{t}_z \leq 0.1 \frac{\text{m}}{\text{s}} \quad (4.41)$$

$$\omega_x, \omega_y, \omega_z = 0 \quad (4.42)$$

### Constant Design Parameters

The spatial CDPR of this case study consists of  $m = 8$  steel cables. Their diameter,  $\phi_c$ , is equal to 2 mm and their linear elastic coefficient,  $k_c$ , is equal to  $2.52 \times 10^6 \frac{\text{N}}{\text{m}}$ . The cable mass is neglected. The cables exit points,  $A_i$ ,  $i = 1, \dots, m$ , are located at the corner of the base frame, as illustrated in Fig. 4.7, according to the following Cartesian coordinates:

$$\mathbf{a}_1^b = \frac{1}{2} \begin{bmatrix} -s_l, -s_w, -s_h \end{bmatrix}^T \quad \mathbf{a}_2^b = \frac{1}{2} \begin{bmatrix} s_l, -s_w, -s_h \end{bmatrix}^T \quad (4.43)$$

$$\mathbf{a}_3^b = \frac{1}{2} \begin{bmatrix} s_l, s_w, -s_h \end{bmatrix}^T \quad \mathbf{a}_4^b = \frac{1}{2} \begin{bmatrix} -s_l, s_w, -s_h \end{bmatrix}^T \quad (4.44)$$

$$\mathbf{a}_5^b = \frac{1}{2} \begin{bmatrix} -s_l, -s_w, s_h \end{bmatrix}^T \quad \mathbf{a}_6^b = \frac{1}{2} \begin{bmatrix} s_l, -s_w, s_h \end{bmatrix}^T \quad (4.45)$$

$$\mathbf{a}_7^b = \frac{1}{2} \begin{bmatrix} s_l, s_w, s_h \end{bmatrix}^T \quad \mathbf{a}_8^b = \frac{1}{2} \begin{bmatrix} -s_l, s_w, s_h \end{bmatrix}^T \quad (4.46)$$

where the base frame length,  $s_l$ , width,  $s_w$ , and height,  $s_h$ , are equal to 1 m, 0.6 m, 0.5 m, respectively.

The cables are connected to the moving platform according to a cross cable layout. The main advantage of this layout is the increase of the CDPR stiffness. The Cartesian coordinates  $\mathbf{b}_i$  of points  $B_i$ ,  $i = 1, \dots, m$  are defined as

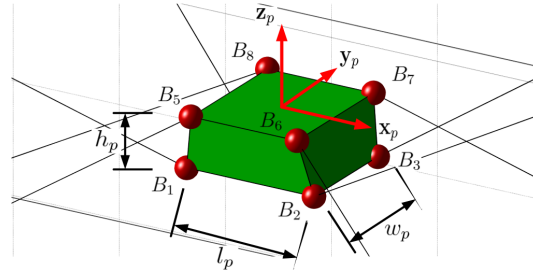


**Fig. 4.8** – Case Study I: Moving Platform of the CDPR

**Tab. 4.2** – DESIGN VARIABLE BOUNDS

Design Variable	$\tau_M$ [Nm]	$\omega_M$ [rpm]	$\phi_w$ [cm]	$\rho_R$
<i>min</i>	0.5	50	1	0.5
<i>Max</i>	1.5	200	5	5

follows:

$$\mathbf{b}_1^p = \frac{1}{2} [-l_p, -w'_p, h_p]^T \quad \mathbf{b}_2^p = \frac{1}{2} [l_p, -w'_p, h_p]^T \quad (4.47)$$

$$\mathbf{b}_3^p = \frac{1}{2} [l_p, w'_p, h_p]^T \quad \mathbf{b}_4^p = \frac{1}{2} [-l_p, w'_p, h_p]^T \quad (4.48)$$

$$\mathbf{b}_5^p = \frac{1}{2} [-l'_p, -w_p, -h_p]^T \quad \mathbf{b}_6^p = \frac{1}{2} [l'_p, -w_p, -h_p]^T \quad (4.49)$$

$$\mathbf{b}_7^p = \frac{1}{2} [l'_p, w_p, -h_p]^T \quad \mathbf{b}_8^p = \frac{1}{2} [-l'_p, w_p, -h_p]^T \quad (4.50)$$

where  $w'_p = w_p + u_0$  and  $l'_p = l_p + u_0$ .  $u_0$  is an offset applied to the cable-platform connection points in order to avoid cable collisions and singularities. Here, this offset is equal to 1 cm. The moving platform is a parallelepiped, as shown in Fig. 4.8. Its width,  $w_p$ , and its length,  $l_p$ , are equal to 10 cm. Its height,  $h_p$ , is equal to 5 cm. Cable properties, moving platform dimensions and the Cartesian coordinates of the exit points of the cables are part of the constant design parameters, collected in vector  $\mathbf{q}$ .

### Design Variables

The design variables are collected in the design variable vector,  $\mathbf{x}$ :

$$\mathbf{x} = [\tau_M, \omega_M, \phi_w, \rho_R]^T \quad (4.51)$$

The ranges of these variables are given in Table 4.2.

### Objective and Constraint Functions

The objective function of the optimisation problem,  $\mathcal{V}$ , is the percentage  $p_f$  of points  $P \in \mathcal{P}$  which are both wrench and twist feasible:

$$\mathcal{V}(\mathbf{x}) = p_f = \frac{\sum_{k=1}^{n_P} F_k}{n_P} \quad (4.52)$$

where  $F_k = 1$  if the the pose associated to the  $k$ -th point,  $P_k$ , is both wrench and twist feasible and  $F_k = 0$  otherwise.

A set of constraints has to be satisfied for all the points  $P_k \in \mathcal{P}$  where the pose assumed by the CDPR is wrench and twist feasible. The constraints include the absence of cable interferences and a maximum moving platform positioning displacement due to the elasticity of the cables. These constraints are detailed in Sec. 4.1.3.

According to all the previous considerations, the design problem is formulated as follows:

$$\begin{aligned}
 &\text{maximise: } \mathcal{V}(\mathbf{x}) = p_f \\
 &\text{over: } \mathbf{x} = [\tau_M, \omega_M, \phi_w, \rho_R]^T \\
 &\text{subject to:} \\
 &\forall P_k \in \mathcal{P} : F_k = 1 \begin{cases} d_{i,j}^{cc} \geq \phi_c & \forall i, j = 1, \dots, m, \quad i \neq j \\ -\delta t_c \leq \delta t_x, \delta t_y, \delta t_z \leq \delta t_c \end{cases}
 \end{aligned}$$

#### 4.5.2 Optimisation Results

The case study has been solved in *Matlab*<sup>®</sup> using the genetic algorithm toolbox and the *GlobalSearch*<sup>®</sup> algorithm developed by Ugray *et al.* [ULP<sup>+</sup>07].

According to the optimal solution, 57.70% of points  $P_k \in \mathcal{P}$  are included in both the WFW and the TFW. The optimal dimensioning of the design variables contemplates a motor nominal torque  $\tau_M = 1.44$  Nm, a motor nominal speed  $\omega_M = 195.6$  rpm, a winch diameter  $\phi_w = 46.5$  mm and a gearbox ratio  $\rho_R = 3.1$ . Figure 4.9 shows the intersection of the WFW and the TFW associated to the optimal solution. For the given values of the design variables, the TFW includes 97.82% of the desired points  $P_k \in \mathcal{P}$ , as illustrated in Fig. 4.10. On the contrary, the WFW includes only 57.73% of points  $P_k \in \mathcal{P}$ .

The correlation between the design variables,  $\mathbf{x}$ , and the optimisation function,  $\mathcal{V}$ , has been investigated by means of the *Matlab*<sup>®</sup> function `corrcoef`<sup>®</sup>. A set of values has been associated to each design variable:

$$[\tau_M] = \{-0.5 \text{ Nm} : 0.1 \text{ Nm} : 1.5 \text{ Nm}\} \quad (4.53)$$

$$[\omega_M] = \{50 \text{ rpm} : 10 \text{ rpm} : 200 \text{ rpm}\} \quad (4.54)$$

$$[\phi_w] = \{1 \text{ cm} : 1 \text{ cm} : 5 \text{ cm}\} \quad (4.55)$$

$$[\rho_R] = \{0.5 : 0.1 : 1, \quad 2 : 1 : 5\} \quad (4.56)$$

The different combinations of design variables have been tested computing the percentage of feasible points belonging to the WFW and the TFW. As illustrated in Fig. 4.11, the size of the WFW increases with respect to the nominal torque of the motor,  $\tau_M$ , and the gearbox transmission ratio,  $\rho_R$ . The diameter of the winch drums,  $\phi_w$ , is inversely proportional to the size of the WFW. Analogously, an increase of the nominal motor speed,  $\omega_M$ , induces an improvement of the TFW size, as well as the increasing of the diameter of the winch drums. The size of the TFW can be augmented by decreasing the the gearbox transmission ratio.

The performed analysis highlights that, regarding the dimensions of both the WFW and the TFW,  $\phi_w$  and  $\rho_R$  have a higher influence with respect to the other design variables. Consequently, dimensioning the gearbox transmission ratio and the drum diameter, the designer should take into account the sensitivity of these design parameters and the trade-off between increasing the WFW size and decreasing the TFW size. For example,

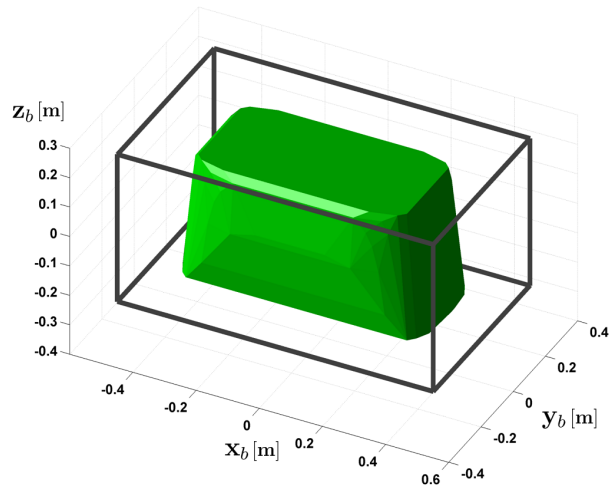


**Fig. 4.9** – Intersection of the WFW and the TFW for the optimal solution ( $\tau_M = 1.44\text{Nm}$ ,  $\omega_M = 195.6\text{rpm}$ ,  $\phi_w = 46.5\text{mm}$ ,  $\rho_R = 3.1$ )

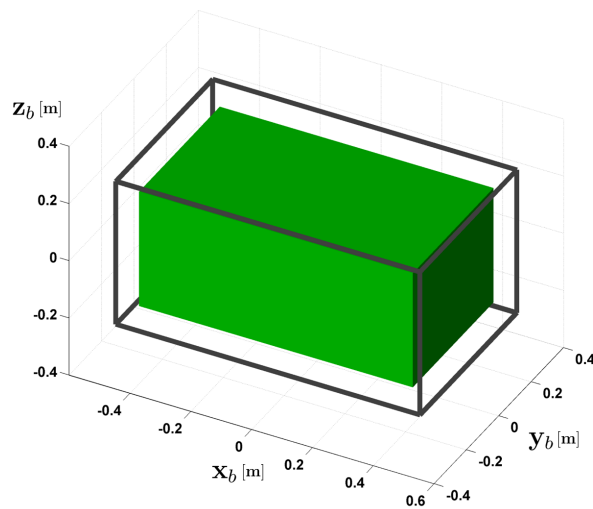


**Fig. 4.10** – Case Study I: TFW of the optimal solution ( $\tau_M = 1.44\text{Nm}$ ,  $\omega_M = 195.6\text{rpm}$ ,  $\phi_w = 46.5\text{mm}$ ,  $\rho_R = 3.1$ )

the largest WFW can be obtained for the design variables at their upper limits:  $\tau_M = 1.5\text{Nm}$ ,  $\omega_M = 200\text{rpm}$ ,  $\phi_w = 50\text{mm}$  and  $\rho_R = 5$ . Under these assumptions, the WFW covers 65.98% of points  $P_k, i = 1, \dots, n_p$  belonging to  $\mathcal{P}$ , as shown in Fig. 4.12. However, due to the relatively large gearbox ratio,  $\rho_R = 5$ , all the points included in the WFW are not twist feasible, the moving platform being not able to attain the prescribed twists.

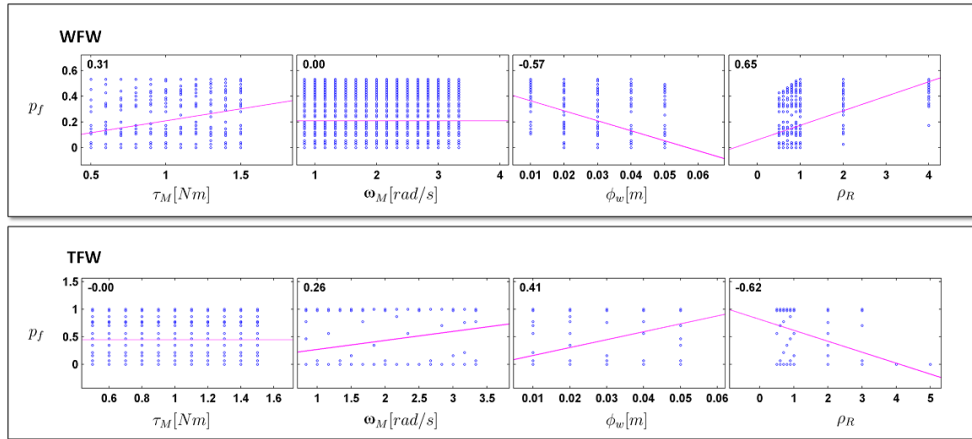


Fig. 4.11 – Analysis of the correlation between the design variables and the optimisation criterion

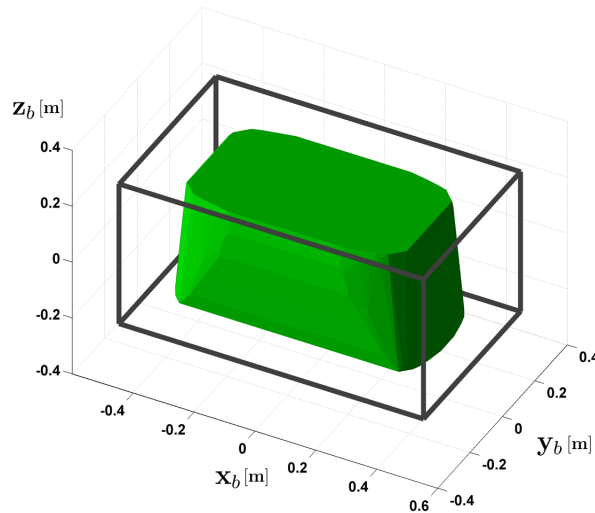
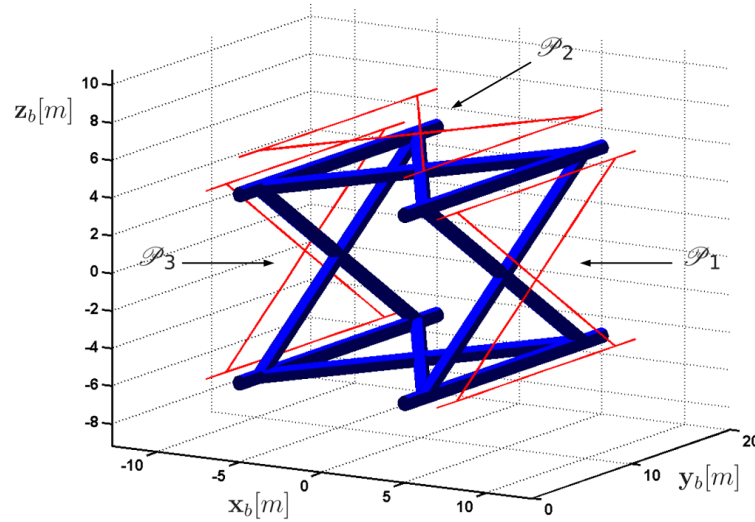


Fig. 4.12 – Case Study I: Larger WFW, covering the 65,98% of the prescribed workspace, obtained for the design variables  $\tau_M = 1.5 \text{ Nm}$ ,  $\omega_M = 200 \text{ rpm}$ ,  $\phi_w = 50 \text{ mm}$ ,  $\rho_R = 5$

## 4.6 Case Study II : Design of a RCDPR for Sandblasting and Painting of a Large Tubular Structure

### 4.6.1 Problem Description

The necessity to improve the production rate of large tubular structures pushed some companies to investigate new technologies. These technologies should be able to reduce the time needed to perform several manufacturing operations, such as the assembly of the structure parts or the treatment of their surfaces. Painting and sandblasting operations over wide tubular structures can be realised by means of RCDPRs, as illustrated in the present case study.



**Fig. 4.13** – Case Study II: Case study model and prescribed paths  $\mathcal{P}_1$ ,  $\mathcal{P}_2$  and  $\mathcal{P}_3$  of the moving platform CoM

### Task and Environment

The tubular structure selected for the given case study is 20 m long, with a cross section of 10 m x 10 m. The number of tubes to be painted is equal to twenty. Their diameter,  $\phi_s$ , is equal to 0.8 m. The sandblasting and painting operations are realised indoor. The structure lies horizontally in order to reduce the dimensions of the painting workshop. The whole system can be described with respect to a fixed reference frame,  $\mathcal{F}_b$ , of origin  $O_b$  and axes  $x_b$ ,  $y_b$ ,  $z_b$ , as illustrated in Fig. 4.13.

Sandblasting and painting tools are embarked on the RCDPR moving platform. The CoM of the moving platform follows the profile of the structure tubes and the tools perform the required operations. The paths to be followed,  $\mathcal{P}_1$ ,  $\mathcal{P}_2$  and  $\mathcal{P}_3$ , are represented in Fig. 4.13. Note that each path  $\mathcal{P}_i, i = 1, \dots, 3$  is discretised into 38 points  $P_{j,i}, j = 1, \dots, 38 \quad i = 1, \dots, 3$ . They are located at a distance of 2 m from the structure tubes. No path has been assigned to the lower external side of the structure, since it is sandblasted and painted from the ground.

### Division of the Prescribed Workspace

In order to avoid collisions between the cables and the structure, the reconfiguration of the cable exit point positions is necessary. Each external side of the structure should be painted by one and only one robot configuration. Three configurations are necessary to work on the exterior of the structure: Configuration  $\mathcal{C}_i$  being associated to path  $\mathcal{P}_i, i = 1, 2$  and 3. This requirement is demanded in order not to interrupt the painting and sandblasting operations during their execution. Passing from a configuration to another, one or more cables are disconnected from their exit points and connected to other exit points located elsewhere. For each configuration, the locations of the cable exit points are defined as variables of the design problem. In the present case study, the dimensions of the moving platform as well as the position of the cable connection points on the moving platform are fixed.

### Constant Design parameters

The number of cables,  $m = 8$ , the cable properties and the dimensions of the moving platform are given. Those parameters are the same for the three robot configurations. The RCDPR developed in this case study is composed of steel cables. The Young Modulus,  $E$ , is equal to 100 GPa. Their diameter,  $\phi_c$  is equal to 4 mm, the stiffness coefficient,  $k_i$ , is equal to 252 KN/m. The maximum allowed tension in the cables,  $\tau_{max}$ , is equal to 34950 N:

$$0 < \tau_i \leq \tau_{max}, \quad \forall i = 1, \dots, 8 \quad (4.57)$$

$l_p$ ,  $w_p$  and  $h_p$  denote the length, width and height of the moving platform, respectively:  $l_p = 30$  cm,  $w_p = 30$  cm and  $h_p = 60$  cm. The design (constant) parameter vector  $\mathbf{q}$  is expressed as:

$$\mathbf{q} = [m, \phi_c, k_i, \tau_{max}, l_p, w_p, h_p]^T \quad (4.58)$$

The design problem aims at identifying the locations of points  $A_{i,c}$  for the configurations  $\mathcal{C}_1$ ,  $\mathcal{C}_2$  and  $\mathcal{C}_3$ . At first, in order to identify the set of feasible locations for the exit points  $A_{i,c}$ , the three robot configurations are parameterised and analysed separately in the following paragraph. A set of exit points will be considered feasible if the design constraints are satisfied along the whole path to be followed by the CoM of the moving platform. The analysed constraints are: Cable interferences, Cable collisions with the structure, and maximum moving platform infinitesimal displacement due to the non-rigid nature of the cables.

### Constraint Functions and Configuration Analysis

A suspended and a non-suspended fully constrained 8-cable CDPR architectures are considered. The suspended architecture is inspired by the CoGiRo CDPR prototype [LGCH13, GCRB15]. For the non-suspended configuration, note that 8 cables is the smallest possible even number of cables that can be used for the moving platform to be fully constrained by the cables. In the suspended architecture, the static equilibrium of the moving platform is obtained thanks to the gravity force that plays the role of an additional cable pulling the moving platform downward.

Since the sandblasting and painting operations are performed at low speed, the motion of the CDPR moving platform can be considered to be quasi-static. Hence, only the static equilibrium of the robot moving platform will be considered. Collisions between the cables as well as collisions between the cables and the structure tubes should be avoided. Besides, the moving platform infinitesimal displacements, due to the elasticity of the cables, are constrained. Here, the cable mass is not considered.

**Configuration  $\mathcal{C}_1$**  A fully constrained architecture has been assigned to configuration  $\mathcal{C}_1$ . The exit points  $A_{i,1}$  have been arranged in a parallelepiped layout. The edges of the parallelepiped are aligned with the axes of frame  $\mathcal{F}_b$ . This layout can be fully described by means of five variables:  $u_1$ ,  $u_2$  and  $u_3$  define the Cartesian coordinates of the parallelepiped centre;  $u_4$  and  $u_5$  represent the half-lengths of the parallelepiped along the axes  $\mathbf{x}_b$  and  $\mathbf{y}_b$ ,

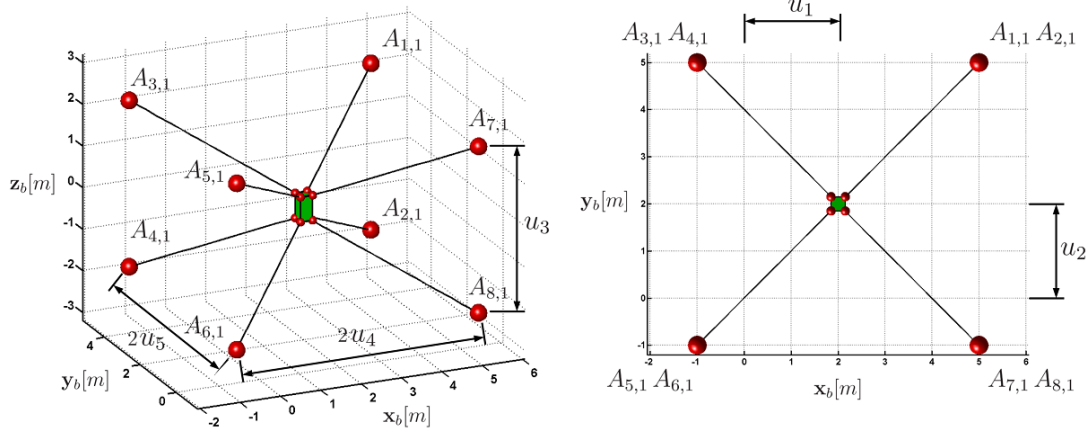


Fig. 4.14 – Case Study II: Design variables parametrising configuration  $\mathcal{C}_1$

respectively. Therefore, the Cartesian coordinates of the exit points  $A_{i,1}, i = 1, \dots, m$  are expressed as follows:

$$\mathbf{a}_{1,1}^b = [u_1 + u_4, u_2 + u_5, u_3]^T \quad \mathbf{a}_{2,1}^b = [u_1 + u_4, u_2 + u_5, -u_3]^T \quad (4.59)$$

$$\mathbf{a}_{3,1}^b = [u_1 - u_4, u_2 + u_5, u_3]^T \quad \mathbf{a}_{4,1}^b = [u_1 - u_4, u_2 + u_5, -u_3]^T \quad (4.60)$$

$$\mathbf{a}_{5,1}^b = [u_1 - u_4, u_2 - u_5, u_3]^T \quad \mathbf{a}_{6,1}^b = [u_1 - u_4, u_2 - u_5, -u_3]^T \quad (4.61)$$

$$\mathbf{a}_{7,1}^b = [u_1 + u_4, u_2 - u_5, u_3]^T \quad \mathbf{a}_{8,1}^b = [u_1 + u_4, u_2 - u_5, -u_3]^T \quad (4.62)$$

The layout of the first robot configuration is described in Fig. 4.14. The design variables of the design problem at hand are collected into the vector  $\mathbf{x}_1$ :

$$\mathbf{x}_1 = [u_1, u_2, u_3, u_4, u_5]^T \quad (4.63)$$

The Cartesian coordinates of the connection points  $B_{i,1}, i = 1, \dots, m$  of the cables on the moving platform are expressed as:

$$\mathbf{b}_{1,1}^b = \frac{1}{2} [l_p, w_p, h_p]^T, \quad \mathbf{b}_{2,1}^b = \frac{1}{2} [l_p, w_p, -h_p]^T \quad (4.64)$$

$$\mathbf{b}_{3,1}^b = \frac{1}{2} [-l_p, w_p, h_p]^T, \quad \mathbf{b}_{4,1}^b = \frac{1}{2} [-l_p, w_p, -h_p]^T \quad (4.65)$$

$$\mathbf{b}_{5,1}^b = \frac{1}{2} [-l_p, -w_p, h_p]^T, \quad \mathbf{b}_{6,1}^b = \frac{1}{2} [-l_p, -w_p, -h_p]^T \quad (4.66)$$

$$\mathbf{b}_{7,1}^b = \frac{1}{2} [l_p, -w_p, h_p]^T, \quad \mathbf{b}_{8,1}^b = \frac{1}{2} [l_p, -w_p, -h_p]^T \quad (4.67)$$

A discretised set of design variables have been considered. The lower and upper bounds, as well as the number of values for each design variable, are given in Table 4.3. 18225 robot configurations have been generated by combining those values. It turns out that 4576 configurations satisfy the design constraints along the 38 discretised points of path  $\mathcal{P}_1$ .

**Configuration  $\mathcal{C}_2$**  A suspended fully constrained architecture has been assigned to configuration  $\mathcal{C}_2$  in order to avoid any possible collision with the tubular structure. The selected architecture is based on CoGiRo prototype, a suspended CDPR designed and built in the framework of the ANR CoGiRo project [LGCH13, GCRB15]. An

advantage of this architecture is the possibility to balance efficiently external wrenches throughout a very large part of the robot footprint. The exit points  $A_{i,2}$  have been arranged in a parallelepiped layout. The Cartesian coordinates  $\mathbf{a}_{i,c}$ ,  $i = 1, \dots, m$  are defined as follows:

$$\mathbf{a}_{1,2}^b = \mathbf{a}_{2,2}^b = [v_1 - v_4, v_2 - v_5, v_3]^T \quad (4.68)$$

$$\mathbf{a}_{3,2}^b = \mathbf{a}_{4,2}^b = [v_1 - v_4, v_2 + v_5, v_3]^T \quad (4.69)$$

$$\mathbf{a}_{5,2}^b = \mathbf{a}_{6,2}^b = [v_1 + v_4, v_2 + v_5, v_3]^T \quad (4.70)$$

$$\mathbf{a}_{7,2}^b = \mathbf{a}_{8,2}^b = [v_1 + v_4, v_2 - v_5, v_3]^T \quad (4.71)$$

Variables  $v_1 = 1, \dots, 5$  assume the same geometric roles assigned to variables  $u_1 = 1, \dots, 5$ . The layout of this configuration is illustrated in Fig. 4.15. The design variables of configuration  $\mathcal{C}_2$  are collected into the vector  $\mathbf{x}_2$ :

$$\mathbf{x}_2 = [v_1, v_2, v_3, v_4, v_5]^T \quad (4.72)$$

Note that this architecture is composed of couples of exit points theoretically connected to the same locations:  $\{A_{1,2}, A_{2,2}\}$ ,  $\{A_{3,2}, A_{4,2}\}$ ,  $\{A_{5,2}, A_{6,2}\}$  and  $\{A_{7,2}, A_{8,2}\}$ . From a technical point of view, in order to avoid any cable interference, the coupled exit points should be separated by a distance at least greater than cable diameter. For the design problem at hand, this distance has been fixed to  $v_0 = 5$  mm.

$$\mathbf{a}_{1,2}^b = [v_1 - v'_4, v_2 - v_5, v_3]^T \quad (4.73)$$

$$\mathbf{a}_{2,2}^b = [v_1 - v_4, v_2 - v'_5, v_3]^T \quad (4.74)$$

$$\mathbf{a}_{3,2}^b = [v_1 - v_4, v_2 + v'_5, v_3]^T \quad (4.75)$$

$$\mathbf{a}_{4,2}^b = [v_1 - v'_4, v_2 + v_5, v_3]^T \quad (4.76)$$

$$\mathbf{a}_{5,2}^b = [v_1 + v'_4, v_2 + v_5, v_3]^T \quad (4.77)$$

$$\mathbf{a}_{6,2}^b = [v_1 + v_4, v_2 + v'_5, v_3]^T \quad (4.78)$$

$$\mathbf{a}_{7,2}^b = [v_1 + v_4, v_2 - v'_5, v_3]^T \quad (4.79)$$

$$\mathbf{a}_{8,2}^b = [v_1 + v'_4, v_2 - v_5, v_3]^T \quad (4.80)$$

where  $v'_4 = v_4 - v_0$  and  $v'_5 = v_5 - v_0$

The Cartesian coordinates of points  $B_{i,2}$ ,  $i = 1, \dots, m$  are defined as:

$$\mathbf{b}_{1,2}^b = \frac{1}{2} [l_p, -w_p, h_p]^T, \quad \mathbf{b}_{2,2}^b = \frac{1}{2} [-l_p, w_p, -h_p]^T \quad (4.81)$$

$$\mathbf{b}_{3,2}^b = \frac{1}{2} [-l_p, -w_p, h_p]^T, \quad \mathbf{b}_{4,2}^b = \frac{1}{2} [l_p, w_p, -h_p]^T \quad (4.82)$$

$$\mathbf{b}_{5,2}^b = \frac{1}{2} [-l_p, w_p, h_p]^T, \quad \mathbf{b}_{6,2}^b = \frac{1}{2} [l_p, -w_p, -h_p]^T \quad (4.83)$$

$$\mathbf{b}_{7,2}^b = \frac{1}{2} [l_p, w_p, h_p]^T, \quad \mathbf{b}_{8,2}^b = \frac{1}{2} [-l_p, -w_p, -h_p]^T \quad (4.84)$$

Table 4.3 describes the lower and upper bounds as well as the number of values considered for configuration  $\mathcal{C}_2$ . Combining these values, 22275 configurations have been generated. Amongst these configurations, only 5579 configurations are feasible.

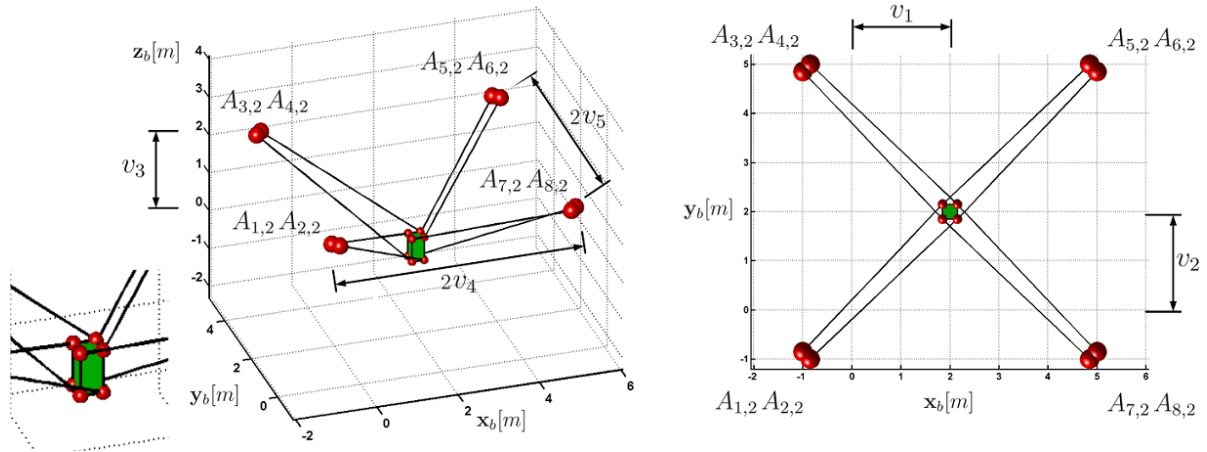


Fig. 4.15 – Case Study II: Design variables parametrising the configuration  $\mathcal{C}_2$

**Configuration  $\mathcal{C}_3$**  Configuration  $\mathcal{C}_3$  follows the path  $\mathcal{P}_3$ . This path is symmetric to the path  $\mathcal{P}_1$  with respect to the plane  $\mathbf{y}_b O \mathbf{z}_b$ ,  $O$ ,  $\mathbf{y}_b$  and  $\mathbf{z}_b$  being the origin, the  $y$ -axis and the  $z$ -axis of the base frame. Considering the symmetry of the tubular structure, the robot architecture used for configuration  $\mathcal{C}_1$  has been assigned to configuration  $\mathcal{C}_3$ . The set of values of the discretised design variables defined for configuration  $\mathcal{C}_3$  is described in Table 4.3. The design variables for configuration  $\mathcal{C}_3$  are collected into the vector  $\mathbf{x}_3$ :

$$\mathbf{x}_3 = [w_1, w_2, w_3, w_4, w_5]^T \quad (4.85)$$

where variables  $w_i, i = 1, \dots, 5$  amount to the variables describing configuration  $\mathcal{C}_1$ ,  $u_i, i = 1, \dots, 5$ . Therefore, the Cartesian coordinates of the exit points  $A_{i,3}, i = 1, \dots, m$  are expressed as follows:

$$\mathbf{a}_{1,3}^b = [w_1 + w_4, w_2 + w_5, -w_3]^T \quad \mathbf{a}_{2,3}^b = [w_1 + w_4, w_2 + w_5, w_3]^T \quad (4.86)$$

$$\mathbf{a}_{3,3}^b = [w_1 - w_4, w_2 + w_5, -w_3]^T \quad \mathbf{a}_{4,3}^b = [w_1 - w_4, w_2 + w_5, w_3]^T \quad (4.87)$$

$$\mathbf{a}_{5,3}^b = [w_1 - w_4, w_2 - w_5, -w_3]^T \quad \mathbf{a}_{6,3}^b = [w_1 - w_4, w_2 - w_5, w_3]^T \quad (4.88)$$

$$\mathbf{a}_{7,3}^b = [w_1 + w_4, w_2 - w_5, -w_3]^T \quad \mathbf{a}_{8,3}^b = [w_1 + w_4, w_2 - w_5, w_3]^T \quad (4.89)$$

### Objective Functions and Design Problem Formulation

The RCDPR should be as cheap and simple as possible. For this reason, the minimisation of the total number of cable exit points,  $\mathcal{V}_1 = n_c$ , is required. Consequently, the number of exit point locations, shared by two or more configurations, should be maximised. The size of the robot is minimised as well, in order to reduce the dimensions of the sandblasting and painting workshop. Finally, the mean of the moving platform infinitesimal displacement due to cable deformations is minimised as well. The optimisations are performed hierarchically, by means of the procedure described in Sec. 4.4.1 and the objective functions collected in Sec. 4.4.2.

**Tab. 4.3** – DESIGN VARIABLES ASSOCIATED WITH CONFIGURATIONS  $\mathcal{C}_1$ ,  $\mathcal{C}_2$  AND  $\mathcal{C}_3$ 

Configuration	Design Variables	Lower Bounds [m]	Upper Bounds [m]	Number of values
$\mathcal{C}_1$	$u_1$	5.5	7.5	9
	$u_2$	8.0	12.0	9
	$u_3$	6	10	5
	$u_4$	0.5	2.5	9
	$u_5$	10	14	5
$\mathcal{C}_2$	$v_1$	-1	1	9
	$v_2$	8.0	12.0	5
	$v_3$	7	11	9
	$v_4$	5	7.5	11
	$v_5$	10	14	5
$\mathcal{C}_3$	$w_1$	-7.5	-5.5	9
	$w_2$	8.0	12.0	9
	$w_3$	6	10	5
	$w_4$	0.5	2.5	9
	$w_5$	10	14	5

Hence, the design problem of the CDPR is formulated as follows:

$$\begin{aligned}
& \text{minimise} && \begin{cases} \mathcal{V}_1 = n_c \\ \mathcal{V}_2 = (\bar{s}_x - \underline{s}_x)(\bar{s}_y - \underline{s}_y)(\bar{s}_z - \underline{s}_z) \\ \mathcal{V}_3 = \frac{\|\delta \mathbf{t}\|_2}{n_p} \end{cases} \\
& \text{over} && \mathbf{x}_1, \mathbf{x}_2, \mathbf{x}_3 \\
& \text{subject to:} && \\
& \forall P_{m,n}, \quad \begin{matrix} m = 1, \dots, 38 \\ n = 1, \dots, 3 \end{matrix} && \begin{cases} \mathbf{C}\mathbf{w} \leq \mathbf{d}, \quad \forall \mathbf{w} \in [\mathbf{w}]_r \\ d_{i,j}^{cc} \geq \phi_c \quad \forall i, j = 1, \dots, 8, \quad i \neq j \\ d_{i,k}^{cs} \geq \frac{(\phi_c + \phi_s)}{2} \quad \forall i = 1, \dots, 8, \forall k = 1, \dots, 12 \\ -5 \text{ cm} \leq \delta t_x, \delta t_y, \delta t_z \leq 5 \text{ cm} \\ -0.1 \text{ rad} \leq \delta r_x, \delta r_y, \delta r_z \leq 0.1 \text{ rad} \end{cases}
\end{aligned} \tag{4.90}$$

Once the set of feasible solutions have been obtained for each configuration, i.e., for each path, a list of RCDPRs with a minimum number of exit points,  $n_c$ , is extracted from the list of feasible RCDPRs. Finally, the most compact and stiff RCDPRs from the list of RCDPRs with a minimum number of exit points are optimal solutions.

#### 4.6.2 Optimisation Results

The feasible robot configurations associated to paths  $\mathcal{P}_1$ ,  $\mathcal{P}_2$  and  $\mathcal{P}_3$  have been identified. For each path, a configuration is selected, aiming at minimising the total number of exit points required by the RCDPR to

**Tab. 4.4** – DESIGN VARIABLES OF THE SELECTED OPTIMUM RCDPR

Conf.	var.1	var.2	var.3	var.4	var.5
$\mathbf{x}_1$	6.25	10.0	8.0	1.0	11.0
$\mathbf{x}_3$	0	10.0	8.0	5.25	11.0
$\mathbf{x}_3$	-6.25	10.0	8.0	1.0	11.0

complete the task. The 4576 feasible RCDPR configurations for path  $\mathcal{P}_1$  are compared with the 5579 feasible RCDPR configurations for path  $\mathcal{P}_2$  and the 4576 feasible RCDPR configurations for path  $\mathcal{P}_3$ . The sets of robot configurations that minimise the number,  $n_c$ , of required exit points along the three paths are identified. According to the discrete optimisation analysis, 16516 triplets of configurations minimise the total number of exit points.

A generic CDPR composed of 8 cables requires 8 exit points  $A_i = 1, \dots, 8$  on the base. It is the case for the non-suspended fully constrained configuration  $\mathcal{C}_1$ . The suspended CDPR presents 4 coincident couples of exit points. Hence, the maximum total number of exit points of the RCDPR is equal to 20. The best results provide a reduction of 4 points. Regarding the configurations  $\mathcal{C}_1$  and  $\mathcal{C}_2$ , points  $A_{5,2}$  and  $A_{7,2}$  can be coincident with points  $A_{3,1}$  and  $A_{5,1}$ , respectively. Alternatively, points  $A_{5,2}$  and  $A_{7,2}$  can be coincident with points  $A_{1,1}$  and  $A_{7,1}$ . As far as configurations  $\mathcal{C}_2$  and  $\mathcal{C}_3$  are concerned, points  $A_{1,2}$  and  $A_{3,2}$  can be coincident with points  $A_{8,3}$  and  $A_{2,3}$ , respectively. Likewise, points  $A_{1,2}$  and  $A_{3,2}$  can be coincident with points  $A_{4,3}$  and  $A_{6,3}$ , respectively.

The total volume of the robot has been computed for the 16516 triplets of configurations minimising the total number of exit points. 96 RCDPRs amongst the 16516 triplets of configurations have the smallest size, this minimum size being equal to 5104 m<sup>3</sup>. The selection of the best solutions has been promoted through the third optimisation criterion, based on the robot stiffness. 20 solutions provided a minimum mean of the moving platform displacement of 1.392 mm due to non-rigid nature of the cables. An optimal solution is illustrated in Fig. 4.16. The corresponding optimal design variables are given in Table 4.4.

Figure 4.17 illustrates the MDoCS introduced in [GCC14] and defined thereafter along the paths  $\mathcal{P}_1$ ,  $\mathcal{P}_2$  and  $\mathcal{P}_3$ , which are discretised into 388 points.

$$s = \min_{i=1,\dots,n} \left( \min_{j=1,\dots,p} s_{j,i} \right) \quad (4.91)$$

It turns out that moving platform is in a static equilibrium along all the paths because the MDoCS remains negative. We remind that the MDoCS is negative when a pose is wrench feasible. Configurations  $\mathcal{C}_1$  and  $\mathcal{C}_3$  maintain their degree of satisfaction lower than the 400 N. On the contrary, configuration  $\mathcal{C}_2$  is often close to 0. The poses where  $s$  vanishes require that two cables of the suspended CDPR are slack.

## 4.7 Conclusions

This chapter dealt with the design of CDPRs. The design of CDPRs has been formulated as an optimisation problem, according to the state of the art [GCG<sup>+</sup>14]. The design problem aims at optimising one or more objective function(s). A set of relevant objective functions, e.g. the maximisation of the workspace size and the maximisation of the *Minimum Degree of Dynamic Constraint Satisfaction* (MDoDCS), has been presented in this chapter. The optimal solution has been computed while considering a set of user-defined constraints. The

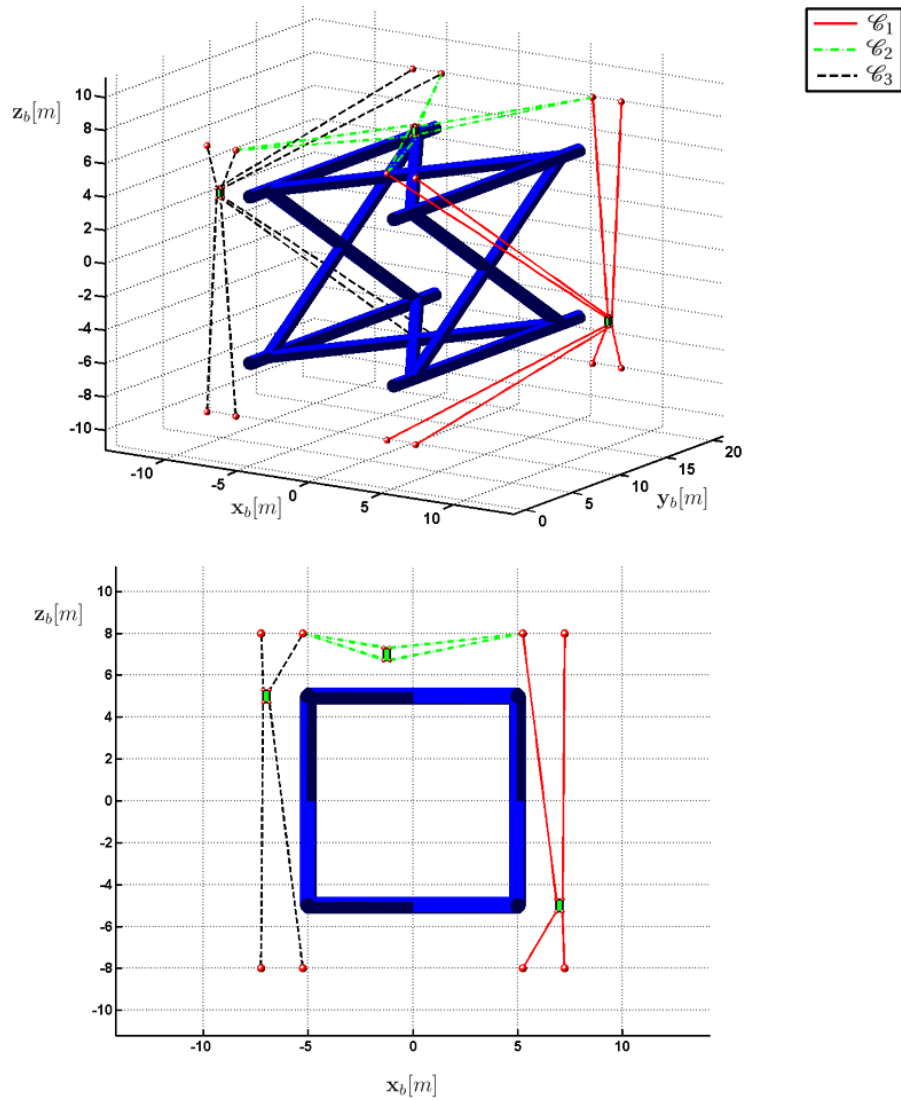
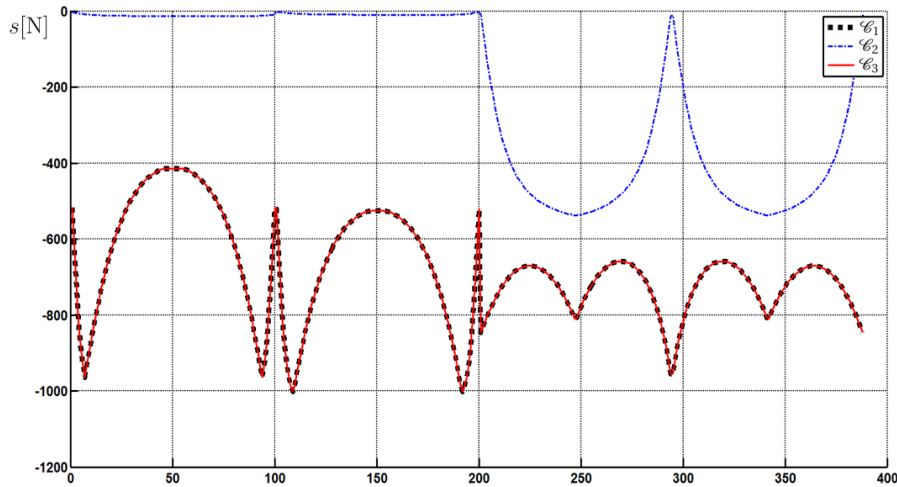


Fig. 4.16 – Case Study II: Optimal Reconfigurable Cable-Driven Parallel Robot

most significant constraints have been described in the previous section including wrench, twist and dynamic feasibility, cable interferences and the collisions between cables and the environment. An illustrative example has been studied to highlight the contributions of this chapter. The sizes of the wrench and twist feasible workspaces of a CDPR have been maximised by means of a global optimisation algorithm.

When the task to be accomplished is complicated, and the working environment is extremely cluttered, CDPRs may not succeed in the task execution. The problem can be solved by means of RCDPRs. Despite several elements of a RCDPR can be reconfigured, this manuscript focuses on the displacement of the exit points. A classification between discrete and continuous reconfigurations of the exit points have been proposed. This chapter introduced a design strategy for discrete RCDPRs, whose exit points can be placed on a predefined grid of locations. This design strategy assumes that the number of configurations necessary to complete the task can be fixed by the designer according to his/her experience [GCG<sup>+</sup>15b]. The designer divides the prescribed path, or the prescribed workspace, into several parts. Each part has to be covered entirely by one and only one configuration. The position



**Fig. 4.17** – Case Study II: MDoCS of the selected optimum RCDPR. The analysis has been performed by discretising the paths  $\mathcal{P}_1$ ,  $\mathcal{P}_2$  and  $\mathcal{P}_3$  into 388 points

of the cable exit points, for all the configurations, is computed by means of an optimisation algorithm. The algorithm optimises one or more global objective function(s) while satisfying a set of user-defined constraints. In this manuscript, global objective functions will be used to optimise the RCDPR size, the number of exit point displacements and the number of configuration changes. A case study has been proposed in order to validate the RCDPR design strategy. The RCDPR has to paint and sandblast three of the four external sides of a tubular structure. Each of the three sides to be painted is covered by one and only one configuration. The design strategy provided several optimal solutions to the case study, minimising hierarchically the number of exit point displacements, the size of the RCDPR and the moving platform displacement due to the non-rigid nature of the cables. The computation of the optimal solution, performed on a Intel® Core™ i7-3630QM 2.40 GHz, required 19 h of computation. More complicated tasks may require high computational efforts. An improvement of the design strategy for RCDPR should be investigated in order to reduce this computational time.



## Chapter 5

# Reconfiguration Planning of RCDPRs

### Chapter Content

5.1 Reconfiguration Procedure . . . . .	90
5.2 Reconfiguration Strategy . . . . .	90
5.3 Case Study I: A Planar RCDPR . . . . .	102
5.4 Case Study II: A Spatial RCDPR . . . . .	104
5.5 Conclusions . . . . .	120

When the working environment is not extremely cluttered, RCDPRs can be designed according to the strategy proposed in Chap. 4. The designer divides the prescribed workspace into  $n_r$  portions. According to the grid of cable exit point locations, the algorithm computes all the possible configurations of the RCDPR. Then, the algorithm analyses, for each portion of the prescribed workspace, the configurations which satisfy the user defined constraints and selects the best configurations with respect to one or more global objective functions.

When the environment is extremely cluttered, it is hard to predict if a given portion of the prescribed workspace can be covered by a unique configuration. To overcome this problem, the RCDPR is designed in such a way the cable exit points can be installed all around the prescribed workspace, on a discrete grid of possibly large but finite number of locations.

From a technical point of view, cable exit points can be reconfigured according to the procedure described in Sec. 5.1, by moving the pulleys which directs the cable toward the moving platform.

Most of the studies on RCDPRs are focused on continuous reconfigurations, performed by several researchers, e.g. in [RZA11, ZRMR14, ZTK12, ZJK13, NGCP14, NG14b]. To the best of our knowledge, none reconfiguration strategy has been proposed in the framework of discrete RCDPRs, yet. This chapter proposes a strategy to compute the optimal reconfiguration strategy for a RCDPR whose exit points can only be placed on a finite set of positions. This strategy will allow the moving platform to follow the prescribed path improving the performance of the RCDPR while satisfying one or more constraint(s). The strategy to optimise the RCDPR exit point reconfiguration is detailed in Sec. 5.2.

The reconfiguration strategy will be verified for two case studies. The first case study, described in Sec. 5.3, deals with a planar task. This case study illustrates the steps of the reconfiguration strategy through a basic example. The second case study aims at optimising the reconfigurations of a spatial RCDPR for sandblasting and painting of

tubular structures. The details of the problem and the results obtained using the proposed reconfiguration strategy are described in Sec. 5.4.

## 5.1 Reconfiguration Procedure

When the working environment is not cluttered, and the ground is free, it is possible to perform the reconfiguration on the ground. The CDPR moving platform is moved from the current pose to a home position on the ground. Then, when no external wrench is applied on the moving platform and the cables are slack, the cables can be disconnected easily from the moving platform. Once the exit points are reconfigured, the cables can be attached again to the moving platform, and the moving platform can be moved to a desired working pose.

However, this strategy cannot always be applied. For instance, a cluttered environment may not permit to put the CDPR moving platform in a home position on the ground. In the strategy proposed hereafter the moving platform of the CDPR is supposed not to change its pose during the reconfiguration:

- a. The robot is located at the desired reconfiguration pose. The current pose of the robot is denoted hereafter as  $\mathcal{C}_a$ . The cables balance the weight of the moving platform and the external wrenches applied on the moving platform, according to the static equilibrium equation  $\mathbf{W}_a \boldsymbol{\tau}_a + \mathbf{w}_e = \mathbf{0}$ .
- b. A new set of cables are connected to the proper exit point locations, according to the new desired configuration, defined hereafter as  $\mathcal{C}_{a'}$ . The other extremities of these cables are connected to the corresponding attachment points on the moving platform. These cables are initially slack and they are coiled in such a way to be "just tensed", their lengths being adjusted to the moving platform pose.
- c. In order to be detached from the moving platform, the cables belonging to  $\mathcal{C}_a$ , but not to  $\mathcal{C}_{a'}$ , should be slack. These cables are gradually uncoiled in such a way that the external wrenches are transferred to the cables belonging to  $\mathcal{C}_{a'}$ .
- d. When the cables belonging exclusively to configuration  $\mathcal{C}_a$  are slack, they can be detached. The RCDPR is now ready to proceed with the task execution.

Figure 5.1 illustrates the proposed procedure.

## 5.2 Reconfiguration Strategy

The user provides a grid of possible exit point locations where the cables can be attached to the base frame. The task to be performed can be realised by combining several configurations, disconnecting one or more cable(s) from their exit points and connecting them to new locations. Accordingly, in order to determine the optimal reconfiguration scheme of a RCDPR based on some user defined criteria, a 10-step algorithm, shown in Fig. 5.2, is explained in the following sub-sections.

### 5.2.1 Step I: Constant Design Parameters

The user defines the constant design parameters of the RCDPR, including:

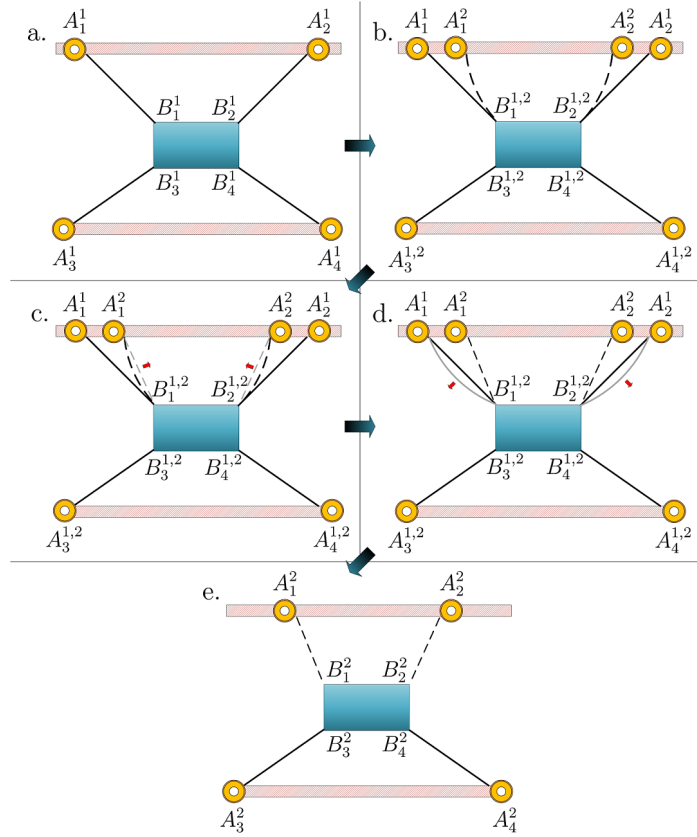


**Fig. 5.1** – Example of reconfiguration procedure for a 4-cable suspended planar robot. The continuous lines represent the cable associated to configuration  $\mathcal{C}_a$ ; the dashed lines represent the cables associated exclusively to configuration  $\mathcal{C}_a'$ . In this example only 2 cables are reconfigured

- The number of cables,  $m$ .
- The cable properties, namely, the Young Modulus,  $E$ , the diameter,  $\phi_c$ , and the linear stiffness coefficient,  $k$ .
- The data of the motorisation, including the nominal torque,  $\tau_M$ , the nominal speed,  $\omega_M$ , the gearbox transmission ratio,  $\rho_R$  and the winch diameter,  $\phi_W$ .
- The position of the cable connection points on the moving platform,  $B_i$ , expressed in the local reference frame  $\mathcal{F}_p$  by the Cartesian coordinate vectors  $\mathbf{b}_i^p$ .

### 5.2.2 Step II: RCDPR Layout Parametrisation

The user provides a point grid where the RCDPR exit points can be located. While placing the exit points at the points of this grid, a huge number of CDPR configurations can be generated. In order to limit the complexity of the problem, the user can parametrise the cable layouts, correlating the relative position of the cable exit points,  $A_{i,c}$ ,  $i = 1, \dots, m$ , with respect to each other and with respect to the reference frame  $\mathcal{F}_b$ . For instance, the cable exit points can be disposed at the vertices of a parallelepiped, as shown in Fig. 5.3. The Cartesian coordinates vectors  $\mathbf{a}_{i,c}^b$ ,  $i = 1, \dots, m$ , are described by means of  $n_v$  design parameters,  $u_v$ ,  $v = 1 \dots, n_v$ . In the previous example, three design parameters,  $x_1$ ,  $x_2$ , and  $x_3$  are sufficient to describe the exit point locations.

Once the exit point locations are parametrised, a set of discrete values,  $[u]_v$ , is assigned to each design

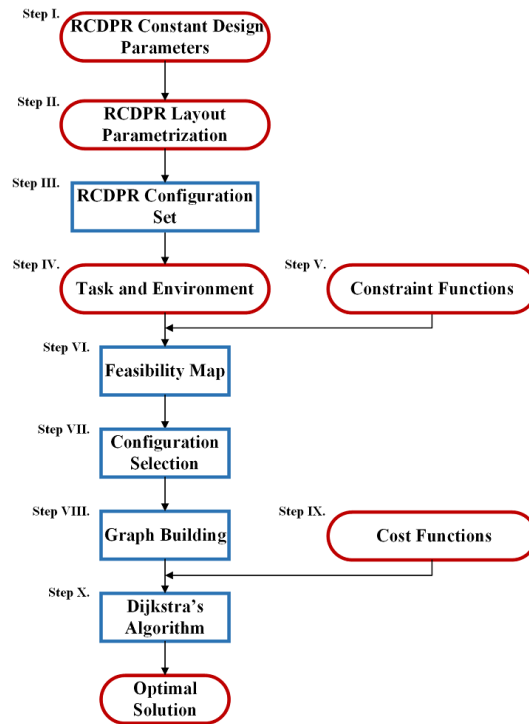


Fig. 5.2 – Scheme of the optimal reconfiguration planning method

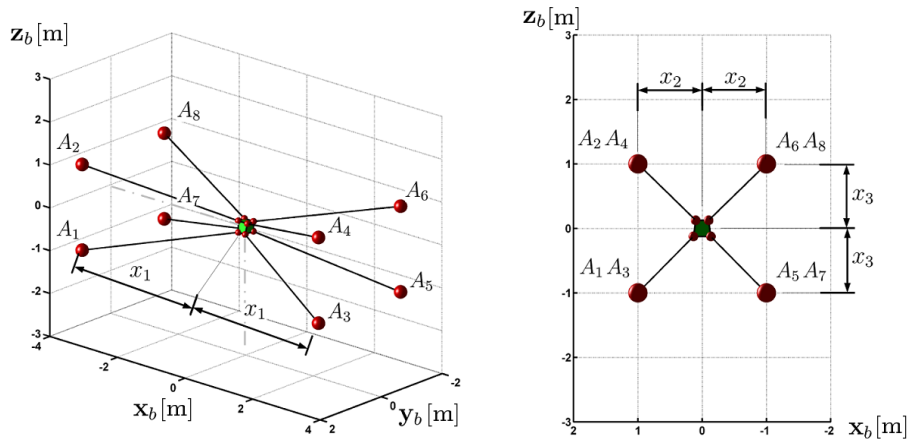
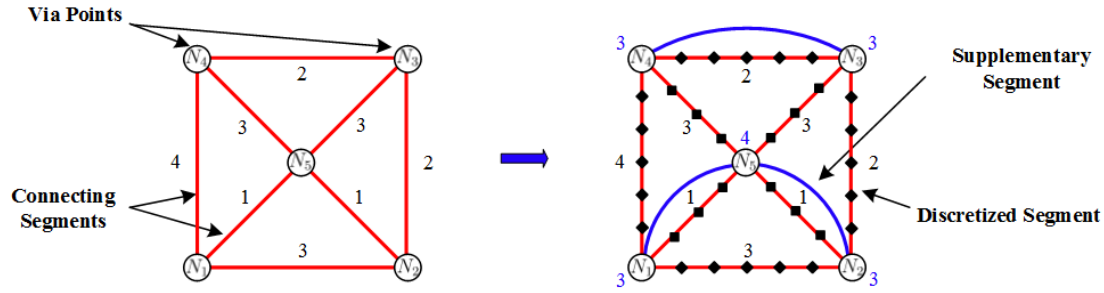


Fig. 5.3 – Location and parametrization of the exit points of a RCDPR, disposed on a parallelepiped layout

parameter. The number of values contained in the  $v$ -th set is equal to  $\varepsilon_v$ . The discrete values  $[u]_v, v = 1, \dots, n_v$  are defined according to the grid where the cable exit points can be located.

### 5.2.3 Step III: RCDPR Configuration Set

The algorithm combines the discrete values  $[u]_v$  provided at Step II. Hence,  $n_{\mathcal{C}} = \prod_{v=1}^{n_v} \varepsilon_v$  configurations of RCDPRs are generated. Each  $j$ -th configuration,  $\mathcal{C}_j$ , is described by a design parameter vector,  $\mathbf{x}_j$ , containing the



**Fig. 5.4** – Computation of one of the possible optimal paths covering the whole set of prescribed segments. In this example, the segments to be followed do not represent an Eulerian graph. To transform it into an Eulerian graph, minimising the cost of the corresponding Eulerian cycles, it is necessary to add three segments (supplementary segments). An optimal path consists in visiting the via points in the following order:  $N_1N_5N_2N_3N_5N_4N_3N_4N_1N_5N_2N_1$

design parameters  $u_{v,v} = 1 \dots, n_v$  associated to this specific configuration. The configurations are analysed in the subsequent steps of the algorithm.

#### 5.2.4 Step IV: Task and Environment

The user provides the data related to the task to be performed and the robot environment, namely:

- The moving platform weight  $w_g$  and the bounds on the external wrench applied on the moving platform,  $f, \bar{f}, m, \bar{m}$ .
- The working environment, modelled by means of simple geometric shapes or approximated by means of polygonal meshes.
- A set of  $n_{vp}$  via points. The via points are connected with each other by segments. All the segments should be followed by the RCDPR moving platform CoM. The minimisation of the length of the corresponding path is a routing inspection problem [EGL95]. The via points and the segments connecting them are represented as a graph. The graph is modified in such a way to contain at least one Eulerian path (a trail which crosses every edge exactly once) or an Eulerian cycle (an Eulerian path starting and ending at the same vertex). The graph is solved by means of Fleury's algorithm [EGL95]. The user can select one of the solutions, representing the path that the moving platform of the RCDPR must follow during the task. The chosen path is discretised into  $n_p$  points,  $\mathcal{P} = \{P_i, i = 1, \dots, n_p\}$ , where  $\mathbf{p}_i, i = 1, \dots, n_p$ , are the moving platform poses associated to these points. The moving platform orientation associated to each pose is defined by the user. Figure 5.4 presents an example of such a path generation in a case where the moving platform has to follow 8 segments starting from the via point  $N_1$ .

#### 5.2.5 Step V: Constraint Functions

The user specifies a set of  $n_\phi$  constraint functions that the RCDPR should satisfy during the task. Some constraints are presented in Sec. 4.1 of Chap. 4.

### 5.2.6 Step VI: Feasibility Map

This step aims at identifying the RCDPR configurations  $\mathcal{C}_j$ ,  $j = 1, \dots, n_{\mathcal{C}}$  which, at a given point  $P_i \in \mathcal{P}$ , satisfies all the constraints defined at Step V. In particular, any pose associated to the  $i$ -th point,  $P_i$ , and the  $j$ -th configuration,  $\mathcal{C}_j$ , is said to be feasible if it satisfies all the  $n_{\phi}$  user defined constraints,  $\phi_l(i, j)$ ,  $l = 1, \dots, n_{\phi}$ . The information associated to the pose feasibility is stored in the variables  $F_{i,j}$ ,  $i = 1, \dots, n_P$ ,  $j = 1, \dots, n_{\mathcal{C}}$  where  $i$  and  $j$  represent the index of the analysed point and the index of the analysed configuration, respectively.

**Definition 5.1.**

$$F_{i,j} = 1 \iff \sum_{l=1}^{n_{\phi}} \phi_l(i, j) = 0 \quad (5.1)$$

where  $\phi_l(i, j)$ ,  $l = 1, \dots, n_{\phi}$  is defined as :

$$\begin{cases} \phi_l(i, j) = 0 & \iff \text{the } l\text{-th constraint is satisfied for the } j\text{-th robot configuration at point } P_i \\ \phi_l(i, j) = 1 & \iff \text{the } l\text{-th constraint is not satisfied for the } j\text{-th robot configuration at point } P_i \end{cases}$$

A *feasibility map* is created according to the values of  $F_{i,j}$ ,  $i = 1, \dots, n_P$ ,  $j = 1, \dots, n_{\mathcal{C}}$ . A simple feasibility map is shown in Fig. 5.5. The horizontal axis represents the points  $P_i$ ,  $i = 1, \dots, n_P$  of the discretised prescribed path. The vertical axis shows the values of  $F_{i,j}$  computed for four configurations  $\mathcal{C}_1$ ,  $\mathcal{C}_2$ ,  $\mathcal{C}_3$  and  $\mathcal{C}_4$ . At a given point  $P_i$ ,  $F_{i,j} = 1$  if the pose assumed by configuration  $\mathcal{C}_j$  is feasible and  $F_{i,j} = 0$  if the pose assumed by configuration  $\mathcal{C}_j$  is infeasible. From the feasibility map, it is apparent that, for a given configuration, several changes in the feasibility conditions are possible between two consecutive points  $P_i$  and  $P_{i+1}$ . These feasibility changes are named *Feasibility Transitions* (FT). Hereafter,  $F_{i,j}$  is said to be a *Positive Feasibility Transition* (PFT) when a transition from an infeasible condition to a feasible one occurs at point  $P_i$  for configuration  $\mathcal{C}_j$ .

**Definition 5.2.**

$$F_{i,j} \text{ is a PFT} \quad \text{if} \quad \begin{cases} F_{i,j} = 1 \\ F_{i-1,j} = 0 \\ F_{i+1,j} = 1 \end{cases} \quad (5.2)$$

On the contrary,  $F_{i,j}$  is said to be a *Negative Feasibility Transition* (NFT) when a transition from a feasible condition to an infeasible one occurs.

**Definition 5.3.**

$$F_{i,j} \text{ is a NFT} \quad \text{if} \quad \begin{cases} F_{i,j} = 1 \\ F_{i+1,j} = 0 \\ F_{i-1,j} = 1 \end{cases} \quad (5.3)$$

For instance, observing the example in Fig. 5.5,  $F_{6,3}$  is a PFT since  $F_{5,3} = 0$  and  $F_{6,3} = F_{7,3} = 1$ . Moreover,  $F_{2,3}$  is a NFT since  $F_{1,3} = F_{2,3} = 1$  and  $F_{3,3} = 0$ . In the following sections, the possible reconfigurations of the RCDPR

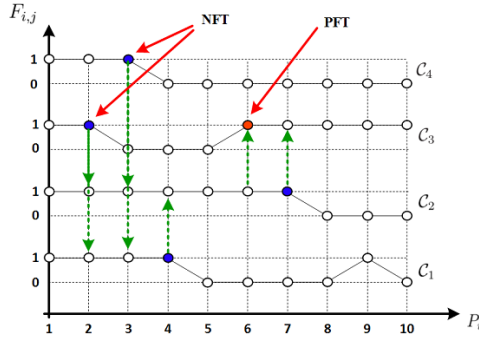


**Fig. 5.5** – A feasibility map: The green arrows represent the possible reconfigurations, the red dots show the Positive Feasibility Transitions (PFTs), and the blue dots show the Negative Feasibility Transitions (NFTs)

will be generated only in presence of a PFT or a NFT. In Fig. 5.5, a so-called *isolated feasible transition* can be seen at  $F_{9,1}$  since the surrounding poses are not feasible, i.e.,  $F_{8,1} = 0$  and  $F_{10,1} = 0$ . Obviously, isolated feasible transitions need not be taken into account during the computation of the optimal reconfiguration strategy.

### 5.2.7 Step VII: Configuration Selection

Some feasibility maps may be composed of a large number  $n_{\mathcal{C}}$  of configurations. The present step aims at reducing the number of configurations of the feasibility map to be used in the following optimisation by analysing the minimum number of configurations,  $n_m$ , that can be used to follow the whole prescribed path  $\mathcal{P}$ . Figure 5.6 illustrates this configuration selection procedure.

a. *Feasibility Map Modification* (Fig. 5.6a). The algorithm simplifies the data stored in the feasibility map. A configuration may present isolated feasible transitions (as illustrated in Sec. 5.2.6) or isolated clusters of few adjacent feasible poses. In both cases, it is not convenient to use these feasible poses. Isolated feasible poses imply that the RCDPR should be reconfigured to cover only a small portion of the prescribed path of the moving platform. This situation does not facilitate the achievement of practical goals such as the minimisation of the number of reconfigurations to be performed to follow the whole prescribed path. Each isolated feasible transition,  $F_{i,j} = 1$ , s.t.  $F_{i-1,j} = 0, F_{i+1,j} = 0$  is transformed directly into an infeasible pose,  $F_{i,j} = 0$ . Regarding the clusters composed of a few feasible poses, they are detected by analysing each configuration  $\mathcal{C}_j$ ,  $j = 1, \dots, n_{\mathcal{C}}$  by means of a clustering algorithm: If the detected cluster contains a number of feasible poses lower than a user defined threshold,  $h_1$ , the poses belonging to this cluster are transformed into infeasible ones.

b. *Filtering* (Fig. 5.6b). The algorithm computes the percentage of feasible poses,  $p_j$ , associated to each configuration  $\mathcal{C}_j$ :

$$p_j = \frac{\sum_{i=1}^{n_p} F_{i,j}}{n_p} \quad (5.4)$$

The configurations with a number of feasible poses lower than a user defined threshold,  $h_2$ , are eliminated from the feasibility map. As a result,  $n_{\mathcal{C}'}$  configurations remain in the feasibility map after this filtering process.

c. *Dominant Solution Computation* (Fig. 5.6c). The algorithm analyses the  $n_{\mathcal{C}'}$  configurations at disposal and identifies the so-called dominated and dominant configurations.

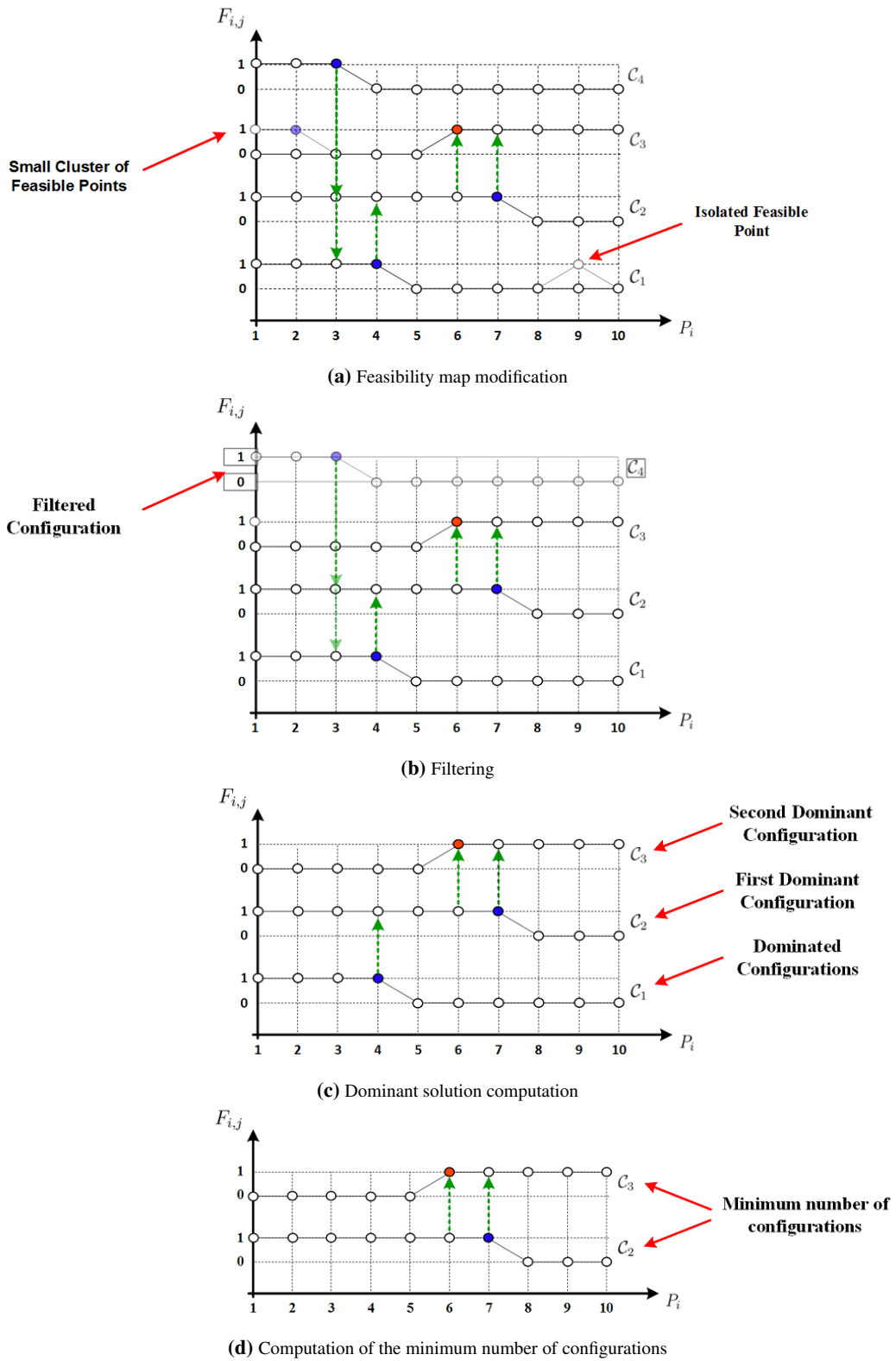


Fig. 5.6 – Example of a feasibility map and minimum set of configurations to be used during the graph building

**Definition 5.4.**

A dominated configuration is a configuration  $\mathcal{C}_j$  such that its feasible poses are all included in the set of feasible poses of another configuration  $\mathcal{C}_k$  and whose percentage of feasible poses,  $p_j$  is strictly lower than  $p_k$

$$\mathcal{C}_j \text{ is a dominated configuration if } \exists \mathcal{C}_k, k \neq j \quad \text{s.t.} \quad \begin{cases} \forall F_{i,j}, i = 1, \dots, n_P : F_{i,j} = 1 & \implies & F_{i,k} = 1 \\ p_j < p_k \end{cases}$$

Consequently, the dominant configurations can be defined as follows.

**Corollary 5.5.**

A dominant configuration is a configuration such that its feasible poses are not all included in the set of feasible poses of another configuration.

- d. *Computation of the Minimum Number of Configurations (Fig. 5.6d).* Given  $n_d$  dominant configurations, the algorithm computes the minimum number of configurations,  $n_m$ , that allow the moving platform to follow the whole prescribed path while satisfying all constraint functions. The computation is performed by analysing the possible combinations of  $\eta$  dominant configurations. The analysis starts with  $\eta = 1$ . The value of  $\eta$  is increased until at least one combination covers all the points of the prescribed path. For a given  $\eta$ , the number of combinations to be tested is equal to  $\binom{\eta}{n_d} = \frac{n_d!}{\eta!(n_d-\eta)!}$ . In the best case, only one configuration is sufficient,  $n_m = \eta = 1$ . In the worst case, all dominant configurations are required to follow the complete path, i.e.,  $n_m = \eta = n_d$ .
- e. *Definition of the Configurations to Build the Graph.* Among all the  $\binom{n_m}{n_d} = \frac{n_d!}{n_m!(n_d-n_m)!}$  combinations of  $n_m$  configurations, all the ones which proved to belong to a combination which covers entirely the prescribed path are retained and will be used to build the graph of the reconfigurations (Step VIII). When the prescribed path cannot be fully covered, due to an extremely cluttered environment or other external constraints, the algorithm selects the set of configurations that let cover the largest number of points of the prescribed path.

An example of the configuration selection procedure, based on a 4-configurations feasibility map, is illustrated in Fig. 5.6.  $\mathcal{C}_1$  contains an isolated feasibility transition at  $P_9$  and configuration  $\mathcal{C}_3$  has a cluster of two feasible points at  $P_1$  and  $P_2$ . With the threshold  $h_1 = 3$ , the feasibility map is modified in such a way that  $F_{9,1} = 0$ ,  $F_{1,3} = 0$  and  $F_{2,3} = 0$  (Fig. 5.6a). According to the number of feasible points of the four configurations, and with a threshold  $h_2 = 0.4$ , configuration  $\mathcal{C}_4$  has been eliminated, since  $p_4 = 0.3$  (Fig. 5.6b). The analysis performed over the remaining configurations shows that configuration  $\mathcal{C}_1$  is dominated by configuration  $\mathcal{C}_2$  (Fig. 5.6c). Configuration  $\mathcal{C}_3$  is also a dominant configuration. Therefore,  $\mathcal{C}_2$  and  $\mathcal{C}_3$  are the two dominant configurations of the problem at hand that can be used to complete the task (Fig. 5.6d).

### 5.2.8 Step VIII: Graph Building

A graph is generated from the reduced feasibility map obtained at Step VII. The nodes of the graph, denoted as  $N_{i,j,k}$ , represent the possible reconfigurations the robot can perform at point  $P_i$  to switch from the actual feasible configuration  $\mathcal{C}_j$  to another feasible configuration  $\mathcal{C}_k$ . The nodes are connected by oriented arcs representing the possible sequences of reconfigurations to be followed in order to follow the whole prescribed path. In fact, two nodes  $N_{i,j,k}$  and  $N_{i',j',k'}$  are adjacent when  $i' > i$ ,  $k = j'$  and all the poses between  $P_{i,k}$  and  $P_{i',k}$  are feasible:

**Definition 5.6.**

$$N_{i,j,k} \text{ and } N_{i',j',k'} \text{ are adjacent if } \begin{cases} i' > i \\ j' = k \\ F_{i'',k} = 1, \forall i'' \text{ s.t. } i \leq i'' \leq i' \end{cases} \quad (5.5)$$

The graph building algorithm is illustrated in Fig. 5.7. It consists of the following steps.

- The first node,  $N_0$ , is a virtual node. This node represents the starting point of the graph. It is associated to a virtual point of the prescribed path,  $P_0$ , and it is not assigned to any configuration. Its adjacent nodes,  $N_{1,0,k}$ , are associated to the point  $P_1$  and they are created only when a configuration  $\mathcal{C}_k$  is feasible at point  $P_1$ , i.e.,  $F_{1,k} = 1$ .
- The intermediate nodes,  $N_{i,j,k}$ , are generated by analysing each feasibility transition of the feasibility map, from point  $P_2$  to point  $P_{n_p-1}$ . Nodes are generated in correspondence to NFTs and PFTs. Given a NFT, a node  $N_{i,j,k}$  is generated if configuration  $\mathcal{C}_k$  is feasible at points  $P_i$  and  $P_{i+1}$ .

**Definition 5.7.**

$$N_{i,j,k} \text{ is generated if } \begin{cases} F_{i,j} \text{ is a NFT} \\ F_{i,k} = 1 \\ F_{i+1,k} = 1 \end{cases} \quad (5.6)$$

Given a PFT, a node  $N_{i,k,j}$  is generated if configuration  $\mathcal{C}_k$  is feasible at points  $P_i$  and  $P_{i-1}$ . Thus:

**Definition 5.8.**

$$N_{i,k,j} \text{ is generated if } \begin{cases} F_{i,j} \text{ is a PFT} \\ F_{i,k} = 1 \\ F_{i-1,k} = 1 \end{cases} \quad (5.7)$$

Thus, the following corollary is verified:

**Corollary 5.9.**

According to Def. 5.7 and 5.8, a node  $N_{i,j,k}$  exists only if both configurations  $\mathcal{C}_j$  and  $\mathcal{C}_k$  are feasible at point  $P_i$ :  $F_{i,j} = 1$  and  $F_{i,k} = 1$

- c. The ending node,  $N_e$ , is a virtual node. This node is associated to point  $P_{n_p}$  and it is not assigned to any configuration. Its adjacent nodes,  $N_{n_p,j,e}$ , are associated to point  $P_{n_p}$  and they are created only when a configuration  $\mathcal{C}_j$  is feasible at point  $P_{n_p}$ , e.g.,  $F_{n_p,j} = 1$ .

Finally, the adjacent nodes are connected to each other, according to Def. 5.6, and a cost is assigned to each arc. Some relevant cost functions are discussed in Sec. 5.2.9.

Figure 5.8 shows the graph associated to the feasibility map given in Fig. 5.5.

### 5.2.9 Step IX: Cost Functions

The user defines a set of  $n_\mu$  cost functions,  $\mu_t$ ,  $t = 1, \dots, n_\mu$ . The cost functions are used to compute the cost of each arc of the graph. The cost functions to be used depend on the task to be performed by the RCDPR or on the user preferences. Nevertheless, five relevant cost functions, bounded between 0 and 1, are presented thereafter.

1. *Number of reconfigurations.* The first cost function,  $\mu_1$ , aims at minimising the number of reconfigurations,  $n_r$ , defined as the number of exit point changes to be performed in order to switch from configuration  $\mathcal{C}_j$  to configuration  $\mathcal{C}_k$ :

$$\mu_1 = \frac{n_r}{m} \quad (5.8)$$

Note that  $\mu_1$  is equal to 1 if all the cables have to be reconfigured. This cost function can be considered in order to reduce the number of cable attaching/detaching operations.

2. *Capacity margin.* The second cost function,  $\mu_2$ , aims at maximising the capacity margin of the RCDPR [CR-CCG15]. The capacity margin quantifies how "close" the RCDPR is to a non static equilibrium configuration, with respect to the REWS,  $[\mathbf{w}_e]_r$ . Given two adjacent nodes,  $N_{i,j,k}$  and  $N_{i',k,k'}$ ,  $\mu_2$  is defined as the inverse of the average of the capacity margin between points  $P_i$  and  $P_{i'}$  of the prescribed path. The evaluation is performed with respect to configuration  $\mathcal{C}_k$ :

$$\mu_2 = \frac{\sum_{i''=i}^{i'} S_{i'',k} (i' - i)}{(i' - i) n_p} = \frac{\sum_{i''=i}^{i'} S_{i'',k}}{n_p} \quad (5.9)$$

where the capacity margin  $S_{i'',k}$ , measured at points  $P_{i''}$ ,  $i'' = i, \dots, i'$  for configuration  $\mathcal{C}_k$ , is defined as follows:

$$S_{i'',k} = \min_{j=1, \dots, n_j} \left( \min_{l=1, \dots, n_l} (s_{i'',j,l}) \right) \quad (5.10)$$

$s_{i'',j,l}$  being the signed distance from the  $j$ -th vertex of  $[\mathbf{w}_e]_r$  to the  $l$ -th face of  $[\mathbf{w}_e]_a$ .  $n_j$  and  $n_l$  are equal to the number of vertices of  $[\mathbf{w}_e]_r$  and the number of faces of  $[\mathbf{w}_e]_a$ , respectively.

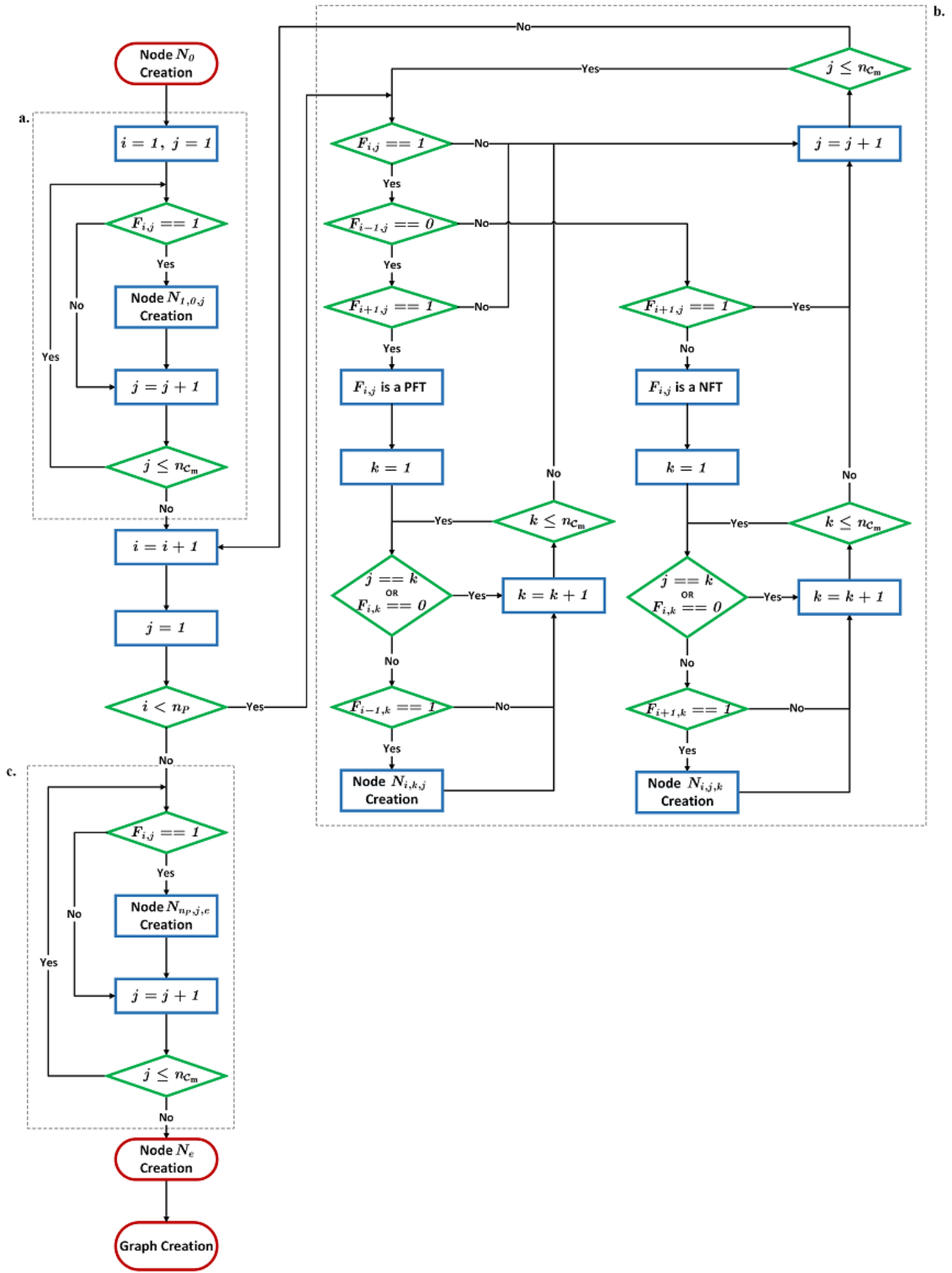


Fig. 5.7 – Flowchart of the graph building algorithm

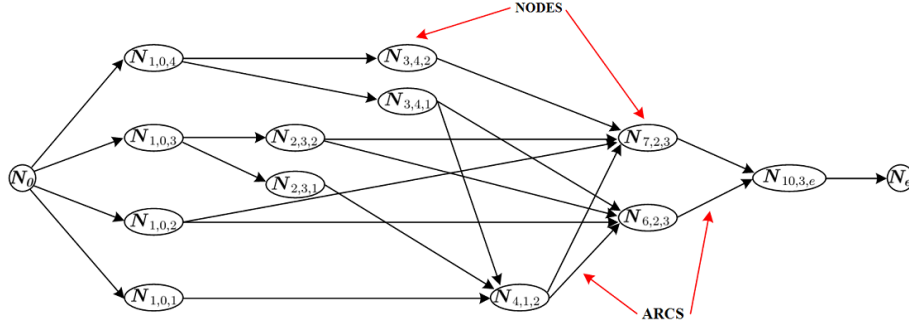


Fig. 5.8 – Graph associated to the feasibility map shown in Fig. 5.5

It has to be noticed that vector  $\mathbf{w}_e$  and matrix  $\mathbf{W}$  (Eq. (2.12)) are not homogeneous. In order to compute the capacity margin, they are normalised as follows:

$$\mathbf{W}_n = \begin{bmatrix} \mathbb{I}_3 & \mathbf{0}_3 \\ \mathbf{0}_3 & \frac{1}{r_g} \mathbb{I}_3 \end{bmatrix} \mathbf{W} \quad (5.11)$$

$$\mathbf{w}_{e, n} = \begin{bmatrix} \mathbb{I}_3 & \mathbf{0}_3 \\ \mathbf{0}_3 & \frac{1}{r_g} \mathbb{I}_3 \end{bmatrix} \mathbf{w}_e \quad (5.12)$$

where  $r_g^2 = (1/m) \sum_{i=1}^m \|\mathbf{b}_i^b\|_2^2$  is the radius of gyration of the moving platform.  $\mathbb{I}_3$  and  $\mathbf{0}_3$  are the [3x3] identity and null matrices, respectively.

3. *Positioning error.* The third cost function,  $\mu_3$ , aims at minimising the norm of the positioning error of the RCDPR moving platform. Given two adjacent nodes,  $N_{i,j,k}$  and  $N_{i',k,k'}$ , this cost function is expressed as the weighted mean of the 2-norm of the positioning error,  $\|\delta\mathbf{t}\|_2$ , of the moving platform between points  $P_i$  and  $P_{i'}$  of the prescribed path. The evaluation is performed with respect to configuration  $\mathcal{C}_k$ :

$$\mu_3 = \frac{\overline{\|\delta\mathbf{t}\|_2}}{n_p} \frac{(i' - i)}{i' - i} = \frac{\sum_{i''=i}^{i'} \|\delta\mathbf{t}_{i'',k}\|_2}{i' - i} \frac{(i' - i)}{n_p} = \frac{\sum_{i''=i}^{i'} \|\delta\mathbf{t}_{i'',k}\|_2}{n_p} \quad (5.13)$$

where  $\|\delta\mathbf{t}_{i'',k}\|_2$  is the 2-norm of the positioning error vector at point  $P_{i''}$  for configuration  $\mathcal{C}_k$ .

4. *Cable tensions.* The fourth cost function,  $\mu_4$ , aims at minimising the cable tensions. Given two adjacent nodes,  $N_{i,j,k}$  and  $N_{i',k,k'}$ ,  $\mu_4$  is equal to the weighted mean of the norm of the cable tension vector,  $\overline{\|\boldsymbol{\tau}\|_2}$ , between points  $P_i$  and  $P_{i'}$  along the prescribed path. As mentioned in Sec. 2.2, the minimal 2-norm of cable tension vector is chosen as the solution to Eq. (2.12). The evaluation is performed with respect to configuration  $\mathcal{C}_k$ :

$$\mu_4 = \frac{\overline{\|\boldsymbol{\tau}\|_2}}{n_p} \frac{(i' - i)}{i' - i} = \frac{\sum_{i''=i}^{i'} \|\boldsymbol{\tau}_{i'',k}\|_2}{i' - i} \frac{(i' - i)}{n_p} = \frac{\sum_{i''=i}^{i'} \|\boldsymbol{\tau}_{i'',k}\|_2}{n_p} \quad (5.14)$$

where  $\|\boldsymbol{\tau}_{i'',k}\|_2$  is the 2-norm of the cable tension vector at point  $P_{i''}$  for configuration  $\mathcal{C}_k$ .

5. *Cable tension variations.* The fifth cost function,  $\mu_5$ , aims at minimising the cable tension variations along the prescribed path. This function is defined by the weighted standard deviation  $\sigma_\tau$  of the norm of the cable

tension vector, between points  $P_i$  and  $P_{i'}$ . The evaluation is performed with respect to configuration  $\mathcal{C}_k$ :

$$\mu_5 = \sigma_\tau \frac{(i' - i)}{n_p} = \sqrt{\frac{\sum_{i''=i}^{i'} \left( \|\tau_{i'',k}\|_2 - \|\tau\|_2 \right)^2}{i' - i}} \frac{(i' - i)}{n_p} \quad (5.15)$$

### 5.2.10 Step X: Dijkstra's Algorithm

A Dijkstra's algorithm [SLL01], [Dik59], [CCH14] is used to select the optimal reconfiguration strategy. It searches for the graph in order to compute the shortest path connecting nodes  $N_0$  and  $N_e$ . The optimal sequence of nodes to be crossed corresponds to the optimal sequence of reconfigurations to be performed to allow the moving platform to follow the whole prescribed path. The optimisation can be performed by analysing different criteria, and consequently different costs associated to the arcs of the graph. The cost of the optimal reconfiguration strategy,  $\Phi_i$ , is equal to the sum of the costs of the arcs connecting the nodes belonging to the shortest path.

## 5.3 Case Study I: A Planar RCDPR

A first case study is considered in order to illustrate the algorithm presented in Sec. 5.2. A closed path  $\mathcal{P}$ , discretised into 164 points,  $P_i, i = 1, \dots, 164$ , has to be followed by the moving platform CoM. The path, lying in the plane  $(O, \mathbf{x}_b, \mathbf{y}_b)$ , is shown in Fig. 5.9. The orientation of the moving platform is constant. The axes of the moving reference frame,  $\mathcal{F}_p$ , are oriented as the ones of the fixed reference frame,  $\mathcal{F}_b$ .

The RCDPR under study is composed of four cables. The properties of the cables have been selected as follows: the Young Modulus,  $E$ , is equal to 100 GPa; their diameter  $\phi_c$  is equal to 4 mm; their stiffness coefficient,  $k_i$ , is equal to 252 KN/m; the maximum allowed tension in the cables,  $\tau_{max}$ , is equal to 34950 N. A safety coefficient  $\eta = 5$  has been taken into account such that:

$$0 < \tau_i \leq \frac{\tau_{max}}{\eta}, \quad \forall i = 1, \dots, 4 \quad (5.16)$$

The dimensions of the moving platform have been set to 0.2 m for the width,  $w_p$ , and 0.3 m for the height,  $h_p$ . The Cartesian coordinates of points  $B_i, i = 1, \dots, 4$ , expressed in the moving platform frame  $\mathcal{F}_p$  are the following:

$$\mathbf{b}_1^p = [w_p/2, h_p/2]^T \quad (5.17)$$

$$\mathbf{b}_2^p = [-w_p/2, h_p/2]^T \quad (5.18)$$

$$\mathbf{b}_3^p = [-w_p/2, -h_p/2]^T \quad (5.19)$$

$$\mathbf{b}_4^p = [w_p/2, -h_p/2]^T \quad (5.20)$$

The cable exit points,  $A_i, i = 1, \dots, 4$  can be reconfigured, according to the following parametrisation:

$$\mathbf{a}_1^b = [u_1 + u_3, u_2]^T \quad (5.21)$$

$$\mathbf{a}_2^b = [-u_1 + u_3, u_2]^T \quad (5.22)$$

$$\mathbf{a}_3^b = [-u_1 + u_3, -u_2]^T \quad (5.23)$$

$$\mathbf{a}_4^b = [u_1 + u_3, -u_2]^T \quad (5.24)$$

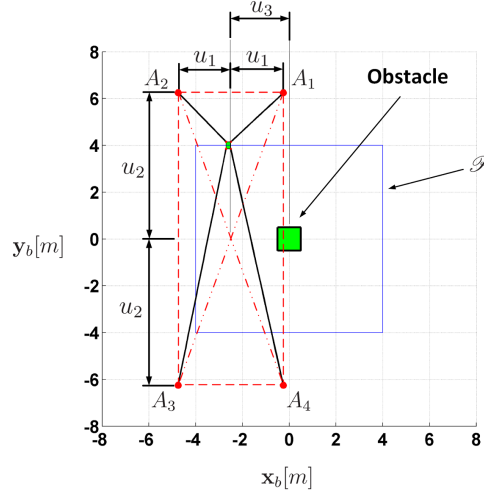


**Fig. 5.9** – Case Study I: Description of the exit point parametrisation for the RCDPR

**Tab. 5.1** – Possible configurations of the first case study

Configuration	$u_1$ [m]	$u_2$ [m]	$u_3$ [m]
$\mathcal{C}_1$	2.25	6.25	2.50
$\mathcal{C}_2$	4.00	7.75	-1.00
$\mathcal{C}_3$	4.00	7.00	-0.25
$\mathcal{C}_4$	2.25	6.25	-2.50

The parameters  $u_1$  and  $u_2$  represent half of the distance between the exit points along  $\mathbf{x}_b$  and  $\mathbf{y}_b$ , respectively.  $u_3$  is the offset of the cable connection point positions along  $\mathbf{x}_b$ . The robot is symmetric with respect to  $\mathbf{x}_b$ , as shown in Fig. 5.9.

An obstacle is included in the environment. It consists of a square of side length equal to 1 m. The obstacle is centred at the origin of the reference frame  $\mathcal{F}_b$  as shown in Fig. 5.9.

The moving platform can be subjected to an external wrench,  $\mathbf{w}_e$ . We assume that the components of  $\mathbf{w}_e$  are bounded as follows:

$$-500 \text{ N} \leq f_x, f_y \leq 500 \text{ N} \quad (5.25)$$

$$-7.5 \text{ N} \leq m_z \leq 7.5 \text{ N} \quad (5.26)$$

where  $f_x$  and  $f_y$  stand for the external force components along  $\mathbf{x}_b$  and  $\mathbf{y}_b$  axes, respectively.  $m_z$  is the external moment about the  $\mathbf{z}_b$  axis.

Four configurations have been considered in this case study. Their parameters are represented in Table 5.1.

The first analysis has been performed by optimising the total number of reconfigurations,  $\mu_1$ . The solution proves that four reconfigurations are sufficient to complete the proposed task. The optimal result is shown in Fig. 5.10. The feasibility map has been built by analysing the constraints assigned to each point of the prescribed path namely, wrench feasibility, cable interferences and obstacle collisions.

For instance, configuration  $\mathcal{C}_4$  is the unique feasible configuration at point  $P_1$  of the desired path. The NFT at

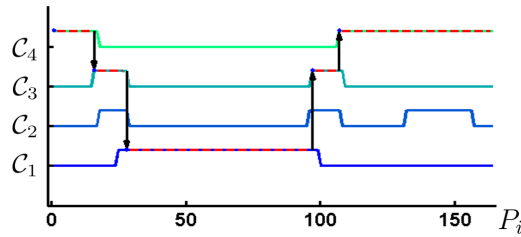


**Fig. 5.10** – Case Study I: Feasibility map and optimal solution with regard to the minimisation of  $\mu_1$

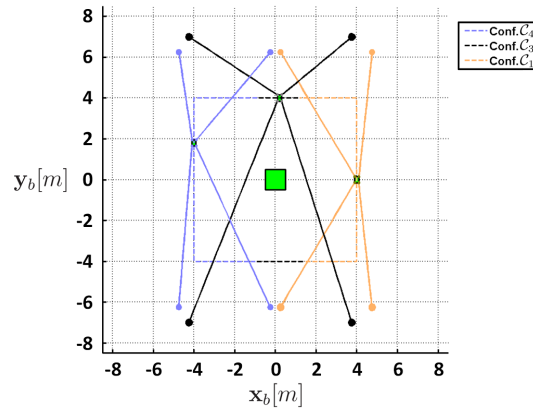


**Fig. 5.11** – Case Study I: Optimal RCDPR configurations, selected by the algorithm in order to complete the task with respect to the minimum number of configurations  $\mu_1$

point  $P_{16}$  requires a change of configuration, from  $\mathcal{C}_4$  to  $\mathcal{C}_3$ . When a new NFT appears at point  $P_{28}$ , the RCDPR adopts the configuration  $\mathcal{C}_1$ . A PFT appears at point  $P_{37}$ . The RCDPR returns to the configuration  $\mathcal{C}_3$  and, later on, to the configuration  $\mathcal{C}_4$ , following the desired path until its end.

The optimal configurations required to complete the task are shown in Fig. 5.11.

A second optimisation has been tested, aiming at minimising the positioning error of the moving platform,  $\mu_3$ , due to the cable non-rigid nature. The result is similar to the one obtained by minimising  $\mu_1$ . In this specific case, the first reconfiguration is performed at  $P_{18}$ . The RCDPR switches from the configuration  $\mathcal{C}_4$  to the configuration  $\mathcal{C}_2$  as shown in Fig. 5.12.

Both the optimal solutions analysed in this case study are represented in the graph shown in Fig. 5.13. The red arrows indicate the path obtained by minimising  $\mu_1$ . The blue arrows describe the path obtained by minimising the moving platform positioning error. The blue optimal path leads to a reduction of the positioning error, with respect to the red optimal path, of almost 18%: The total cost of the red path, in terms of positioning error, is equal to 1.7663 while the cost associated to the blue path is equal to 1.4545.

## 5.4 Case Study II: A Spatial RCDPR

The reconfiguration planning method introduced in Sec. sec:5.2 is implemented in the following case study, which aims at painting and sandblasting the yellow tubular structure shown in Fig. 5.14. This structure is 5 m long, 2 m wide at its extremities and 1.5 m wide at its centre and lies on the ground. The tubes have a diameter  $\phi_t$  equal

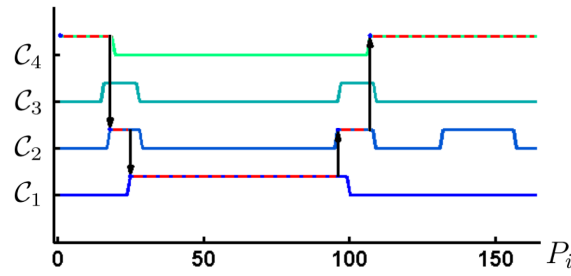


Fig. 5.12 – Case Study I: Feasibility map and optimal solution with regard to the minimisation of  $\mu_3$

to 10 cm. The RCDPR should paint and sandblast both the inner and the outer faces of the structure. A robotic arm, embarked on the moving platform, aims at manipulating the sandblasting and painting tools. Therefore, the orientation of the moving platform can be kept constant and the  $\mathbf{x}_p$ ,  $\mathbf{y}_p$  and  $\mathbf{z}_p$  axes of the moving platform frame  $\mathcal{F}_p$  are supposed to be parallel to the  $\mathbf{x}_b$ ,  $\mathbf{y}_b$  and  $\mathbf{z}_b$  axes of the base frame  $\mathcal{F}_b$ .

### 5.4.1 Problem Description

#### Constant Design Parameters (Step I)

The RCDPR consists of a moving platform connected to the base by  $m = 8$  cables, as shown in Fig. 5.14. The characteristics of the cables of the RCDPR are the following: The Young Modulus,  $E$ , is equal to 100 GPa; the diameter,  $\phi_c$ , is equal to 4 mm; their stiffness coefficient,  $k_i$ , is equal to 252 KN/m; the structural maximum cable tension is equal to 34.95 KN. A tension safety coefficient,  $k_{s1} = 5$ , has been applied in this case study so that  $\tau_{max1} = 6.99$  KN.

The base length,  $l_s$ , is equal to 7 m, the base width,  $w_s$ , is equal to 4.5 m and the base height,  $h_s$ , is equal to 4 m. The cables are connected to the base frame through some pulleys. The pulleys can be installed on a predefined grid of locations, which are located on ten sliding bars. The sliding bars are installed on the lateral and top sides of the base. Their motion is discretised with a constant step of 25 cm.

The cables are coiled and uncoiled on winches, which are actuated by electric motors. The characteristics of the power system are the following: The nominal motor torque,  $\tau_M$ , is equal to 45 Nm, the nominal speed,  $\omega_M$ , is equal to 3000 rpm, the gearbox transmission ratio,  $\rho_R$ , is equal to 10, the diameter of the winches,  $\rho_W$ , is equal to 15 cm. The cable tension limit  $\tau_{max}$  is equal to  $\tau_{max} = \min\{\tau_{max1}, \tau_{max2}\} = 6000$  N. Considering that  $\tau_{max2} = \frac{2}{\phi_w} \rho_R \tau_M = 6000$  N,  $\tau_{max} = \tau_{max2}$  since the tension that can be provided to the cables is lower than  $\tau_{max1}$ .

The moving platform is represented in Fig. 5.15. Its width,  $w_p$ , is equal to 20 cm, its length,  $l_p$ , is equal to 20 cm and its height is equal to 25 cm. The Cartesian coordinates of points  $B_i, i = 1, \dots, 8$ , are expressed in frame

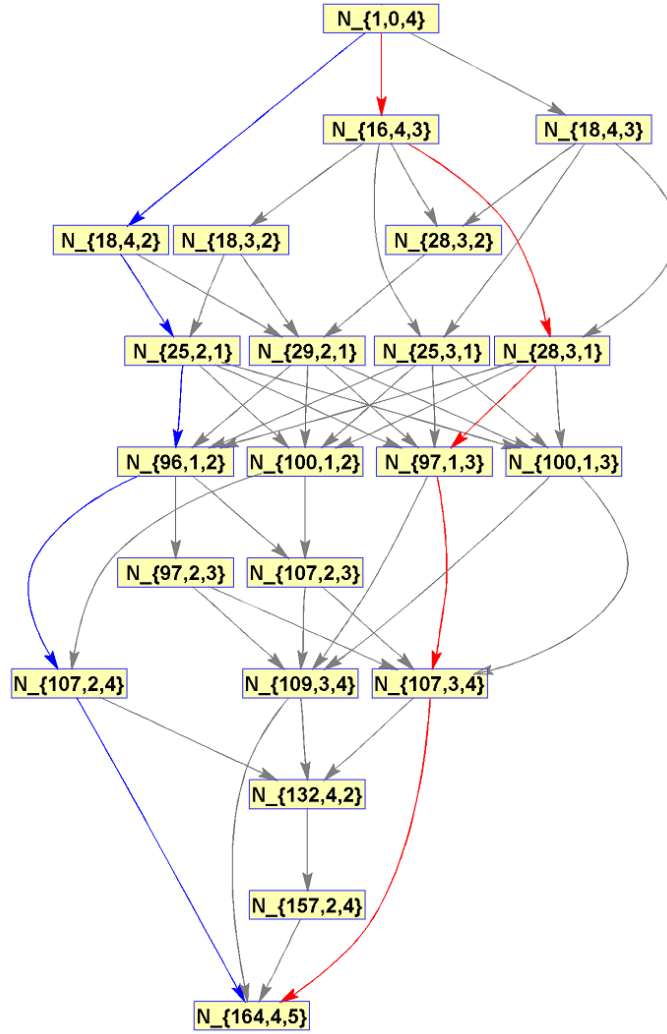


Fig. 5.13 – Case Study I: Graph of the two optimisation problems

$\mathcal{F}_p$  as follows:

$$\mathbf{b}_1^p = [-w_p/2 - c_0, -l_p/2, -h_p/2] \quad (5.27)$$

$$\mathbf{b}_2^p = [-w_p/2, -l_p/2 - c_0, h_p/2] \quad (5.28)$$

$$\mathbf{b}_3^p = [-w_p/2 - c_0, l_p/2, -h_p/2] \quad (5.29)$$

$$\mathbf{b}_4^p = [-w_p/2, l_p/2 + c_0, h_p/2] \quad (5.30)$$

$$\mathbf{b}_5^p = [w_p/2 + c_0, l_p/2, -h_p/2] \quad (5.31)$$

$$\mathbf{b}_6^p = [w_p/2, l_p/2 + c_0, h_p/2] \quad (5.32)$$

$$\mathbf{b}_7^p = [w_p/2 + c_0, -l_p/2, -h_p/2] \quad (5.33)$$

$$\mathbf{b}_8^p = [w_p/2, -l_p/2 - c_0, h_p/2] \quad (5.34)$$

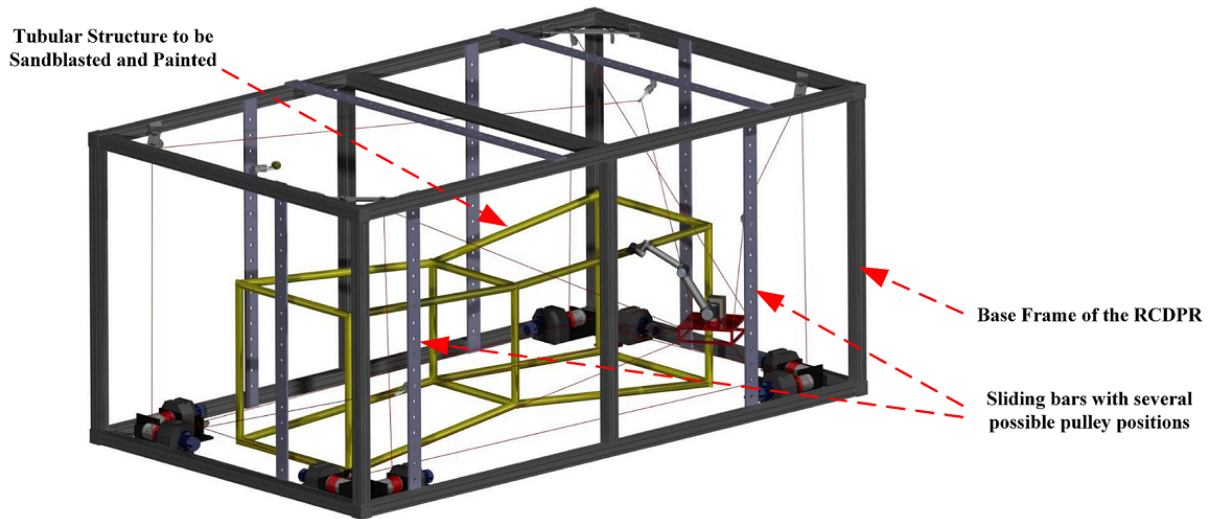


**Fig. 5.14** – Case study II: The yellow tubular structure should be sandblasted and painted by the RCDPR. The RCDPR consists of a moving platform, eight cables and a base with some sliding bars

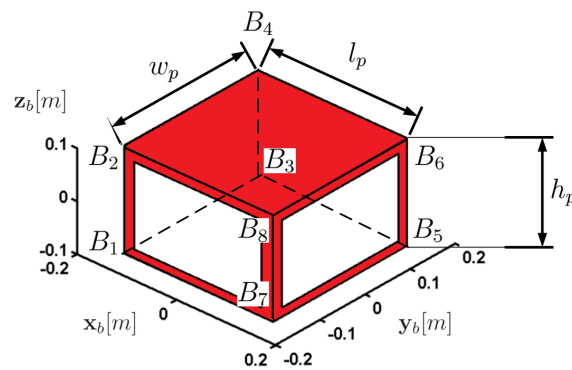


**Fig. 5.15** – Case study II: Moving platform

where  $c_0$  is an offset used to avoid both the collisions between the cables and the parallel singularities of the RCDPR (the wrench matrix  $\mathbf{W}$  has not full rank). The offset helps to prevent this situation by introducing an asymmetry between the layout of the cable exit points and the layout of the cable connection points on the moving platform. In this case study, the offset is equal to 3.5 cm.

### RCDPR Layout Parametrisation and Configuration Set (Steps II and III)

Two different layouts and parametrisations of the RCDPR are used in order to cover the inner and the outer areas of the tubular structure. In the layout chosen for the outer faces of the structure, the exit points,  $A_i$ ,  $i = 1, \dots, 8$ , are located at the vertices of a parallelepiped. The Cartesian coordinates of points  $A_i$ ,  $i = 1, \dots, 8$  are parametrised

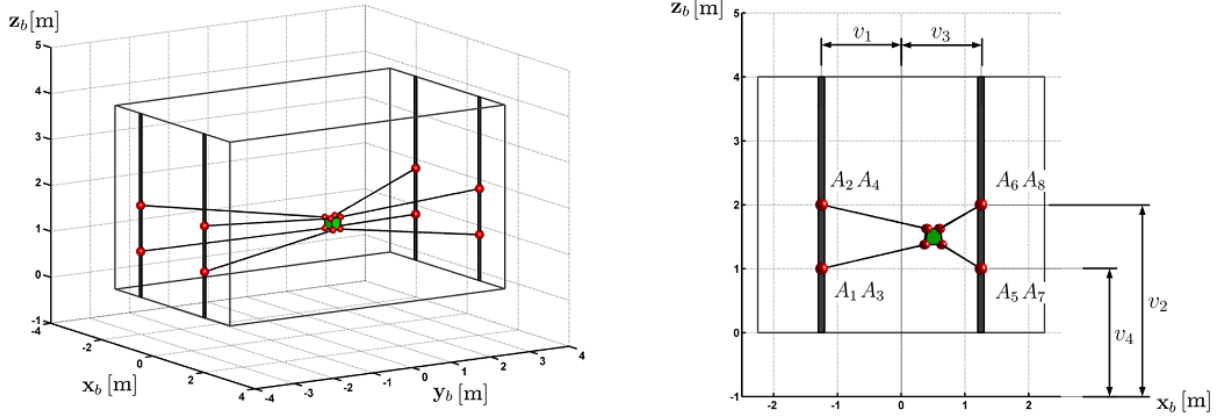


Fig. 5.16 – Case study II: Parametrisation of the RCDPR while operating on the outer faces of the tubular structure

by means of four parameters  $v_1$ ,  $v_2$ ,  $v_3$  and  $v_4$  as shown in Fig. 5.16:

$$\mathbf{a}_1^b = [v_1 \quad -l_s/2 \quad v_4]^T \quad \mathbf{a}_2^b = [v_1 \quad -l_s/2 \quad v_2]^T \quad (5.35)$$

$$\mathbf{a}_3^b = [v_1 \quad l_s/2 \quad v_4]^T \quad \mathbf{a}_4^b = [v_1 \quad l_s/2 \quad v_2]^T \quad (5.36)$$

$$\mathbf{a}_5^b = [v_3 \quad l_s/2 \quad v_4]^T \quad \mathbf{a}_6^b = [v_3 \quad l_s/2 \quad v_2]^T \quad (5.37)$$

$$\mathbf{a}_7^b = [v_3 \quad -l_s/2 \quad v_4]^T \quad \mathbf{a}_8^b = [v_3 \quad -l_s/2 \quad v_2]^T \quad (5.38)$$

The four parameters can take the following values:

$$[v]_1 = \{-2.10, -1.85, -1.60, -1.35, -1.10, 1.10, 1.35, 1.60, 1.85, 2.10\} \quad (5.39)$$

$$[v]_2 = \{0.10, 0.35, 0.60, 0.85, 1.10, 1.90, 2.15, 2.40, 2.65, 2.90, 3.15, 3.40\} \quad (5.40)$$

$$[v]_3 = \{-2.10, -1.85, -1.60, -1.35, -1.10, 1.10, 1.35, 1.60, 1.85, 2.10\} \quad (5.41)$$

$$[v]_4 = \{0.10, 0.35, 0.60, 0.85, 1.10, 1.90, 2.15, 2.40, 2.65, 2.90, 3.15, 3.40\} \quad (5.42)$$

$$(5.43)$$

Those values for parameters  $v_1$ ,  $v_2$ ,  $v_3$  and  $v_4$  lead to  $n_{\mathcal{C}} = 14400$  possible configurations of the RCDPR.

The exit point layout used to cover the inner faces of the structure is a parallelepiped too, as shown in Fig. 5.17. However, considering the symmetry of the task, the exit points  $A_i$ ,  $i = 1, \dots, 8$  are located symmetrically with respect to planes  $\mathbf{x}_b O \mathbf{z}_b$  and  $\mathbf{y}_b O \mathbf{z}_b$ . As a consequence, the three parameters  $w_1$ ,  $w_2$  and  $w_3$  are considered to be sufficient to define the Cartesian coordinates of points  $A_i$ :

$$\mathbf{a}_1^b = [-w_1 \quad -l_s/2 \quad w_2]^T \quad \mathbf{a}_2^b = [-w_1 \quad -l_s/2 \quad w_3]^T \quad (5.44)$$

$$\mathbf{a}_3^b = [-w_1 \quad l_s/2 \quad w_2]^T \quad \mathbf{a}_4^b = [-w_1 \quad l_s/2 \quad w_3]^T \quad (5.45)$$

$$\mathbf{a}_5^b = [w_1 \quad l_s/2 \quad w_2]^T \quad \mathbf{a}_6^b = [w_1 \quad l_s/2 \quad w_3]^T \quad (5.46)$$

$$\mathbf{a}_7^b = [w_1 \quad -l_s/2 \quad w_2]^T \quad \mathbf{a}_8^b = [w_1 \quad -l_s/2 \quad w_3]^T \quad (5.47)$$

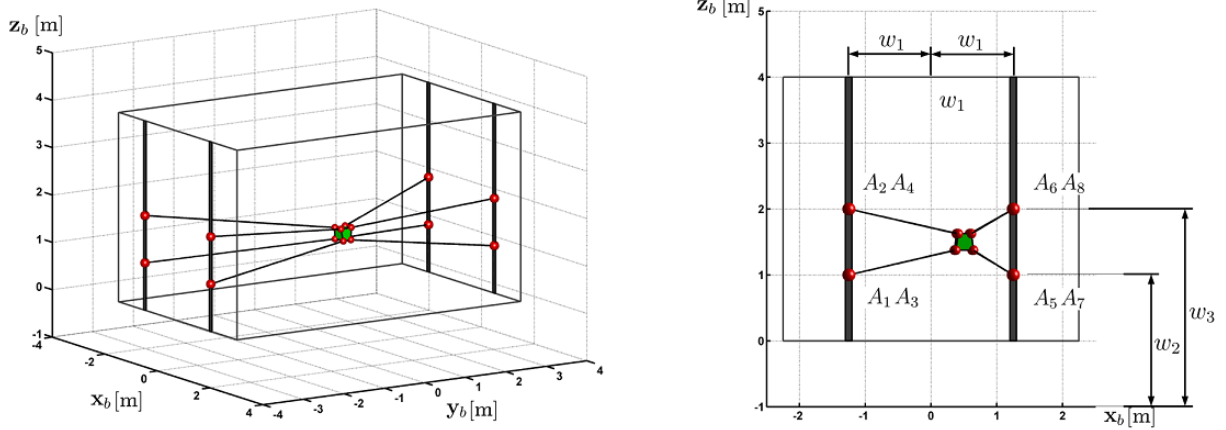


Fig. 5.17 – Case study II: Parametrisation of the RCDPR while operating on the inner faces of the tubular structure

Parameters  $w_1$ ,  $w_2$  and  $w_3$  can take the following values:

$$[w]_1 = \{0, 0.25, 0.5, 0.75, 1.0, 1.25, 1.5, 1.75, 2.0, 2.25\} \quad (5.48)$$

$$[w]_2 = \{0.25, 0.5, 0.75, 1.0, 1.25, 1.5, 1.75, 2.0, 2.25\} \quad (5.49)$$

$$[w]_3 = \{0.25, 0.5, 0.75, 1.0, 1.25, 1.5, 1.75, 2.0, 2.25\} \quad (5.50)$$

$$(5.51)$$

Those values for parameters  $w_1$ ,  $w_2$  and  $w_3$  lead to  $n_{\mathcal{C}} = 810$  possible configurations of the RCDPR.

#### Task and Environment (Step IV)

The weight of the moving platform and the embarked tools is equal to 31 Kg. The forces transmitted by the painting and sandblasting tools to the moving platform are bounded as follows:

$$-30\text{N} \leq f_x, f_y \leq 30\text{N} \quad (5.52)$$

$$f_z = -310\text{N} \quad (5.53)$$

The moments  $m_x$ ,  $m_y$  and  $m_z$  about axes  $\mathbf{x}_b$ ,  $\mathbf{y}_b$  and  $\mathbf{z}_b$  are neglected:  $m_x, m_y, m_z = 0$ . In order to complete the operations, the CoM of the moving platform should follow the profile of the tubular structure with an offset  $d_t = 80\text{cm}$  with respect to the central axes of the tubes. Figure 5.18 shows the red segments and the green via points that the moving platform should follow. According to the procedure described in Sec. 5.2.4, an Eulerian path,  $\mathcal{P}_{out}$ , and an Eulerian cycle,  $\mathcal{P}_{in}$ , covering the outer and inner faces of the tubular structure, respectively, can be defined.  $\mathcal{P}_{out}$  is discretised into 450 points and  $\mathcal{P}_{in}$  is discretised into 500 points. The Eulerian path,  $\mathcal{P}_{out}$ , is illustrated in Fig. 5.19. The moving platform should go through the green via points while respecting a prescribed order. For instance, the moving platform should follow the Eulerian path,  $\mathcal{P}_{out}$ , while passing through 23 points in sequence, namely from point  $P_1$  to point  $P_{23}$ , as shown in Fig. 5.19. Note that points  $P_1$ ,  $P_5$ ,  $P_{11}$  and  $P_{23}$  are coincident and are named  $P_{1,5,11,23}$ .

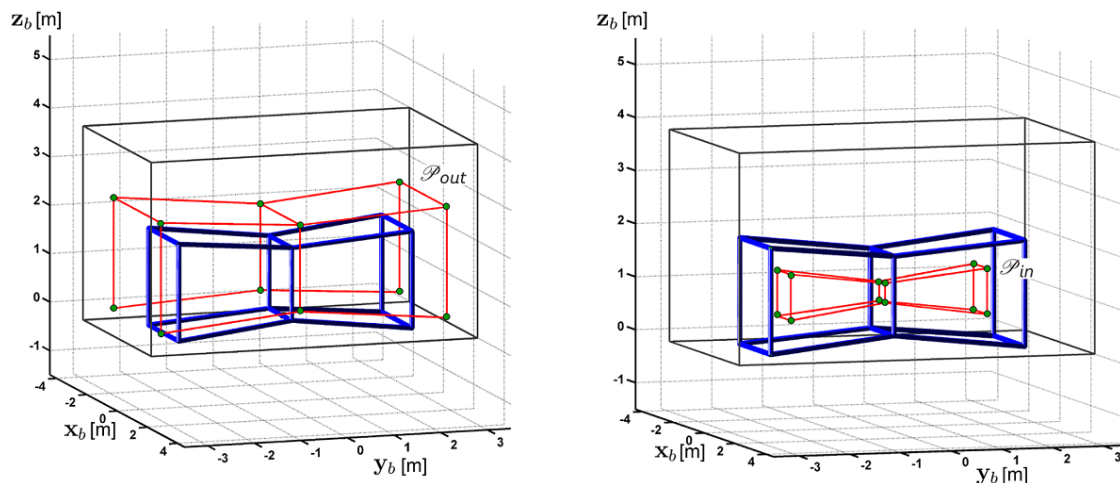


Fig. 5.18 – Case Study II: Sets of red segments and green via points to be covered by the moving platform CoM

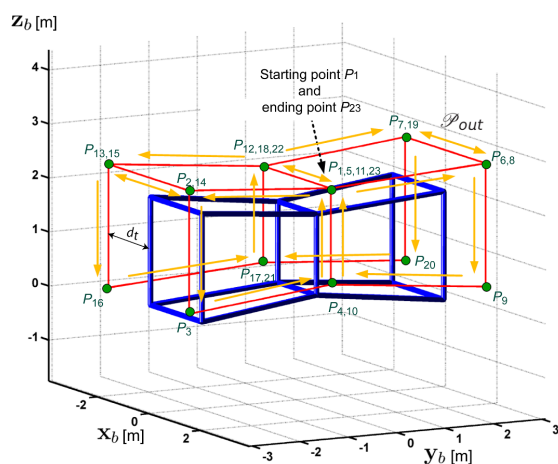


Fig. 5.19 – Case Study II: Eulerian path  $\mathcal{P}_{out}$  to be followed by the moving platform CoM when moving on the outer faces of the tubular structure

## 5.4.2 Results for the Outer Faces of the Tubular Structure

### Feasibility Map and Configuration Selection (Steps VI and VII)

The  $n_{\mathcal{C}} = 14400$  possible configurations of the RCDPR obtained in the previous section are analysed in order to identify the segments of  $\mathcal{P}_{out}$  that can be covered by each configuration. Then, the constraints introduced in Sec. 5.2.5 are considered leading to trace a feasibility map composed of 14400 lines, each line corresponding to one RCDPR configuration. The problem turns out to be fairly complex because of the large number of lines in the feasibility map. In order to reduce the problem complexity, the configuration selection approach explained in Sec. 5.2.7 is used to reduce the number of configurations to be considered with the following thresholds:  $h_1 = 20$  and  $h_2 = 0.25$ . As a result,  $n_d = 76$  dominant configurations are obtained among  $n_{\mathcal{C}'} = 1186$  filtered configurations. It is noteworthy that the minimum number of configurations required to complete the task amongst the 76 dominant configurations is equal to  $n_{\mathcal{C}_m} = 3$ . Moreover, 784 triplets of dominant configurations can be used to cover the prescribed path  $\mathcal{P}_{out}$  completely. Note that 57 configurations can be considered amongst the 76 dominant ones to generate the 784 triplets. The 19 remaining dominant configurations necessarily lead to a combination of more than three dominant configurations to cover the whole prescribed path.

### Graph Building and Cost Functions (Steps VIII and IX)

Figure 5.20 illustrates the graph obtained from the selected 57 dominant configurations. The graph is composed of 452 nodes and 10752 arcs. Due to the size of this graph, only a partial representation has been provided in Fig. 5.20.

The corresponding reconfiguration planning problem has been solved using a Dijkstra's algorithm with respect to each cost function,  $\mu_i = i = 1, \dots, 5$ , proposed in Sec. 5.2.9. The optimal solutions associated to each of the five cost functions are represented on the feasibility map shown in Fig. 5.21. For the sake of clarity, only the 10 configurations,  $\mathcal{C}_i^*, i = 1, \dots, 10$ , composing the five different optimal solutions are displayed in the feasibility map. Table 5.2 gives the design parameters corresponding to those 10 configurations.

### Results Analysis

From Fig. 5.21, it is apparent that configurations  $\mathcal{C}_{[1-4]}^*$  have the same feasibility map, as well as configurations  $\mathcal{C}_{[6-10]}^*$ . Indeed, from Def. 5.4, two dominant configurations, generated by different design parameters, can share the same feasibility map. Note that different configurations can present the same feasibility map but generally provide different performances. For instance, configuration  $\mathcal{C}_{10}^*$  is better in terms of cable tensions than configurations  $\mathcal{C}_{[6-9]}^*$ .

While using  $\mu_1$  as the cost function (arc cost in Dijkstra's algorithm), the number of required reconfigurations to complete the task is minimised. Five reconfigurations turn out to be sufficient to complete the task.  $\mathcal{C}_{10}^*$  is the starting configuration. At the 11<sup>th</sup> point,  $P_{11}$ , of the discretised path  $\mathcal{P}_{out}$ , all the constraints of the optimisation problem at hand are not satisfied anymore for configuration  $\mathcal{C}_{10}^*$ . As a consequence, the RCDPR switches from configuration  $\mathcal{C}_{10}^*$  to configuration  $\mathcal{C}_5^*$ . During the reconfiguration, all the exit points have to be displaced, except points  $A_5$  and  $A_7$ . A NFT is then encountered at  $P_{155}$  and the RCDPR switches to configuration  $\mathcal{C}_9^*$ . During this reconfiguration, exit points  $A_5$  and  $A_7$  are not displaced. The RCDPR meets another NFT at  $P_{209}$  and six of the exit points are displaced. Between points  $P_{209}$  and  $P_{294}$ , the RCDPR remains in configuration  $\mathcal{C}_5^*$ . Two other

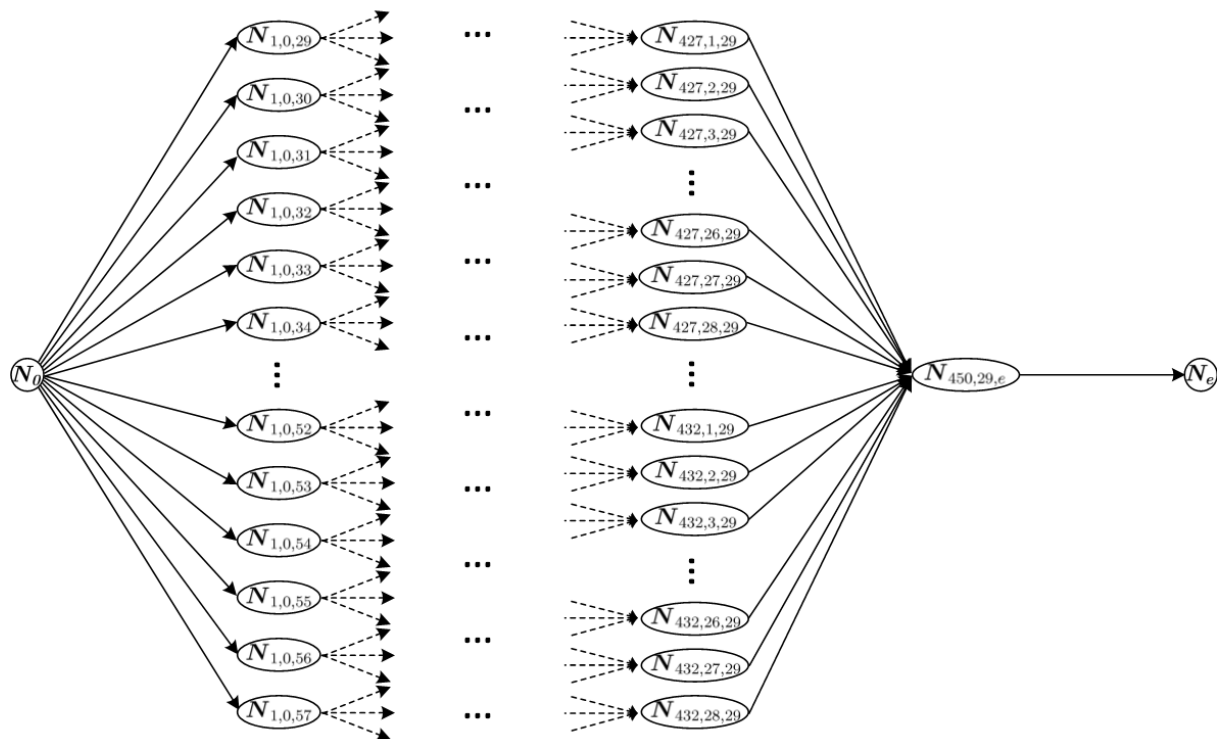


**Fig. 5.20** – Case Study II: Partial representation of the reconfiguration graph. The graph is composed of 452 nodes and 10752 arcs

**Tab. 5.2** – Optimal configurations for the spatial RCDPR

Configuration	$v_1$ [m]	$v_2$ [m]	$v_3$ [m]	$v_4$ [m]
$\mathcal{C}_1^*$	-2.1	0.1	-1.1	3.4
$\mathcal{C}_2^*$	-1.85	0.1	-1.1	3.4
$\mathcal{C}_3^*$	-1.85	0.35	-1.1	3.4
$\mathcal{C}_4^*$	-1.85	0.85	-1.1	3.4
$\mathcal{C}_5^*$	-1.85	2.4	1.85	3.4
$\mathcal{C}_6^*$	1.1	0.1	1.85	2.65
$\mathcal{C}_7^*$	1.1	0.1	1.85	3.4
$\mathcal{C}_8^*$	1.1	0.1	2.1	3.4
$\mathcal{C}_9^*$	1.1	0.6	1.85	3.4
$\mathcal{C}_{10}^*$	1.1	0.85	1.85	3.4

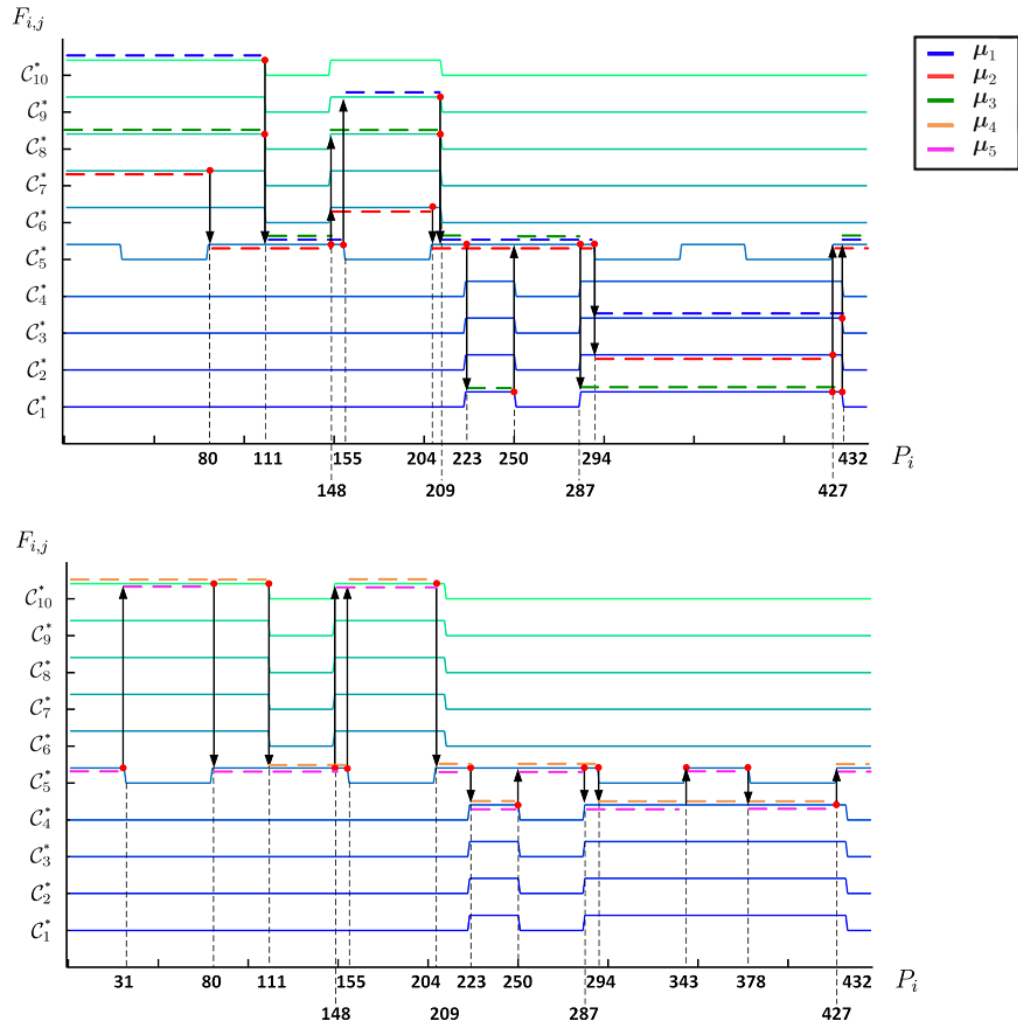


Fig. 5.21 – Case Study II: Feasibility map and optimal solutions for the spatial RCDPR

**Tab. 5.3** – Optimal reconfiguration planning and the associated cost functions for the outer faces of the tubular structure. For each reconfiguration strategy, the optimised cost function is surrounded by a red box

Optimal Reconfiguration Planning	Cost of the reconfiguration strategy				
	$\mu_1$ [°]	$\mu_2$ [N]	$\mu_3$ [mm]	$\mu_4$ [N]	$\mu_5$ [N]
Optimal planning w.r.t. $\mu_1$	30	234.8	0.208	578.1	233.9
Optimal planning w.r.t. $\mu_2$	34	281.3	0.217	615.0	232.8
Optimal planning w.r.t. $\mu_3$	56	260.4	0.132	751.2	504.5
Optimal planning w.r.t. $\mu_4$	42	238.9	0.205	542.3	203.5
Optimal planning w.r.t. $\mu_5$	60	135.0	0.227	561.8	158.5

reconfigurations are necessary to reach the end of  $\mathcal{P}_{out}$ , as shown in Fig. 5.21. Table 5.3 gives the optimal value of each cost function  $\mu_i = i = 1, \dots, 5$ , obtained with Dijkstra's algorithm <sup>1</sup>.

The optimisation performed with respect to  $\mu_2$  leads to five reconfigurations, as well, while maximising the capacity margin of the RCDPR.  $\mathcal{C}_7^*$  is the starting configuration. The first reconfiguration occurs at point  $P_{80}$ , in presence of a PFT. The RCDPR switches to configuration  $\mathcal{C}_5^*$ . The portions of  $\mathcal{P}_{out}$  between  $P_{80}$  and  $P_{148}$  and between  $P_{204}$  and  $P_{294}$  cover the upper face of the tubular structure. Configuration  $\mathcal{C}_5^*$  is assigned to these portions of  $\mathcal{P}_{out}$  since it improves the capacity margin. In fact, it should be noticed that  $\mathcal{C}_5^*$  is a suspended configuration and suspended configurations usually provide a higher capacity margin than fully constrained ones. The fully constrained configurations  $\mathcal{C}_6^*$  and  $\mathcal{C}_2^*$  are used on the lateral faces of the tubular structure. The RCDPS switches to these configurations when a PFT or a NFT is encountered.

The optimisation performed while considering  $\mu_3$  minimises the use of the suspended configuration  $\mathcal{C}_5^*$ . In order to maintain a static equilibrium, a fully constrained configuration usually requires higher cable tensions than a suspended configuration. Larger cable tensions allow us to increase the RCDPR stiffness, reducing the positioning errors. The positioning error optimisation leads to configuration  $\mathcal{C}_8^*$  at the beginning of  $\mathcal{P}_{out}$ . When a NFT is encountered, at  $P_{111}$ , the RCDPR switches to configuration  $\mathcal{C}_5^*$ , coming back to configuration  $\mathcal{C}_8^*$  when a PFT is encountered at  $P_{148}$ . Following the same principle, the RCDPR uses configuration  $\mathcal{C}_5^*$  only when the fully constrained configurations become infeasible. It goes back to configurations  $\mathcal{C}_1^*$  or  $\mathcal{C}_8^*$ , as soon as possible, when following configuration  $\mathcal{C}_5^*$  a PFT is encountered. It is noteworthy that, despite the high number of reconfigurations, only three configurations ( $\mathcal{C}_1^*$ ,  $\mathcal{C}_5^*$  and  $\mathcal{C}_8^*$ ) are required to complete the task. The fully constrained ones,  $\mathcal{C}_1^*$  and  $\mathcal{C}_8^*$ , are symmetric with respect to the plane  $\mathbf{y}_b \mathbf{Oz}_b$ , as shown in Fig. 5.22. Furthermore, it has to be noticed that, despite an improvement of the moving platform positioning error, the optimal reconfiguration planning increases the cable tension average to 751.2 N and the average of the cable tension variations to 504.5 N.

The optimisations performed while considering  $\mu_4$  and  $\mu_5$  as cost functions are similar: The two solutions assign the same configurations to a large portion of  $\mathcal{P}_{out}$ . In both the optimisation problems, the configurations

<sup>1</sup>The reader is referred to as the following link <http://www.irccyn.ec-nantes.fr/~caro/MMT/VideosMMTGCGG/TestExtMu1.avi> to visualise the optimal reconfiguration planning associated to the first cost function  $\mu_1$ . The reader is referred to as the following link <http://www.irccyn.ec-nantes.fr/~caro/MMT/VideosMMTGCGG/TestExtMu2.avi> to visualise the optimal reconfiguration planning associated to the second cost function  $\mu_2$ . The reader is referred to as the following link <http://www.irccyn.ec-nantes.fr/~caro/MMT/VideosMMTGCGG/TestExtMu3.avi> to visualise the optimal reconfiguration planning associated to the third cost function  $\mu_3$ . The reader is referred to as the following link <http://www.irccyn.ec-nantes.fr/~caro/MMT/VideosMMTGCGG/TestExtMu4.avi> to visualise the optimal reconfiguration planning associated to the fourth cost function  $\mu_4$ . The reader is referred to as the following link <http://www.irccyn.ec-nantes.fr/~caro/MMT/VideosMMTGCGG/TestExtMu5.avi> to visualise the optimal reconfiguration planning associated to the fifth cost function  $\mu_5$ .

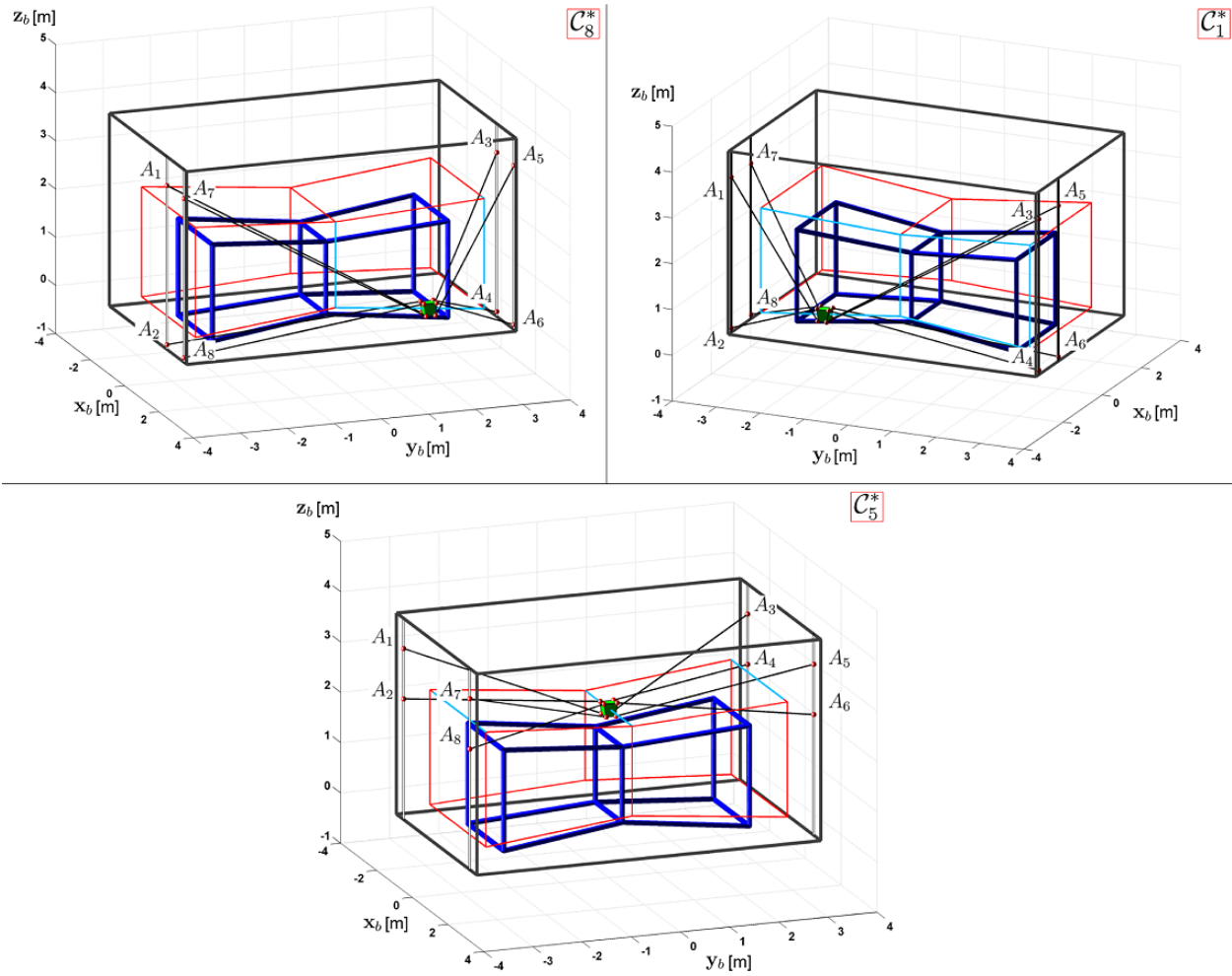
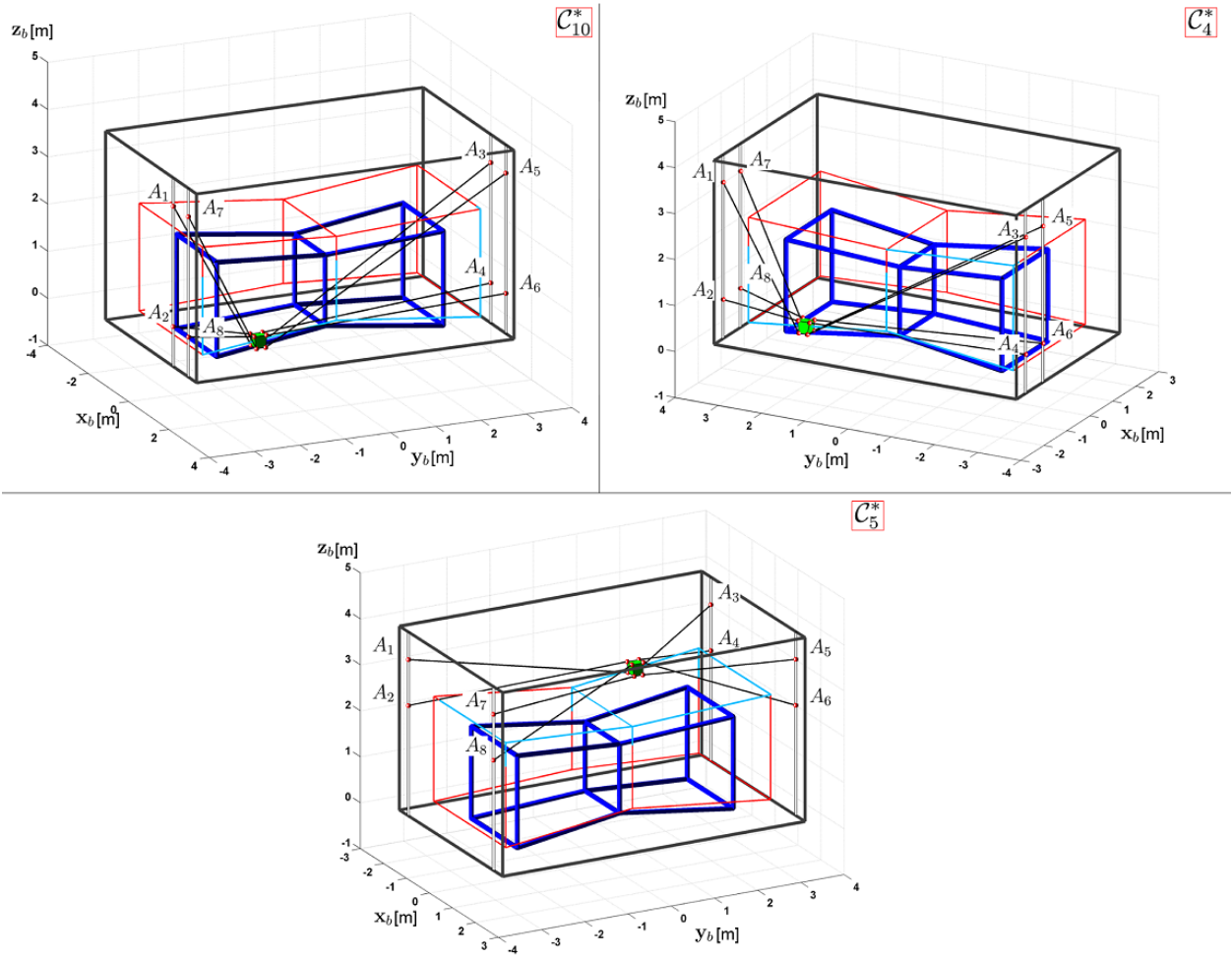


Fig. 5.22 – Case Study II: Configurations  $C_1^*$ ,  $C_5^*$  and  $C_8^*$ , composing the optimal reconfiguration planning with respect to cost function  $\mu_3$



**Fig. 5.23** – Configurations  $\mathcal{C}_4^*$ ,  $\mathcal{C}_5^*$  and  $\mathcal{C}_{10}^*$ , composing the optimal reconfiguration planning with respect to cost function  $\mu_5$

taking part to the optimal solutions are  $\mathcal{C}_4^*$ ,  $\mathcal{C}_5^*$  and  $\mathcal{C}_{10}^*$ . The optimal reconfiguration planning with respect to  $\mu_4$  requires the RCDPR to perform seven reconfigurations and displaces 42 exit points. The number of reconfigurations is equal to 10 when the cable tension variation (represented by  $\mu_5$ ) is optimised, and the number of exit point displacements is equal to 60. Figure 5.23 illustrates the optimal reconfiguration scheme of the RCDPR obtained for cost function  $\mu_5$ .

Figure 5.24 illustrates the parallel graph associated to the 832 quadruplets of dominant configurations that can be used to cover the whole prescribed path  $\mathcal{P}_{out}$ . The parallel graph of Fig. 5.24 is composed of 9 columns. The first four columns groups the configurations according to the segments of  $\mathcal{P}_{out}$  they are covering. These columns of the parallel graph let define the composition of the quadruplets: the first column defines which configuration,  $[\mathcal{C}_{bottom}] = \{\mathcal{C}_5, \dots, \mathcal{C}_{12}\}$ , is used to paint the lower part of the structure; the second and the third columns refer to the configurations used to paint the lateral sides of the structure,  $[\mathcal{C}_{right}] = \{\mathcal{C}_{13}, \mathcal{C}_{14}\}$  and  $[\mathcal{C}_{left}] = \{\mathcal{C}_{15}, \mathcal{C}_{16}\}$ ; the fourth column defines the configurations,  $[\mathcal{C}_{up}] = \{\mathcal{C}_{17}, \dots, \mathcal{C}_{42}\}$ , that can be used to paint the upper part of the tubular structure. The remaining five columns of the parallel graph represent the cost functions  $\mu_i$ ,  $i = 1, \dots, 5$ . The coloured lines in Fig. 5.24 describe the optimal reconfiguration schemes corresponding to the five objective

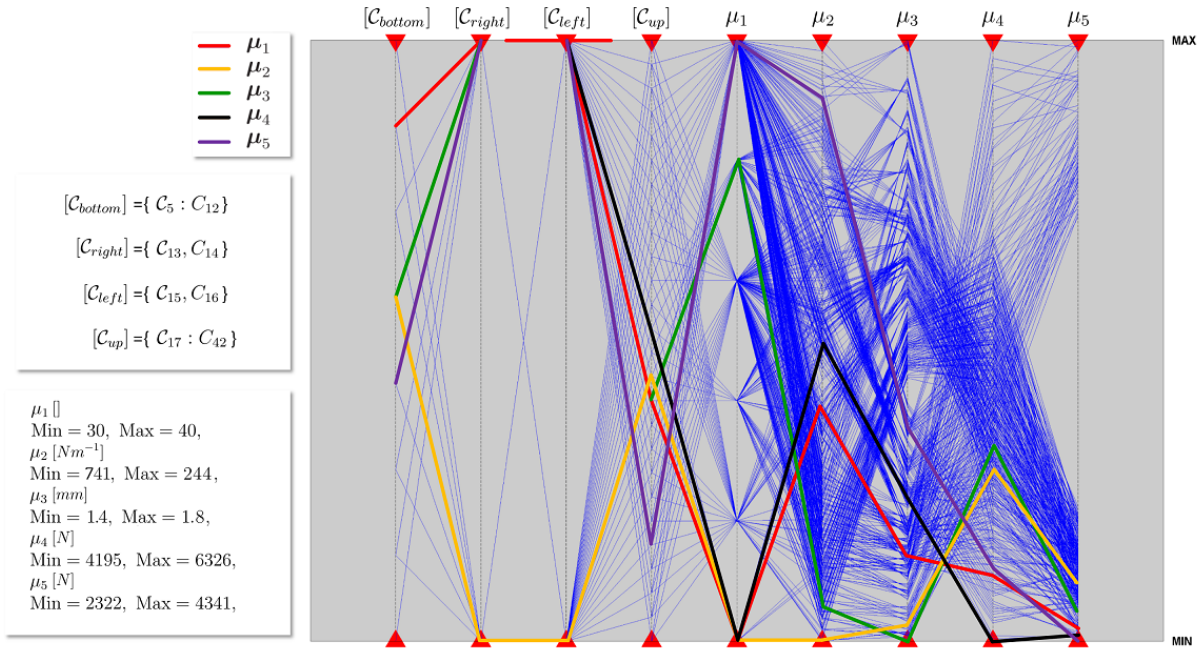


Fig. 5.24 – Case Study II: Parallel graph associated to the 832 quadruplets of dominant configurations

functions  $\mu_i$ ,  $i = 1, \dots, 5$ .

In addition, the parallel graph allows the user to select the quadruplets whose optimal solutions satisfy a set of requirements over all the five optimisation criteria. For instance, Fig. 5.25 illustrates the solutions for which the five criteria  $\mu_i$ ,  $i = 1, \dots, 5$  are lower than 30 % of their maximum value, respectively.

- According to the layout of configurations  $\mathcal{C}_i^*$ ,  $i = 1, \dots, 11$ , all the cables are crossing with each other. Crossing cable layouts provide better performance than non-crossing cable layouts. According to the layout description given in Sec. 5.2.2, the algorithm has been able to detect automatically the best layout for the RCDPR.
- The capacity margin, related to the cost function  $\mu_2$ , is strictly associated to the robot architecture (configuration).
- A high positioning error, characterised by the cost function  $\mu_3$ , is always associated to low cable tensions, and consequently to  $\mu_4$ . On the contrary, a low positioning error can be associated to both low and high cable tensions.
- The cost  $\mu_4$ , measuring the norm of the cable tension vector, is usually proportional to the cost  $\mu_5$ , measuring the standard variation of the cable tensions along the prescribed path.

### 5.4.3 Results for the Inner Faces of the Tubular Structure

According to Sec. 5.4.1, mixing the design parameters in  $[w]_1$ ,  $[w]_2$  and  $[w]_3$ ,  $n_{\mathcal{C}} = 810$  configurations are obtained. Performing the constraint analysis, a feasibility map has been built and simplified according to the configuration selection procedure described in Sec. 5.2.7. The thresholds  $h_1$  and  $h_2$  have been initialised with the same values used to compute the optimal reconfiguration strategy for the outer faces of the tubular structure.

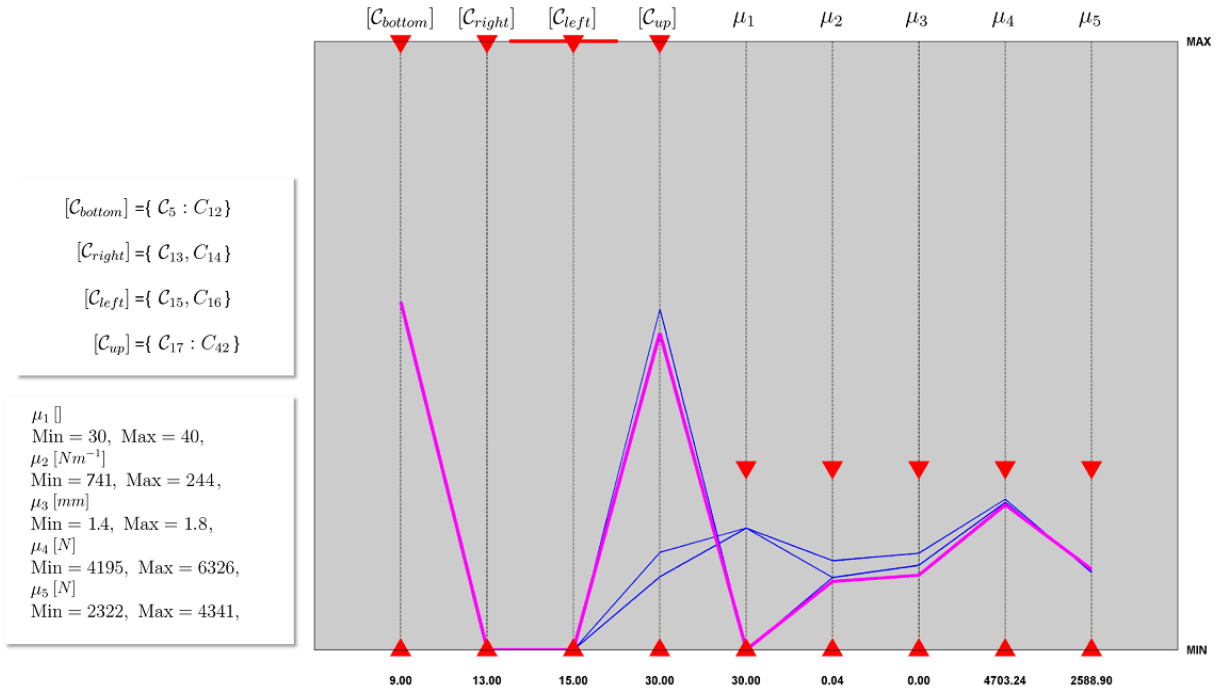


**Fig. 5.25** – Case Study II: Filtered parallel graph corresponding to cost functions lower than 30% of their maximum values

**Tab. 5.4** – Optimal configurations and the associated cost functions for the inner faces of the tubular structure. For each configuration, the optimal cost functions are surrounded by red boxes

Optimal Configurations	$\mu_2$ [N]	$\mu_3$ [ $\mu m$ ]	$\mu_4$ [N]	$\mu_5$ [N]
$w_1 = 0.75$ m, $w_2 = 2$ m, $w_3 = 1.25$ m (See Fig. 5.26)	526.31	157	841.99	365.67
$w_1 = 0.75$ m, $w_2 = 2$ m, $w_3 = 0.25$ m (See Fig. 5.27)	166.67	331	625.81	205.69

The analysis of the feasibility map leads to  $n_d = 14$  dominant configurations. Each of these configurations allows the moving platform to cover entirely the path  $\mathcal{P}_m$  without any reconfiguration of the robot. Hence, the task can be performed by selecting only one of the dominant configurations. Among those configurations, two of them lead to some optimal solutions.

The configuration whose design parameters  $w_1$ ,  $w_2$  and  $w_3$  are equal to 0.75 m, 2 m and 0.25 m, respectively, minimises the cost functions  $\mu_2$  and  $\mu_3$ , according to the values given in Table 5.4. According to this configuration, the RCDPR is fully constrained, as shown in Fig. 5.26. The cables of the RCDPR are crossing (but without any cable-cable collision), improving the RCDPR accuracy and stiffness.

The configuration whose design parameters  $w_1$ ,  $w_2$  and  $w_3$  are equal to 0.75 m, 2 m and 1.25 m, respectively, is shown in Fig. 5.27. The RCDPR is suspended above the prescribed path. Being suspended, the cable tensions are minimised. This configuration optimises the cost functions  $\mu_4$  and  $\mu_5$ . The optimal values are collected in Table 5.4<sup>1</sup>.

<sup>1</sup>The reader is referred to as the following link <http://www.irccyn.ec-nantes.fr/~caro/MMT/VideosMMTGCGG/TestInt.avi> to visualise the optimal reconfiguration planning associated to cost functions  $\mu_4$  and  $\mu_5$  to cover the inner faces of the tubular structure.

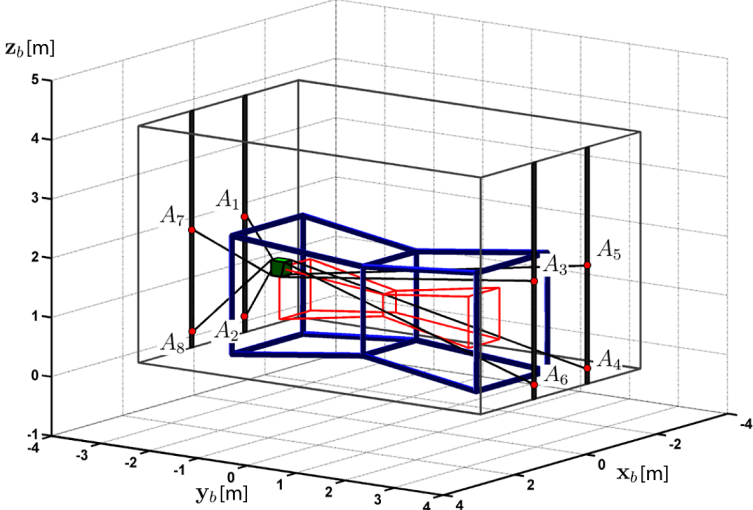


**Fig. 5.26** – Case Study II: RCDPR configuration, with  $w_1 = 0.75$  m,  $w_2 = 2$  m and  $w_3 = 0.25$  m, which optimises  $\mu_2$  and  $\mu_3$  for the inner prescribed path  $\mathcal{P}_{in}$

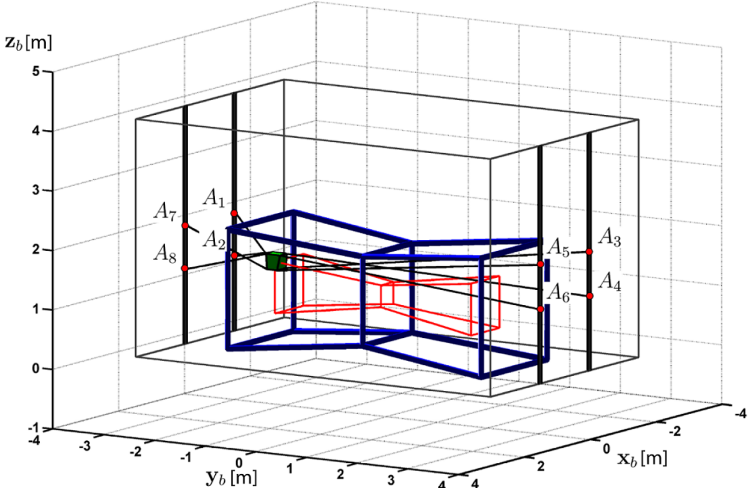


**Fig. 5.27** – Case Study II: RCDPR configuration, with  $w_1 = 0.75$  m,  $w_2 = 2$  m and  $w_3 = 1.25$  m, which optimises  $\mu_4$  and  $\mu_5$  for the inner prescribed path  $\mathcal{P}_{in}$

**Tab. 5.5** – Analysis of the computational time and number of operations for the second case study

Algorithm Step	Computational Time [s]	Nb of Operations	Complexity of Operations
Step III (RCDPR Configuration Set)	0.019	$\prod_{v=1}^{n_v} \varepsilon_v$	Low
Step VI (Feasibility Map)	142335	$\prod_{v=1}^{n_v} \varepsilon_v n_p$	High
Step VII (Configuration Selection)	10.61	Non Predictable	Medium
Step VIII (Graph Building)	492.64	$n_p n_\phi$	High
Step X (Dijkstra's Algorithm)	0.018	Non Predictable	Low

#### 5.4.4 Computational Time

The simulation has been performed on an Intel(R) Core(TM) i7-3630QM CPU @ 2.40 Ghz, with 8 GB of RAM. The results collected in Table 5.5 show that Step III (RCDPR Configuration Set) and Step X (Dijkstra's Algorithm), presented in Sec. 5.2, are performed in less than 0.02 s. On the contrary, Step VI (Feasibility Map), which involves the constraint analysis of a large number of configurations, required 39 hours of computation. Step VII (Configuration Selection) and Step VIII (Graph Building) required 10.1 s and 8.2 minutes of computation, respectively. The low computational effort required to perform Step VIII is due to the configuration selection performed at Step VII. Building the graph using the full set of configurations generated at Step III would require several days of intensive computation. The result would lead to such a wide graph that the analysis will be prohibitive.

### 5.5 Conclusions

This chapter dealt with RCDPRs discrete reconfiguration planning [GCG<sup>+</sup>15c, GCGG16, GGC<sup>+</sup>16b]. The considered task consists of low force operations, such as sandblasting and painting, in cluttered industrial environments and the RCDPR reconfigurability results from movable cable exit points. These exit points can be positioned at a possibly large but discrete set of possible locations. Means to select and optimise the sequence of discrete reconfigurations allowing the RCDPR moving platform to follow a prescribed path were introduced. A so-called feasibility map was first defined and generated. This map reflects the feasibility of all possible RCDPR configurations at all points of the discretised prescribed path, with respect to a set of constraints. In this chapter, the latter set included wrench-feasibility, cable collision, and pose error constraints. Then, the feasibility map is analysed and filtered in order to determine minimum sets of configurations, which allow the RCDPR to follow the whole prescribed path. Based on these minimum sets, a graph-based approach was proposed to solve the discrete reconfiguration planning problem by providing a reconfiguration sequence which is optimal with respect to one of several possible user-defined cost functions.

A planar case study has been used in order to validate the proposed reconfiguration strategy. The results show that the algorithm is able to compute the optimal solutions with respect to a set of configurations proposed by the user. The results have been extended to a three-dimensional case study, which consists in following a path covering the whole inner and outer parts a tubular structure. The results notably show that an optimal solution, which minimises the number of required RCDPR reconfigurations, can be found.

The proposed discrete reconfiguration planning method may require further improvements, notably in order to reduce the computational time of the constraint analysis (feasibility map). As part of our future work, heuristic

approaches will be considered. Indeed, with such approaches, it is presumably possible to obtain solutions to the discrete reconfiguration problem without analysing all the constraints of all the possible configurations. Such solutions would not be optimal as the ones considered in this chapter but should be much faster to compute.



# Chapter 6

## Conclusions and Perspectives

### Chapter Content

6.1 General Conclusions . . . . .	123
6.2 Perspectives . . . . .	125

### 6.1 General Conclusions

During the last decades, several research studies have been performed in the field of *Cable-Driven Parallel Robots* (CDPRs). CDPRs provide several advantages, including a wide workspace and a high payload to weight ratio. However, when the working environment is cluttered, CDPR cannot be used to accomplish complicated tasks. Under these circumstances, it may be necessary to use *Reconfigurable Cable-Driven Parallel Robots* (RCDPRs). The geometric parameters of RCDPRs can be modified in order to avoid the obstacles contained in the working environment and improve the RCDPR performances.

The research work presented in this manuscript is mainly related to the development of a design and a reconfiguration strategy for RCDPR whose exit points can be displaced on a large discrete set of locations.

#### 6.1.1 Modelling

In order to define a design and a reconfiguration strategy for RCDPRs, it is necessary to describe the static, kinematic, and dynamic behaviour of such RCDPRs by means of mathematical models. Some models have been presented in Chap. 2. Most of these models, e.g. the geometric, kinematic and dynamic models, consider the cables as linear segments. When the mass of the cables is not negligible, cables have been described by means of the sagging model. The sagging cable model has been used uniquely to define the quasi-static model of the RCDPRs.

Despite the previous models are well known in the literature, the elasto-static models of CDPRs and RCDPRs require further improvements. The elasto-static model can be used to analyse the displacement of the moving platform due to the non-rigid nature of the cables or the compliance of moving platform. The analysis is usually performed while observing the stiffness matrix of the RCDPR. In this manuscript, the stiffness matrix of CDPRs

and RCDPRs with linear non-rigid cables and pulleys has been expressed, by developing the model using a different formalism with respect to the ones proposed in the literature. By using a similar approach, the stiffness matrix of RCDPRs with sagging cables has been analysed. While in the literature the active stiffness component of the stiffness matrix is usually neglected, both the active and passive stiffness matrices have been taken into account in the proposed model. The model has been computed by differentiating the external wrench acting on the moving platform with respect to the pose of the moving platform.

### 6.1.2 Workspace Analysis

Designing a RCDPR requires the computation and the analysis of the RCDPR capabilities, including the size and the shape of its workspace. In Chap. 3, the workspace of a RCDPR is computed by verifying the poses of the moving platform where the cables are able to assure the static or dynamic equilibrium of the moving platform. A mathematical description of the workspaces appearing in the literature has been provided, including: the *Wrench Feasible Workspace* (WFW), the *Dynamic Feasible Workspace* (DFW), the *Static Feasible Workspace* (SFW), the *Interference Free Workspace* (IFW), and the *Collision Free Workspace* (CFW). Thus, two novel workspace have been defined: the *Twist Feasible Workspace* (TFW) [GCG15a], and the *Improved Dynamic Feasible Workspace* (IDFW) [GGC16a].

The TFW has been defined as the set of twist feasible poses of the moving platform *Centre of Mass* (CoM). A pose is *twist feasible* if the CDPR is able to provide a given set of twists to the moving platform, while considering the torque and the power limitations of the actuators and the winches. From a mathematical point of view, the bounds of this workspace can be represented by a system of linear equations, similarly to the WFW. The bounds have been computed according to the shifting hyperplanes method.

The DFW is defined in the literature as the set of dynamic feasible poses of the moving platform CoM. A pose is dynamic feasible if the cables are able to transmit on the platform the tensions required to displace the moving platform within a given range of accelerations. In the literature, the DFW contemplates only the inertia of the moving platform, while neglecting the external wrenches applied on the moving platform and the Coriolis forces. In this manuscript, the following components are accounted for the IDFW: the external wrench acting on the moving platform, the weight of the moving platform, the inertia of the moving platform, Coriolis and centrifugal forces of the moving platform. Coriolis and centrifugal forces have been considered as constant in order to preserve the linear form of the dynamic equations. The bounds of the IDFW are obtained according to the shifting hyperplanes method.

### 6.1.3 Design of CDPRs and RCDPRs

The design of CDPRs has been formulated as an optimisation problem, aiming at optimising one or more objective function(s) [GCG<sup>+</sup>14]. Several objective functions have been presented in this manuscript, including: the maximisation of the workspace size and the maximisation of the *Minimum Degree of Dynamic Constraint Satisfaction* (MDoDCS). The solutions have been computed while considering a set of user-defined constraints over the CDPR workspaces and performances. The most significant constraints have been described in Chap. 4, including: wrench, twist and dynamic feasibility, cable interferences, and collisions between cables and the environment. A case study has been illustrated in order to validate the efficacy of the proposed design problem.

When the task to be performed is complicated, and the working environment is cluttered, CDPRs may not be able to accomplish the task. A solution may be provided by RCDPRs. This manuscript mainly focuses on discrete

RCDPRs, where the reconfiguration of cable exit points, defined as the connection points of the cables on the fixed base of the RCDPR, is performed by attaching and detaching the cables on a predefined grid of locations.

A novel design strategy for discrete RCDPRs has been proposed [GCG<sup>+</sup>15b]. This design strategy assumes that the number of configurations necessary to complete the task can be fixed by the designer according to his/her experience. The prescribed path, or the prescribed workspace, are divided into several parts. Each part has to be covered by one and only one configuration. The configurations are computed by means of an optimisation algorithm, which optimises one or more global objective function(s) while satisfying a set of user-defined constraints. A case study has been proposed in order to validate the RCDPR design strategy. A RCDPR has to paint and sandblast a tubular structure. The design strategy provided several optimal solutions to the case study, minimising hierarchically the number of exit point displacements, the size of the RCDPR and the moving platform displacement due to the non-rigid nature of the cables. The computation of the optimal solution, performed on a Intel® Core™ i7-3630QM 2.40 GHz, required 19 hours of computation. More complicated tasks may require high computational efforts.

#### 6.1.4 Reconfiguration Strategy for discrete RCDPRs

When the working environment is complex, and it is not possible to predict the number of configurations needed to complete the tasks, a reconfiguration strategy is necessary to define the optimal placements of the RCDPR exit points [GCG<sup>+</sup>15c, GCGG16, GGC<sup>+</sup>16b].

In this manuscript, we proposed an optimal reconfiguration strategy for optimising and selecting the sequence of discrete reconfigurations allowing the RCDPR moving platform to follow a prescribed path. The exit points can be positioned at a possibly large but discrete set of possible locations. A so-called feasibility map was first defined and generated. This map reflects the feasibility of all possible RCDPR configurations at all points of the discretised prescribed path, with respect to a set of constraints, including: wrench-feasibility, cable collision, and pose error constraints. Then, the feasibility map is analysed and filtered out in order to determine the minimum sets of configurations, which allow the RCDPR to follow the whole prescribed path. Based on these minimum sets, a graph-based approach was proposed to solve the discrete reconfiguration planning problem by providing a reconfiguration sequence, which is optimal with respect to one of several possible user-defined cost functions.

Two case studies have been proposed: (i) a planar case study, which validates the proposed reconfiguration strategy and whose results show that the algorithm is able to compute the optimal solutions with respect to a set of configurations proposed by the user; (ii) a three-dimensional case study, which consists in following a path covering the whole inner and outer parts a tubular structure. The results notably show that an optimal solution, which minimises the number of required RCDPR reconfigurations, can be found.

## 6.2 Perspectives

This manuscript focuses on the modelling, design and reconfiguration of *Reconfigurable Cable-Driven Parallel Robots* (RCDPRs). Tools for the elasto-static, kinematic and dynamic modelling of RCDPRs have been provided. These tools have been used in order to analyse the characteristics of RCDPRs, including their workspace. A reconfiguration strategy for discrete RCDPRs has been provided. Based on the previous discussions and developments, summarised in Sec. 6.1, some perspectives for future work are proposed hereafter.

### 6.2.1 Modelling

The elasto-static models introduced in Chap. 2 are based on the linear and the sagging models of cables. While most of the elasto-static models in the literature neglect the effects of the active stiffness matrix, the contribution of this component on the CDPR stiffness may be relevant according to the external wrenches applied on the moving platform. A detailed analysis of the effect of the active stiffness matrix onto the stiffness of the CDPR should be performed. This analysis should define the CDPR layouts and the working conditions for which the active stiffness matrix is not negligible with respect to the passive stiffness matrix. The analysis should also take into account the pulleys in the proposed sagging cable stiffness model described in Sec. 2.3.3. Finally, more efficient numerical approaches may be investigated in order to reduce the computational time required to compute the elasto-static model. Finally, the obtained elasto-static model should be validated experimentally and should be efficient from a practical viewpoint.

### 6.2.2 Workspace Analysis

The workspace of CDPRs and RCDPRs can be analysed according to several criteria, e.g. the static, kinematic and dynamic behaviour of the moving platform. Chapter 3 describes some relevant workspaces, including: the *Static Feasible Workspace* (SFW), the *Wrench Feasible Workspace* (WFW) and the *Dynamic Feasible Workspace* (DFW). Two workspaces have been introduced in this thesis: the *Twist Feasible Workspace* (TFW) and the *Improved Dynamic Feasible Workspace* (IDFW). According to the working conditions of the CDPR, its workspace may be defined as the intersection of the proposed workspaces. A formal definition of the generalised CDPR workspaces should be defined. A *Global Minimum Degree of Constraint Satisfaction* (GMDoCS) should be associated to this workspace, proving a comprehensive tool quantifying the workspace capabilities of a CDPR.

### 6.2.3 Reconfiguration of the Cable Connection Points on the Moving Platform

Several components of a RCDPR may be reconfigured. This manuscript focused on the reconfiguration of cable exit points. However, the layout and the geometry of a RCDPR can be reconfigured by displacing the cable connection points on the moving platform.

Changes in the location of the cable connection points may introduce several advantages, e.g. the increase of the RCDPR workspace size. The influence of positions of the cable connection points onto the workspace of the RCDPR should be analysed. Eventually, a reconfiguration strategy of the cable connection points on the moving platform should be developed.

### 6.2.4 Routing of the Cables

The cables that connect the winches to the moving platform are oriented into the workspace by means of passive pulleys located on the exit points. The displacement of the exit points of a RCDPR amounts to the displacement of the pulleys installed at the exit point locations. According to the complexity of the RCDPR, and the grid of possible exit point locations, cables may be routed to the exit points by means of supplementary passive pulleys, as shown in Fig. 6.1. Some of these pulleys may be fixed to the base of the RCDPR while the remaining pulleys can be displaced.

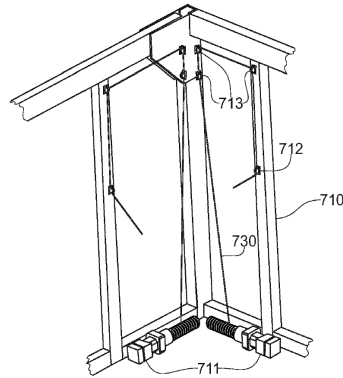


**Fig. 6.1** – Example of cable routing for a RCDPR, described in the European Patent EP2982483 (A2) [GGC+16b]. This design has been developed in the framework of the *IRT Jules Verne* (IRT JV) CAROCA project

Accordingly, a strategy to determine the optimal routing of the cables should be developed. This strategy should guarantee the possibility to displace the passive pulleys of the RCDPR without producing any interference between the cables. The number of required pulleys to guide the cables should be minimised and their displacement should be simplified, reducing the complexity of the RCDPR. The passive pulleys may have one, two or three degree(s) of freedom.

### 6.2.5 Macro-micro RCDPRs and Control Laws

According to the task specification, the RCDPR may consist of a macro-micro system. The micro system, such as a robotic arm, may be embarked onto the platform of the RCDPR. In that case, the robotic arm transfers an external wrench onto the moving platform. This wrench is generated by the motion of the robotic arm and the action performed by its end-effector. According to this context, the stability of the mobile platform can be influenced by the micro system. Furthermore, the micro system could also induce vibrations on the mobile platform.

Further research works should be dedicated to the analysis of the influence of such a macro-micro system onto the moving-platform of the RCDPR. A design strategy and a control strategy should be developed specifically for this kind of systems. The design and control strategies should aim at compensating the potential vibrations induced by both the micro and macro systems. The control strategy should integrate the trajectory planning. The trajectory planning has to prevent any interference between the cables. Furthermore, it should coordinate and optimise the motion of the micro and macro systems.



# Bibliography

- [ABAASV11] A. Alikhani, S. Behzadipour, A. Alasty, and S. Ali Sadough Vanini. Design of a large-scale cable-driven robot with translational motion. *Robotics and Computer-Integrated Manufacturing*, 27:357–366, July 2011.
- [ABB] ABB [Online]. Available: <http://www.abb.com/>.
- [ABD92] J. Albus, R. Bostelman, and N. Dagalakis. The NIST spider, a robot crane. *J. of Research of the Nat. Inst. of Standards and Technology*, 97(3):373–385, July 1992.
- [ABJ03] J. Albus, R. Bostelman, and A. Jacoff. Modular suspended manipulator, May 2003.
- [AC12] K. Azizian and P. Cardou. The dimensional synthesis of planar parallel cable-driven mechanisms through convex relaxations. *ASME J. of Mechanisms and Robotics*, 4(3), July 2012.
- [AC13] K. Azizian and P. Cardou. The dimensional synthesis of spatial cable-driven parallel mechanisms. *ASME J. of Mechanisms and Robotics*, 5(4), Sept. 2013.
- [AC15] G. Abbasnejad and M. Carricato. Direct geometrico-static problem of underconstrained cable-driven parallel robots with  $n$  cables. *IEEE Trans. on Robotics*, 31(2):468–478, Apr. 2015.
- [Ars10] M. Arsenault. Optimization of the prestress stable wrench closure workspace of planar parallel three-degree-of-freedom cable-driven mechanisms with four cables. In *Proc. of the IEEE Int. Conf. on Robotics and Automation (ICRA 2010)*, pages 1182–1187, Anchorage, AK, May 2010.
- [Ars13] M. Arsenault. Workspace and stiffness analysis of a three-degree-of-freedom spatial cable-suspended parallel mechanism while considering cable mass. *Mechanism and Machine Theory*, 66:1–13, Aug. 2013.
- [BADJ94] R. Bostelman, J. Albus, N. Dagalakis, and A. Jacoff. Applications of the NIST RoboCrane. In *Proc. of the 5th Int. Symp. on Robotics and Manufacturing*, Maui, HI, Aug. 1994.
- [BBGA07] S. Briot, C. Baradat, S. Guegan, and V.A. Arakelian. Contribution to the mechanical behavior improvement of the robotic navigation device surgiscope. In *Proc. of the ASME Int. Design Eng. Tech. Conf. & Comput. and Inform. in Eng. Conf. (IDETC/CIE 2007)*, pages 653–661, Las Vegas, NV, Sept. 2007.
- [BEM<sup>+</sup>97] C. Bonivento, A. Eusebi, C. Melchiorri, M. Montanari, and G. Vassura. Wireman: A portable wire manipulator for touch-rendering of bas-relief virtual surfaces. In *Proc. of the IEEE Int. Conf. on Robotics and Automation (ICRA 1997)*, pages 13–18, Monterey, CA, July 1997.
- [BG05] G. Barrette and C.M. Gosselin. Determination of the dynamic workspace of cable-driven planar parallel mechanisms. *ASME J. of Mech. Design*, 127(2):242–248, 2005.
- [BG07] S. Bouchard and C.M. Gosselin. Workspace optimization of a very large cable-driven parallel mechanism for a radiotelescope application. In *Proc. of the ASME Int. Design Eng. Tech. Conf. & Comput. and Inform. in Eng. Conf. (IDETC/CIE 2007)*, pages 963–970, Las Vegas, NV, Sept. 2007.
- [BGM08] S. Bouchard, C. M. Gosselin, and B. Moore. On the ability of a cable-driven robot to generate a prescribed set of wrenches. In *Proc. of the ASME Int. Design Eng. Tech. Conf. & Comput. and Inform. in Eng. Conf. (IDETC/CIE 2008)*, pages 47–58, Brooklyn, NY, Aug. 2008.

- [BJP<sup>+</sup>00] R. Bostelman, A. Jacoff, F. Proctor, T. Kramer, and A. Wavering. Cable-based reconfigurable machines for large scale manufacturing. In *Proc. of the 2000 Japan-USA Symp. on Flexible Automation*, Ann Arbor, MI, July 2000.
- [BJS<sup>+</sup>09] P.H. Borgstrm, B.L. Jordan, G.S Sukhatme, M.A. Batalin, and W.J Kaiser. Rapid computation of optimally safe tension distributions for parallel cable-driven robots. *IEEE Trans. on Robotics*, 25(6):1271–1281, Dec. 2009.
- [BK05a] S. Behzadipour and A. Khajepour. A new cable-based parallel robot with three dof. *J. of Multibody Syst. Dynamics*, 13(4):371–383, May 2005.
- [BK05b] S. Behzadipour and A. Khajepour. Stiffness of cable-based parallel manipulators with application to stability analysis. *ASME J. of Mech. Design*, 128(1):303–310, Apr. 2005.
- [Bla15] L. Blanchet. *Contribution à la modélisation de robots à câbles pour leur commande et leur conception*. PhD thesis, Université de Nice Sophia-Antipolis, Mai 2015.
- [BMB<sup>+</sup>09a] T. Bruckmann, L. Mikelsons, T. Brandt, M. Hiller, and D. Schramm. Design approaches for wire robots. In *Proc. of the ASME Int. Design Eng. Tech. Conf. & Comput. and Inform. in Eng. Conf. (IDETC/CIE 2009)*, pages 25–34, San Diego, CA, Aug. 2009.
- [BMB<sup>+</sup>09b] T. Bruckmann, L. Mikelsons, T. Brandt, M. Hiller, D. Schramm, A. Pott, and M. Abdel-Maskoud. A novel tensed mechanism for simulation of maneuvers in wind tunnels. In *Proc. of the ASME Int. Design Eng. Tech. Conf. & Comput. and Inform. in Eng. Conf. (IDETC/CIE 2009)*, pages 17–24, San Diego, CA, Aug. 2009.
- [BMC13] A. Berti, J.-P. Merlet, and M. Carricato. Solving the direct geometrico-static problem of 3-3 cable-driven parallel robots by interval analysis: Preliminary results. In *Cable-Driven Parallel Robots*, volume 12 of *Mechanisms and Machine Science*, pages 251–268. Springer, 2013.
- [BMC15] A. Berti, J.-P. Merlet, and M. Carricato. Workspace analysis of redundant cable-suspended parallel robots. In *Cable-Driven Parallel Robots*, volume 32 of *Mechanisms and Machine Science*, pages 41–53. Springer, 2015.
- [BMC16] A. Berti, J.-P. Merlet, and M. Carricato. Solving the direct geometrico-static problem of underconstrained cable-driven parallel robots by interval analysis. *Int. J. of Robotics Research*, 35(6):723–739, 2016.
- [BMHS07] T. Bruckmann, L. Mikelsons, M. Hiller, and D. Schramm. A new force calculation algorithm for tendon-based parallel manipulators. In *Proc. of the IEEE/ASME Int. Conf. on Advanced Intelligent Mechatronics (AIM 2007)*, pages 1–6, Zurich, Switzerland, Sept. 2007.
- [BR15] M. Beck and S. Robins. *Computing the Continuous Discretely*, chapter Zonotopes. Springer, 2015.
- [BREU06] P. Bosscher, A.T. Riechel, and I. Ebert-Uphoff. Wrench-feasible workspace generation for cable-driven robots. *IEEE Trans. on Robotics*, 22(5):890–902, Oct. 2006.
- [Bru10] T. Bruckmann. *Auslegung und Betrieb redundanter paralleler Seilroboter*. PhD thesis, Universität Duisburg-Essen, Sept. 2010.
- [BWT05] P. Bosscher, R.L. Williams, and M. Tummino. A concept for rapidly-deployable cable robot search and rescue systems. In *Proc. of the ASME Int. Design Eng. Tech. Conf. & Comput. and Inform. in Eng. Conf. (IDETC/CIE 2005)*, pages 589–598, Long Beach, CA, Sept. 2005.
- [CA13] M. Carricato and G. Abbasnejad. Direct geometrico-static analysis of under-constrained cable-driven parallel robots with 4 cables. In *Cable-Driven Parallel Robots*, volume 12 of *Mechanisms and Machine Science*, pages 269–285. Springer, 2013.
- [Caba] CableBOT [Online]. Available: <http://www.cablebot.eu/en/>.
- [Cabb] Cablecam [Online]. Available: [www.cablecam.com](http://www.cablecam.com).
- [Cap67] K.L. Cappel. Motion simulator, Jan. 1967.

- [Car13] M. Carricato. Direct geometrico-static problem of underconstrained cable-driven parallel robots with three cables. *ASME J. of Mechanisms and Robotics*, 5(3), June 2013.
- [CC13] J.-F. Collard and P. Cardou. Computing the lowest equilibrium pose of a cable-suspended rigid body. *Optimization and Engineering*, 14(3):457–476, Sept. 2013.
- [CCH14] S. Caro, D. Chablat, and Y. Hu. Algorithm for the actuation mode selection of the parallel manipulator NaVARo. In *Proc. of the ASME Int. Design Eng. Tech. Conf. & Comput. and Inform. in Eng. Conf. (IDETC/CIE 2014)*, volume 5B, Buffalo, NY, Aug. 2014.
- [CE90] R. Clavel and Ecublens. Device for the movement and positioning of an element in space, Dec. 1990.
- [CM13] M. Carricato and J.-P. Merlet. Stability analysis of underconstrained cable-driven parallel robots. *IEEE Trans. on Robotics*, 29(1), Feb. 2013.
- [CRCCG15] A. Cruz Ruiz, S. Caro, P. Cardou, and F. Guay. Arachnis : Analysis of robots actuated by cables with handy and neat interface software. In *Cable-Driven Parallel Robots*, volume 32 of *Mechanisms and Machine Science*, pages 293–305. Springer, 2015.
- [CW03] D. Chablat and P. Wenger. Architecture optimization of a 3-dof translational parallel mechanism for machining applications, the orthoglide. *IEEE Tans. on Robotics and Automation*, 19(3):403–410, June 2003.
- [DDB13] J. Du, W. Ding, and H. Bao. Cable vibration analysis for large workspace cable-driven parallel manipulators. In *Cable-Driven Parallel Robots*, volume 12 of *Mechanisms and Machine Science*, pages 437–449. Springer, 2013.
- [DGAD12] T. Dallej, M. Gouttefarde, N. Andreff, and R. Dahmouche. Vision-based modeling and control of large-dimension cable-driven parallel robots. In *Proc. of the IEEE/RSJ Int. Conf. on Intelligent Robots and Syst. (IROS 2012)*, pages 1581–1586, Vilamoura, Portugal, Oct. 2012.
- [Dik59] E.W. Dijkstra. A note on two problems in connection with graphs. *Numerische Mathematik*, 1(1):269–271, 1959.
- [DLP<sup>+</sup>07] J.-D. Deschenes, P. Lambert, D. Perrault, N. Martel-Brisson, N. Zoso, A. Zaccarin, P. Herbert, S. Bouchard, and C. Gosselin. A cable-driven parallel mechanism for capturing object appearance from multiple viewpoints. In *6th Int. Conf. on 3-D Digital Imaging and Modeling*, Montréal, QC, Aug. 2007.
- [DM09] X. Diao and O. Ma. Vibration analysis of cable-driven parallel manipulators. *Multibody System Dynamics*, 21(4):347–460, 2009.
- [DPL07] L. Dominjon, L. Perret, and A. Lécuyer. Novel devices and interaction techniques for human-scale haptics. *The Visual Computer*, 23(4):257–266, Apr. 2007.
- [DQZZ09] B.Y. Duan, Y.Y. Qiu, F.S. Zhang, and B. Zi. On design and experiment of the feed cable-suspended structure for super antenna. *Mechatronics*, 19(4):503–509, June 2009.
- [Dua99] B.Y. Duan. A new design project of the line feed structure for large spherical radio telescope and its nonlinear dynamic analysis. *Mechatronics*, 9(1):53–64, Feb. 1999.
- [EGGC15] G. El-Ghazaly, M. Gouttefarde, and V. Creuze. Hybrid cable-thruster actuated underwater vehicle-manipulator systems: A study on force capabilities. In *Proc. of the IEEE/RSJ Int. Conf. on Intelligent Robots and Syst. (IROS 2015)*, Hamburg, Germany, Sept. 2015.
- [EGL95] H.A. Eiselt, Michel Gendreau, and Gilbert Laporte. Arc routing problems, Part I: The chinese postman problem. *Operational Research*, 43(2):231–242, 1995.
- [EUV04] I. Ebert-Uphoff and P.A. Voglewede. On the connections between cable-driven robots, parallel robots and grasping. In *Proc. of the IEEE Int. Conf. on Robotics and Automation (ICRA 2004)*, volume 5, pages 4521–4526, New Orleans, LA, Apr. 2004.

- [FCCG14] A. Fortin-Coté, P. Cardou, and C. Gosselin. An admittance control scheme for haptic interfaces based on cable-driven parallel mechanisms. In *Proc. of the IEEE Int. Conf. on Robotics and Automation (ICRA 2014)*, pages 819–925, Hong Kong, May 2014.
- [FFT<sup>+</sup>04] S. Fang, D. Franitza, M. Torlo, F. Bekes, and M. Hiller. Motion control of a tendon-based parallel manipulator using optimal tension distribution. *IEEE/ASME Trans. on Mechatronics*, 9(3):561–568, Sept. 2004.
- [FMKK11] J. Fink, N. Michael, S. Kim, and V. Kumar. Planning and control for cooperative manipulation and transportation with aerial robots. In *Robotics Research*, volume 70 of *Springer Tracts in Advanced Robotics*, pages 643–659. Springer, 2011.
- [Fou] Four Cable Drawing Machine by D. Bynoe [Online]. Available: <http://dbynoe.blogspot.fr/>.
- [GCC14] F. Guay, P. Cardou, A.L. Cruz, and S. Caro. Measuring how well a structure supports varying external wrenches. In *New Advances in Mechanisms, Transmissions and Applications*, volume 17 of *Mechanisms and Machine Science*, pages 385–392. Springer, 2014.
- [GCG<sup>+</sup>14] L. Gagliardini, S. Caro, M. Gouttefarde, P. Wenger, and A. Girin. Optimal design of cable-driven parallel robots for large industrial structures. In *Proc. of the IEEE Int. Conf. on Robotics and Automation (ICRA 2014)*, pages 5744–5749, Hong Kong, China, May 2014.
- [GCG15a] L. Gagliardini, S. Caro, and M. Gouttefarde. Dimensioning of cable-driven parallel robot actuators, gear head and winches according to the twist feasible workspace. In *Proc. of the IEEE Int. Conf. on Automation Science and Engineering (CASE 2015)*, pages 99–105, Gothenburg, Sweden, Aug. 2015.
- [GCG<sup>+</sup>15b] L. Gagliardini, S. Caro, M. Gouttefarde, P. Wenger, and A. Girin. A reconfigurable cable-driven parallel robot for sandblasting and painting of large structures. In *Cable-Driven Parallel Robots*, volume 32 of *Mechanisms and Machine Science*, pages 275–291. Springer, 2015.
- [GCG<sup>+</sup>15c] L. Gagliardini, S. Caro, M. Gouttefarde, P. Wenger, and A. Girin. A reconfiguration strategy for reconfigurable cable-driven parallel robots. In *Proc. of the IEEE Int. Conf. on Robotics and Automation (ICRA 2015)*, pages 1613–1620, Seattle, WA, May 2015.
- [GCGG16] L. Gagliardini, S. Caro, M. Gouttefarde, and A. Girin. Discrete reconfiguration planning for cable-driven parallel robots. *Mechanism and Machine Theory*, 100:313–337, 2016.
- [GCRB12] M. Gouttefarde, J.-F. Collard, N. Riehl, and C. Baradat. Simplified static analysis of large-dimension parallel cable-driven robots. In *Proc. of the IEEE Int. Conf. on Robotics and Automation (ICRA 2012)*, pages 2299–2305, Saint Paul, MN, May 2012.
- [GCRB15] M. Gouttefarde, J.-F. Collard, N. Riehl, and C. Baradat. Geometry selection of a redundantly actuated cable-suspended parallel robot. *IEEE Trans. on Robotics*, 31(2):501–510, Feb. 2015.
- [GDM11] M. Gouttefarde, D. Daney, and J.-P. Merlet. Interval-analysis-based determination of the wrench-feasible workspace of parallel cable-driven robots. *IEEE Trans. on Robotics*, 27(1):1–13, Feb. 2011.
- [GG04] M. Gouttefarde and C.M. Gosselin. On the properties and the determination of the wrench-closure workspace of planar parallel cable-driven mechanisms. In *Proc. of the ASME Int. Design Eng. Tech. Conf. & Comput. and Inform. in Eng. Conf. (IDETC/CIE 2004)*, pages 337–346, Salt Lake City, UT, Sept. 2004.
- [GG06] M. Gouttefarde and C.M. Gosselin. Analysis of the wrench-closure workspace of planar parallel cable-driven mechanisms. *IEEE Trans. on Robotics*, 22(3):434–445, June 2006.
- [GG11] C. Gosselin and M. Grenier. On the determination of the force distribution in overconstrained cable-driven parallel mechanisms. *Meccanica*, 46(1):3–15, 2011.
- [GGC16a] L. Gagliardini, M. Gouttefarde, and S. Caro. *Advances in Robot Kinematics*, chapter Determination of a Dynamic Feasible Workspace for Cable-Driven Parallel Robots. Springer, 2016.

- [GGC<sup>+</sup>16b] A. Girin, L. Gagliardini, S. Caro, M. Gouttefarde, and P. Yvan. European patent ep2982483 (a2), Feb. 2016.
- [GJC01] J.J. German, K. Jablokow, and D.J. Cannon. The cable array robot: theory and experiment. In *Proc. of the IEEE Int. Conf. on Robotics and Automation (ICRA 2001)*, volume 3, pages 2804–2810, Seoul, Korea, May 2001.
- [GK10] M. Gouttefarde and S. Krut. *Advances in Robot Kinematics*, chapter Characterization of parallel manipulator available wrench set facets, pages 475–484. Springer, 2010.
- [GKC<sup>+</sup>08] M. Gouttefarde, S. Krut, O. Company, F. Pierrot, and N. Ramdani. *Advances in Robot Kinematics*, chapter On the Design of Fully Constrained Parallel Cable-Driven Robots, pages 71–78. Springer, 2008.
- [GMP11] M. Gobbi, G. Mastinu, and G. Previati. A method for measuring the inertia properties of rigid bodies. *Mechanical Systems and Signal Processing (MSSP)*, 25:305–318, 2011.
- [GNB14] M. Gouttefarde, D.Q. Nguyen, and C. Baradat. *Advances in Robot Kinematics*, chapter Kinetostatic Analysis of Cable-Driven Parallel Robots with Consideration of Sagging and Pulleys, pages 213–221. Springer, 2014.
- [Gos13] C. Gosselin. Global planning of dynamically feasible trajectories for three-DOF spatial Cable-Suspended parallel robots. In *Cable-Driven Parallel Robots*, volume 12 of *Mechanisms and Machine Science*, pages 3–22. Springer, 2013.
- [GR02] P. Gallina and G. Rosati. Manipulability of a planar wire driven haptic device. *Mechanism and Machine Theory*, 37(2):215–228, Feb. 2002.
- [GRR01] P. Gallina, G. Rosati, and A. Rossi. 3-dof wire driven planar haptic interface. *J. of Intelligent and Robotic Syst.*, 32(1):23–36, Sept. 2001.
- [HA95] K. Homma and T. Arai. Design of an upper limb motion assist system with parallel mechanisms. In *Proc. of the IEEE Int. Conf. on Robotics and Automation (ICRA 1995)*, volume 2, pages 1302–1307, Nagoya, Japan, May 1995.
- [HC04] C.S. Holland and D.J. Cannon. Cable array robot for material handling, Nov. 2004.
- [Hek] Hektor [Online]. Available: <http://juerglehni.com/works/hektor>.
- [HK09] M. Hassan and A. Khajepour. Analysis of large-workspace cable-actuated manipulator for warehousing applications. In *Proc. of the ASME Int. Design Eng. Tech. Conf. & Comput. and Inform. in Eng. Conf. (IDETC/CIE 2009)*, pages 45–53, San Diego, CA, Aug. 2009.
- [HkMP15] W.Y. Ho, W. kraus, A. Mangold, and A. Pott. Haptic interaction with a cable-driven parallel robot using admittance control. In *Cable-Driven Parallel Robots*, volume 32 of *Mechanisms and Machine Science*, pages 201–212. Springer, 2015.
- [HS92] Y. Hirata and M. Sato. 3-dimensional interface device for virtual work space. In *Proc. of the IEEE Int. Conf. on Intelligent Robots and Syst. (IROS 1992)*, page 889–896, Raleigh, NC, July 1992.
- [IGCS13] J.-B Izard, C. Gouttefarde, Baradat, D. Culla, and D. Sallé. Integration of a parallel cable-driven robot on an existing building façade. In *Cable-Driven Parallel Robots*, volume 12 of *Mechanisms and Machine Science*, pages 149–164. Springer, 2013.
- [IGM<sup>+</sup>13] J.-B Izard, M. Gouttefarde, M. Michelin, O. Tempier, and C. Baradat. A reconfigurable robot for cable-driven parallel robotic research and industrial scenario proofing. In *Cable-Driven Parallel Robots*, volume 12 of *Mechanisms and Machine Science*, pages 135–148. Springer, 2013.
- [Int] Intelligent Surgical Instruments & Systems [Online]. Available: <http://www.isis-robotics.com/>.
- [Irv92] M. Irvine. *Cable structures*. Dover Publications, June 1992.
- [IS94] M. Ishii and M. Sato. A 3d spatial interface device using tensed strings. *Teleoperators and Virtual Environments - Presence*, 3(1):81–86, 1994.

- [JK13] Q. Jiang and V. Kumar. The inverse kinematics of cooperative transport with multiple aerial robots. *IEEE Trans. on Robotics*, 29(1):136–145, Feb. 2013.
- [KBT14] H. Khakpour, L. Birglen, and S.-A Tahan. Synthesis of differentially driven planar cable parallel manipulators. *IEEE Trans. on Robotics*, 30(3):619–630, Jan. 2014.
- [KCTP95] S. Kawamura, W. Choe, S. Tanaka, and S.R. Pandian. Development of an ultrahigh speed robot FALCON using wire driven system. In *Proc. of the IEEE Int. Conf. on Robotics and Automation (ICRA 1995)*, volume 1, pages 215–220, Nagoya, Japan, May 1995.
- [KJ75] W.P. Koevermans and C.J. Jansen. Design and performance of the four dof motion system of the nlr research flight simulator. In *Proc. of AGARD Conf. No 198*, pages 17–1/17–11, The Hague, Netherlands, Oct. 1975.
- [KKW00] S. Kamawura, H. Kino, and C. Won. High-speed manipulation by using parallel wire-driven robots. *Robotica*, 18(1):13–21, Jan. 2000.
- [Koz14] V. Kozlov. A graphical user interface for the design of cable-driven parallel robots. Master’s thesis, École Centrale de Nantes, Aug. 2014.
- [KZW06] K. Kozak, Qian Zhou, and Jinsong Wang. Static analysis of cable-driven manipulators with non-negligible cable mass. *IEEE Trans. on Robotics*, 22(3):425–433, June 2006.
- [Laf04] P. Lafourcade. *Etude des manipulateurs parallèles à câbles, conception d’une suspension active pour soufflerie*. PhD thesis, Thèse de Docteur Ingénieur ENSAE, 2004.
- [LCH04] R. Loureiro, C.F. Collin, and W. Harwin. Robot aided therapy: Challenges ahead for upper limb stroke rehabilitation. In *Proc. of the 5th Int. Conf. on Disability, Virtual Reality and Associated Technologies*, pages 33–39, Oxford, UK, 2004.
- [LG13] J. Lamaury and M. Gouttefarde. Control of a large redundantly actuated cable-suspended parallel robot. In *Proc. of the IEEE/RSJ Int. Conf. on Intelligent Robots and Syst. (IROS 2013)*, pages 4659–4664, Karlsruhe, Germany, May 2013.
- [LGCH13] J. Lamaury, M. Gouttefarde, A. Chemori, and P.-E. Herve. Dual-space adaptive control of redundantly actuated cable-driven parallel robots. In *Proc. of the IEEE Int. Conf. on Robotics and Automation (ICRA 2013)*, pages 4879–4886, Tokyo, Japan, Nov. 2013.
- [Li15] H. Li. On the static stiffness of incompletely restrained cable-driven robot. In *Cable-Driven Parallel Robots*, volume 32 of *Mechanisms and Machine Science*, pages 55–69. Springer, 2015.
- [LLR02] P. Lafourcade, M. Llibre, and C. Reboulet. Design of a parallel wire-driven manipulator for wind tunnels. In *Proc. of the Workshop on Fundamental Issues and Future Directions for Parallel Mechanisms and Manipulators*, pages 187–194, Quebec City, QC, Oct. 2002.
- [LNC07] C. Lambert, M. Nahon, and D. Chalmers. Implementation of an aerostat positioning system with cable control. *IEEE/ASME Trans. on Mechatronics*, 12(1):32–40, Feb. 2007.
- [Lum85] V.J. Lumelsky. On fast computation of distance between line segments. *Inform. Process. Lett.*, 21(3):55–61, Aug. 1985.
- [MA12] Y. Mao and S.K. Agrawal. Design of cable-driven arm exoskeleton (carex) for neural rehabilitation. *IEEE Trans. on Robotics*, 28(4):922–931, Aug. 2012.
- [MBHS08] L. Mikelsons, T. Bruckman, M. Hiller, and D. Schramm. A real-time capable force calculation algorithm for redundant tendon-based parallel manipulators. In *Proc. of the IEEE Int. Conf. on Robotics and Automation (ICRA 2008)*, pages 3869–3874, Pasadena, CA, May 2008.
- [MD05] O. Ma and X. Diao. Dynamics analysis of a cable-driven parallel manipulator for hardware-in-the-loop dynamic simulation. In *Proc. of the IEEE/ASME Int. Conf. on Advanced Intelligent Mechatronics (AIM 2005)*, pages 837–842, Monterey, CA, July 2005.

- [MD06] J.-P. Merlet and D. Daney. Legs interference checking of parallel robots over a given workspace or trajectory. In *Proc. of the IEEE Int. Conf. on Robotics and Automation (ICRA 2006)*, pages 757–762, Orlando, FL, May 2006.
- [MD10] J.-P. Merlet and D. Daney. A portable, modular parallel wire crane for rescue operations. In *Proc. of the IEEE Int. Conf. on Robotics and Automation (ICRA 2010)*, pages 2834–2839, Anchorage, AK, May 2010.
- [MDRC13] M. Manubens, D. Devaurs, L. Ros, and J. Cortés. Motion planning for 6-d manipulation with aerial towed-cable systems. In *Proceedings of Robotics: Science and Systems*, Berlin, Germany, June 2013.
- [Mer01] J.-P. Merlet. Micro parallel robot mips for medical applications. In *Proc. of the IEEE Int. Conf. on Emerging Technologies and Factory Automation (ETFA 2001)*, pages 611–619, Antibes-Juan les Pins, France, Oct. 2001.
- [Mer04] J.-P. Merlet. *Advances in Robot Kinematics*, chapter Analysis of the influence of wire interference on the workspace of wire robots, page 211–218. Springer, 2004.
- [Mer06] J.-P. Merlet. *Parallel Robots*. Springer, 2 edition, 2006.
- [Mer08] J.-P. Merlet. Kinematics of the wire-driven parallel robot marionet using linear actuators. In *Proc. of the IEEE Int. Conf. on Robotics and Automation (ICRA 2008)*, pages 3857–3862, Pasadena, CA, May 2008.
- [Mer15a] J.-P. Merlet. The kinematics of cable-driven parallel robots with sagging cables: preliminary results. In *Proc. of the IEEE Int. Conf. on Robotics and Automation (ICRA 2015)*, pages 1593–1598, Seattle, WA, May 2015.
- [Mer15b] J.-P. Merlet. On the inverse kinematics of cable-driven parallel robots with up to 6 sagging cables. In *Proc. of the IEEE Int. Conf. on Intelligent Robots and Syst. (IROS 2015)*, pages 4356–4361, Hamburg, Germany, Sept. 2015.
- [MI93] S. Mawamura and K. Ito. A new type of master robot for teleoperation using a radial wire drive system. In *Proc. of the IEEE/RSJ Int. Conf. on Intelligent Robots and Syst. (IROS 1993)*, volume 1, pages 55–60, Yokohama, Japan, July 1993.
- [MKK97] T. Morizono, K. Kurahashi, and S. Kawamura. Realization of a virtual sports training system with parallel wire mechanism. In *Proc. of the IEEE Int. Conf. on Robotics and Automation (ICRA 1997)*, pages 3025–3030, Albuquerque, NM, Apr. 1997.
- [MKK98] T. Morizono, K. Kurahashi, and S. Kawamura. Analysis and control of a force display system driven by parallel wire mechanism. *Robotica*, 16(5):551–563, Sept. 1998.
- [MRB15] K. Müller, C. Reichert, and T. Bruckmann. Analysis of a real-time capable force computation method. In *Cable-Driven Parallel Robots*, volume 32 of *Mechanisms and Machine Science*, pages 227–238. Springer, 2015.
- [MTT+99] K. Maeda, S. Tadokoro, T. Takamori, M. Hiller, and R. Verhoeven. On design of a redundant wire-driven parallel robot WARP manipulator. In *Proc. of the IEEE Int. Conf. on Robotics and Automation (ICRA 1999)*, volume 2, pages 895–900, Detroit, MI, May 1999.
- [NAD06] M. Nikkhah, H. Ashrafiuon, and E.J. Dougherty. Motion control and design of an aerial robotic system. In *Proc. of the ASME Int. Design Eng. Tech. Conf. & Comput. and Inform. in Eng. Conf. (IDETC/CIE 2008)*, pages 877–883, Philadelphia, PA, Sept. 2006.
- [NG13] D.-Q. Nguyen and M. Gouttefarde. On the simplifications of cable model in static analysis of large dimension cable-driven parallel robots. In *Proc. of the IEEE Int. Conf. on Intelligent Robots and Syst. (IROS 2013)*, pages 928–934, Tokyo, Japan, Nov. 2013.
- [NG14a] D.-Q. Nguyen and M. Gouttefarde. *Advances in Robot Kinematics*, chapter Stiffness Matrix of 6-DOF Cable-Driven Parallel Robots and Its Homogenization, pages 181–191. Springer, 2014.

- [NG14b] D.-Q. Nguyen and M. Gouttefarde. Study of reconfigurable suspended cable-driven parallel robots for airplane maintenance. In *Proc. of the IEEE Int. Conf. on Intelligent Robots and Syst. (IROS 2014)*, pages 1682–1689, Chicago, IL, Sept. 2014.
- [NGCP14] D.-Q. Nguyen, M. Gouttefarde, O. Company, and F. Pierrot. On the analysis of large-dimension reconfigurable suspended cable-driven parallel robots. In *Proc. of the IEEE Int. Conf. on Robotics and Automation (ICRA 2014)*, pages 5728–5735, Hong Kong, Mai 2014.
- [OA05] S.-R Oh and S.K. Agrawal. Cable suspended planar robots with redundant cables: Controllers with positive tensions. *IEEE Trans. on Robotics*, 21(3):457–465, June 2005.
- [OMDT<sup>+</sup>08] M.-D Otis, M. Mokhtari, C. Du Tremblay, D. Laurendeau, F.-M. De Rainville, and C. M. Gosselin. Hybrid control with multi-contact interactions for 6dof haptic foot platform on a cable-driven locomotion interface. In *IEEE Symp. on Haptics*, pages 161–168, Vancouver, Canada, Mar. 2008.
- [PBM09] A. Pott, T. Bruckmann, and L. Mikelsons. *Computational Kinematics*, chapter Closed-form force distribution for parallel wire robots, pages 25–34. Springer, 2009.
- [PCGO10] Simon Perreault, Philippe Cardou, Clément M. Gosselin, and Martin J.-D. Otis. Geometric determination of the interference-free-constant-orientation workspace of parallel cable-driven mechanisms. *ASME J. of Mechanisms and Robotics*, 2(3), July 2010.
- [PFAM04] J. Pusey, A. Fattah, S. Agrawal, and E. Messina. Design and workspace analysis of a 6-6 cable-suspended parallel robot. *Mechanism and Machine Theory*, 39(7):761–778, July 2004.
- [PG07] S. Perreault and C.M. Gosselin. Cable-driven parallel mechanism: Application to a locomotion interface. In *Proc. of the ASME Int. Design Eng. Tech. Conf. & Comput. and Inform. in Eng. Conf. (IDETC/CIE 2007)*, pages 791–799, Las Vegas, NV, Sept. 2007.
- [PMK<sup>+</sup>13] A. Pott, H. Mütherich, W. Kraus, V. Schmidt, P. Miermeister, and A. Verl. IPAnema: a family of cable-driven parallel robots for industrial applications. In *Cable-Driven Parallel Robots*, volume 12 of *Mechanisms and Machine Science*, pages 119–134. Springer, 2013.
- [PMV10] A. Pott, C. Meyer, and A. Verl. Large-scale assembly of solar power plants with parallel cable robots. In *Proc. of the Int. Symp. on Robotics and 6th German Conf. on Robotics (ISR/ROBOTIK 2010)*, pages 1–6, Munich, Germany, June 2010.
- [PRF90] F. Pierrot, C. Reynaud, and A. Fournier. Delta: a simple and efficient parallel robot. *Robotica*, 8(2):105–109, Apr. 1990.
- [Pro] Project ANR CoGiRo [Online]. Available: <http://www.lirmm.fr/cogiro/>.
- [RABG07] G. Rosati, M. Andreolli, A. Biondi, and P. Gallina. Performance of cable suspended robots for upper limb rehabilitation. In *Proc. of the IEEE 10th International Conference on Rehabilitation Robotics (ICORR 2007)*, pages 385–392, Noordwijk, Netherlands, June 2007.
- [RGBP10a] N. Riehl, M. Gouttefarde, C. Baradat, and F. Pierrot. On the determination of cable characteristics for large dimension cable-driven parallel mechanisms. In *Proc. of the IEEE Int. Conf. on Robotics and Automation (ICRA 2010)*, pages 4709–4714, Anchorage, AK, May 2010.
- [RGBP10b] N. Riehl, M. Gouttefarde, C. Baradat, and F. Pierrot. On the static workspace of large dimensions cable-suspended robots with non-negligible cable mass. In *Proc. of the ASME Int. Design Eng. Tech. Conf. & Comput. and Inform. in Eng. Conf. (IDETC/CIE 2010)*, pages 261–270, Montréal, QC, Aug. 2010.
- [RGK<sup>+</sup>09] N Riehl, M. Gouttefarde, S. Krut, C. Baradat, and F. Pierrot. Effects of non-negligible cable mass on the static behavior of large workspace cable-driven parallel mechanisms. In *Proc. of the IEEE Int. Conf. on Robotics and Automation (ICRA 2009)*, pages 2193–2198, Kobe, Japan, May 2009.
- [RGL98] R.G. Roberts, T. Graham, and T. Lippitt. On the inverse kinematics, statics, and fault tolerance of cable-suspended robots. *J. of Robotic Syst.*, 15(10):581–597, Oct. 1998.

- [RGM07] G. Rosati, P. Gallina, and S. Masiero. Design, implementation and clinical test of a wire-based robot for neurorehabilitation. *IEEE Trans. on Neural Syst. and Rehabilitation Eng.*, 15(4):560–569, Dec. 2007.
- [RMB15] C. Reichert, K. Müller, and T. Bruckman. Robust internal force-based impedance control for cable-driven parallel robots. In *Cable-Driven Parallel Robots*, volume 32 of *Mechanisms and Machine Science*, pages 131–143. Springer, 2015.
- [RZA11] G. Rosati, D. Zanotto, and S. K. Agrawal. On the design of adaptive cable-driven systems. *ASME J. of Mechanisms and Robotics*, 3(2), May 2011.
- [SD00] Y.X. Su and B.Y. Duan. The mechanical design and kinematics accuracy analysis of a fine tuning stable platform for the large spherical radio telescope. *Mechatronics*, 10(7):819–834, Oct. 2000.
- [SDJB08] Y.X. Su, B.Y. Duan, Du J.L., and H. Bao. Dynamic modeling and active control of a cable-suspended parallel robot. *Mechatronics*, 18(1):1–12, Feb. 2008.
- [SK04] E. Stump and V. Kumar. Workspace delineation of cable-actuated parallel manipulators. In *Proc. of the ASME Int. Design Eng. Tech. Conf. (DETC 2004)*, Salt Lake City, UT, Sept. 2004.
- [SK06] Ethan Stump and Vijay Kumar. Workspaces of cable-actuated parallel manipulators. *ASME J. of Mech. Design*, 128(1):159–167, Jan. 2006.
- [Sky] SkyCam [Online]. Available: <http://skycam.tv/>.
- [SLL01] J.G. Siek, L.-Q. Lee, and A. Lumsdaine. *The Boost Graph Library: User Guide and Reference Manual*. Addison Wesley, Dec. 2001.
- [SPSA15] Z. Sheng, J.-H. Park, P. Stegall, and K. Agrawal. Analytic determination of wrench closure workspace of spatial cable driven parallel mechanisms. In *Proc. of the ASME Int. Design Eng. Tech. Conf. & Comput. and Inform. in Eng. Conf. (IDETC/CIE 2015)*, pages 1–10, Boston, MA, Aug. 2015.
- [Spy] SpyderCam [Online]. Available: <http://spydercam.com/>.
- [SRK13] D. Surdilovic, J. Radojicic, and J. Krüger. Geometric stiffness analysis of wire robots: A mechanical approach. In *Cable-Driven Parallel Robots*, volume 12 of *Mechanisms and Machine Science*, pages 389–404. Springer, 2013.
- [Ste65] D. Stewart. A platform with six degrees of freedom. In *Proc. of the Institution of Mech. Engineers*, volume 180, pages 371–386, May 1965.
- [SWB11] C. Sturm, L. Wildan, and T. Bruckmann. *Wind Tunnels and Experimental Fluid Dynamics Research*, chapter Wire Robot Suspension Systems for Wind Tunnels. InTech, July 2011.
- [SZB07] D. Surdilovic, J. Zhang, and R. Bernhardt. STRING-MAN: Wire-robot technology for safe, flexible and human- friendly gait rehabilitation. In *Proc. of the IEEE 10th International Conference on Rehabilitation Robotics (ICORR 2007)*, pages 446–453, Noordwijk, Netherlands, June 2007.
- [TB05] R.R. Thompson and M.S. Blackstone. Three-dimensional moving camera assembly with an informational cover housing, Mar. 2005.
- [TB11] H.R. Taghirad and Y.B. Bedoustani. An analytic-iterative redundancy resolution scheme for cable-driven redundant parallel manipulators. *IEEE Trans. on Robotics*, 27(6):1137–1143, Dec. 2011.
- [TET+05] F. Takemura, M. Enomoto, T. Tanaka, K. Denou, and Y. Kobayashi. Development of the balloon-cable driven robot for information collection from sky and proposal of the search strategy at a major disaster. In *Proc. of the IEEE/ASME Int. Conf. on Advanced Intelligent Mechatronics (AIM 2005)*, pages 658–663, Monterey, CA, July 2005.
- [TMH+02] S. Tadokoro, Y. Murao, M. Hiller, R. Murata, H. Kohkawa, and T. Matsushima. A motion base with 6-dof by parallel cable drive architecture. *IEEE/ASME Trans. on Mechatronics*, 7(2):115–123, June 2002.

- [TSPE15] P. Tempel, F. Schenelle, A. Pott, and P. Eberhard. Design and programming for cable-driven parallel robots in the german pavilion at the expo 2015. *IMachines*, 3:223–241, 2015.
- [TVHT99] S. Tadokoro, R. Verhoeven, M. Hiller, and T. Takamori. A portable parallel manipulator for search and rescue at large-scale urban earthquakes and an identification algorithm for the installation in unstructured environments. In *Proc. of the IEEE/RSJ Int. Conf. on Intelligent Robots and Syst. (IROS 1999)*, volume 2, pages 1222–1227, Kyongju, South Korea, Oct. 1999.
- [ULP<sup>+</sup>07] Z. Ugray, L. Lasdon, J. Plummer, F. Glover, J. Kelly, and R. Marti. Scatter search and local nlp solvers: A multistart framework for global optimization. *INFORMS J. on Computing*, 19(3):328–340, July 2007.
- [VH00] R. Verhoeven and Hiller. *Advances in Robot Kinematics*, chapter Estimating the controllable workspace of tendon-based Stewart platforms, page 277–284. Springer, 2000.
- [VHT98] R. Verhoeven, M. Hiller, and S. Tadokoro. *Advances in Robot Kinematics*, chapter Workspace, stiffness, singularities and classification of tendon-driven Stewart platforms, pages 105–114. Springer, 1998.
- [Wil98] R.L. Williams. Cable suspended haptic interface. *Int. J. of Virtual Reality*, 3(3):13–21, 1998.
- [WS02] M. Weck and D. Staimer. Parallel kinematic machine tools - current state and future potentials. *CIRP Annals - Manufacturing Technology*, 51(2):671–683, Jan. 2002.
- [WXB08] R.L. Williams, M. Xin, and P. Bosscher. Contour-crafting-cartesian-cable robot system concepts: Workspace and stiffness comparisons. In *Proc. of the ASME Int. Design Eng. Tech. Conf. & Comput. and Inform. in Eng. Conf. (IDETC/CIE 2008)*, volume 2, pages 31–38, Brooklyn, NY, Aug. 2008.
- [YCD15] H. Yuan, E. Courteille, and D. Deblaise. Workspace and stiffness analysis of a three-degree-of-freedom spatial cable-suspended parallel mechanism while considering cable mass. *Mechanism and Machine Theory*, 85:64–81, Mar. 2015.
- [YLZ13] R. Yao, H. Li, and X. Zhang. A modeling method of the cable driven parallel manipulator for FAST. In *Cable-Driven Parallel Robots*, volume 12 of *Mechanisms and Machine Science*, pages 423–436. Springer, 2013.
- [YTWH10] R. Yao, X. Tang, J. Wang, and P. Huang. Dimensional optimization design for the four-cable driven parallel manipulator in FAST. *IEEE/ASME Trans. on Mechatronics*, 15(6):932–941, 2010.
- [ZJK13] X. Zhou, S. Jun, and V. Krovi. Tension distribution shaping via reconfigurable attachment in planar mobile cable robots. *Robotica*, 32(2):245–256, Mar. 2013.
- [ZJK14] X. Zhou, S. Jun, and V. Krovi. Stiffness modulation exploiting configuration redundancy in mobile cable robots. In *Proc. of the IEEE Int. Conf. on Robotics and Automation (ICRA 2014)*, pages 5934–5939, Hong Kong, Mai 2014.
- [ZLL10] Y. Zheng, Q. Lin, and X. Liu. *Robot Manipulators Trends and Development*, chapter A Wire-Driven Parallel Suspension System with 8 Wires (WDPSS-8) for Low-Speed Wind Tunnels. InTech, Mar. 2010.
- [ZRM14] D. Zanotto, G. Rosati, S. Minto, and A. Rossi. Sophia-3: A semiadaptive cable-driven rehabilitation device with a tilting working plane. *IEEE Trans. on Robotics*, 30(4):974–979, Aug. 2014.
- [ZRS<sup>+</sup>09] J. Zitzewitz, G. Rauter, R. Steiner, A. Brunschweiler, and R. Riener. A versatile wire robot concept as a haptic interface for sport simulation. In *Proc. of the IEEE Int. Conf. on Robotics and Automation (ICRA 2009)*, pages 313–318, Kobe, Japan, May 2009.
- [ZTK12] A. Zhou, C. P. Tang, and V. Krovi. Analysis framework for cooperating mobile cable robots. In *Proc. of the IEEE Int. Conf. on Robotics and Automation (ICRA 2012)*, pages 3128–3133, Saint Paul, MN, May 2012.

# Appendix A

## Modelling Complements

### A.1 Angular Speeds and Accelerations

The angular velocity of the moving platform,  $\omega = [\omega_x, \omega_y, \omega_z]$ , can be described with respect to the RPY angles. Thus, according to the RPY definition,  $\omega$  can be considered as the composition of three consecutive angular velocities,  $\dot{\phi}$  around  $\mathbf{z}_b$ ,  $\dot{\theta}$  around  $\mathbf{y}_b$  and  $\dot{\psi}$  around  $\mathbf{x}_b$ , as shown in Fig. A.1:

$$\omega = \dot{\phi}\mathbf{z}_b + \dot{\theta}\mathbf{R}_z(\phi)\mathbf{y}_b + \dot{\psi}\mathbf{R}_z(\phi)\mathbf{R}_y(\theta)\mathbf{x}_b = \dot{\phi} \begin{bmatrix} 0 \\ 0 \\ 1 \end{bmatrix} + \dot{\theta} \begin{bmatrix} -s\phi \\ c\phi \\ 0 \end{bmatrix} + \dot{\psi} \begin{bmatrix} c\phi c\theta \\ s\phi c\theta \\ -s\theta \end{bmatrix} = \begin{bmatrix} -\dot{\theta}s\phi + \dot{\psi}c\phi c\theta \\ \dot{\theta}c\phi + \dot{\psi}s\phi c\theta \\ \dot{\phi} - \dot{\psi}s\theta \end{bmatrix} \quad (\text{A.1})$$

Equation (A.1) can be rewritten as follows:

$$\omega = \begin{bmatrix} c\phi c\theta & -s\phi & 0 \\ s\phi c\theta & c\phi & 0 \\ -s\theta & 0 & 1 \end{bmatrix} \begin{bmatrix} \dot{\psi} \\ \dot{\theta} \\ \dot{\phi} \end{bmatrix} = \mathbf{S}\omega_{RPY} \quad (\text{A.2})$$

where  $\omega_{RPY} = [\dot{\psi}, \dot{\theta}, \dot{\phi}]^T$  is the vector collecting the RPY angular velocities.

Therefore, the twist of the moving platform,  $\dot{\mathbf{p}}$ , can be described with respect to the RPY angles:

$$\dot{\mathbf{p}}_{RPY} = \begin{bmatrix} \dot{\mathbf{t}} \\ \omega_{RPY} \end{bmatrix} = \mathbb{S}_{RPY}\dot{\mathbf{p}} \quad (\text{A.3})$$

where  $\mathbb{S}_{RPY}$  is the transformation matrix to express the moving platform twist in terms of the RPY angles.

$$\mathbb{S}_{RPY} = \begin{bmatrix} \mathbf{I}_3 & \mathbf{0}_3 \\ \mathbf{0}_3 & \mathbf{S}^{-1} \end{bmatrix} \quad (\text{A.4})$$

The moving platform angular accelerations,  $\alpha = [\alpha_x, \alpha_y, \alpha_z]^T$ , are computed by deriving Eq. (A.2):

$$\dot{\alpha} = \dot{\mathbf{S}}\omega_{RPY} + \mathbf{S}\dot{\omega}_{RPY} \quad (\text{A.5})$$

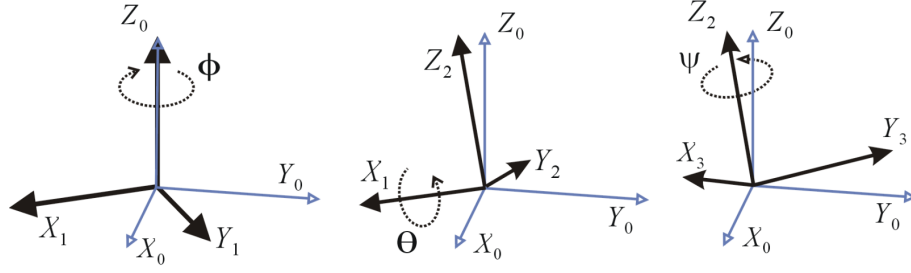


Fig. A.1 – RPY angle representation

where  $\alpha_{RPY} = [\ddot{\psi}, \ddot{\theta}, \ddot{\phi}]^T$  is the vector collecting the RPY angular accelerations and  $\dot{\mathbf{S}}$  is the time derivative of the transformation matrix  $\mathbf{S}$ .

$$\dot{\mathbf{S}} = \begin{bmatrix} -\dot{\phi}s\phi c\theta - \dot{\theta}c\phi s\theta & -\dot{\phi}c\phi & 0 \\ \dot{\phi}c\phi c\theta - \dot{\theta}s\phi s\theta & -\dot{\phi}s\phi & 0 \\ -\dot{\theta}c\theta & 0 & 0 \end{bmatrix} \quad (\text{A.6})$$

Equation (A.5) can be rewritten as follows:

$$\begin{aligned} \dot{\omega} &= \begin{bmatrix} -\dot{\phi}s\phi c\theta - \dot{\theta}c\phi s\theta & -\dot{\phi}c\phi & 0 \\ \dot{\phi}c\phi c\theta - \dot{\theta}s\phi s\theta & -\dot{\phi}s\phi & 0 \\ -\dot{\theta}c\theta & 0 & 0 \end{bmatrix} \begin{bmatrix} \ddot{\psi} \\ \ddot{\theta} \\ \ddot{\phi} \end{bmatrix} + \begin{bmatrix} c\phi c\theta & -s\phi & 0 \\ s\phi c\theta & c\phi & 0 \\ -s\theta & 0 & 1 \end{bmatrix} \begin{bmatrix} \ddot{\psi} \\ \ddot{\theta} \\ \ddot{\phi} \end{bmatrix} = \\ &= \begin{bmatrix} -\dot{\phi}\ddot{\psi}s\phi c\theta - \dot{\theta}\ddot{\psi}c\phi s\theta - \dot{\phi}\dot{\theta}c\phi + \ddot{\psi}c\phi c\theta - \dot{\theta}s\phi\dot{\phi} \\ \dot{\phi}\ddot{\psi}c\phi c\theta - \dot{\theta}\ddot{\psi}s\phi s\theta - \dot{\phi}\dot{\theta}s\phi + \ddot{\psi}s\phi c\theta + \dot{\theta}c\phi\dot{\phi} \\ -\dot{\theta}\dot{\phi}c\theta - \ddot{\psi}s\theta + \ddot{\phi} \end{bmatrix} \quad (\text{A.7}) \end{aligned}$$

Thus, the angular acceleration of the moving platform can be expressed in terms of the RPY angles, according to the following transformation:

$$\alpha_{RPY} = \mathbf{S}^{-1}\dot{\alpha} - \mathbf{S}^{-1}\dot{\mathbf{S}}\omega_{RPY} = \mathbf{S}^{-1}\dot{\alpha} - \mathbf{S}^{-1}\dot{\mathbf{S}}\mathbf{S}^{-1}\omega \quad (\text{A.8})$$

## A.2 Wrench Matrix Time Derivative

The SOIKM requires the computation of the time derivative of the wrench matrix  $\mathbf{W}$ . Its columns represent the cable wrench,  $\mathbf{w}_i = [\mathbf{d}_i^b, \mathbf{b}_i^r \times \mathbf{d}_i^b], i = 1, \dots, m$ .

The time derivative of  $\mathbf{d}_i^b$  is defined as follows:

$$\frac{d\mathbf{d}_i^b}{dt} = \dot{\mathbf{d}}_i^b = \frac{\mathbf{i}_i^b - (\mathbf{i}_i^{bT} \mathbf{d}_i^b) \mathbf{d}_i^b}{l_i} \quad (\text{A.9})$$

where  $\mathbf{i}_i^b = -\dot{\mathbf{t}} - \dot{\omega} \mathbf{b}_i^r$ .

The time derivative of  $\mathbf{b}_i^r \times \mathbf{d}_i^b$  is defined as follows:

$$\frac{d(\mathbf{b}_i^r \times \mathbf{d}_i^b)}{dt} = \dot{\mathbf{b}}_i^r \times \mathbf{d}_i^b + \mathbf{b}_i^r \times \dot{\mathbf{d}}_i^b \quad (\text{A.10})$$

### A.3 Active Stiffness Matrix Detailed Computation for Sagging Cables

Several elasto-static models, based on sagging cables, have been proposed in the literature. Most of them do not develop the active stiffness matrix,  $\mathbf{K}_a$ , which is one of the two components of the CDPR stiffness matrix,  $\mathbf{K}$ . The remaining models have been derived taking into account matrix  $\mathbf{K}_a$  and developing it according to different procedures [Ars13, NG14a].

Hereafter, the active stiffness matrix described in Sec. 2.3.3 is computed in details. For sake of simplicity, matrix  $\mathbf{K}_a$  can be decomposed as follows:

$$\mathbf{K}_a = \sum_{i=1}^m \frac{d\mathbf{W}_i}{d\mathbf{p}} \mathbf{F}_i = \sum_{j=1}^3 \frac{d\mathbf{w}_{i,j}}{d\mathbf{p}} F_{i,j} \quad (\text{A.11})$$

where  $\mathbf{w}_{i,j}$  represents the  $j$ -th column of the wrench matrix  $\mathbf{W}_i$  and  $F_{i,j}$  the  $j$ -th force component associated to the  $i$ -th cable. The wrench projection matrix  $\mathbf{W}_i$  is defined as follows:

$$\mathbf{W}_i = \begin{bmatrix} \mathbf{w}_{i,1}^T \\ \mathbf{w}_{i,2}^T \\ \mathbf{w}_{i,3}^T \end{bmatrix}^T = \begin{bmatrix} c\theta_i & s\theta_i & 0 & -b_{z,i}^r s\theta_i & b_{z,i}^r c\theta_i & b_{x,i}^r s\theta_i - b_{y,i}^r c\theta_i \\ -s\theta_i & c\theta_i & 0 & -b_{z,i}^r c\theta_i & -b_{z,i}^r s\theta_i & b_{x,i}^r c\theta_i + b_{y,i}^r s\theta_i \\ 0 & 0 & 1 & b_{y,i}^r & -b_{x,i}^r & 0 \end{bmatrix}^T \quad (\text{A.12})$$

Each term of  $\mathbf{W}_i$  is derived with respect to the pose  $\mathbf{p}$ . In order to improve the readability of the result, the Jacobian matrices  $\frac{d\mathbf{w}_{i,1}}{d\mathbf{p}}$  have been decomposed:

$$\frac{d\mathbf{w}_{i,1}}{d\mathbf{p}} = \left[ \left( \frac{d\mathbf{w}_{i,11}}{d\mathbf{p}} \right)^T, \left( \frac{d\mathbf{w}_{i,12}}{d\mathbf{p}} \right)^T, \left( \frac{d\mathbf{w}_{i,13}}{d\mathbf{p}} \right)^T, \left( \frac{d\mathbf{w}_{i,14}}{d\mathbf{p}} \right)^T, \left( \frac{d\mathbf{w}_{i,15}}{d\mathbf{p}} \right)^T, \left( \frac{d\mathbf{w}_{i,16}}{d\mathbf{p}} \right)^T \right]^T \quad (\text{A.13})$$

Hereafter, each gradient  $\frac{d\mathbf{w}_{i,1j}}{d\mathbf{p}}, j = 1, \dots, 6$  is computed:

$$\frac{d\mathbf{w}_{i,11}}{d\mathbf{p}} = \left[ -s\theta_i \frac{l_{y,i,c}}{l_{x,i,c}^2 + l_{y,i,c}^2}, s\theta_i \frac{l_{x,i,c}}{l_{x,i,c}^2 + l_{y,i,c}^2}, 0, -s\theta_i \frac{b_{z,i}^r l_{x,i,c}}{l_{x,i,c}^2 + l_{y,i,c}^2}, -s\theta_i \frac{b_{z,i}^r l_{y,i,c}}{l_{x,i,c}^2 + l_{y,i,c}^2}, s\theta_i \frac{b_{x,i}^r l_{x,i,c} + b_{y,i}^r l_{y,i,c}}{l_{x,i,c}^2 + l_{y,i,c}^2} \right] \quad (\text{A.14})$$

$$\frac{d\mathbf{w}_{i,12}}{d\mathbf{p}} = \left[ c\theta_i \frac{l_{y,i,c}}{l_{x,i,c}^2 + l_{y,i,c}^2}, -c\theta_i \frac{l_{x,i,c}}{l_{x,i,c}^2 + l_{y,i,c}^2}, 0, c\theta_i \frac{b_{z,i}^r l_{x,i,c}}{l_{x,i,c}^2 + l_{y,i,c}^2}, c\theta_i \frac{b_{z,i}^r l_{y,i,c}}{l_{x,i,c}^2 + l_{y,i,c}^2}, -c\theta_i \frac{b_{x,i}^r l_{x,i,c} + b_{y,i}^r l_{y,i,c}}{l_{x,i,c}^2 + l_{y,i,c}^2} \right] \quad (\text{A.15})$$

$$\frac{d\mathbf{w}_{i,13}}{d\mathbf{p}} = [0, 0, 0, 0, 0, 0] \quad (\text{A.16})$$

$$\frac{d\mathbf{w}_{i,14}}{d\mathbf{p}} = \left[ -b_{z,i}^r c\theta_i \frac{l_{y,i,c}}{l_{x,i,c}^2 + l_{y,i,c}^2}, b_{z,i}^r c\theta_i \frac{l_{x,i,c}}{l_{x,i,c}^2 + l_{y,i,c}^2}, 0, -b_{y,i}^r s\theta_i - b_{z,i}^r c\theta_i \frac{b_{z,i}^r l_{x,i,c}}{l_{x,i,c}^2 + l_{y,i,c}^2}, \right. \\ \left. b_{x,i}^r s\theta_i - b_{z,i}^r c\theta_i \frac{b_{z,i}^r l_{y,i,c}}{l_{x,i,c}^2 + l_{y,i,c}^2}, b_{z,i}^r c\theta_i \frac{b_{x,i}^r l_{x,i,c} + b_{y,i}^r l_{y,i,c}}{l_{x,i,c}^2 + l_{y,i,c}^2} \right] \quad (\text{A.17})$$

$$\frac{d\mathbf{w}_{i,15}}{d\mathbf{p}} = \left[ -b_{z,i}^r s\theta_i \frac{l_{y,i,c}}{l_{x,i,c}^2 + l_{y,i,c}^2}, b_{z,i}^r s\theta_i \frac{l_{x,i,c}}{l_{x,i,c}^2 + l_{y,i,c}^2}, 0, b_{y,i}^r c\theta_i - b_{z,i}^r s\theta_i \frac{b_{z,i}^r l_{x,i,c}}{l_{x,i,c}^2 + l_{y,i,c}^2}, \right. \\ \left. -b_{x,i}^r c\theta_i - b_{z,i}^r s\theta_i \frac{b_{z,i}^r l_{y,i,c}}{l_{x,i,c}^2 + l_{y,i,c}^2}, b_{z,i}^r s\theta_i \frac{b_{x,i}^r l_{x,i,c} + b_{y,i}^r l_{y,i,c}}{l_{x,i,c}^2 + l_{y,i,c}^2} \right] \quad (\text{A.18})$$

$$\begin{aligned}
\frac{dw_{i,61}}{dp} = & \left[ b_{y,i}^r s \theta_i \frac{l_{y,i,c}}{l_{x,i,c}^2 + l_{y,i,c}^2} + b_{x,i}^r c \theta_i \frac{l_{y,i,c}}{l_{x,i,c}^2 + l_{y,i,c}^2}, -b_{y,i}^r s \theta_i \frac{l_{x,i,c}}{l_{x,i,c}^2 + l_{y,i,c}^2} - b_{x,i}^r c \theta_i \frac{l_{x,i,c}}{l_{x,i,c}^2 + l_{y,i,c}^2}, 0, \right. \\
& b_{z,i}^r c \theta_i + b_{y,i}^r s \theta_i \frac{b_{z,i}^r l_{x,i,c}}{l_{x,i,c}^2 + l_{y,i,c}^2} + b_{x,i}^r c \theta_i \frac{b_{z,i}^r l_{x,i,c}}{l_{x,i,c}^2 + l_{y,i,c}^2}, b_{z,i}^r s \theta_i + b_{y,i}^r s \theta_i \frac{b_{z,i}^r l_{y,i,c}}{l_{x,i,c}^2 + l_{y,i,c}^2} + b_{x,i}^r c \theta_i \frac{b_{z,i}^r l_{y,i,c}}{l_{x,i,c}^2 + l_{y,i,c}^2}, \\
& \left. -b_{x,i}^r c \theta_i - b_{y,i}^r s \theta_i - b_{y,i}^r s \theta_i \frac{b_{x,i}^r l_{x,i,c} + b_{y,i}^r l_{y,i,c}}{l_{x,i,c}^2 + l_{y,i,c}^2} - b_{x,i}^r c \theta_i \frac{b_{x,i}^r l_{x,i,c} + b_{y,i}^r l_{y,i,c}}{l_{x,i,c}^2 + l_{y,i,c}^2} \right] \quad (A.19)
\end{aligned}$$

Considering  $F_{i,y}$  is always equal to 0, it is not necessary to take into account the Jacobian matrices  $\frac{dw_{i,2}}{dp}$ . On the contrary, the Jacobian matrix  $\frac{dw_{i,3}}{dp}$  has been developed as follows:

$$\frac{dw_{i,3}}{dp} = \begin{bmatrix} 0 & 0 & 0 & 0 & 0 & 0 \\ 0 & 0 & 0 & 0 & 0 & 0 \\ 0 & 0 & 0 & 0 & 0 & 0 \\ 0 & 0 & 0 & -b_{z,i}^r & 0 & b_{x,i}^r \\ 0 & 0 & 0 & 0 & -b_{z,i}^r & b_{y,i}^r \\ 0 & 0 & 0 & 0 & 0 & 0 \end{bmatrix} \quad (A.20)$$

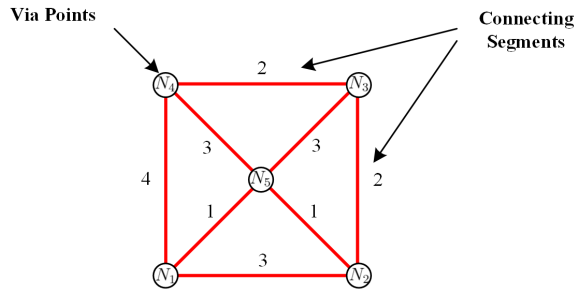
## Appendix B

# Routing Inspection Problem

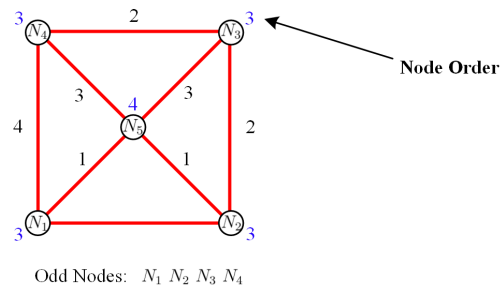
According to the reconfiguration algorithm introduced in Chap. 5, the user provides a list of  $n_{vp}$  via points that the moving platform should cross. The via points are connected by segments. In order to optimise the path planning of the moving platform, the length of the path necessary to cover all the via points and the connecting segments should be minimised. Hence, this optimisation problem is formulated as a routing inspection problem through a graph representation. The problem is solved according to Fleury's algorithm:

- a. *Graph Building.* Build a graph such that the nodes represent the via points and the arcs the segments connecting them. The costs of the arcs are the lengths of the corresponding segments.
- b. *Analysis of the Node Orders.* Analyse the graph in order to verify if it is an Eulerian graph. A graph is Eulerian if all the nodes have an even order. The order of a node is equivalent to the number of segments connected to the node. An Eulerian graph contemplates one or more Eulerian cycle, a trail which cross every edge exactly once, starting and ending at the same vertex. If the graph is Eulerian, steps c., d. and e. has to be skipped.
- c. *Pair up the Odd Nodes.* If there exist some odd nodes, pair up each node of odd order and for each pairing find the arcs which connect the odd nodes with the shortest possible path.
- d. *Combining the Pairings of Odd Nodes.* Determine the combination of pairings that has the shortest total length.
- e. *Eulerian Graph Computation.* Duplicate in the original graph the arcs connecting the odd nodes according to the combination of pairings identified in the previous step. The modified graph is now Eulerian.
- f. *Eulerian Cycle Computation.* Compute one or several Eulerian cycle(s) by means of Fleury's algorithm [EGL95]. The total length of the Eulerian cycle is equal to the sum of the arc costs of the modified graph. Fig. B.1 presents an example of the path planning for a task demanding to the platform to cover 8 segments, starting from via point  $N_1$ .
- g. *Discretisation of the Shortest Path.* Select an Eulerian cycle which represents the path that platform of the RCDPR will follows during the task. The chosen path will be discretised into  $n_P$  points,  $\mathcal{P} = \{P_i, i = 1, \dots, n_P\}$ , where  $\mathbf{p}_i, i = 1, \dots, n_P$ , are the moving-platform pose vectors expressed in  $\mathcal{F}_b$ .

**a. Graph Building**



**b. Analysis of the Node Orders**



**c. Pair Up of the Odd Nodes**

Pair Up the Odd Nodes:

- $\overline{N_1 N_2} = 2$
- $\overline{N_1 N_3} = 3$
- $\overline{N_1 N_4} = 4$
- $\overline{N_2 N_3} = 2$
- $\overline{N_2 N_4} = 4$
- $\overline{N_3 N_4} = 2$

**d. Combining the Pairings of Odd Nodes.**

Combine the Pairings of

- $\overline{N_1 N_2}$   $\overline{N_3 N_4} = 4$
- Odd Nodes:  $\overline{N_1 N_3}$   $\overline{N_2 N_4} = 7$
- $\overline{N_1 N_4}$   $\overline{N_2 N_3} = 6$

**e,f,g. Eulerian Graph Computation, Eulerian Cycle Determination and Discretization**

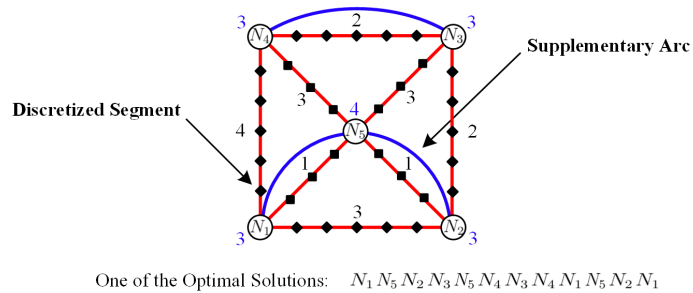


**Fig. B.1** – Computation of one of the possible optimal path covering the whole set of prescribed segments. In this example the segments to be crossed do not represent an Eulerian graph. To transform it into an Eulerian graph, minimising the cost of the corresponding Eulerian cycles, it is necessary to add three segments

# Appendix C

## Publications

### Journals

L. Gagliardini, S. Caro, M. Gouttefarde, and A. Girin. Discrete reconfiguration planning for cable-driven parallel robots. *Mechanism and Machine Theory*, 100:313–337, 2016.

### Book Chapter

L. Gagliardini, M. Gouttefarde, and S. Caro. Design of Reconfigurable Cable-Driven Parallel Robot. *Mechatronics for Cultural Heritage and Civil Engineering*, Springer, 2017. [Accepted]

### Patents

A. Girin, L. Gagliardini, S. Caro, M. Gouttefarde, and P. Yvan. European patent ep2982483 (a2), Feb. 2016.

### International Conferences

L. Gagliardini, S. Caro, M. Gouttefarde, P. Wenger, and A. Girin. Optimal design of cable-driven parallel robots for large industrial structures. In *Proc. of the IEEE Int. Conf. on Robotics and Automation (ICRA 2014)*, pages 5744–5749, Hong Kong, China, May 2014.

L. Gagliardini, S. Caro, and M. Gouttefarde. Dimensioning of cable-driven parallel robot actuators, gear head and winches according to the twist feasible workspace. In *Proc. of the IEEE Int. Conf. on Automation Science and Engineering (CASE 2015)*, pages 99–105, Gothenburg, Sweden, Aug. 2015.

L. Gagliardini, S. Caro, M. Gouttefarde, P. Wenger, and A. Girin. A reconfigurable cable-driven parallel robot for sandblasting and painting of large structures. In *Cable-Driven Parallel Robots*, volume 32 of Mechanisms and Machine Science, pages 275–291. Springer, 2015.

L. Gagliardini, S. Caro, M. Gouttefarde, P. Wenger, and A. Girin. A reconfiguration strategy for reconfigurable cable-driven parallel robots. In *Proc. of the IEEE Int. Conf. on Robotics and Automation (ICRA 2015)*, pages 1613–1620, Seattle, WA, May 2015.

L. Gagliardini, M. Gouttefarde, and S. Caro. Determination of a Dynamic Feasible Workspace for Cable-Driven Parallel Robots. In *Proc. of the IFToMM Int. Conf. on Advances in Robot Kinematics (ARK 2016)*, Grasse, France, June 2016.

### **Workshops**

L. Gagliardini, S. Caro, and M. Gouttefarde. Optimal path planning and reconfiguration strategy for reconfigurable cable-driven parallel robots. In *Optimal Robot Motion Planning Workshop (WORMP) at IEEE Int. Conf. on Robotics and Automation (ICRA 2015)*, Seattle, WA, May 2015.

# Index

- Active stiffness matrix (linear cables with pulleys), [39](#)
- Active stiffness matrix (linear cables), [35](#)
- Active stiffness matrix (sagging cables), [41](#)
- Adjacent node, [99](#)
  
- Cable tension distribution, [33](#)
- Cable-Driven Parallel Robot, [2](#)
- CAROCA Project, [9](#)
- Collision Free Workspace (CFW), [48](#)
- Configuration, [8](#)
- Constant design parameter, [59](#)
- Continuous RCDPR, [68](#)
- Cost function, [102](#)
  
- Degrees of Freedom, [6](#)
- Design Problem Formulation for CDPRs, [60](#)
- Design problem formulation for RCDPRs, [69](#)
- Design variables, [59](#)
- Dijkstra's Algorithm, [102](#)
- Direct Kinematic Model (DKM), [26](#)
- Discrete RCDPR, [68](#)
- Dominant configuration, [97](#)
- Dominated configuration, [97](#)
- Dynamic Feasible Workspace (DFW), [50](#)
  
- Elasto-Static Model (linear cables), [34](#)
- Exit points, [2](#)
  
- Feasibility map, [95](#)
- Fully constrained CDPR, [7](#)
  
- Global objective function, [71](#)
- Graph, [99](#)
  
- Improved Dynamic Feasible Workspace (IDFW), [51](#)
- Interference Free Workspace (IFW), [48](#)
- Inverse Dynamic Model (IDM), [29](#)
- Inverse Geometric Model (IGM) (linear cables), [23](#)
- Inverse geometrico-static problem, [30](#)
- Inverse Kinematic Model (IKM), [26](#)
- Inverse Static Model (ISM), [25](#)
  
- Minimum Degree of Constraint Satisfaction (MDoCS), [61](#)
- Minimum Degree of Dynamic Constraint Satisfaction (MDoDCS), [62](#)
  
- Negative Feasibility Transition (PFT), [95](#)
- NFT node, [99](#)
  
- Parallel Robot, [1](#)
- Passive stiffness matrix (linear cables with pulleys), [37](#)
- Passive stiffness matrix (linear cables), [35](#)
- Passive stiffness matrix (sagging cables), [40](#)
- PFT node, [99](#)
- Planar CDPR, [7](#)
- Positive Feasibility Transition (PFT), [95](#)
  
- Reconfigurable Cable-Driven Parallel Robot, [8](#)
- Reconfiguration Strategy for Discrete RCDPRs, [90](#)
  
- Sagging cable model, [29](#)
- Second Order Direct Kinematic Model (SODKM), [26](#)
- Second Order Inverse Kinematic Model (SOIKM), [27](#)
- Spatial CDPR, [7](#)
- Static Feasible Workspace (SFW), [47](#)
- Stiffness matrix (sagging cables), [39](#)
- Suspended CDPR, [7](#)
  
- Twist Feasible Workspace (TFW), [49](#)
  
- Under-constrained CDPR, [7](#)
  
- Wrench Closure Workspace (WCW), [47](#)
- Wrench Feasible Workspace (WFW), [45](#)

# Thèse de Doctorat

Lorenzo GAGLIARDINI

Reconfigurations Discrètes de Robots Parallèles à Câbles

Discrete Reconfigurations of Cable-Driven Parallel Robots

## Résumé

Les *Robots Parallèles à Câbles* (RPCs) sont des robots parallèles dont les jambes se composent de câbles. Les applications industrielles potentielles des RPCs sont nombreuses telles que le grenailage et la peinture de structures massives et de grandes dimensions.

La première partie de ce manuscrit est dédiée à la modélisation des RPCs. Deux modèles élasto-statiques ont été introduits dans ce manuscrit, pour décrire le petit déplacement de la plate-forme mobile en raison de la nature non-rigide des câbles. Le modèle élasto-statique basé sur des câbles pesants a été exprimé en faisant la différence entre la matrice de raideur active et la matrice de raideur passive du RPC.

La deuxième partie de ce manuscrit traite de l'analyse d'espaces de travail de RPCs vis-à-vis de leurs performances statiques et dynamiques. Deux nouveaux espaces de travail ont été définis : (i) *l'Espace des Vitesses Générables* (EVG); (ii) *l'Espace de Travail Dynamique Amélioré* (ETDA).

La troisième partie de ce manuscrit décrit une stratégie de conception générique de RPCs et des *Robots Parallèles à Câbles Reconfigurables* (RPCRs). Les reconfigurations sont limitées uniquement aux points de sortie des câbles. Dans ce manuscrit, les points de sortie des câbles peuvent être placés dans une large mais limité ensemble de positions. La stratégie proposée envisage la possibilité de déplacer les points de sortie des câbles du RPCR sur une grille prédéfinie d'emplacements.

La quatrième partie de ce manuscrit présente un algorithme pour calculer une stratégie de reconfiguration optimale pour les RPCRs. Cette stratégie peut être utilisée lorsque l'environnement de travail de RPCRs est extrêmement encombré et qu'il n'est pas possible de prévoir le nombre de configurations nécessaires pour compléter la tâche. L'efficacité de l'algorithme a été analysée en étudiant les reconfigurations d'un robot parallèle à câbles planaire et d'un robot parallèle à câbles spatial en lien avec des applications industrielles.

## Mots-clés

**Robots Parallèles à Câbles, Reconfigurations Discrètes, Espaces de travail, Modélisation Elasto-Statique, Conception**

## Abstract

*Cable-Driven Parallel Robots* (CDPRs) are parallel robots whose legs consist of cables. CDPRs may be used successfully in several industrial applications such as sandblasting and painting of large and heavy structures.

The first part of this manuscript is dedicated to the modelling of CDPRs. Two elasto-static models have been introduced in this manuscript, in order to describe the small displacement of the moving platform due to the non-rigid nature of the cables. These models can be used for the modal analysis of the CDPRs, as well. The elasto-static model based on linear cables has been computed including the effect of the pulleys orienting the cables into the CDPR workspace.

The second part of this manuscript deals with the investigation of the workspace of CDPRs, in terms of their moving platform static and dynamic equilibria, and in terms of their moving platform kinematic constraints. Two novel workspaces have been defined: (i) the *Twist Feasible Workspace* (TFW); (ii) the *Improved Dynamic Feasible Workspace* (IDFW).

The third part of this manuscript describes a generic design strategy for CDPRs and a novel design strategy for *Reconfigurable Cable-Driven Parallel Robots* (RCDPRs). In this manuscript, reconfigurations are limited to the displacement of the cable exit points, assuming the cables exit points can be installed on a large but finite set of locations.

The fourth part of this manuscript introduces an algorithm to compute an optimal reconfiguration strategy for RCDPRs. This strategy can be used when the working environment of the RCDPR is extremely cluttered and when it is not possible to predict how many configurations are necessary to complete the task. The effectiveness of the algorithm has been analysed by means of a planar and a spatial case studies reproducing some industrial tasks.

## Key Words

**Cable-Driven Parallel Robots, Discrete Reconfigurations, Workspaces, Elasto-Static Modelling, Design.**

